

NASA CR-111887

PARAMETRIC STUDIES OF THE ACOUSTIC BEHAVIOR  
OF LINED DUCTS AND DUCT-LINING MATERIALS  
FOR TURBOFAN ENGINE APPLICATIONS

By J. Atvars

Prepared Under Contract NAS1-10272 by  
THE BOEING COMPANY  
Commercial Airplane Group  
Seattle, Washington

for

LANGLEY RESEARCH CENTER  
NATIONAL AERONAUTICS AND SPACE ADMINISTRATION



## CONTENTS

	Page
SUMMARY . . . . .	1
INTRODUCTION . . . . .	1
SYMBOLS . . . . .	2
DESCRIPTION OF THE FLOW-DUCT FACILITY . . . . .	4
Instrumentation . . . . .	5
Acoustic Instrumentation . . . . .	5
Aerodynamic Instrumentation . . . . .	5
Performance of the Flow-Duct Facility . . . . .	5
Signal-to-Noise Ratio . . . . .	5
Input Sound Pressure Levels . . . . .	5
Flow-Velocity Profiles . . . . .	5
DESCRIPTION OF PROGRAM PROCEDURE . . . . .	6
Test Procedure . . . . .	6
Data Reduction . . . . .	6
Description of Duct Linings . . . . .	6
FLOW DUCT TEST RESULTS . . . . .	7
Assumptions in Data Analysis . . . . .	7
Power Insertion Loss . . . . .	7
One Wall Lined Versus Two Walls Lined . . . . .	7
Temperature and Pressure . . . . .	8
Turbulence Effects . . . . .	8
Attenuation of Broadband Versus Discrete-Frequency Noise . . . . .	8
Qualitative Discussion of Test Results . . . . .	8
Tuned Frequency of Ducts With Single-Layer Linings . . . . .	8
Attenuation in Ducts With Single-Layer Linings . . . . .	9
Flow Resistance Optimization . . . . .	11
Empirical Prediction Method for the Acoustic Performance of Single-Layer Linings . . . . .	12
Prediction of Tuned Frequency . . . . .	12
Prediction of Attenuation . . . . .	13
Miscellaneous Lining Design Concepts . . . . .	15
Double-Layer Linings . . . . .	15
Slanted-Core Linings . . . . .	15
Mixed-Depth Single-Layer Linings . . . . .	15
Acoustic Splitters . . . . .	16
Multiwall Treatments . . . . .	16
Curved Ducts . . . . .	16
NASA Material . . . . .	16
Effect of Sound Refraction in Lined Ducts . . . . .	16
Acoustically Lined Duct Fluctuating Wall Pressure Spectra . . . . .	16
Skin Friction Drag of Acoustic Linings . . . . .	17

CONTENTS.—Concluded

	Page
CONCLUDING REMARKS . . . . .	17
REFERENCES . . . . .	19
APPENDIX—FLOW-DUCT TEST RESULTS . . . . .	61

FIGURES

No.		Page
1	Boeing Flow-Duct Facility . . . . .	20
2	View of Plenum Chamber and Inlet Diffuser . . . . .	21
3	Multinozzle Jet Noise Source . . . . .	21
4	Semireverberant Chamber With Microphone Boom . . . . .	22
5	S-Bend Test Duct . . . . .	22
6	Aerodynamic Instrumentation of Flow Duct . . . . .	23
7	Test Duct With Remote-Controlled Total-Pressure Rake Mechanisms . . . . .	23
8	Maximum Baseline Broadband Input SPL Spectra at $M = 0.19$ . . . . .	24
9	Upstream Velocity Profiles in the 6- by 10-In. Flow Duct . . . . .	25
10	Upstream Velocity Profiles in the 4- by 10-In. Flow Duct . . . . .	26
11	Method of Flow Velocity Profile Shaping . . . . .	26
12	Graphic Method of Acoustic Data Reduction . . . . .	27
13	Resistive-Resonator Lining Panel Construction . . . . .	28
14	Polyimide Acoustic Liner Construction . . . . .	28
15	Acoustically Treated Duct/Liner Parameters . . . . .	29
16	Variation of Peak Frequency With Lining Depth in a 6-In. Duct at $M = 0.28$ . . . . .	30
17	Variation of Peak Frequency With Lining Separation for a 0.5-In.-Deep Lining at $M = 0.28$ . . . . .	30
18	Variation of Peak Frequency With Cell Length for a 0.5-in.-Deep Lining in a 6-In. Duct at $M = 0.28$ . . . . .	31
19	Variation of Peak Frequency With Airflow Mach Number for a Range of High-Reactance Linings 0.5 In. Deep in a 6-In. Duct . . . . .	31
20	Acoustic Performance of High- and Low-Reactance Linings . . . . .	32
21	Reactive Impedance Characteristics of Different Types of Lining Materials at $M = 0$ . . . . .	32
22	Variation of Peak Frequency With Lining Reactance for a 30-Rayl (CGS) Effective Flow Resistance Material 0.5 In. Deep in a 6-In. Duct . . . . .	33
23	Typical Attenuation Spectra for Various Lining Lengths of a 30-Rayl (CGS) High-Reactance Material 0.5 In. Deep in a 6-In. Duct at $M = 0.28$ . . . . .	33
24	Variation of Attenuation With Lining Length for a 30-Rayl (CGS) High-Reactance Material 0.5 In. Deep in a 6-In. Duct at $M = 0.28$ . . . . .	34
25	Variation of Attenuation With Lining Separation for a 30-Rayl (CGS) High-Reactance Material 0.5 In. Deep at $M = 0.28$ . . . . .	34
26	Variation of Attenuation With Lining Depth for Optimum High-Reactance Materials in a 6-In. Duct at $M = 0.28$ . . . . .	35
27	Variation of Attenuation With Cell Length for a High Reactance Material 0.5 In. Deep in a 6-In. Duct at $M = 0.28$ . . . . .	35



FIGURES.—Continued

No.		Page
28	Variation of Attenuation With Airflow Mach Number for a 30-Rayl (CGS) High-Reactance Material 0.5 In. Deep in a 6-In. Duct . . . . .	36
29	Variation of Attenuation With Laminar Flow Resistance for a High-Reactance Material 0.5 In. Deep in a 6-In. Duct at $M = 0.28$ . . . . .	36
30	Variation of Flow Resistance With Particle Velocity for the Two Major Types of Porous Acoustic Lining Materials . . . . .	37
31	Variation of Attenuation With Nominal Flow Resistance for 0.5-In.-Deep Linings in a 4-In. Duct . . . . .	38
32	Variation of Attenuation With Nominal Flow Resistance for 0.5-In.-Deep Linings in a 6-In. Duct . . . . .	39
33	Variation of Attenuation With Nominal Flow Resistance for 0.5-In.-Deep Linings in an 8-In. Duct . . . . .	40
34	Variation of Attenuation With Nominal Flow Resistance for 0.5-In.-Deep Linings in a 12-In. Duct . . . . .	41
35	Variation of Attenuation With Nominal Flow Resistance for 0.25-In.-Deep Linings in a 6-In. Duct . . . . .	42
36	Variation of Attenuation With Nominal Flow Resistance for 1-In.-Deep Linings in a 6-In. Duct . . . . .	43
37	Variation of Attenuation With Nominal Flow Resistance for 0.25-In.-Deep Linings in a 12-In. Duct . . . . .	44
38	Variation of Attenuation With Nominal Flow Resistance for 1-In. Deep Linings in a 12-In. Duct . . . . .	45
39	Variation of the Optimum Effective Flow Resistance With Attenuation Bandwidth and Mach Number for 0.5-In.-Deep Linings in a 6-In. Duct . . . . .	46
40	Variation of the Optimum Effective Flow Resistance With Lining Depth and Duct Size for One-Octave Bandwidth at $M = 0.3$ . . . . .	46
41	Variation of the Optimum Effective Flow Resistance With Lining Depth and Mach Number for One-Octave Bandwidth in a 6-In. Duct . . . . .	47
42	Variation of Attenuation With Effective Flow Resistance for High- and Low-Reactance Materials . . . . .	48
43	Variation of Attenuation With Mach Number for Various Lining Depths, 9-Rayl (CGS) Nominal Flow Resistance Material in a 6-In. Duct . . . . .	49
44	Variation of Peak Frequency With Duct Size and Lining Depth for 30-Rayl (CGS), Nominal Flow Resistance, High-Reactance Linings at $M = 0.28$ . . . . .	49
45	Variation of Attenuation Band Center Frequency . . . . .	50
46	Increase in Peak Frequency for Low-Reactance Linings as Compared to High-Reactance Linings . . . . .	50
47	Variation of Attenuation With Lining Length for a 30-Rayl (CGS) High-Reactance Material 0.5-In. Deep at $M = 0.28$ . . . . .	51
48	Rate of Change of Attenuation With Lining Length for Various Duct Sizes . . . . .	51
49	Variation of Attenuation With Lining Depth for Optimum Effective Flow Resistance for High-Reactance Material . . . . .	52
50	Variation of Attenuation With Bandwidth and Airflow Mach Number in the Exhaust Mode . . . . .	53
51	Variation of Attenuation With Bandwidth and Airflow Mach Number in the Inlet Mode . . . . .	53
52	Comparison of Attenuation Spectra of Typical Single- and Double-Layer Linings . . . . .	54

FIGURES.—Concluded

No.		Page
53	Difference in Attenuation Between Double- and Single-Layer Linings of Equal Total Depth $d_t$ in a 6-In. Duct at $M = 0.28$ . . . . .	54
54	Attenuation Spectra for Slanted and Upright Honeycomb Core Linings in a 6-In. Duct at $M = 0.28$ . . . . .	55
55	Attenuation Spectra for Slanted Double-Layer Linings in a 6-In. Duct . . . . .	56
56	Attenuation Spectra for Various Combinations of Single-Layer Lining Depths in a 6-In. Duct at $M = 0.28$ . . . . .	57
57	Attenuation Spectra for Two Different Combinations of Single-Layer Linings of Equal Total Length in a 6-In. Duct at $M = 0.28$ . . . . .	57
58	Attenuation Spectra for Different Types of Duct Acoustic Splitters of the Same Total Thickness . . . . .	57
59	Attenuation Spectra for Different Numbers of Walls Lined . . . . .	58
60	Comparison of Acoustic Performance of NASA and Equivalent Polyimide Lining . . . . .	59
61	Attenuation Spectra for a Fixed Length of 0.5-In.-Deep Lining Exposed to a Distorted Velocity Profile . . . . .	60
62	Duct Wall Pressure Spectra as Measured by Flush-Mounted Microphones in a 6-In. Duct at $M = 0.28$ . . . . .	60

PARAMETRIC STUDIES OF THE ACOUSTIC BEHAVIOR OF  
LINED DUCTS AND DUCT-LINING MATERIALS  
FOR TURBOJET ENGINE APPLICATIONS

By J. Atvars  
The Boeing Company  
Seattle, Washington

SUMMARY

Fan noise radiated from the engine inlet and fan discharge ducts of current fan-jet airplanes makes the largest contribution to perceived noise during landing approach. This noise can be reduced by lining the engine inlet and duct walls with sound-absorbing materials. Because of the scarcity of analytical lining design methods, including duct airflow effects, an experimental program was conducted. A flow-duct test facility was developed to simulate turbofan engine bypass duct geometry and noise environment in the laboratory. The facility was used to study the effects of various parameters of sound-absorbent wall liners. The liners consisted basically of a honeycomb sandwich and a porous face sheet.

In this report, a description is given of the flow-duct test facility and the data reduction techniques, along with a listing of the reduced test results.

Analyses of the test data showed that the significant design parameters are the face sheet impedance, treatment length, treatment depth, honeycomb cell dimensions, duct size, number of walls lined, number of layers in the linings, air velocity, and direction of flow with reference to sound propagation. The influence of these parameters is discussed. For simple single-layer linings, a design technology has been developed by means of empirical equations. Experimental results show that this technology is valid for duct sizes (or lining separations) from 4 to 12 in., lining depths of 0.25 to 1 in., and duct airflow Mach numbers from -0.4 to +0.4.

It is concluded that the flow-duct facility is a useful tool for investigating the basic properties of acoustically lined ducts.

INTRODUCTION

Since the advent of jet-powered aircraft, there has been a requirement for devices and techniques to reduce the noise generated by jet engines. With the introduction of turbofan engines, noise generated by the fan has become more prominent to people at or near the airports than jet exhaust noise, especially during the approach and landing phase.

The most desirable way to reduce engine noise would be to eliminate noise generation by suitable engine design. The current state of the art, however, will not provide levels low enough to satisfy expected requirements; thus, it is necessary to attenuate the noise that is generated.

An experimental research program was initiated at The Boeing Company to develop an acoustic duct lining technology to attenuate fan noise that is propagated along the fan exhaust ducts or out of the engine inlet. This program was sponsored by and in support of a NASA Langley contract (NAS 1-7129, ref. 1) to The Boeing Company for the study and development of turbofan nacelle modifications to minimize fan noise on 707-type airplanes.

The aim of the experimental program was to develop an acoustic lining technology by investigating the effects of various acoustic and geometric parameters on the attenuation characteristics of lined ducts. These parameters were evaluated in a simulated engine environment in a flow-duct facility in the frequency range between 800 and 10 000 Hz. The bulk of the work was conducted in the Boeing Seattle flow-duct facility, a brief description of which is given in this report. Since the Seattle flow duct was only capable of simulating the fan exhaust duct environment (airflow and noise propagating in the same direction), a limited number of inlet tests were conducted in the Boeing Wichita flow-duct facility, which was capable of simulating engine inlet conditions where the noise propagates in a direction opposite to the airflow. Since the Wichita flow duct was similar in principle to the Seattle facility, a separate description will not be given.

Although the program was initially oriented toward low bypass ratio turbofans, such as the JT3D engine used to power the 707 airplane, the technology developed in this report is quite general and can be applied to other engines and engine noise problems (e.g., turbo-machinery noise).

The type of acoustic liner developed and tested in this program had to be rugged enough to withstand the environment and the operational requirements of an aircraft engine. The liners consisted basically of a honeycomb sandwich with a porous face sheet. The acoustic properties of the lined ducts were evaluated for a range of grazing airflow velocities up to  $M = 0.4$ .

The analysis of the test data and an interpretation of the results is given in this report. A compilation of all the reduced test data from both test facilities is presented in the appendix.

## SYMBOLS

$A_N$	attenuation, decibels
$A^*$	normalized attenuation
$c$	speed of sound, centimeters/second or feet/second

d	lining depth, inches
f	frequency, hertz
$f_{bc}$	band center frequency, hertz
$f_n$	center frequency of band number n, hertz
$f_o$	frequency at which $X_s = R_s$ , hertz
$f_p$	frequency of peak attenuation, hertz
$*f_p$	frequency of peak attenuation at $M = 0.28$ , hertz
h	lining separation, inches
j	imaginary operator, $\sqrt{-1}$
ℓ	cell length, inches
L	lining length, inches
M	Mach number
p	rms acoustic pressure, dynes/square centimeter
R	flow resistance, rayls (cgs)
$R_s$	resistive component of acoustic impedance, rayls (cgs)
rayl (cgs)	unit of acoustic resistance, dyne-seconds/cubic centimeter
$R_E$	effective flow resistance at velocity u, rayls (cgs)
$R_N$	nominal flow resistance at velocity $u = 25$ cm/sec, rayls (cgs)
u	rms particle velocity, centimeters/second
$u_s$	velocity through a porous media, centimeters/second
$X_s$	reactive component of acoustic impedance, rayls (cgs)
$Z_s$	specific acoustic impedance, rayls (cgs)
$\nu$	constant
$\tau$	constant

$\mu$ bar      microbar

$\rho$             density of air, grams/cubic centimeter or pounds/cubic foot

## DESCRIPTION OF THE FLOW-DUCT FACILITY

The flow-duct facility was developed for evaluating the acoustic characteristics of lined ducts. Test provisions included a variable, high-velocity airflow through the duct test section, with airflow and noise propagating in the same direction, to simulate the fan exhaust ducts of a turbofan engine. Aerodynamic instrumentation was added to provide a capability of measuring pressure profiles and pressure distributions in the test section.

A schematic diagram of the facility is shown in figure 1. A reverberant chamber provided a diffuse acoustic source for the test duct and also acted as a plenum chamber to ensure uniform airflow into the duct test section. Figure 2 shows the plenum chamber in more detail. The volume of the plenum chamber was approximately 45 cu ft. The large diffuser in the air supply line reduced the entry air velocity into the plenum chamber and, hence, improved the flow duct aerodynamic inlet conditions. The bellmouth at the duct inlet ensured minimum aerodynamic distortion and, thus, minimized the generation of aerodynamic noise in the test section.

Three noise sources were available in the plenum chamber:

(1) Aerodynamic noise radiated from the air supply line.

(2) A jet noise source to augment the above source. Details of the multinozzle jet-noise generator are shown in figure 3.

(3) An air-driven siren generating discrete tones over the frequency range from 2000 to 8000 Hz with a fundamental peak amplitude of 150 dB measured in the plenum chamber with a 1/10-octave-bandwidth filter.

The test duct was connected to a calibrated semireverberant chamber in which the total acoustic power transmitted through the duct was measured. An interior view of the chamber is shown in figure 4. The volume of the semireverberant chamber was approximately 1750 cu ft. The chamber was vented by an acoustically lined duct at one end.

Three sizes of test sections, measuring 6 by 10 in., 4 by 10 in., and 6 by 7 in., were used in the test program. The walls were adjustable to maintain constant test section dimensions for various thicknesses of lining treatments. The acoustic panel test specimen linear lengths could be varied from 0 to 44 in., which was the full length on one test section. Longer ducts could be tested by bolting two or more test sections together. An S-bend duct 24 in. long with a 6-in. offset, figure 5, was also used. Lining test specimens could be mounted on any one or all of the four walls in the test section.

## Instrumentation

Acoustic instrumentation.—The flow-duct facility was equipped with the following range of acoustic instrumentation:

- (1) A Photocon microphone inside the plenum chamber to monitor the sound input conditions.
- (2) A Bruel and Kjaer condenser microphone, with a windshield, attached to a rotating boom in the semireverberant receiving chamber, figure 4, to measure the sound power radiated from the duct.
- (3) For some tests, Photocon microphones, flush mounted in the surface of the lining materials, measured local pressure fluctuations.

The acoustic signals were filtered by a General Radio Co. wave analyzer, and the frequency spectra were automatically plotted on a graphic level recorder.

Aerodynamic instrumentation.—A schematic diagram of the aerodynamic instrumentation of the flow-duct facility is shown in figure 6. Two remotely controlled traversing rakes were used to obtain velocity profile data at the inlet and exit of the test section, as shown in figure 7.

## Performance of the Flow-Duct Facility

Signal-to-noise ratio.—The background noise level or noise floor in the test facility was a limit to the maximum power insertion loss (i.e., noise reduction due to acoustic treatment) that could be measured. The noise floor was attributed mainly to the noise radiated into the test area from control valves, pipe bends, etc., in the compressed air supply system. Based on various measurements in the test area, it was estimated that the noise floor inside the semireverberant chamber was approximately 40 dB below the unlined duct (baseline) spectrum.

Input sound pressure levels.—The maximum input broadband sound pressure levels that could be generated in the plenum and the reverberant chambers are shown in figure 8 at an airflow Mach number of 0.19. The sound pressure levels inside the duct were about 3 dB below those of the plenum chamber. The reverberant chamber spectrum was recorded with a hard-wall test section. Discrete frequency tones could be superimposed on the broadband spectrum by including the siren in the system. The siren was capable of generating peak SPLs of 150 dB in the plenum chamber in the frequency range of 2000 to 8000 Hz.

Flow-velocity profiles.—Typical flow-velocity profiles that have been recorded during normal acoustic tests are shown in figures 9 and 10 for two duct sizes. A number of special tests were conducted where a highly distorted velocity profile was required to investigate the refractive effects of flow velocity on sound absorption in lined ducts. The velocity profiles were distorted by means of a ramp restricting the inlet flow ahead of the test section. A schematic of the ramp and the resultant velocity profiles are shown in figure 11.

## DESCRIPTION OF PROGRAM PROCEDURE

### Test Procedure

The purpose of the flow-duct tests was to measure the amount of power insertion loss (or attenuation) achieved with various configurations of sound-absorbing materials on the test section walls. A series of reference or baseline tests was conducted over a range of airflow Mach numbers with an unlined, smooth, metal-wall duct test section. Subsequently, corresponding airflow Mach number cases were repeated with acoustic linings in the duct working section. Most commonly, the tests were conducted using only the maximum broadband noise input, i.e., a combination of airflow noise and jet noise. In special cases, the siren signal was added to the broadband noise to give spectra with "spikes" (discrete tones) resembling those found in full-scale turbofan engine spectra. Acoustic measurements consisted of recordings of sound pressure level spectra taken in the plenum chamber and the semireverberant chamber. In some special cases, additional spectra were recorded from flush-mounted microphones in the lining surface.

The 1/10-octave-bandwidth spectra were registered by a graphic level recorder for each of the microphones in the plenum and reverberant chambers. The input noise levels in the plenum chamber were found to be steady and repeatable for each airflow condition and were only recorded to monitor the quality of the tests. The reverberant chamber noise spectra were used in the data analysis.

### Data Reduction

It was established that, because of the diffuse sound-field characteristics of the reverberant chamber, the recording microphones measured an average sound pressure level spectrum. Hence, by subtracting the noise levels of an acoustically lined duct from those of an unlined duct, as measured in the reverberant chamber, the insertion loss, or attenuation due to the lining, in decibels, was obtained. As an example, a composite strip chart of corresponding graphic level recorder traces is shown in figure 12. The power insertion loss spectra were subsequently analyzed for parametric variations.

### Description of Duct Linings

A review of various lining concepts has been made in reference 2. For this investigation, a broadband resistive-resonator concept was selected as the basic model from which to develop duct linings because it provides substantial attenuation over a wide frequency range and was judged the most suitable concept for use in an engine environment.

The acoustic attenuation provided by a duct lined with the resistive-resonator type of liner is the result of conversion of acoustical energy into heat due to both viscous friction within the face sheet and the orifice expansion losses on either side of the face sheet. The frequency of peak attenuation is mainly a function of lining depth and duct size. For duct sizes and frequencies of interest for current turbofan engines, the required lining depth of



bulk absorbers would tend to make linings too heavy. The effective depth of the lining, however, can be increased economically by including an airspace behind it. To prevent longitudinal wave motion in the airspace behind the lining and thus lose efficiency, it was necessary to insert rigid, airtight, transverse partitions perpendicular to the duct wall.

The resistive-resonator linings tested in this program consisted of a thin layer of porous material with a honeycomb backing that provided the resonant property of the lining (fig. 13). The components of the linings were usually bonded together, although, in some cases, welded construction was used. The test panels were single layer or multilayer with either vertical or oblique cellular honeycomb spacers. Some curved panels were also tested to investigate line-of-sight absorption effects.

A range of metallic and nonmetallic lining and core materials was evaluated in this program. The most commonly tested porous materials were:

- (1) Polyimide-resin-impregnated glass fabric (developed by Boeing)
- (2) Felted metallic fiber
- (3) Woven metallic fiber

Since polyimide/fiberglass was the most readily available material, it was used for testing parameters independent of its material properties. The acoustic layer consisted of a number of laminates bonded together with different orientations of the weave to produce the required impedance properties. A cutaway of a polyimide panel is shown in figure 14. Full details are given in reference 1.

The most commonly used honeycomb core material was a paper impregnated with phenolic resin, with a hexagonal-shape core, and in a variety of cell sizes.

## FLOW-DUCT TEST RESULTS

### Assumptions in Data Analysis

Power insertion loss.—The power insertion loss of the acoustically lined ducts was measured in a calibrated semireverberant chamber. Since the sound power level in a reverberant chamber is equal to the product of the average sound pressure level and a constant (calibration characteristic of the chamber), the difference between two sound power spectra is equal to the difference between the corresponding sound pressure spectra. Hence, in the following discussions, the term “attenuation of SPL” is used instead of power insertion loss.

One wall lined versus two walls lined.—In the analysis of lining separation effects for opposite duct walls lined, the concept of image sources was used. This infers that results from tests with one wall lined in a 6-in. duct are equivalent to two opposite walls lined in a 12-in. duct.

Temperature and pressure.—The experiments were conducted at approximately ambient, sea level temperature and pressure conditions. Hence, the results of the following analysis are true only for these same conditions. Large changes in temperature and pressure, however, can be accommodated by appropriate corrections of  $\rho$  and  $c$  in the duct airflow Mach number and in the reactive and resistive impedance values for the lining.

Turbulence effects.—Airflow turbulence in the test section was low because of the care taken with the aerodynamic design of the bellmouth inlet into the test section. The vertical and horizontal velocity profiles in the test section were found to be uniform with a normal boundary layer growth along the test section walls, this produced a downstream boundary layer thickness of approximately 0.5 in. in the 6-in. duct. Turbulence and boundary layer effects on the acoustic attenuation in ducts were not studied separately.

Attenuation of broadband versus discrete-frequency noise.—The noise generated by the fan and compressor of a jet engine contains both broadband and discrete-frequency characteristics. Early tests in the flow duct were conducted to determine whether linings responded differently to the two types of noise. It was concluded that duct linings absorbed equal amounts of acoustic energy per bandwidth whether its content was broadband or discrete. Subsequently, to simplify the test procedure, the flow-duct tests were conducted using only broadband noise inputs.

### Qualitative Discussion of Test Results

The basic parametric studies of the acoustic behavior of lined ducts and duct linings were conducted using single-layer, constant-depth liners. After the fundamental trends had been established and understood, further tests were conducted to investigate more complex liner concepts and geometries. The acoustic behavior of a lined duct system is characterized by the attenuation frequency spectrum. The effect of varying duct/liner parameters (identified in fig. 15) on the peak attenuation frequency and the attenuation levels will be discussed separately.

Tuned frequency of ducts with single-layer linings.—The influence of various parameters on the peak attenuation frequency of lined ducts was investigated by isolating the effects, i.e., varying one parameter at a time. Unless otherwise stated, the following test results were taken at an airflow Mach number of 0.28, which closely approximates the average Mach number in the fan duct of the JT3D turbofan engine at approach power settings.

Lining cavity depth  $d$ : A strong influence on the peak attenuation frequency is shown in figure 16. For a typical duct size of 6 in., the tuned frequency varies inversely as the cavity depth. The rate of change becomes substantially nonlinear for cavities less than 0.5-in. deep.

Duct size  $h$ : The lining separation is the next strongest parameter affecting the peak attenuation frequency. Figure 17 shows that the tuned frequency varies inversely with the distance between linings.

Cavity cell length (in the direction of duct airflow): Cell length has very little effect on the peak frequency over the limited range of cell lengths tested, as shown in figure 18. Some recent tests of long and narrow cells, however, indicated a significant increase in the tuned frequency.

Duct airflow Mach number  $M$ : Mach number, as well as airflow direction with respect to noise propagation, will influence peak attenuation, as shown in figure 19. An approximately linear relationship is apparent between the inlet and exhaust modes of airflow, with the peak frequency increasing in the positive direction of airflow Mach number. The band-spread in the test data shown for the various linings tested is attributed partly to data scatter and partly to changes in the reactive impedance for the various polyimide layups.

Reactive impedance: The impedance of lining surface laminates is related to the tuned frequency of a given duct and lining configuration. Results from identical tests of linings with different reactive impedances disclosed a shift in peak frequency, as shown in figure 20. Metallic linings, which have a low reactive impedance (fig. 21), exhibit attenuation peaks at a higher frequency than nonmetallic linings of high reactive impedance. Theoretical analyses indicate that a decrease in peak frequency is to be expected with increasing lining reactance, as shown in figure 22. Order-of-magnitude variations for lining design purposes will be discussed later.

Attenuation in ducts with single-layer linings.—The attenuation of noise in lined ducts depends on a number of parameters, the most important of which are: length of treatment, duct size, lining cavity depth, cavity cell size, and resistive and reactive impedances. The parametric results discussed below were conducted with a fixed cross-sectional geometry and, unless otherwise stated, at a duct airflow Mach number of 0.28.

A typical family of attenuation spectra for varying lining lengths tested in the flow duct is shown in figure 23. The simplest way to examine attenuation is to study the narrow-band peak values, but, for turbofan applications, broader bandwidth coverage is usually required. Hence, in the following discussion, the attenuation effects were examined both for the narrowband peak and one-octave bandwidth aspects. Care had to be exercised in the analysis of peak data because, with long lining lengths in small ducts, the peak values were often obscured by noise floor limitations. In this study, the octave-bandwidth attenuation is defined as the maximum height of a rectangle one octave wide that fitted within the attenuation curve, as shown in figure 23. This meant that only the minimum value of attenuation over the bandwidth was the index of lining performance.

Lining length  $L$ : For a given duct cross-sectional area, lining length is the single most important attenuation parameter. Two rates of change of attenuation with lining length are observed in figure 24. It is postulated that this is due to the fact that, out of the randomly oriented sound waves entering the duct, the more oblique waves are absorbed rapidly in the initial lining length leaving the grazing, or close to plane, waves to propagate. The plane waves are more difficult to attenuate, so the phenomena shows up as a reduced slope in figure 24. Analytically, Mangiarotty (ref. 2) also has shown that higher order modes generated in the duct are attenuated at a faster rate than the lower order modes.

Propagating acoustic modes: In any given duct system, propagating modes will affect the initial rate of attenuation, as discussed above. In this test program, a random distribution of acoustic energy in the various modes was assumed. Because of the lack of a simple technique for measuring the modal energy distribution at the duct entrance, no attempt was made to verify this assumption. It is conceivable that, in other installations, a different modal distribution would exist from that in this particular facility. Hence, some variations in the absolute attenuation levels can be expected between various test facilities and/or engine installations for the same lining configuration.

Duct size  $h$ : The lining separation is also a very strong parameter affecting attenuation levels for a given lining length. It was found that attenuation varied inversely with duct size, as shown in figure 25. In other words, to increase the rate of sound absorption per unit length of lining, the distance between linings on opposite walls has to be reduced. In figure 25, it is estimated that the facility noise floor is responsible for suppressing the peak attenuation levels for the small ducts. The one-octave-bandwidth data, however, are unaffected by the noise floor.

Lining cavity depth  $d$ : Depth appears to have a smaller effect on attenuation levels, as shown in figure 26. There was a strong indication that, for lining cavity depths below 0.25 in., the attenuation fell off rapidly, but this may have been due to manufacturing difficulties in maintaining tolerances for very thin cavities. For that reason, care should be taken in working with very thin liner sandwiches.

Cell length (in the direction of duct airflow): For a given cavity depth, cell length influences the attenuation, as shown in figure 27. An optimum cavity length is indicated. The range of cell sizes tested was representative of those expected to be used in lining design applications. Some recent tests with liners with long channel-type core construction substantiated the trend of rapid falloff in attenuation for long cells.

Duct airflow Mach number  $M$ : Effects for both inlet and exhaust modes of operation are shown in figure 28. It can be seen that, for a given lining length, the broadband attenuation stays fairly constant in the exhaust mode. It probably falls off as the exhaust Mach number increases beyond 0.4. In the inlet mode, however, the broadband attenuation increases with Mach number and probably approaches an infinite value as an aerodynamic choke is established in the inlet duct. The peak attenuation curve appears to be more sensitive to Mach number effects in the exhaust mode than in the inlet mode. On the other hand, it was never established beyond doubt that the peak data at high inlet Mach numbers may not have been affected by signal-to-noise ratio problems.

Resistive impedance: Flow resistance  $R$ , which approximates resistive impedance, is another important parameter influencing the attenuation. Up to this point in the discussion, the nominal flow resistance was assumed to be at or near its optimum value. However, varying the flow resistance for the liner with all other parameters kept constant will affect the attenuation, as shown in figure 29 for various bandwidths. The sensitivity to flow resistance decreases as the attenuation bandwidth is increased. There also appears to be a shift in the optimum value of the flow resistance with increasing attenuation bandwidth.

Reactive impedance: Reactance is a parameter that affects attenuation indirectly through its influence on the tuned frequency. As shown earlier in figure 20, low-reactance linings peaked at a higher frequency than high-reactance linings. To have both types of lining perform the same job or have identical performance, one of them has to be “retuned” by either changing its cavity depth or the lining separation. In the process of retuning either of the liner concepts, the attenuation level is going to change up or down depending on the circumstances.

Flow resistance optimization.—The resistive impedance has a greater influence on lining attenuation than the reactive component. Since the steady flow resistance is a good approximation of the resistive impedance and is easy to measure, it was used extensively in preliminary duct lining design (ref. 2). The rates of change of flow resistance with particle velocity for representative types of materials are shown in figure 30 where the mean flow duct environment levels were calculated using the following relationship:

$$\bar{u} = \left( \sum_{n=1}^N \left| \frac{p(f_n)}{R(f_n) + jX(f_n)} \right|^2 \right)^{1/2} \quad (1)$$

where:

- $\bar{u}$  = rms particle velocity in the lining material
- $p$  = rms sound pressure at lining surface
- $R$  = resistive impedance
- $X$  = reactive impedance
- $f_n$  = center frequency of band number  $n$
- $N$  = total number of bands

The sound pressure levels at the lining surface were measured with a flush-mounted wall microphone. A relatively flat flow resistance characteristic (e.g., metallic linings) is a desirable feature, but, for a single design point, it is not essential if the acoustic environment is known. For example, figure 30 shows that, for the mean flow duct environment levels at a Mach number of 0.37, the 8-nominal-rayl nonmetallic lining has the same effective flow resistance as the 21-nominal-rayl metallic lining.

In the foregoing discussion it was shown how attenuation varied mainly with duct size, lining cavity depth, flow resistance, and Mach number. These effects are presented in terms of flow resistance in figures 31 through 38. From the curves of figures 31 through 38, the variation of the optimum effective flow resistance has been extracted in figures 39 through 41. Decreasing duct size or attenuation bandwidth requires decreased values of optimum effective flow resistance, whereas increasing values of Mach number and lining depth go with decreasing optimum effective flow resistance. Reactive impedance did not appear to influence the optimum effective flow resistance, as verified by the examples in figure 42.

It has been assumed that the flow resistance of porous linings is determined by the local pressure fluctuations at their surface, which were generated by acoustic or aerodynamic phenomena or a combination of both. Since the test input noise levels in the flow-duct system remained fairly constant with the Mach number, the measured changes in attenuation were attributed to the variation of the effective flow resistance with flow

velocity during the experiment. It was found, for example, that linings that were below optimum flow resistance improved their attenuation with increasing flow velocity. Although this was generally true, exceptions to this observation were found for thin linings (0.25 in. or less), as shown in figure 43. The reasons for this latter behavior are not clearly understood at this time. They may be due to the previously discussed problem of maintaining reasonable fabrication tolerances with thin linings. In the meantime, however, caution should be exercised to make certain that the effective flow resistance is not below the design optimum.

### Empirical Prediction Method for the Acoustic Performance of Single-Layer Linings

There exist basic acoustic theories describing the sound transmission through ducts with absorbent walls (ref. 3). These theories do not take into account cases of duct systems with airflow. The solution of the duct attenuation problem usually requires sophisticated computer programs. Hence, it was decided to attempt to produce a simplified attenuation prediction method for quick-look analysis based on the extensive test data obtained in this flow-duct test series. To keep the equations as simple as possible, it was decided to perform the analysis in the dimensional form and also to limit the range of validity of the various test parameters to that used in the test series (duct sizes from 4 to 12 in. high; lining cavity depths from 0.25 to 1 in.; and airflow Mach numbers from -0.4 to +0.4). The numerical range of the parameters is typical of that encountered with the low bypass ratio JT3D size of turbofan engines. The basic derivation of the empirical equations was done for an exhaust mode Mach number of 0.28, which closely approximates the design Mach number for the exhaust ducts of the JT3D engine. The obvious choice of  $M = 0$  could not be used since the Seattle flow-duct facility could only operate with airflow.

Prediction of tuned frequency.—To start the analysis, the data points representing the effects of lining cavity depth and duct size were combined in figure 44. Parabolic curves were drawn through the data points as shown. They can be represented by the equation

$$f_p^* = K(h - h_{\min})^2 + f_{p\min} \quad (2)$$

where:

$K$  = a constant

Subscript min = minimum value on parabolic curve

$f_p = f_p^*$  at  $M = 0.28$

The minimum value  $h$  varies linearly with lining depth  $d$  as

$$h_{\min} = -5.3d + 19.3 \quad (3)$$

From the data in figure 43, the minimum value of  $f_p$  varies parabolically with lining depth as

$$f_{p\min} = 1530(d - 1.2)^2 + 1200 \quad (4)$$

Finally, a linear variation of  $f_p$  with Mach number is introduced as

$$f_p = 800M + (f_p \text{ at } M = 0) \quad (5)$$

Therefore,

$$f_p = f_p^* + 800(M - 0.28) \quad (6)$$

Substituting equations (2), (3), and (4) into (6) and evaluating K from the experimental results (i.e.,  $K = 4.86$ ), the final expression obtained for the peak attenuation frequency is

$$f_p = [4.86(h + 5.3d - 19.3)^2 + 1530(d - 1.2)^2 + 800M + 980] \text{ Hz} \quad (7)$$

for  $0.25 \text{ in.} \leq d \leq 1.0 \text{ in.}$ ,  $4 \text{ in.} \leq h \leq 12 \text{ in.}$ , and  $-0.4 \leq M \leq +0.4$ .

Because of the quadratic nature of equation (7), when solving for either h or d, care must be taken in choosing the answer that fits the valid range for h or d indicated above.

In the practical application of duct linings to fan noise reduction, broadband absorption is usually required to cover the unsteady characteristics of the fan noise as well as the deliberate variation of engine rpm during the landing approach operation. The bandwidth center frequency ( $f_{bc}$ ) was found to vary as shown in figure 45. This relationship should be used to modify equation (7) for predicting tuned frequency for bandwidths other than peak.

Although equation (7) was derived for nonmetallic linings of high reactive impedance, it is also applicable to metallic linings, provided a correction accounting for the change of reactance is made. Some information on the effect of reactive impedance was obtained by a careful comparison of experimentally measured and theoretically predicted attenuation spectra at low Mach numbers. The analysis showed that the peak frequency for low-reactance linings was increased by the amounts shown in figure 46. The results for linings 0.5 to 1.0 in. deep collapsed on a single curve and correlated well with experiment. The deviations observed for the 0.25-in.-deep linings are not understood, requiring further work with thin linings to clarify the reactance effects. It is therefore suggested that, at present, the lower curve of figure 46 be used to express the frequency change of low-reactance linings for all depths from 0.25 to 1.0 in.

Prediction of attenuation.—To avoid the problem that some of the peak attenuation levels for tests of long-lining configurations may have been obscured by the facility noise floor, the basic derivation is carried out for an attenuation bandwidth of one octave. Additional curves will be provided at the end of the analysis to modify the basic equation to apply to other bandwidths as well as other effects, such as airflow velocity and direction. It has also been assumed that lining width does not influence attenuation in rectangular ducts, provided the width is at least twice the duct height, because, under those conditions, infinite-width liners are approximated.

A composite summary plot of attenuation varying with lining length and duct size is shown in figure 47. For lining lengths greater than 10 in., a linear variation of attenuation is observed. The lines corresponding to the different duct sizes converge to the 4.5-dB point on the ordinate. Hence, they can be represented by

$$A_N = \frac{dA_N}{dL}L + 4.5 \text{ dB} \quad (8)$$

where  $dA_N/dL$  varies with duct size  $h$ , as shown in figure 48. The curve drawn through the data points is of the form

$$\frac{dA_N}{dL} = \nu 10^{\tau h} \quad (9)$$

The two constants,  $\nu$  and  $\tau$ , are evaluated as  $\nu = 1.26$  and  $\tau = -0.09$ . Hence,

$$\frac{dA_N}{dL} = 1.26(10^{-0.09h}) \quad (10)$$

By substituting equation (10) into equation (8),

$$A_N = 1.26(10^{-0.09h})L + 4.5 \text{ dB} \quad (11)$$

for  $L \geq 10$  in.

Variation in attenuation with lining depth was adjusted by means of the normalized curve of experimentally measured data shown in figure 49, where

$$A^* = \frac{\text{attenuation for depth } d}{\text{attenuation for } d = 0.5 \text{ in.}}$$

In an earlier analysis of these data (ref. 4), it was assumed that a 30-rayl nominal flow resistance closely approximated the optimum flow resistance for all lining depths in a 6-in. duct. Reanalysis of the flow resistance effects in the previous section, figures 31 to 38, clearly shows that optimum flow resistance and, hence, attenuation varies significantly with lining depth in a given duct, especially for narrow bandwidths. Therefore, figure 20 and equation (11) of reference 4 are revised by the new curve given in figure 49 of this report, which reflects the above change.

The curve in figure 49 can be represented by the following parabolic function:

$$A^* = \{0.1(d - 0.1)\}^{1/2} + 0.8 \quad (12)$$

for  $0.25 \text{ in.} \leq d \leq 1.0 \text{ in.}$

Multiplying equation (11) by equation (12), the attenuation over one octave bandwidth is

$$A_N = \left[ 1.26(10^{-0.09h})L + 4.5 \right] \left[ \{0.1(d - 0.1)\}^{1/2} + 0.8 \right] \text{ dB} \quad (13)$$

for  $L \geq 10$  in.,  $0.25 \leq d \leq 1$  in.,  $4 \leq h \leq 12$  in., and  $0 \leq M \leq +0.4$ .



To apply equation (13) to other attenuation bandwidths, as well as inlet and exhaust Mach numbers, the normalized attenuation curves in figures 50 and 51 should be used. The families of curves in the above two figures have been normalized with respect to equation (13).

### Miscellaneous Lining Design Concepts

In addition to the extensive test program with single-layer linings carried out to establish a basis for a simplified design technology, various other lining concepts were evaluated. A qualitative discussion of the results of these tests follows.

Double-layer linings.—The double-layer linings tested in this program consisted of two porous laminates separated by honeycomb core. It was expected that the double-layer linings would provide higher attenuation levels over broader bandwidths than were obtained from single-layer linings discussed in the previous section. Because the double-layer linings were heavier, more complex to manufacture, and early tests showed that the acoustic advantages were not as great as expected, the test program was less extensive than for single-layer linings. Most of the double-layer linings tested were of equal core spacing with the outer laminate having a smaller flow resistance than the inner one—typically 10 and 40 rayls (cgs), respectively. Double-layer lining results had a characteristic spectrum shape with two peaks, as shown in figure 52, where the first peak was greater than the second and was associated in frequency with the total lining depth. The second peak could not be identified in a simple way with any combination of the depth dimensions of the double-layer panel. The increased attenuation achieved with double-layer linings, as compared to single-layer linings of equal total depth, is shown in figure 53. A significant increase in attenuation occurred at higher frequencies. The increased attenuation was a strong function of lining depth, as shown in figure 53. The excess attenuation increased with both lining depth and attenuation bandwidth.

Slanted-core linings.—Tests with slanted honeycomb core linings were conducted to investigate if the peak frequency was controlled by the honeycomb cell height or by the lining depth measured normal to the panel surface. The results in figure 54 indicate that the peak frequency is determined by a factor in between the normal and slanted depths of the lining. A comparison of the slanted and equivalent upright core lining spectra in figure 54 indicates that the upright core linings have better attenuation characteristics. The direction of slant with respect to the noise propagation had no systematic influence on the attenuation, as shown in figure 55. Hence, it is concluded that there is no acoustic advantage in slanting the lining core.

Mixed-depth single-layer linings.—An effort was made to develop single-layer lining configurations with improved broader attenuation bandwidth coverage by testing single-layer linings with different depths on opposite walls. The results were compared with a standard configuration of equal lining depth in figure 56. It is evident that, for the same amount of lining material, the peak attenuation decreases rapidly as the difference between lining depths increases. For broadband attenuation 1.5 octaves wide or greater, a slight improvement in attenuation is observed. If the same linings of different depths are rearranged so that the duct contained two sections, end to end, of equal-depth linings facing each other, then considerably higher broadband attenuation is achieved, as shown in figure 57.

Acoustic splitters.—Ducts that are too large for efficient acoustic treatment per unit length can be subdivided into smaller channels by means of acoustically treated splitters. A number of tests were conducted to investigate optimum splitter configurations. A summary of the results, figure 58, shows that treated splitters with an impervious center layer (infinite flow resistance) are far superior to splitters that are porous right through. Hence, if splitters are designed with an impervious center layer from the start, then the ducts on either side of a splitter can be analyzed independently by the methods described earlier.

Multiwall treatments.—The attenuation of a fixed length of lined duct increases with the number of walls treated, as shown in figure 59. It is evident that lining a second and opposite wall of a duct produces a substantial increase in attenuation. Treating the additional shorter sides, which are farther apart, gives lesser increases in attenuation.

Curved ducts.—A number of tests were conducted with an S-bend duct section added to the basic flow duct to produce line-of-sight blockage for the acoustic waves. Although the results of these tests were inconclusive, Beranek (ref. 5) states that curved ducts change plane waves into higher modes thus increasing the attenuation, provided additional linings are installed downstream of the bend.

NASA material.—NASA Langley Research Center developed several acoustic test panels similar in construction to those manufactured and tested by The Boeing Company. The panels consisted of a porous laminate approximately 0.125-in. thick made from several layers of wire screen spot welded together and backed by a 0.5-in.-deep honeycomb core. These panels, which had a low flow resistance, were tested in the flow duct and found to behave in a similar manner to the 3-rayl polyimide panels, as shown in figure 60.

Effects of sound refraction in lined ducts.—Early full-scale engine tests with acoustically treated fan exhaust ducts indicated that the same lining placed on different walls of the exhaust duct produced different amounts of attenuation. Because of large velocity gradients measured in the fan ducts, refraction of sound was postulated as a mechanism causing the uneven rates of attenuation of the acoustic liners. This was verified by flow-duct tests where velocity profiles were distorted in order that sound waves entering the duct were refracted away from one wall and towards the other. The results are shown in figure 61 where it can be seen that the lining on the wall towards which the sound is being refracted is more effective than the lining for the reference case of uniform velocity profile or zero refraction.

#### Acoustically Lined Duct Fluctuating Wall Pressure Spectra

The rms pressure fluctuations at the surface of the sound-absorptive linings generates oscillating flow through the material. Flow resistance, being a function of the flow velocity through a material, is proportional to the pressure fluctuations at the duct wall. To calculate the effective flow resistance, duct wall pressure spectra were measured with microphones flush mounted in the walls at each end of the acoustic lining. The difference in sound pressure levels between the two ends of the lining, as shown typically in figure 62, were smaller than those measured in the downstream reverberant chamber. The downstream acoustic signal spectrum in figure 62 was derived by subtracting the measured attenuation from the

upstream spectrum at the duct wall. Based on this comparison, it is deduced that the downstream microphone in figure 62 measures a predominantly aerodynamic (boundary layer) pressure field. Therefore, in lining design, boundary layer pressure fluctuations may be of equal importance with the acoustic pressure field in determining the effective flow resistance of lining materials.

### Skin Friction Drag of Acoustic Linings

Acoustic linings that inherently have a certain amount of surface roughness may be installed in the walls of fan exhaust ducts and engine inlet ducts where they are exposed to airflow velocities up to Mach numbers of 0.6, for example. Under such conditions, skin friction drag over the acoustic material could account for measurable engine performance losses. Aerodynamic tests were made to compare the measured skin friction of various samples of acoustic lining materials with that of a smooth, flat plate. Both metallic and non-metallic lining materials were tested in the Boeing 14.4- by 18.0-in. model low-speed wind tunnel over a Reynolds number range of 1.0 to  $5.0 \times 10^6$  (ref. 6).

The test results showed:

(1) The relative increase in skin friction coefficient for both metallic and nonmetallic linings was 36% to 50% over that of a plexiglass plate in the range of Reynolds numbers investigated. This increase in skin friction coefficient was not affected by changes of flow resistance or porosity, nor by the honeycomb core cell size, slant, or depth.

(2) It was found that the local skin friction coefficient results did not correlate well with the measurements of the average skin friction coefficients. It is recommended, however, that the average skin friction coefficient of acoustic linings be increased 50% over that of a smooth, flat wall when estimating the internal losses in acoustically lined ducts.

### CONCLUDING REMARKS

(1) The Boeing flow-duct test facility, which was built and developed for this test program, was found to perform satisfactorily.

(2) The flow duct is a useful tool for investigating the basic properties of acoustically lined ducts.

(3) The resistive-resonator linings developed and tested in this program were judged to be suitable for potential applications in an engine environment for fan noise reduction.

(4) It was shown in this program that the significant parameters for designing acoustically lined ducts are the face sheet impedance, treatment length, treatment depth, honeycomb cell dimensions, duct size, number of duct walls treated, number of layers in the linings, and duct airflow velocity and direction with respect to sound propagation.

(5) For the simple case of single-layer linings, empirical equations have been derived from the test data to describe the acoustic performance of acoustically lined ducts over the limited range of lining separations from 4 to 12 in., lining depths of 0.25 to 1 in., and duct airflow Mach numbers from -0.4 to +0.4.

(6) Aerodynamic measurements of skin friction losses over acoustic liners indicate that the average skin friction coefficient of acoustic linings should be about 50% more than that of a smooth, flat wall when making estimates of internal losses in acoustically lined ducts.

(7) The effects of the modal distribution of acoustic energy on the attenuation of sound in a duct system were not studied in this program because of the lack of a suitable experimental technique. This subject, however, is important enough to warrant the effort to develop the methods required to provide a complete understanding of the physics of sound absorption in a lined duct.

The Boeing Company  
Commercial Airplane Group  
Seattle, Washington, March 1971

## REFERENCES

1. The Boeing Company: Study and Development of Turbofan Nacelle Modifications to Minimize Fan-Compressor Noise Radiation. NASA CR-1711 through 1717, 1971.
2. Mangiarotty, R. A.: Acoustic Linings Concepts and Materials for Engine Ducts. Paper S.2, 77th ASA Meeting, 8 April 1969. J. Acoust. Soc. Am., vol. 48, no. 3 (part 3), 1970.
3. Morse, Philip M.: Vibration and Sound. Second ed., McGraw-Hill Book Co., Inc., 1948, ch. VII.
4. Atvars, J; and Mangiarotty, R. A.: Parametric Studies of the Acoustic Behavior of Duct-Lining Materials. Paper S.4, 77th ASA Meeting, 8 April 1969. J. Acoust. Soc. Am., vol. 48, no. 3 (part 3), 1970.
5. Beranek, Leo L.: Noise Reduction. McGraw-Hill Book Co., Inc., 1960, ch. 17.4.
6. Unpublished Boeing Company data.

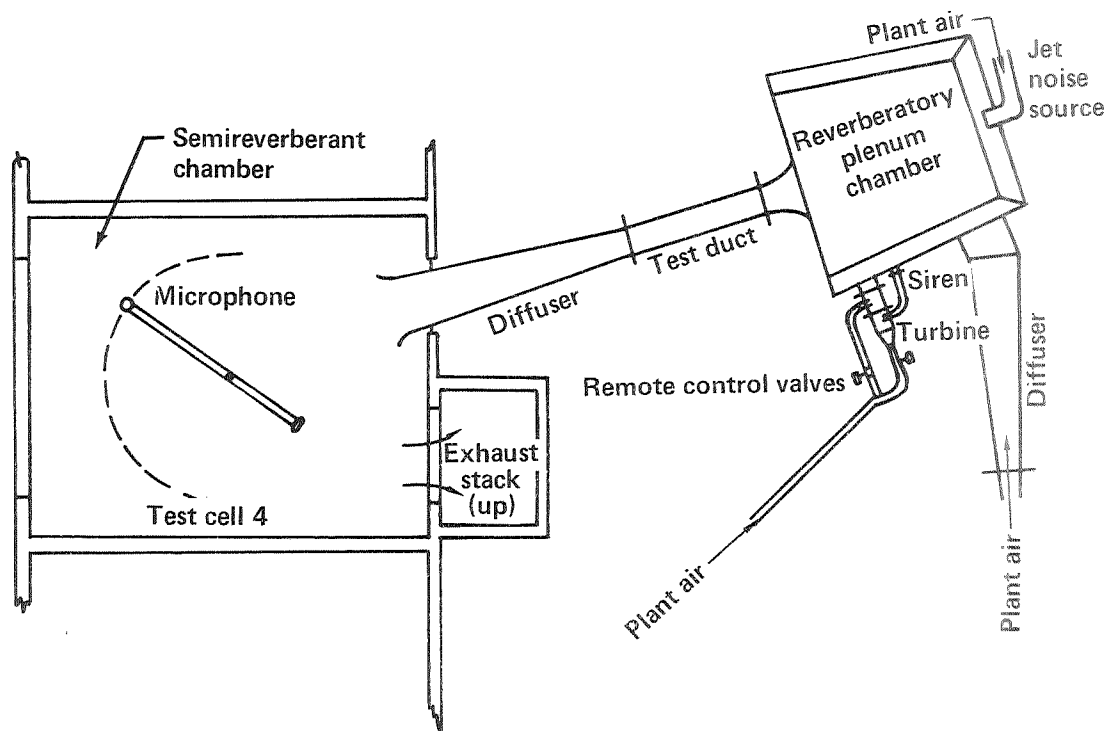
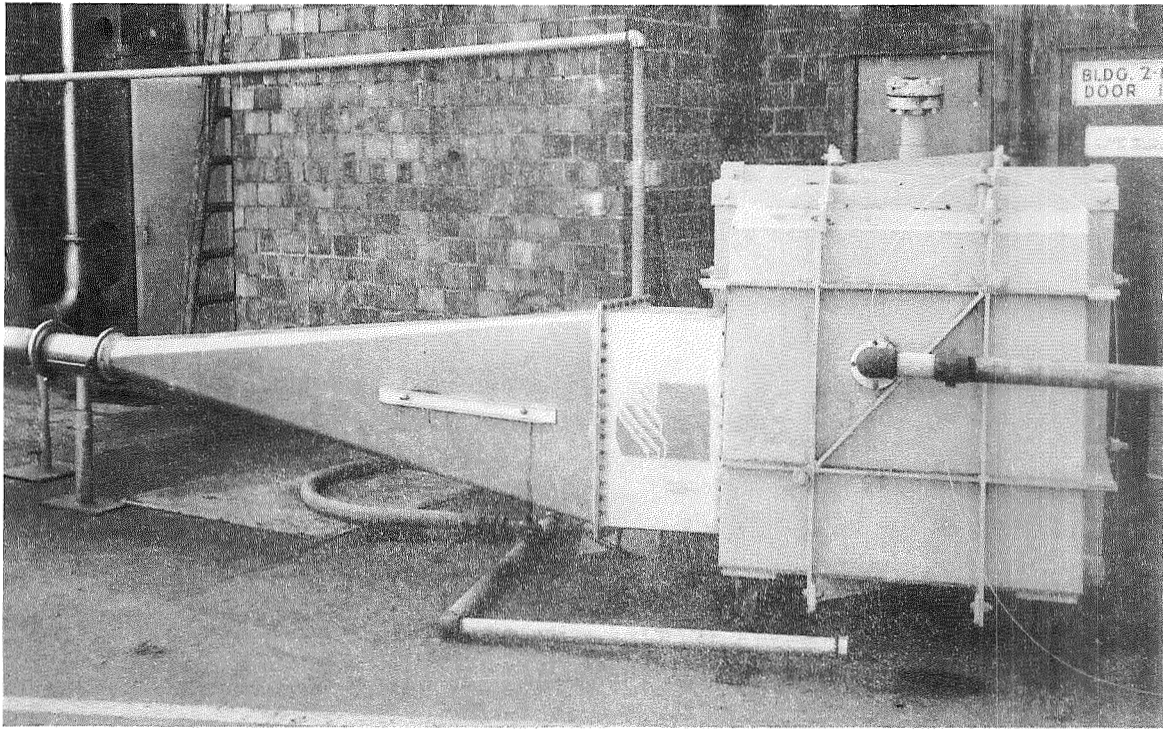
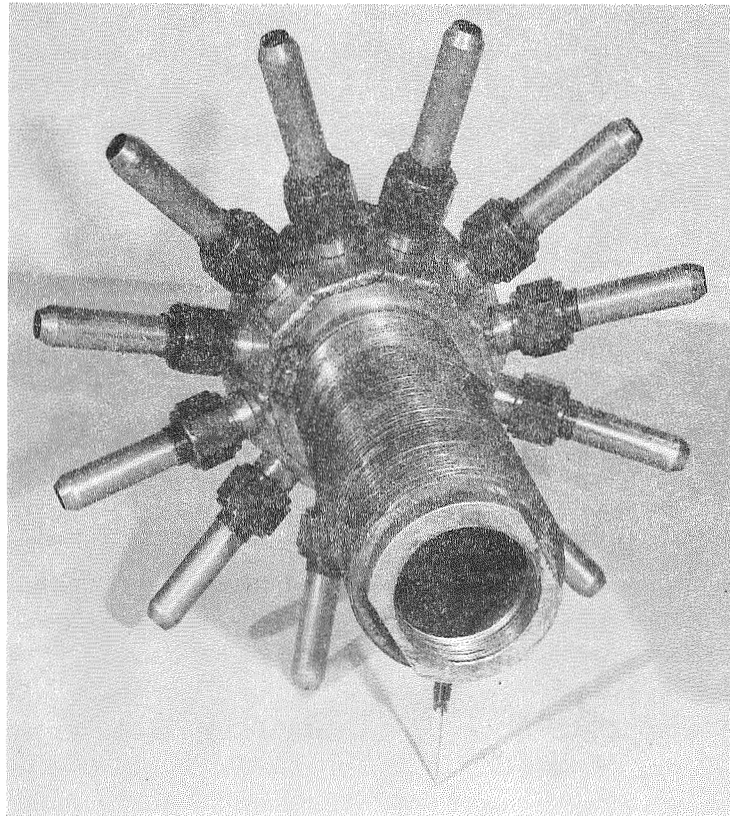


Figure 1.—Boeing Flow-Duct Facility

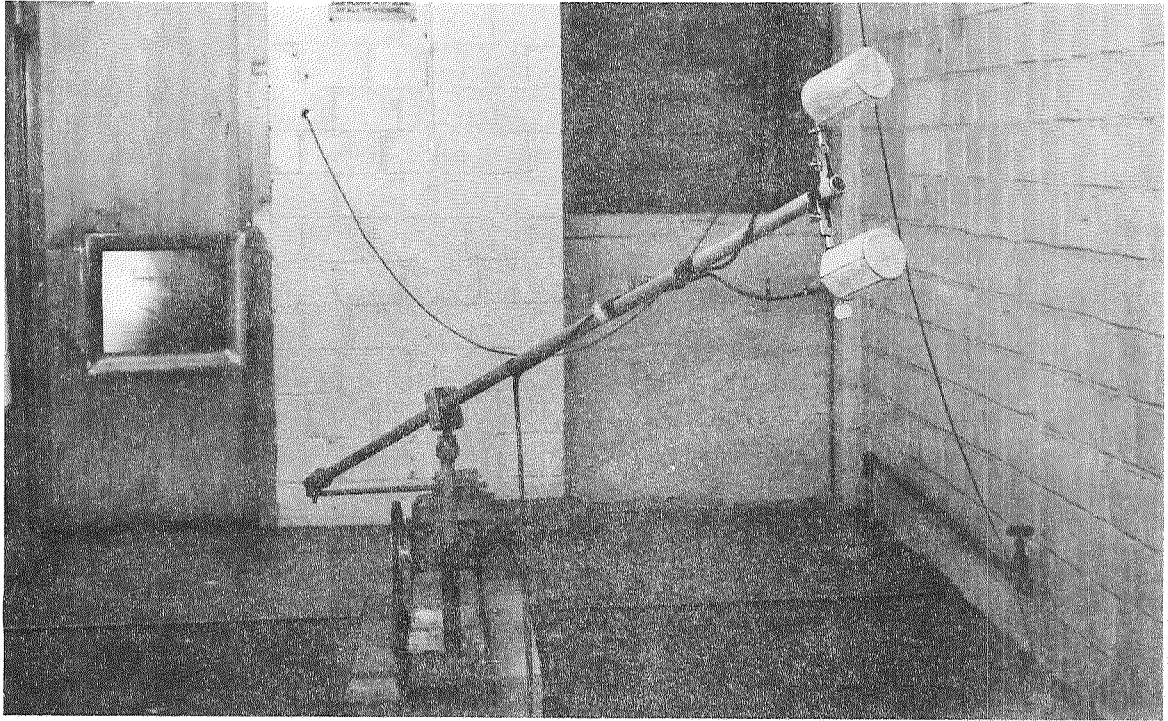


*Figure 2.—View of Plenum Chamber and Inlet Diffuser*

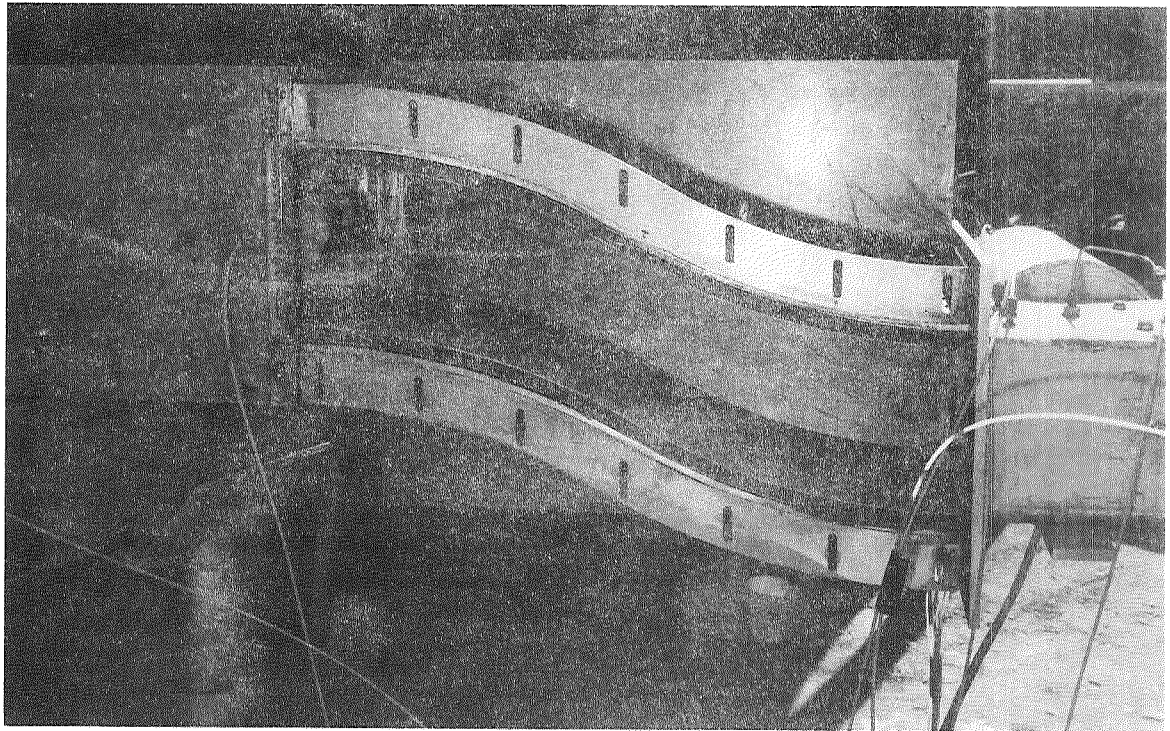


*Figure 3.—Multinozzle Jet Noise Source*





*Figure 4.—Semireverberant Chamber With Microphone Boom*



*Figure 5.—S-Bend Test Duct*



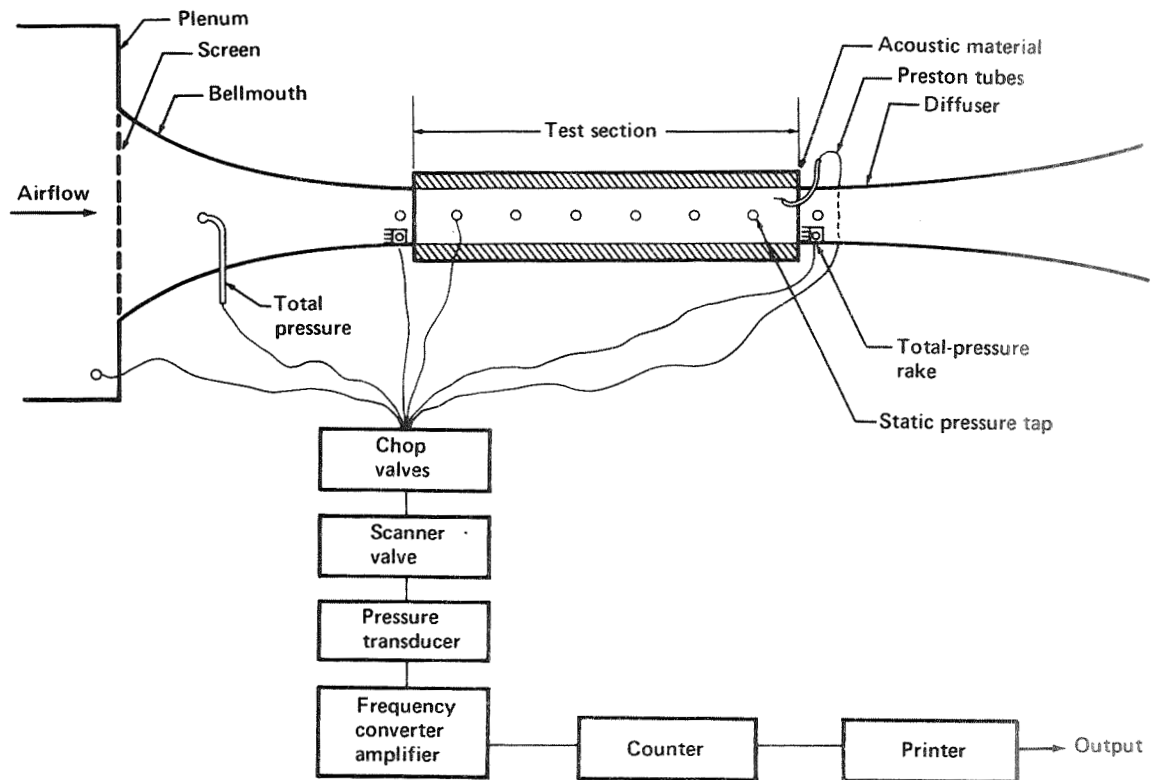


Figure 6.—Aerodynamic Instrumentation of Flow Duct

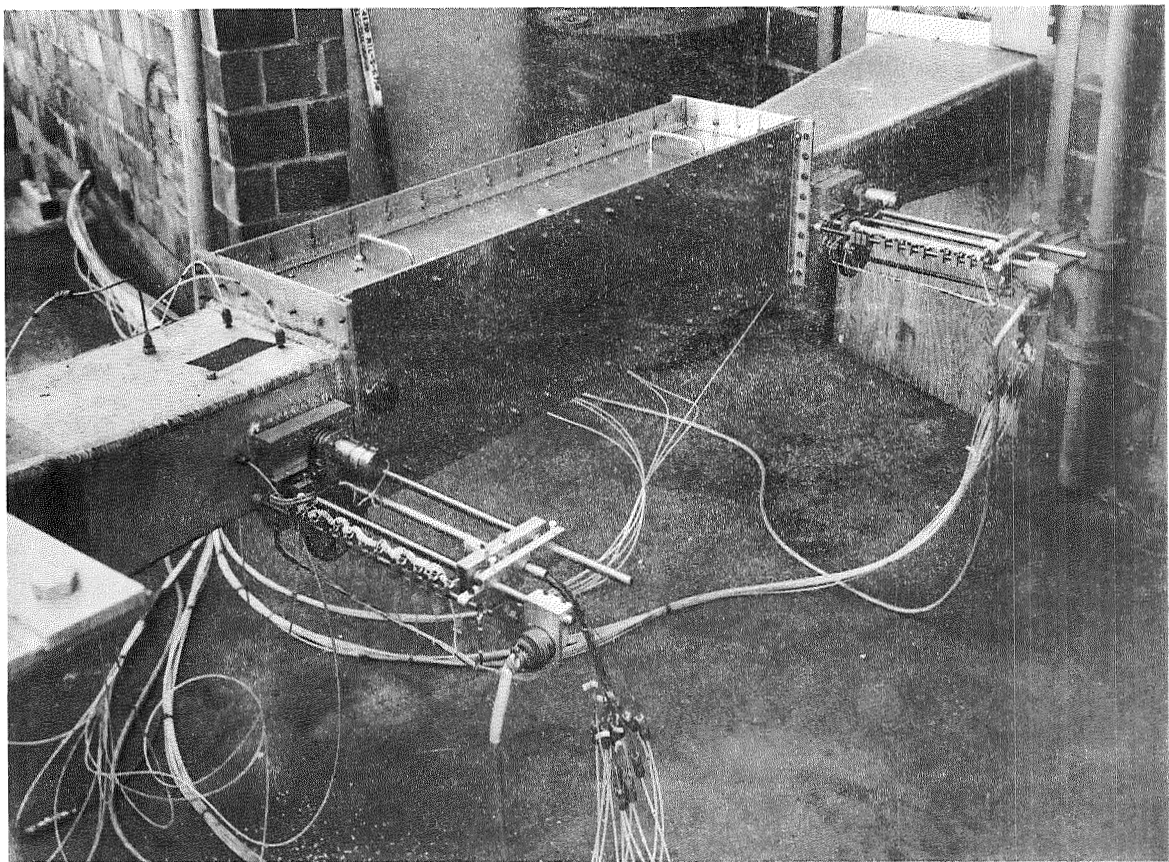


Figure 7.—Test Duct With Remote-Controlled Total-Pressure Rake Mechanisms

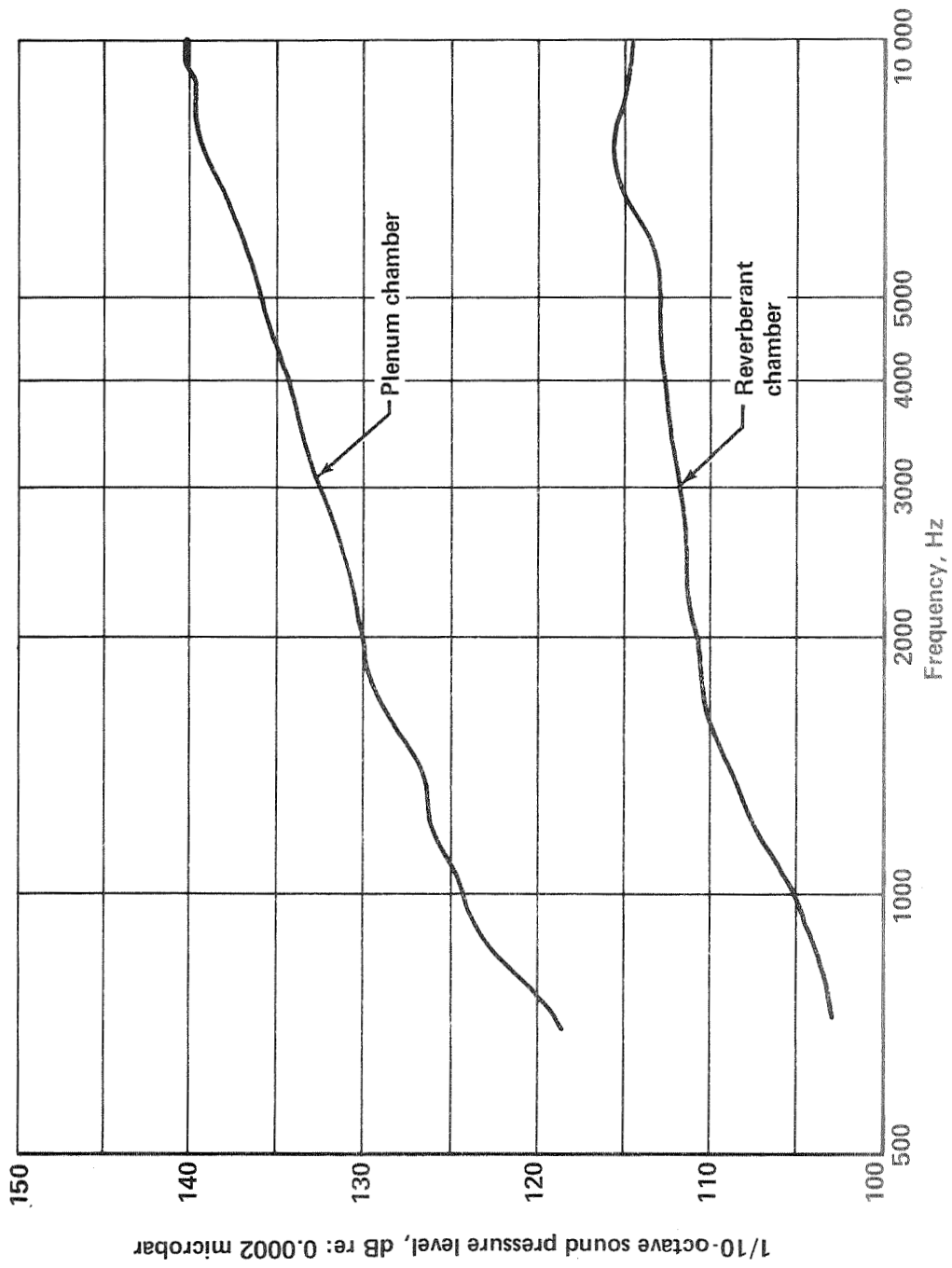


Figure 8.—Maximum Baseline Broadband Input SPL Spectra at  $M = 0.19$

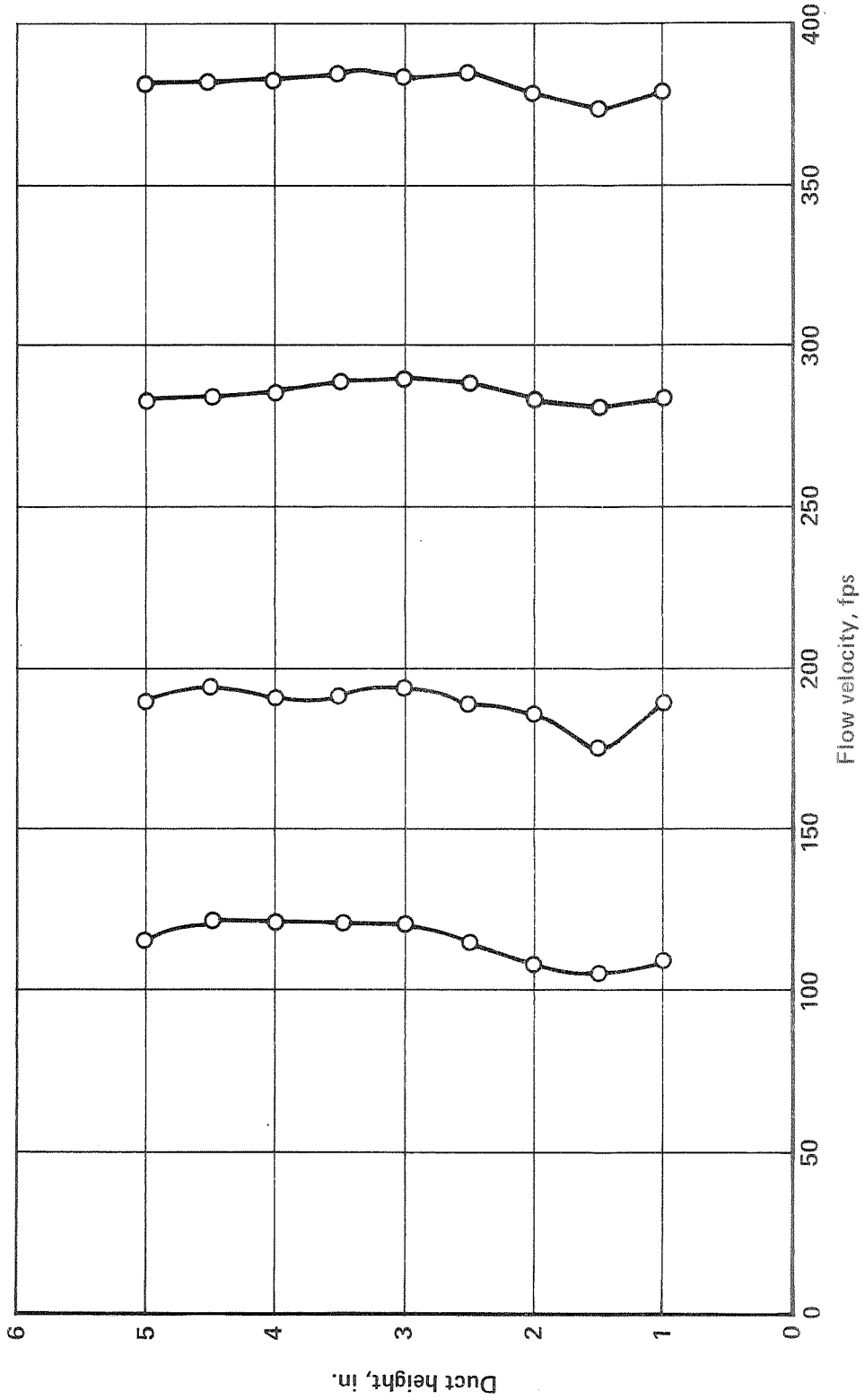


Figure 9.—Upstream Velocity Profiles in the 6-by 10-In. Flow Duct

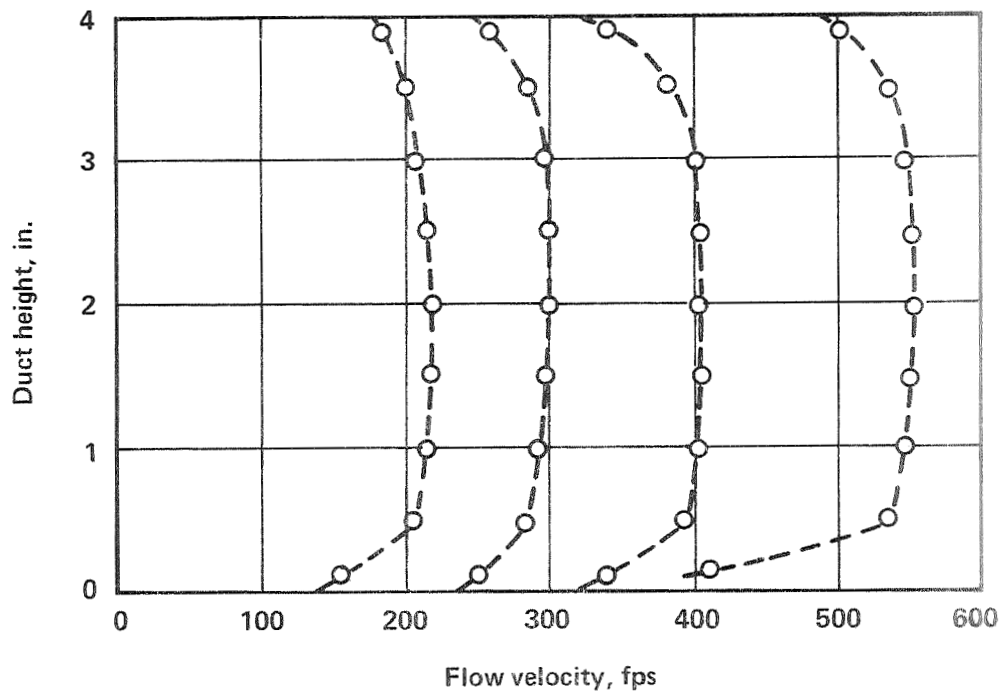


Figure 10.—Upstream Velocity Profiles in the 4- by 10-In. Flow Duct

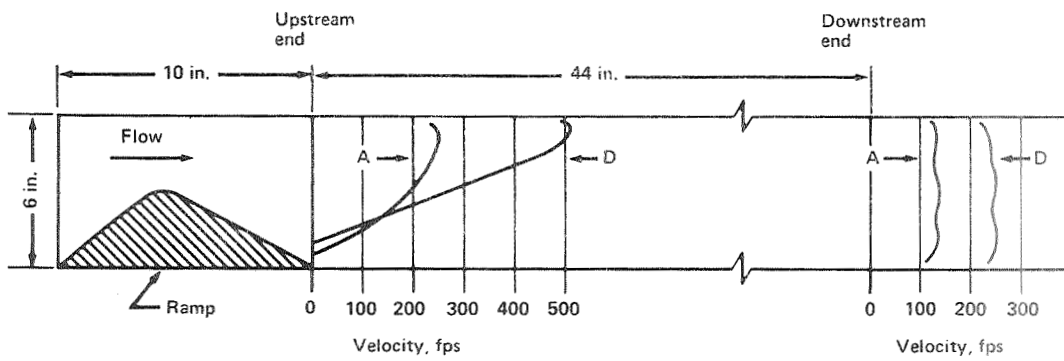


Figure 11.—Method of Flow Velocity Profile Shaping

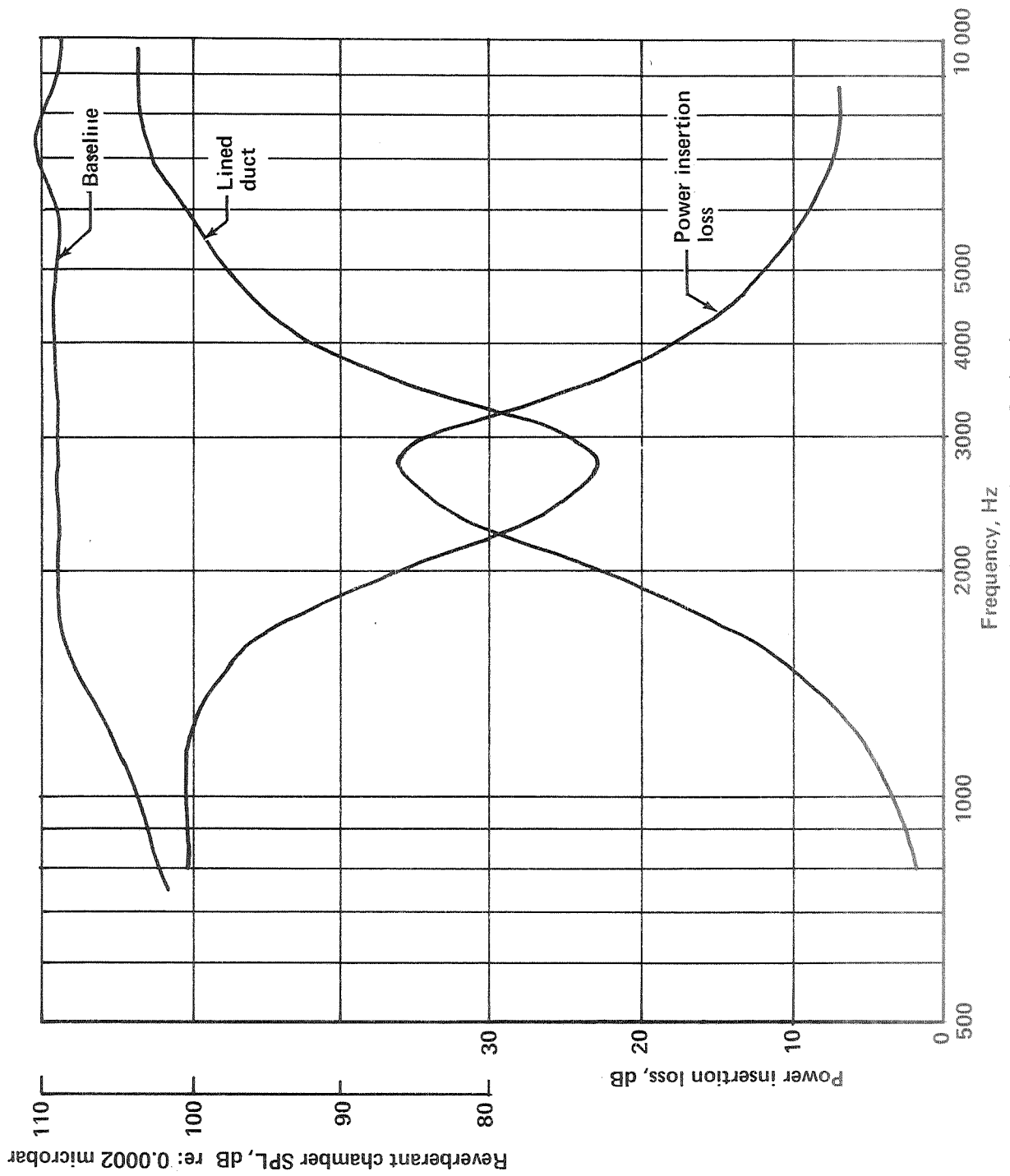
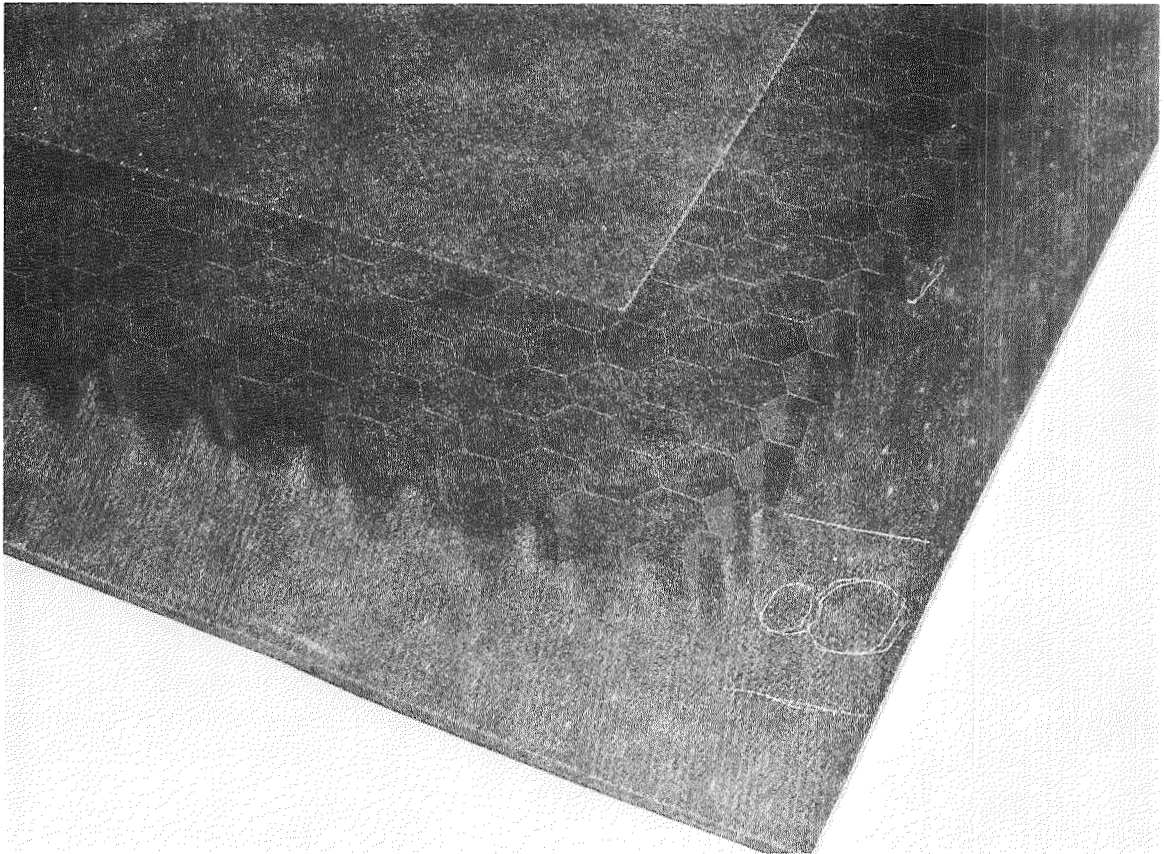
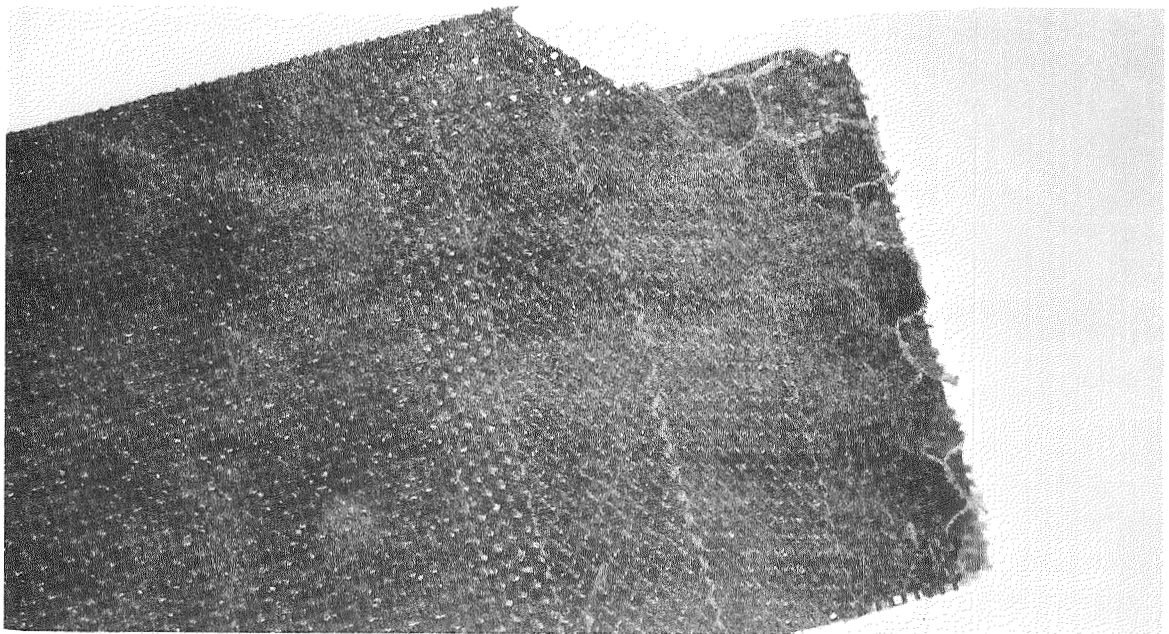


Figure 12.—Graphic Method of Acoustic Data Reduction



*Figure 13.—Resistive-Resonator Lining Panel Construction*



*Figure 14.—Polyimide Acoustic Liner Construction*

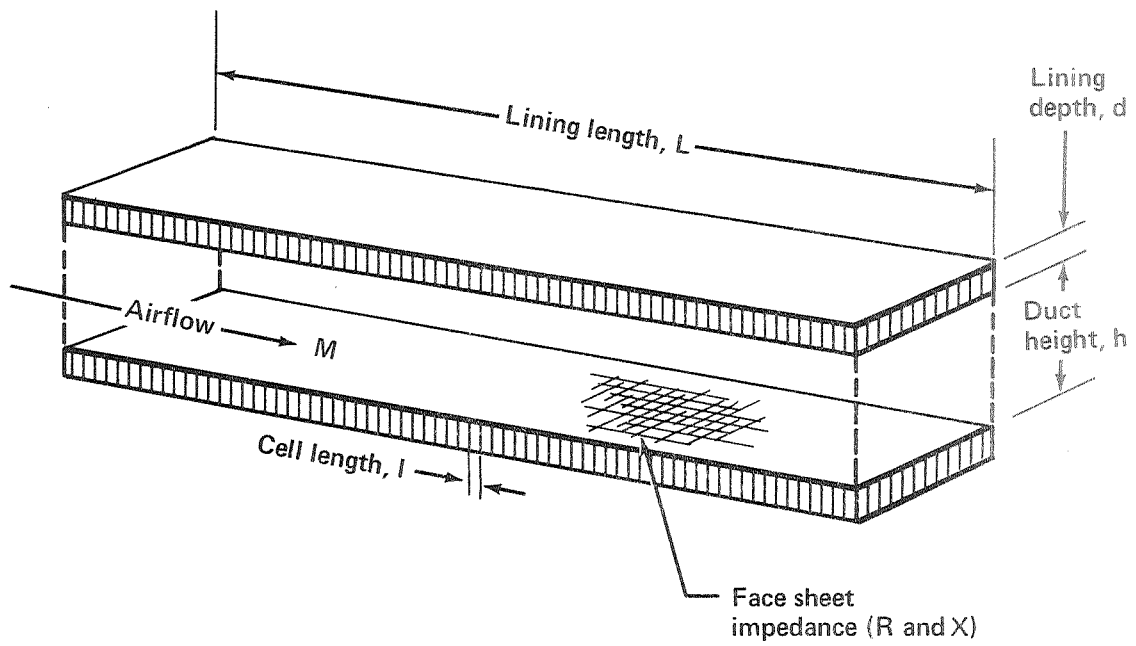


Figure 15.—Acoustically Treated Duct/Liner Parameters

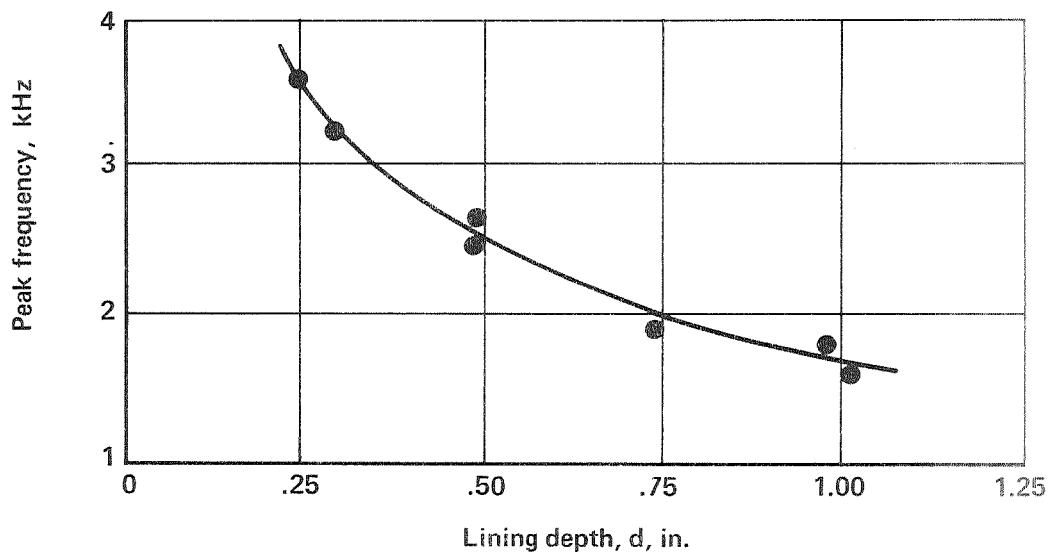


Figure 16.—Variation of Peak Frequency With Lining Depth in a 6-In. Duct at  $M = 0.28$

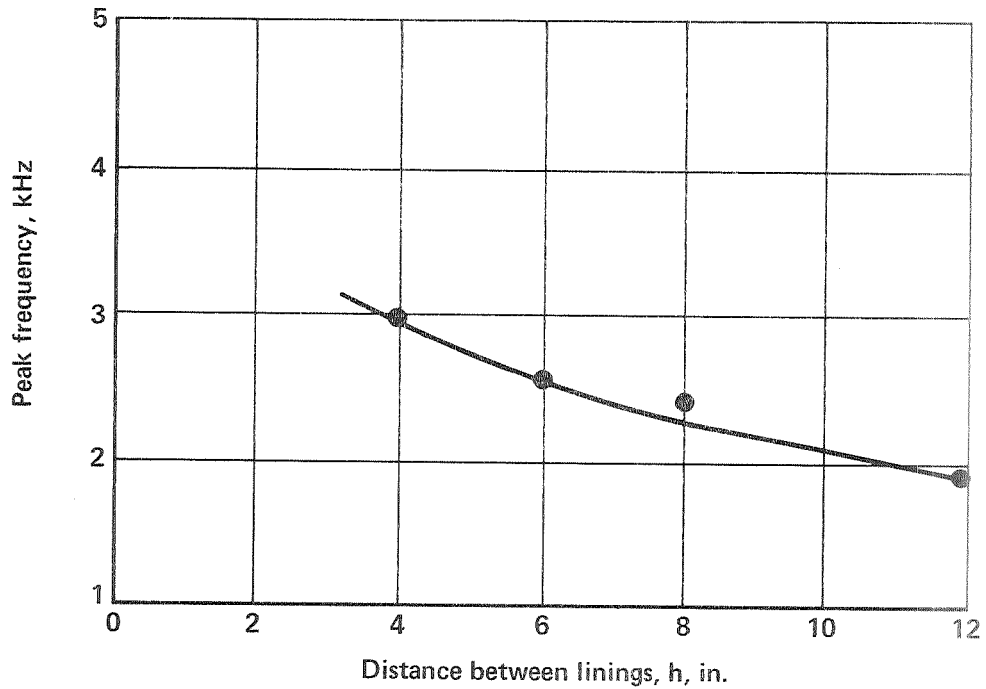


Figure 17.—Variation of Peak Frequency With Lining Separation for a 0.5-In.-Deep Lining at  $M = 0.28$



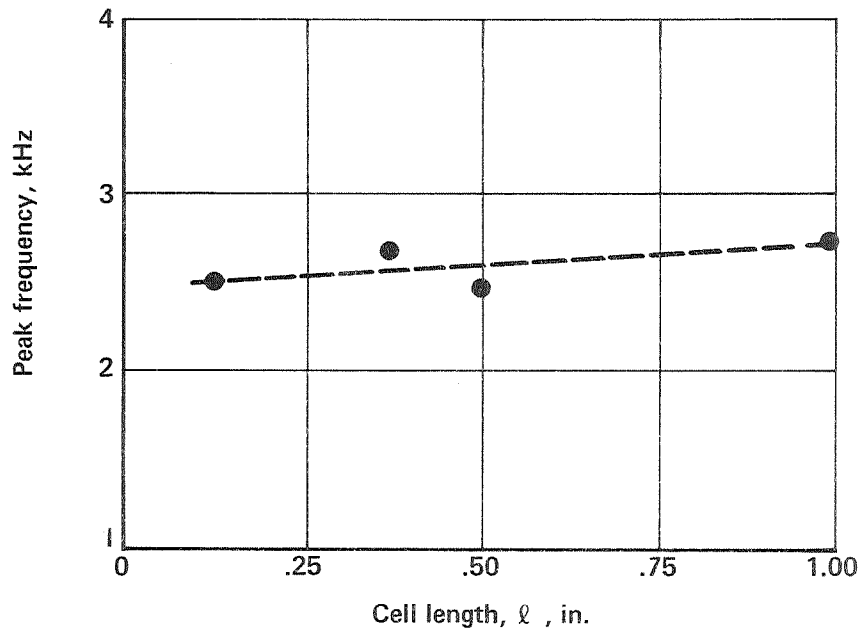


Figure 18.—Variation of Peak Frequency With Cell Length for a 0.5-In.-Deep Lining in a 6-In. Duct at  $M = 0.28$

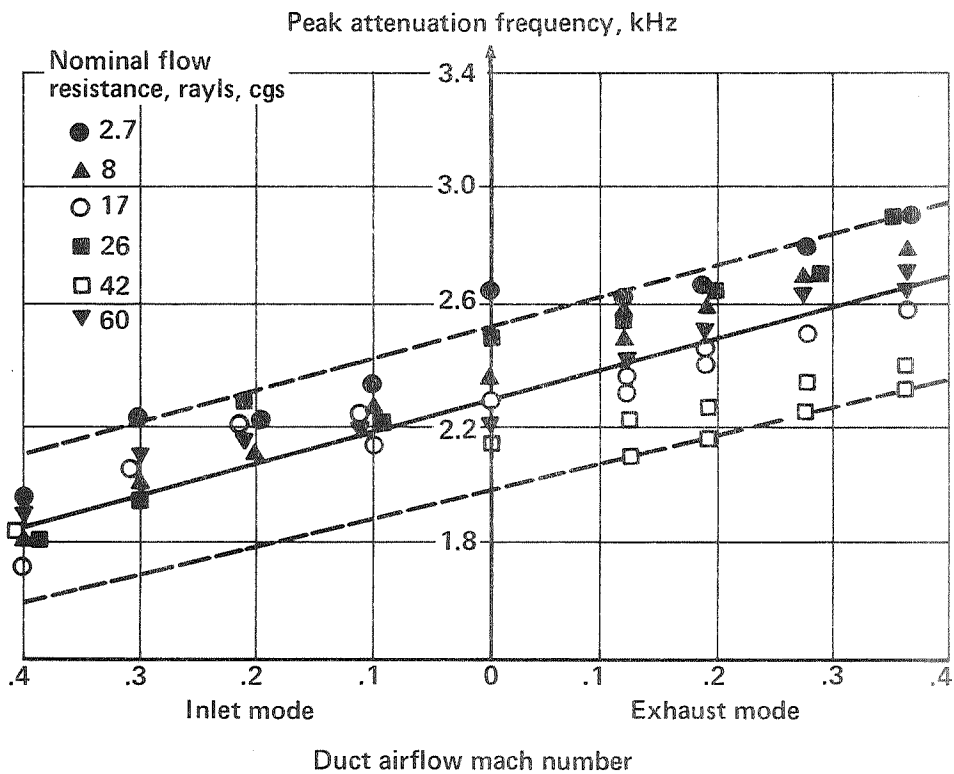


Figure 19.—Variation of Peak Frequency With Airflow Mach Number for a Range of High-Reactance Linings 0.5 In. Deep in a 6-In. Duct

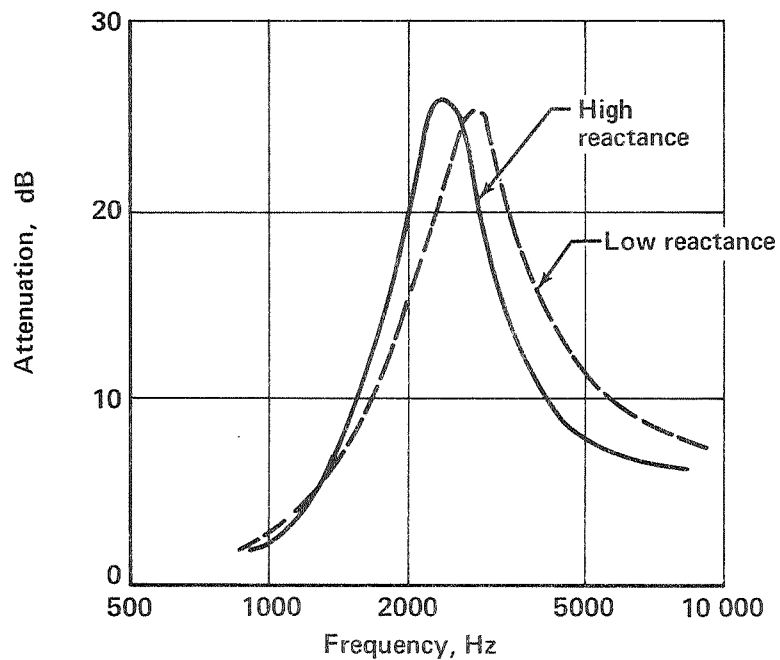


Figure 20.—Acoustic Performance of High- and Low-Reactance Linings

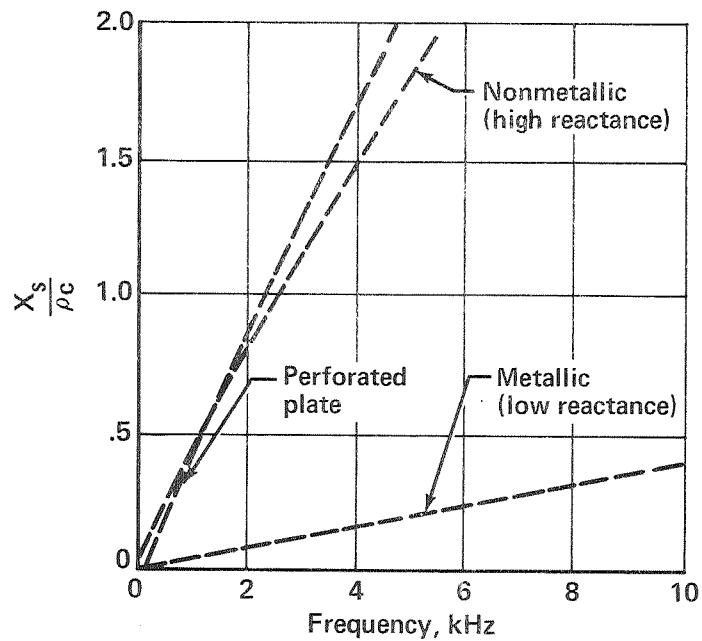


Figure 21.—Reactive Impedance Characteristics of Different Types of Lining Materials at  $M=0$

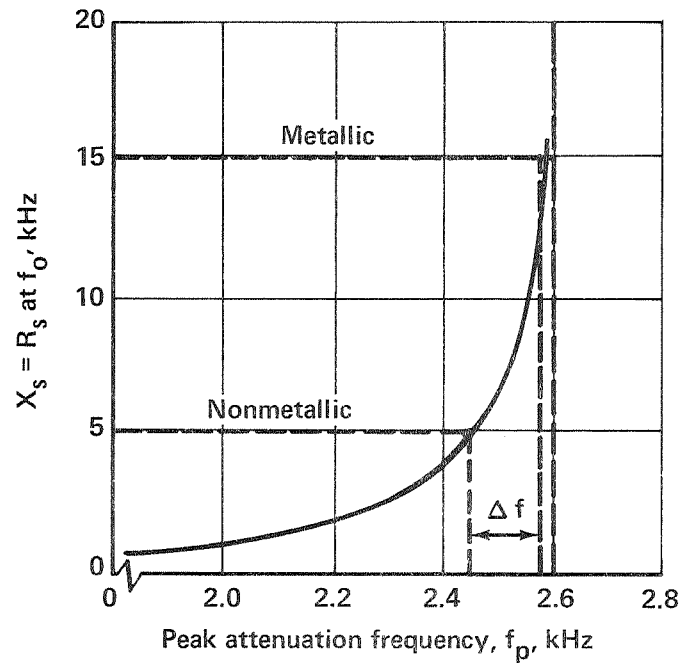


Figure 22.—Variation of Peak Frequency With Lining Reactance for a 30-Rayl (CGS) Effective Flow Resistance Material 0.5 In. Deep in a 6-In. Duct

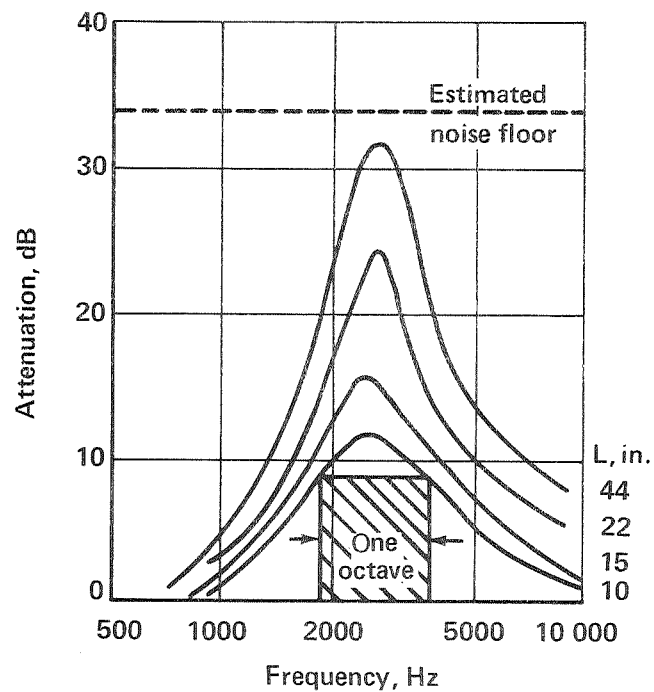


Figure 23.—Typical Attenuation Spectra for Various Lining Lengths of a 30-Rayl (CGS) High-Reactance Material 0.5 In. Deep in a 6-In. Duct at  $M = 0.28$

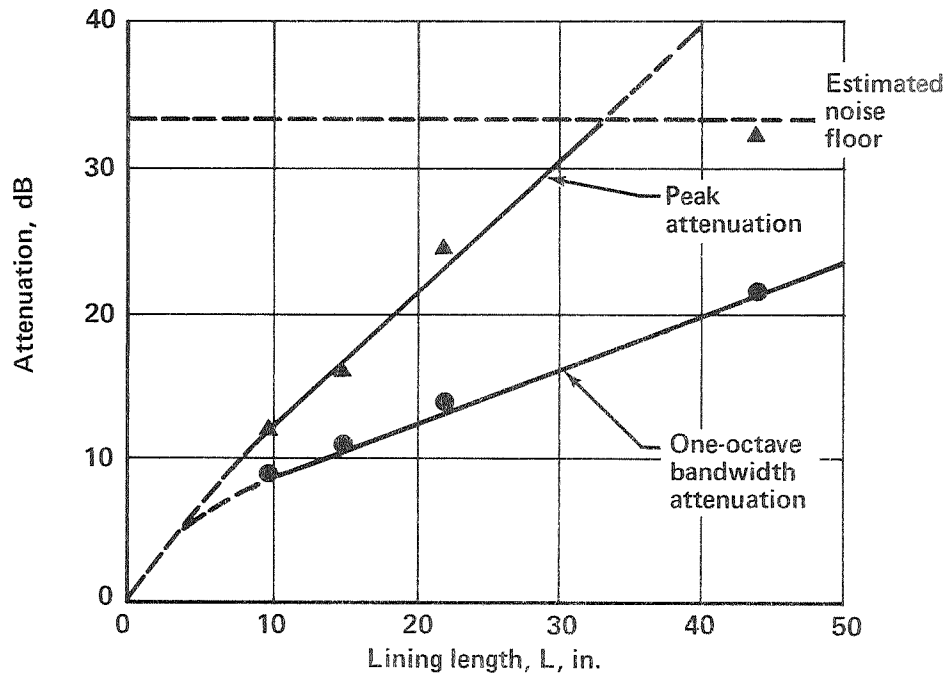


Figure 24.—Variation of Attenuation With Lining Length for a 30-Rayl (CGS) High-Reactance Material 0.5 In. Deep in a 6-In. Duct at  $M = 0.28$

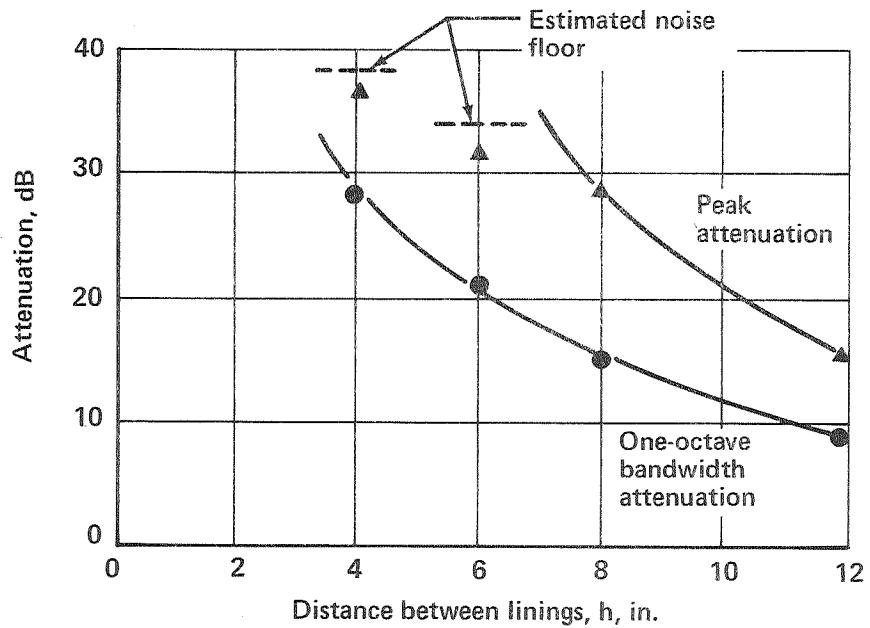


Figure 25.—Variation of Attenuation With Lining Separation for a 30-Rayl (CGS) High-Reactance Material 0.5 In. Deep at  $M = 0.28$

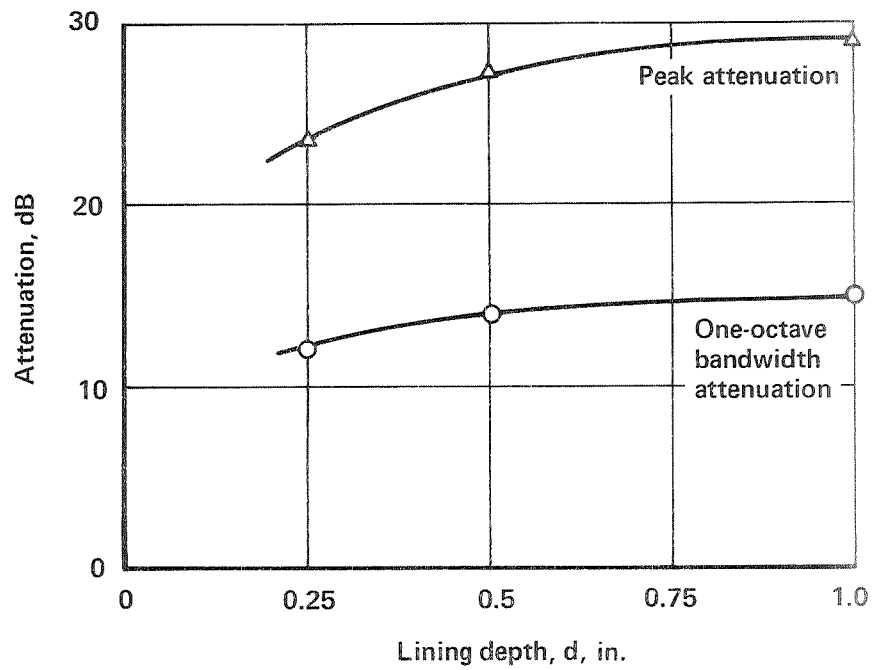


Figure 26.—Variation of Attenuation With Lining Depth for Optimum High-Reactance Materials in a 6-In. Duct at  $M = 0.28$

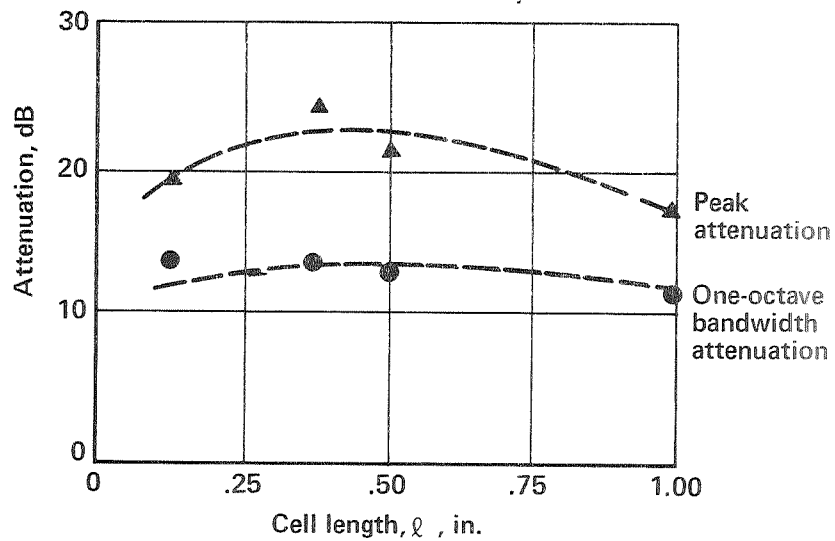


Figure 27.—Variation of Attenuation With Cell Length for a High-Reactance Material 0.5 In. Deep in a 6-In. Duct at  $M = 0.28$

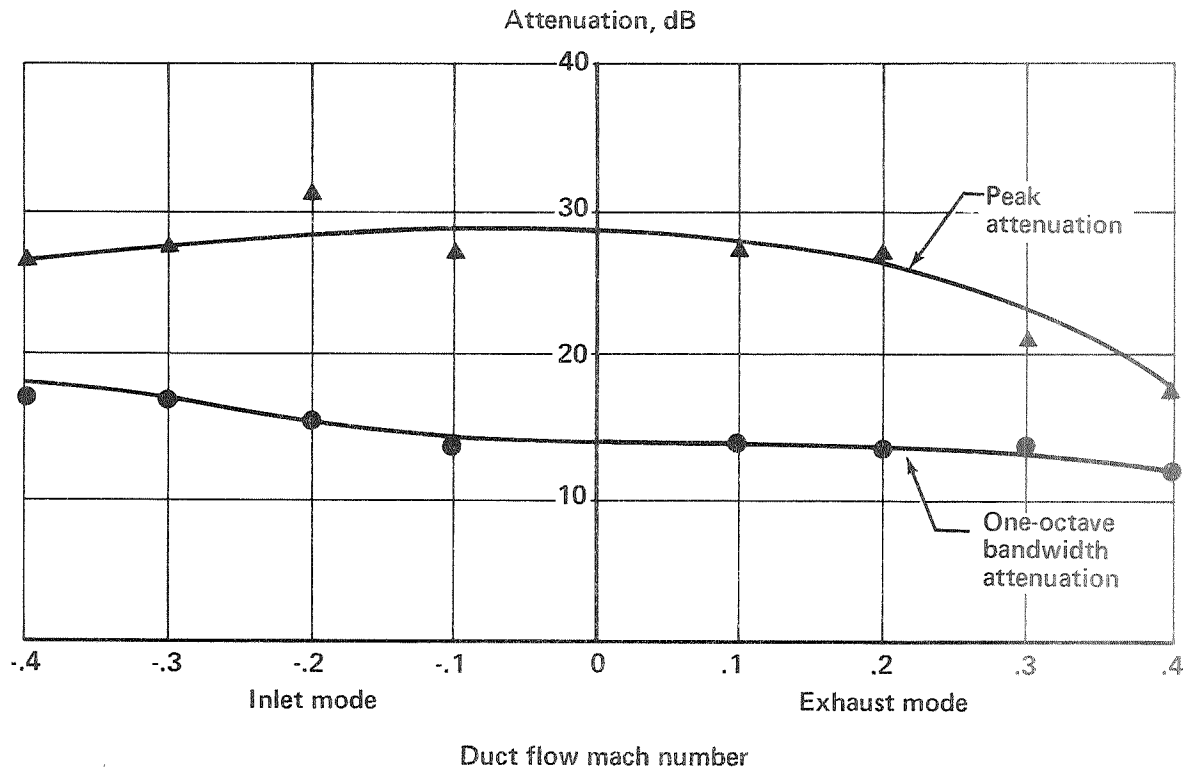


Figure 28.—Variation of Attenuation With Airflow Mach Number for a 30-Rayl (CGS) High-Reactance Material 0.5 In. Deep in a 6-In. Duct

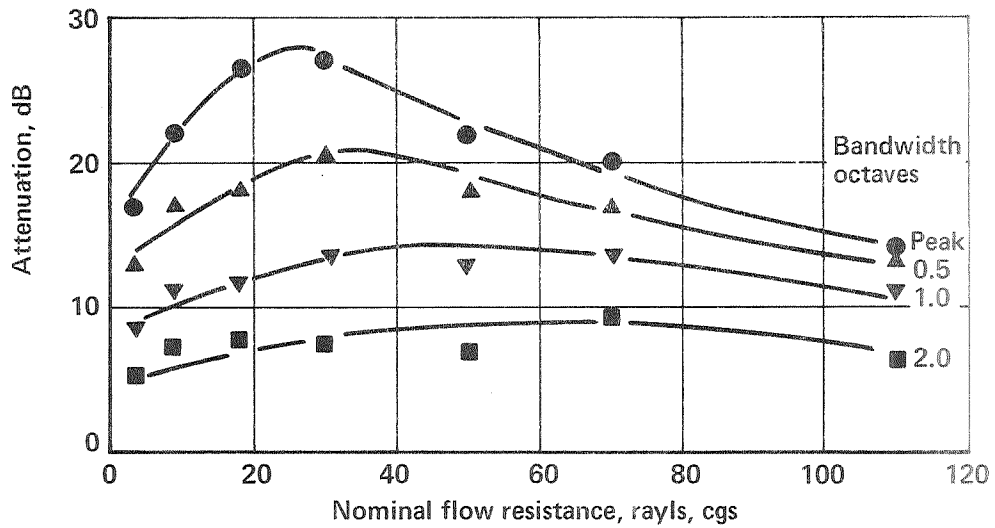


Figure 29.—Variation of Attenuation With Laminar Flow Resistance for a High-Reactance Material 0.5 In. Deep in a 6-In. Duct at  $M = 0.28$

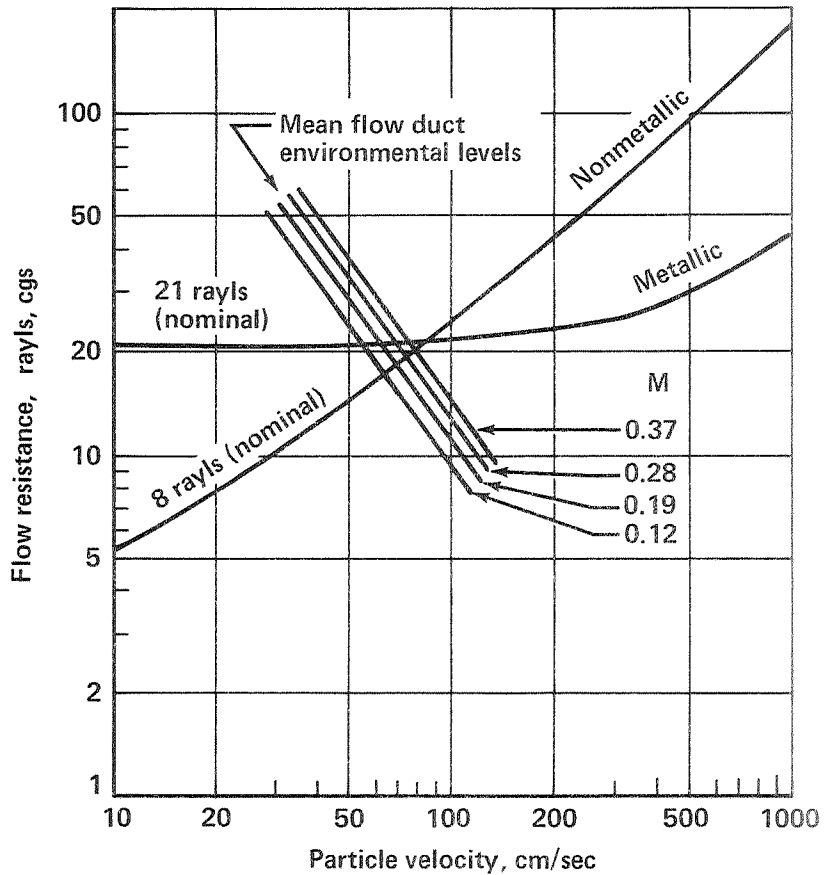


Figure 30.—Variation of Flow Resistance With Particle Velocity for the Two Major Types of Porous Acoustic Lining Materials

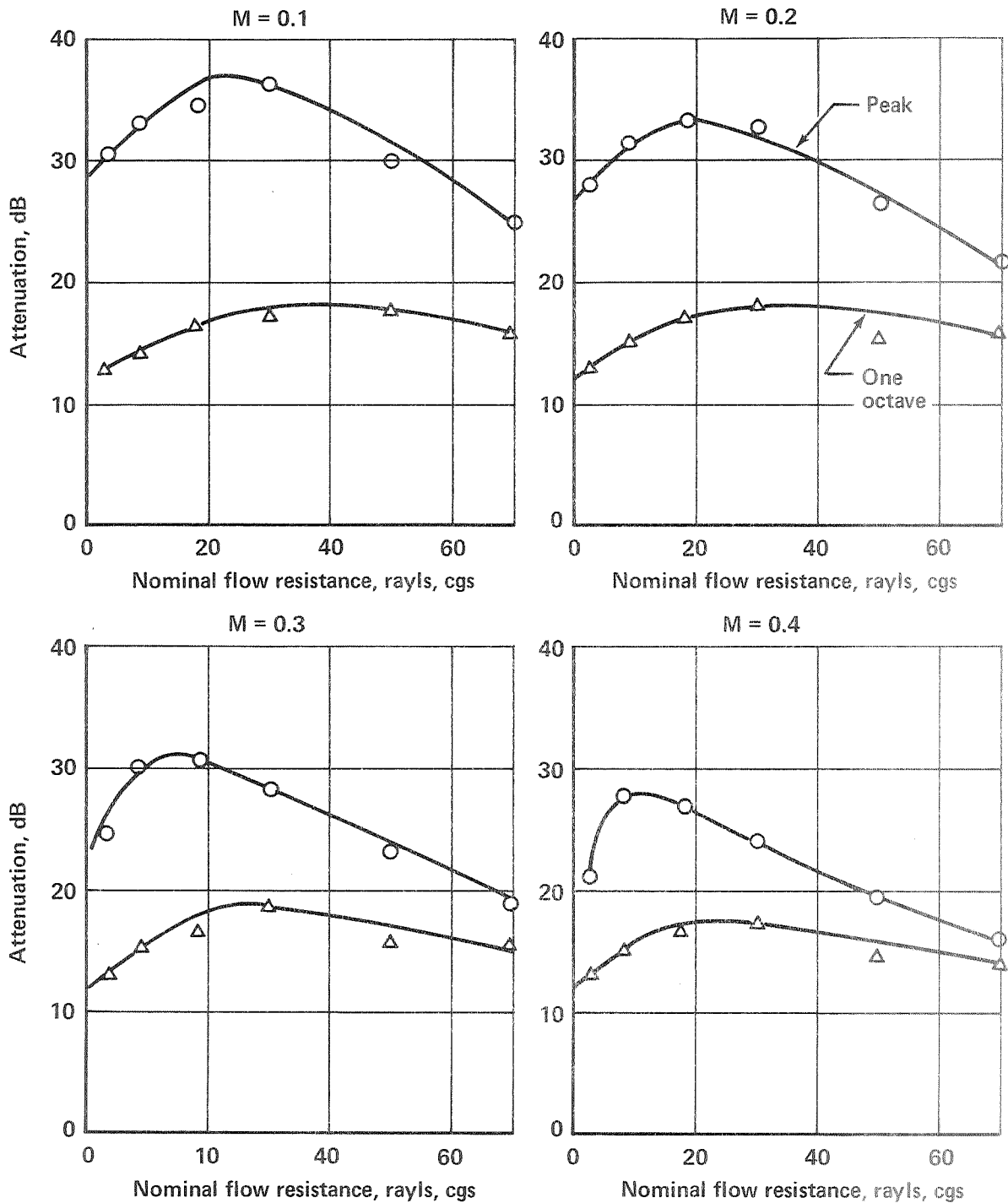


Figure 31.—Variation of Attenuation With Nominal Flow Resistance for 0.5-In.-Deep Lining in a 4-In. Duct



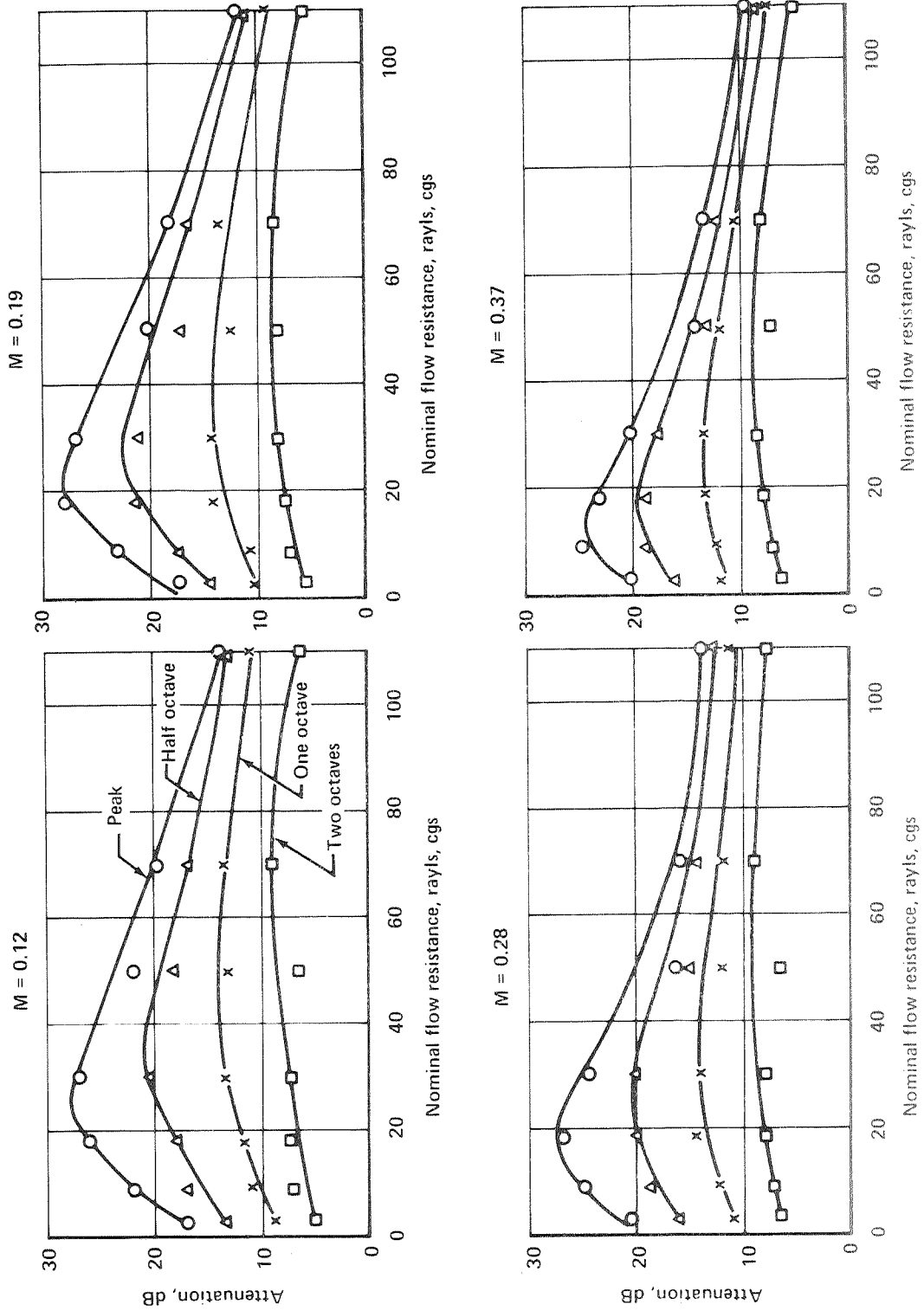


Figure 32. — Variation of Attenuation With Nominal Flow Resistance for 0.5-In.-Deep Lining in a 6-In. Duct

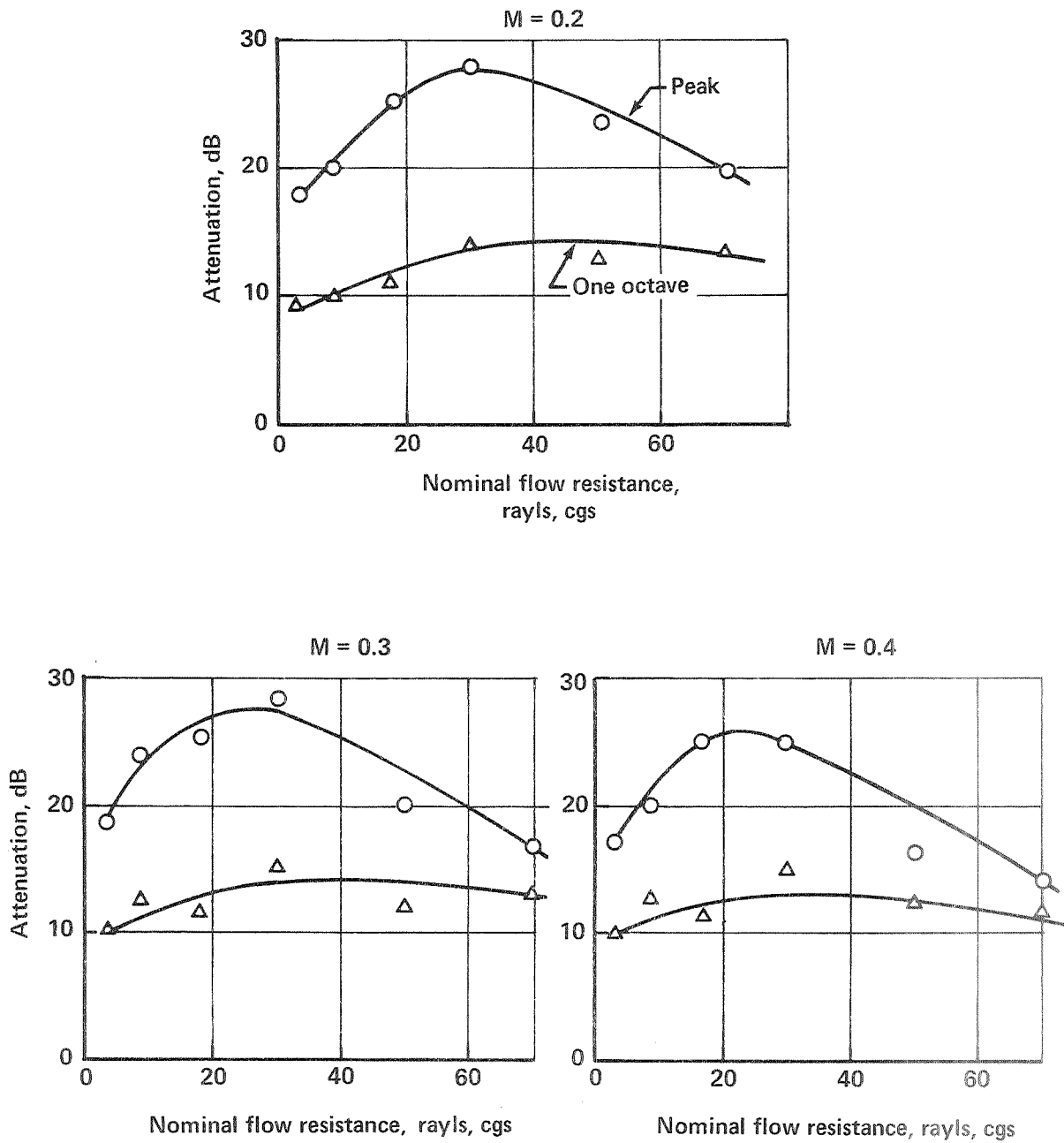


Figure 33.—Variation of Attenuation With Nominal Flow Resistance for 0.5-In.-Deep Lining in an 8-In. Duct

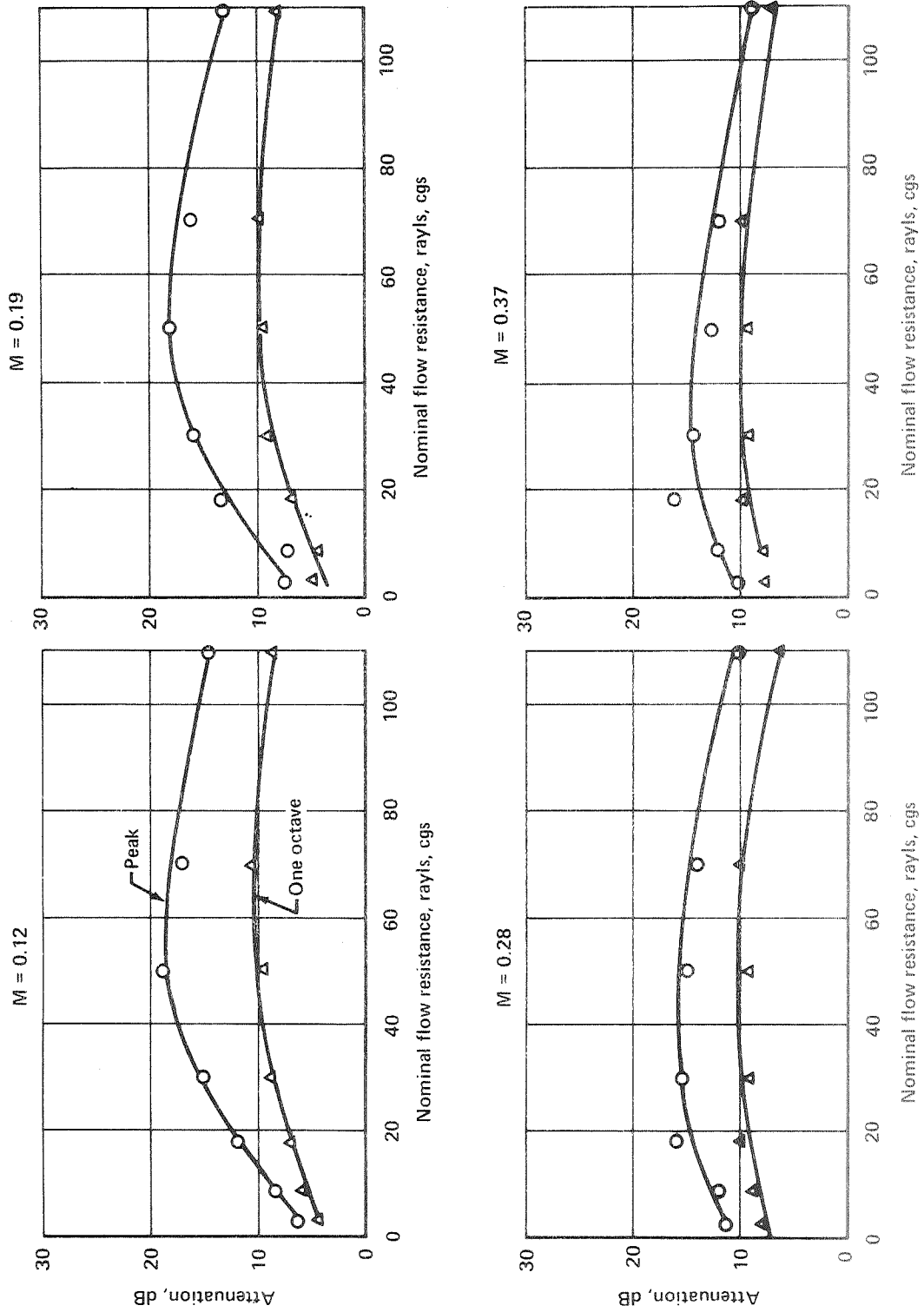


Figure 34. — Variation of Attenuation With Nominal Flow Resistance for 0.5-In. Deep Lining in a 12-In. Duct

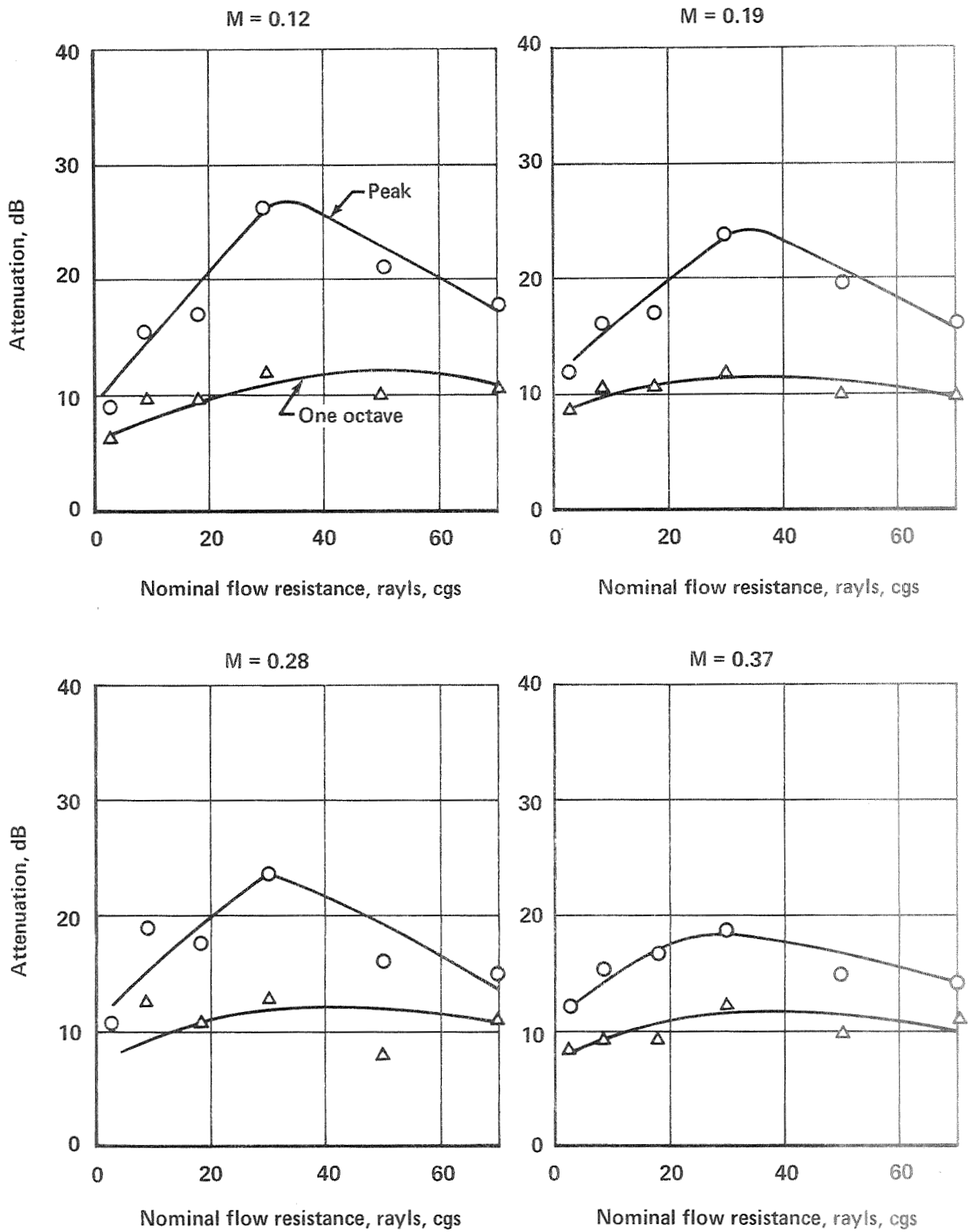


Figure 35.—Variation of Attenuation With Nominal Flow Resistance for 0.25-In.-Deep Lining in a 6-In. Duct

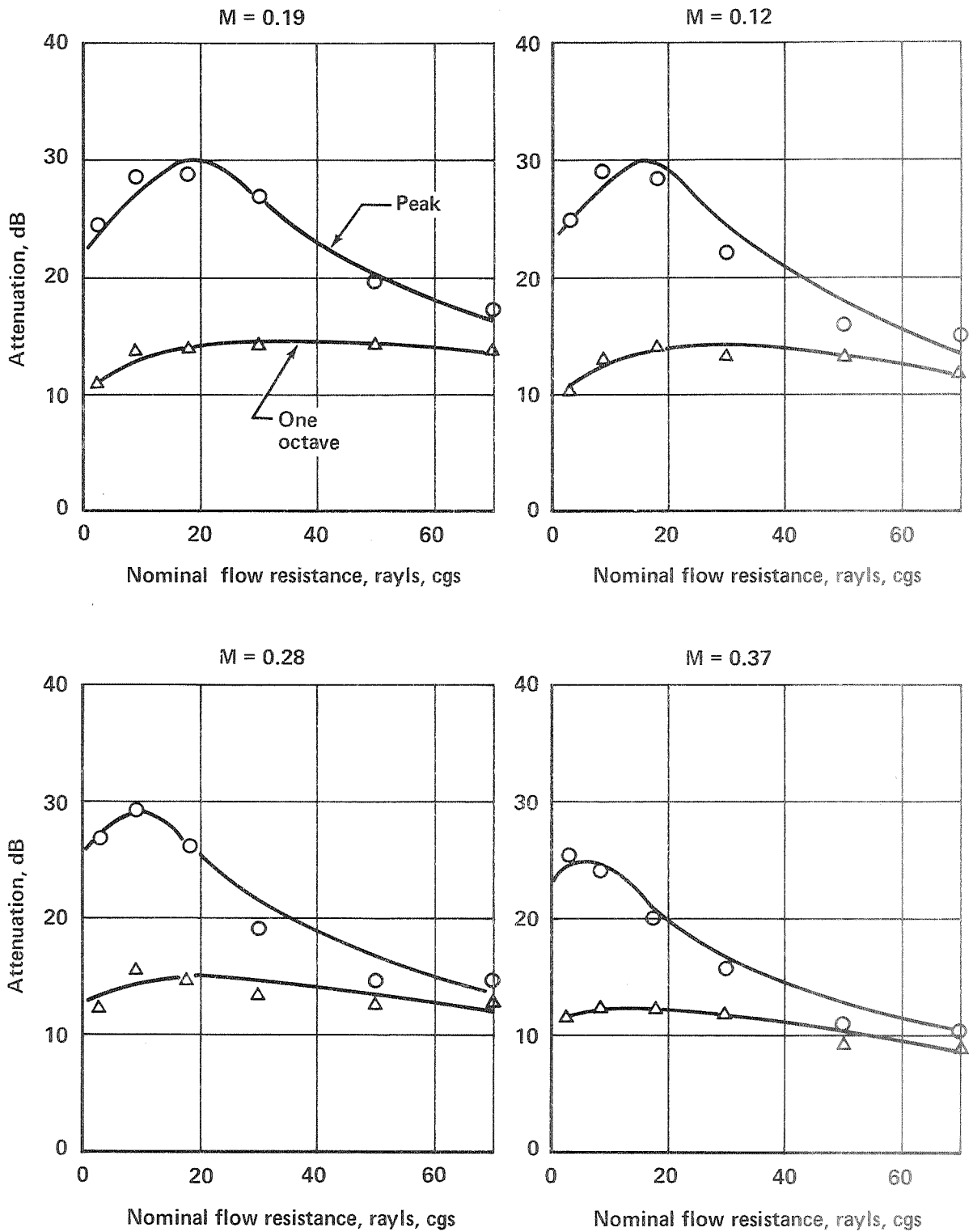


Figure 36.—Variation of Attenuation With Nominal Flow Resistance for 1.0-In.-Deep Lining in a 6-In. Duct

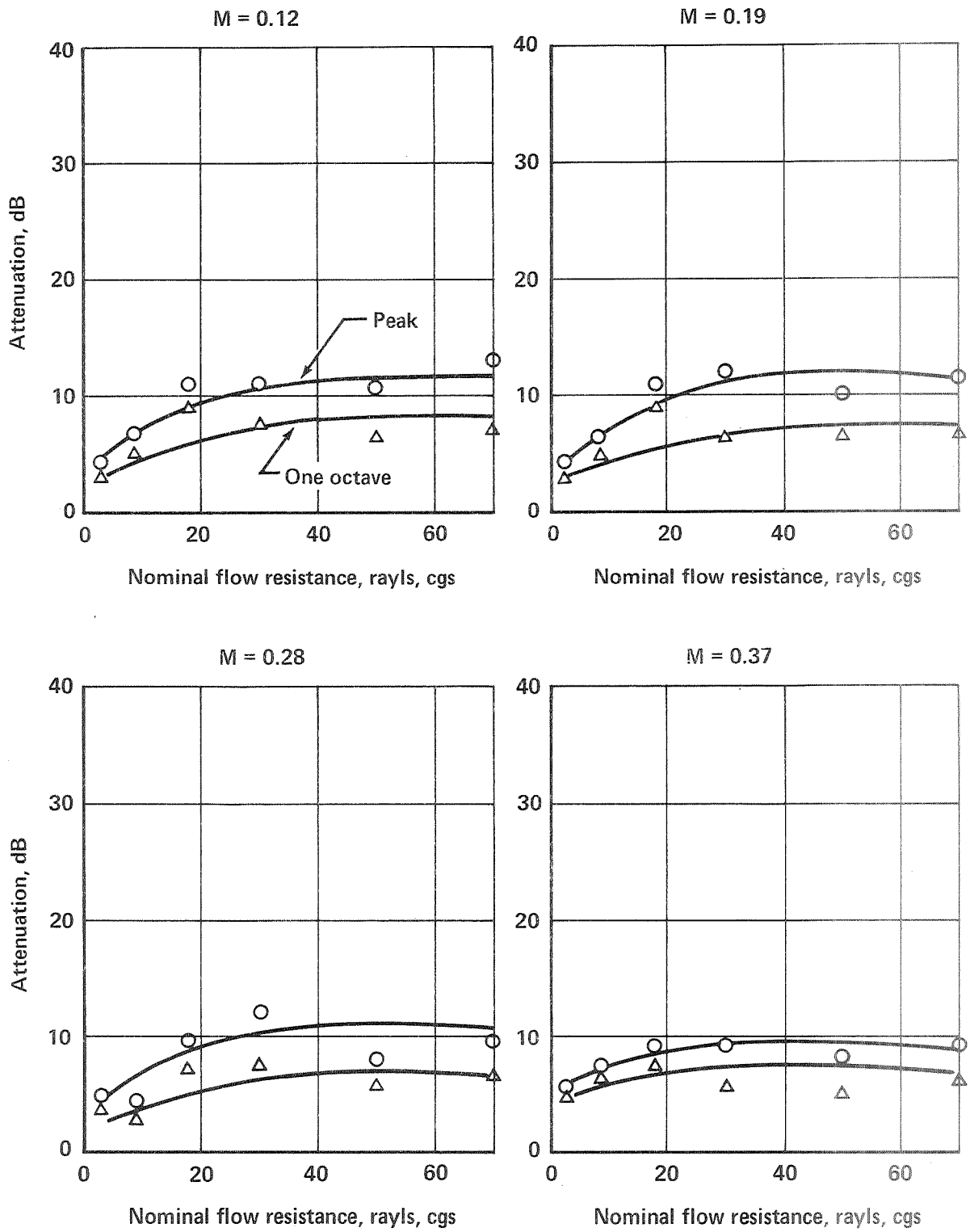


Figure 37.—Variation of Attenuation With Nominal Flow Resistance for 0.25-In.-Deep Lining in a 12-In. Duct

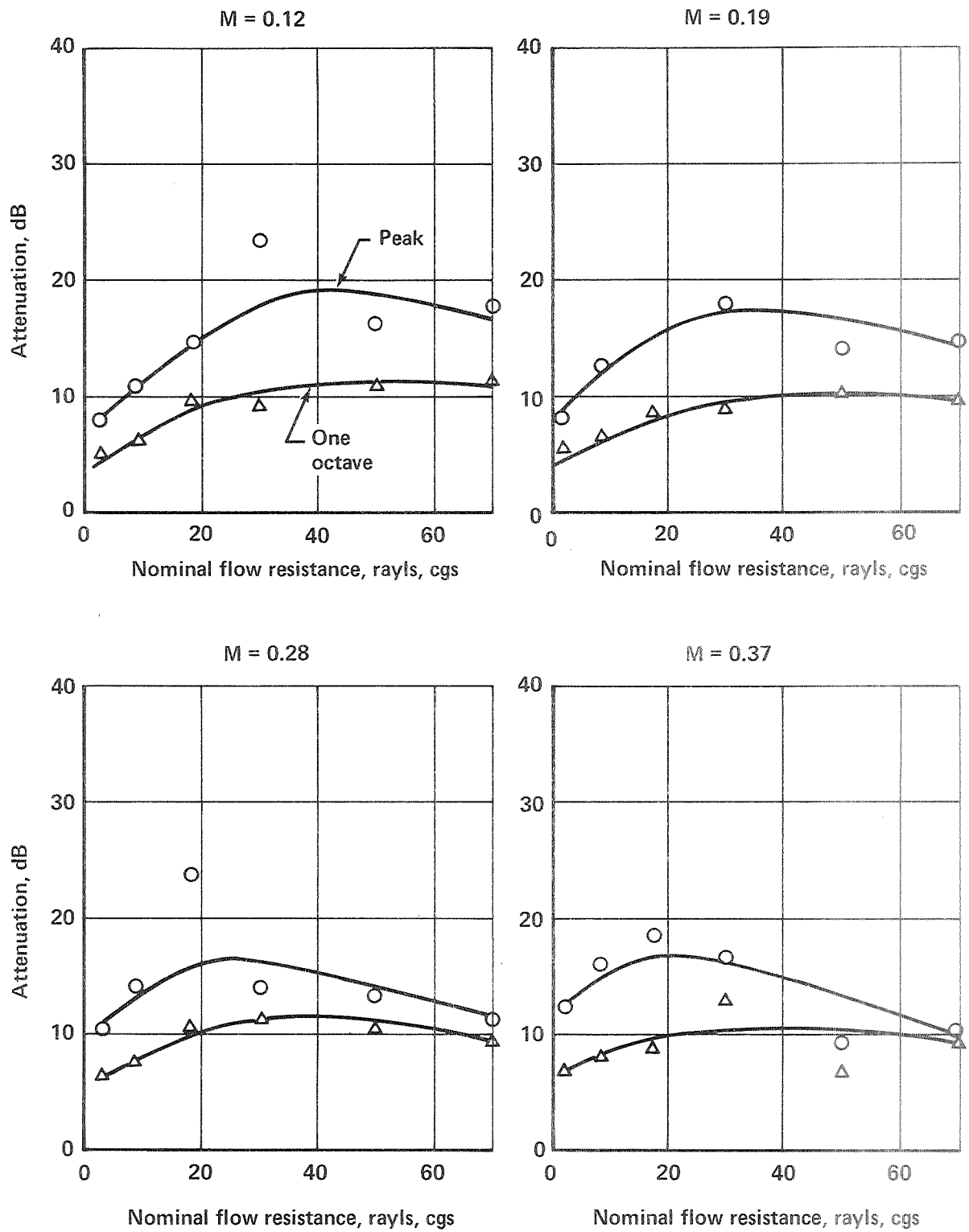


Figure 38.—Variation of Attenuation With Nominal Flow Resistance for 1.0-In.-Deep Lining in a 12-In. Duct

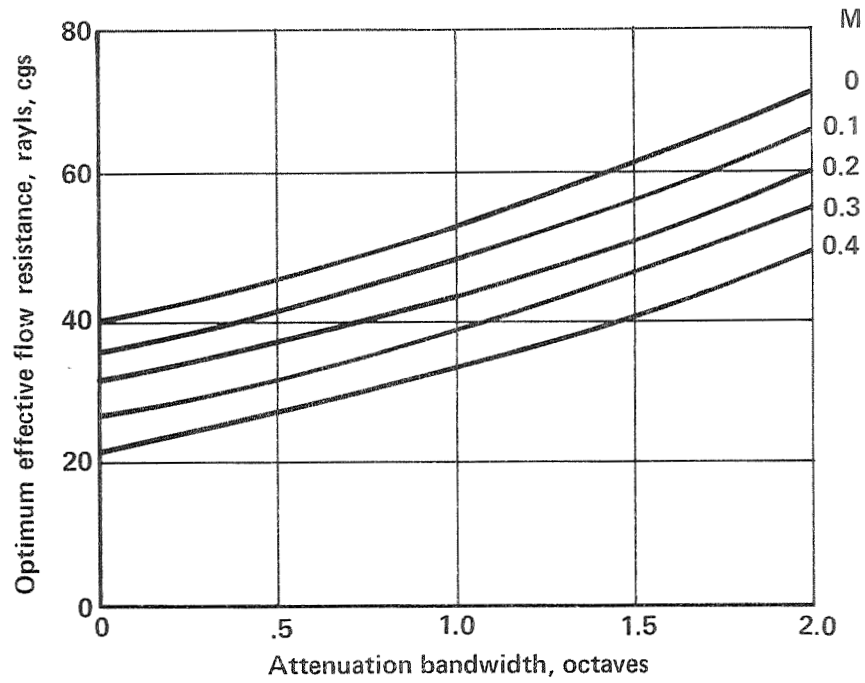


Figure 39.—Variation of the Optimum Effective Flow Resistance With Attenuation Bandwidth and Mach Number for 0.5-In.-Deep Linings in a 6-In. Duct

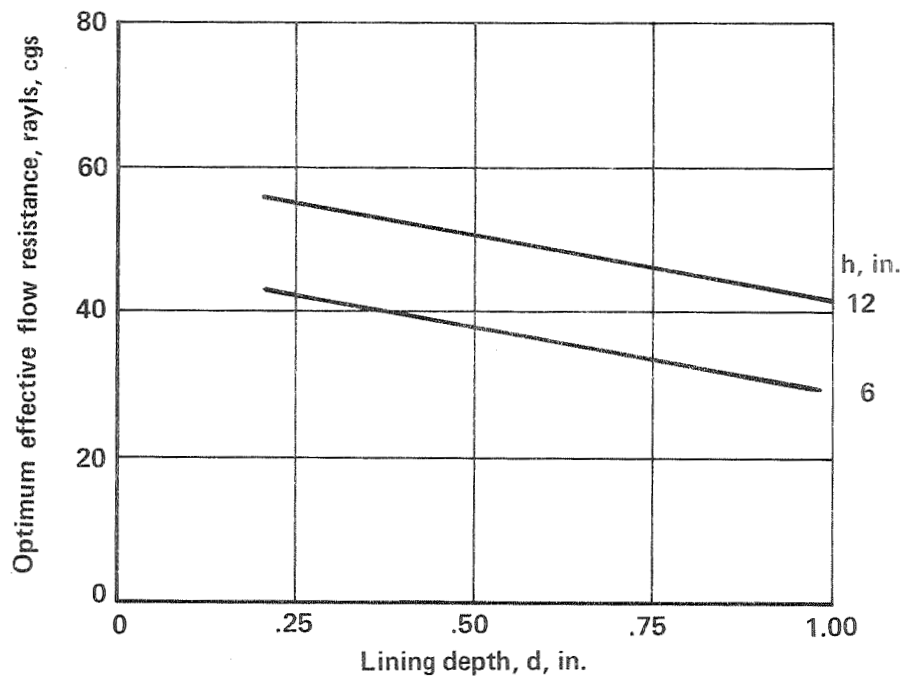


Figure 40.—Variation of the Optimum Effective Flow Resistance With Lining Depth and Duct Size for One-Octave Bandwidth at  $M = 0.3$



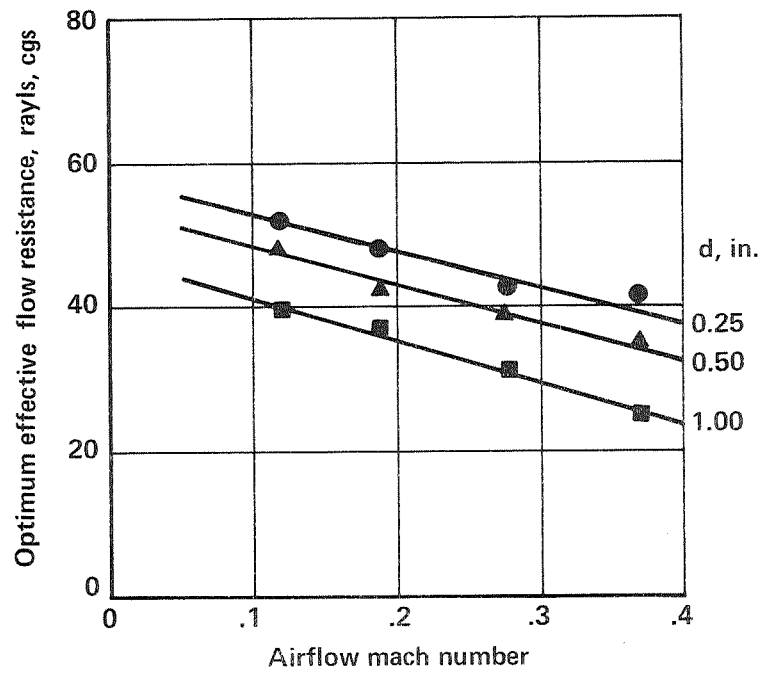


Figure 41.—Variation of the Optimum Effective Flow Resistance With Lining Depth and Mach Number for One-Octave Bandwidth in a 6-In. Duct

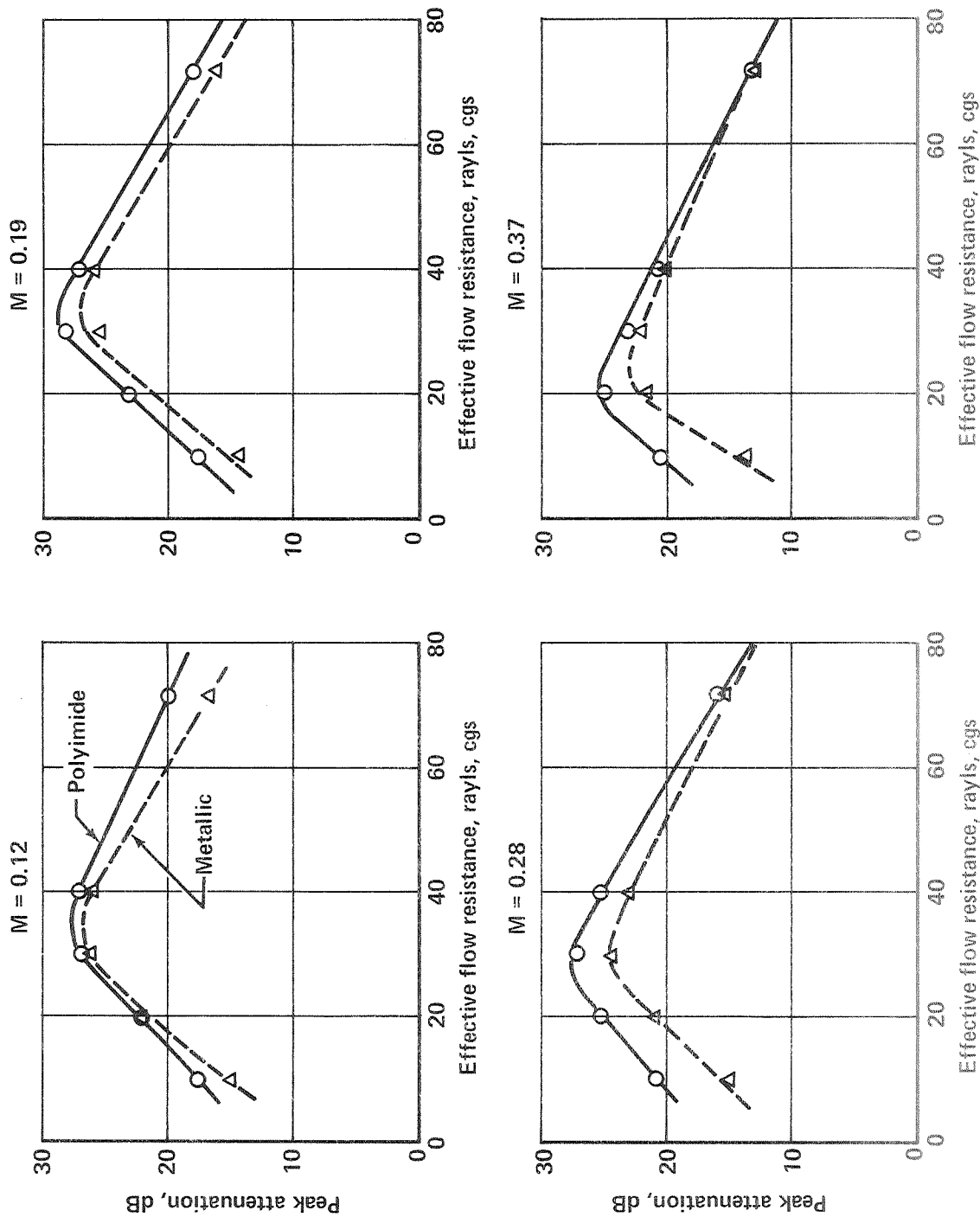


Figure 42.—Variation of Attenuation With Effective Flow Resistance for High- and Low-Reactance Materials

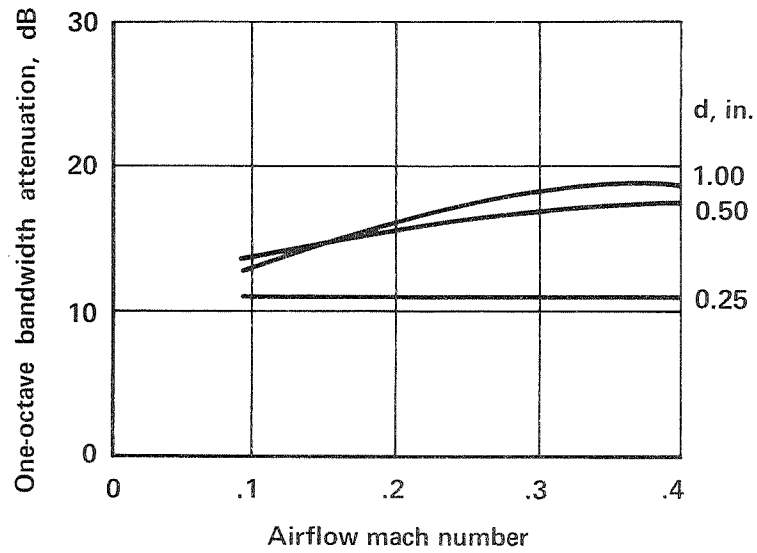


Figure 43.—Variation of Attenuation With Mach Number for Various Lining Depths, 9-Rayl (CGS), Nominal Flow Resistance Material in a 6-In. Duct

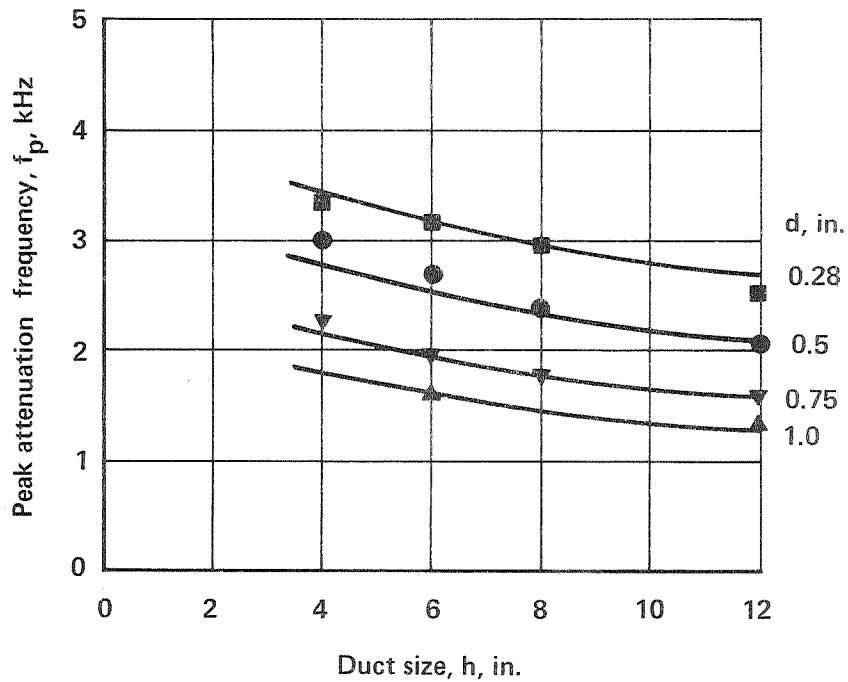


Figure 44.—Variation of Peak Frequency With Duct Size and Lining Depth for 30-Rayl (CGS), Nominal Flow Resistance, High-Reactance Linings at  $M = 0.28$

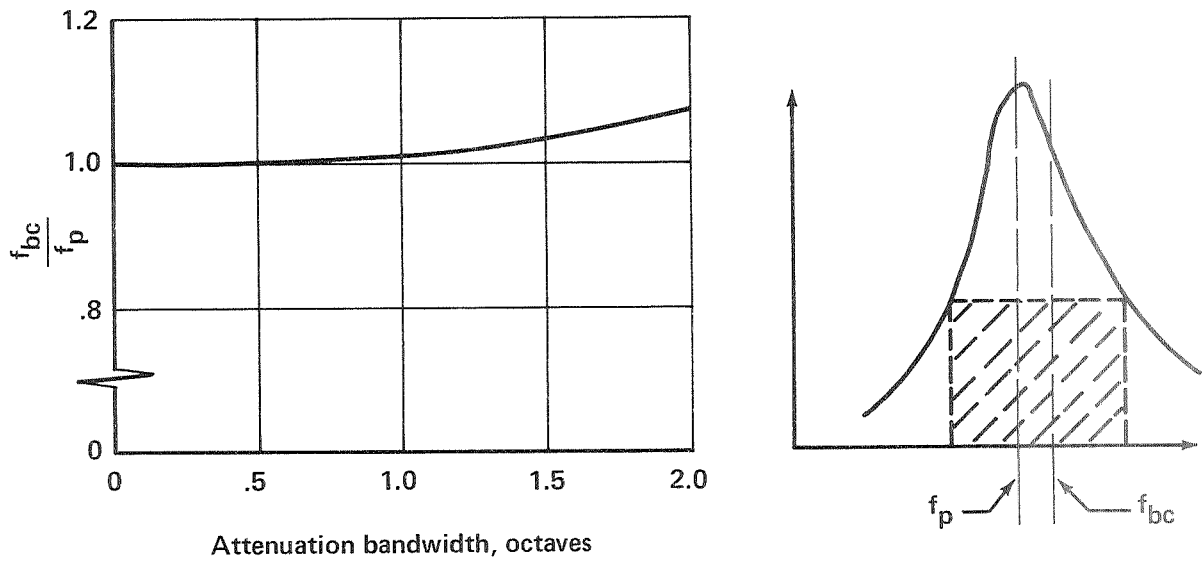


Figure 45.—Variation of Attenuation Band Center Frequency

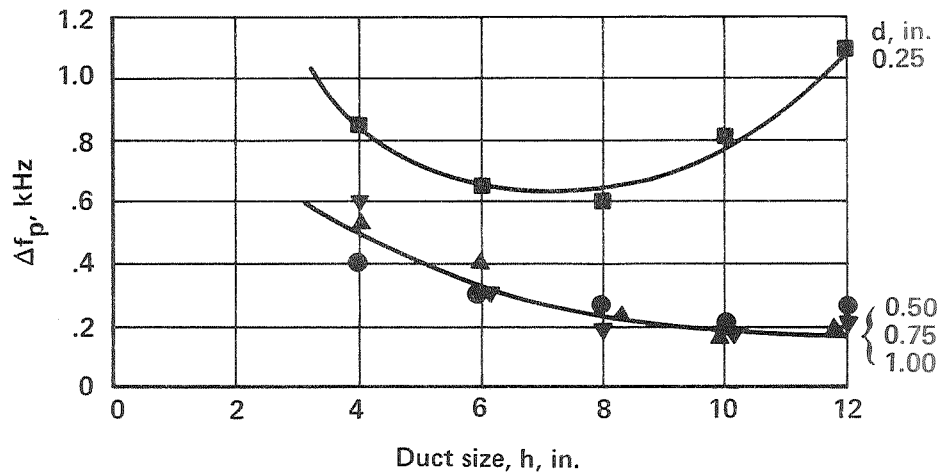


Figure 46.—Increase in Peak Frequency for Low-Reactance Linings as Compared to High-Reactance Linings

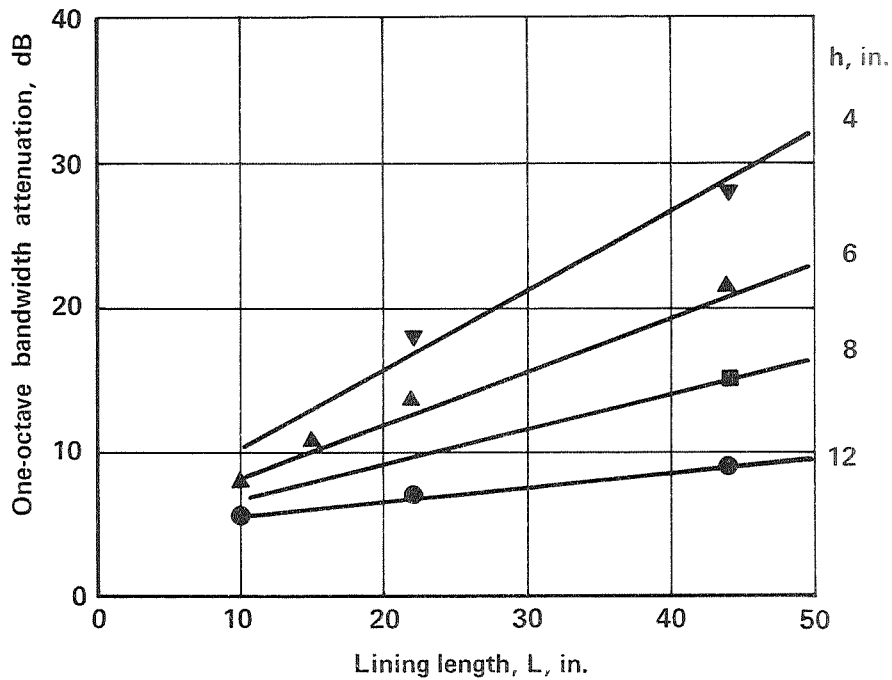


Figure 47.—Variation of Attenuation With Lining Length for a 30-Rayl (CGS) High-Reactance Material 0.5 In. Deep at  $M = 0.28$

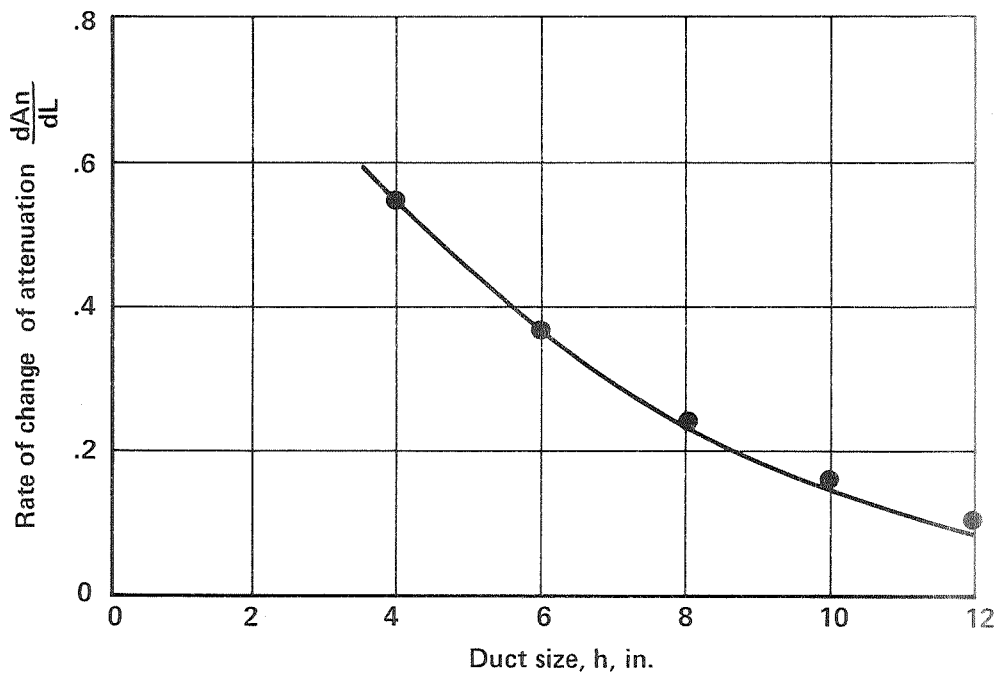


Figure 48.—Rate of Change of Attenuation With Lining Length for Various Duct Sizes

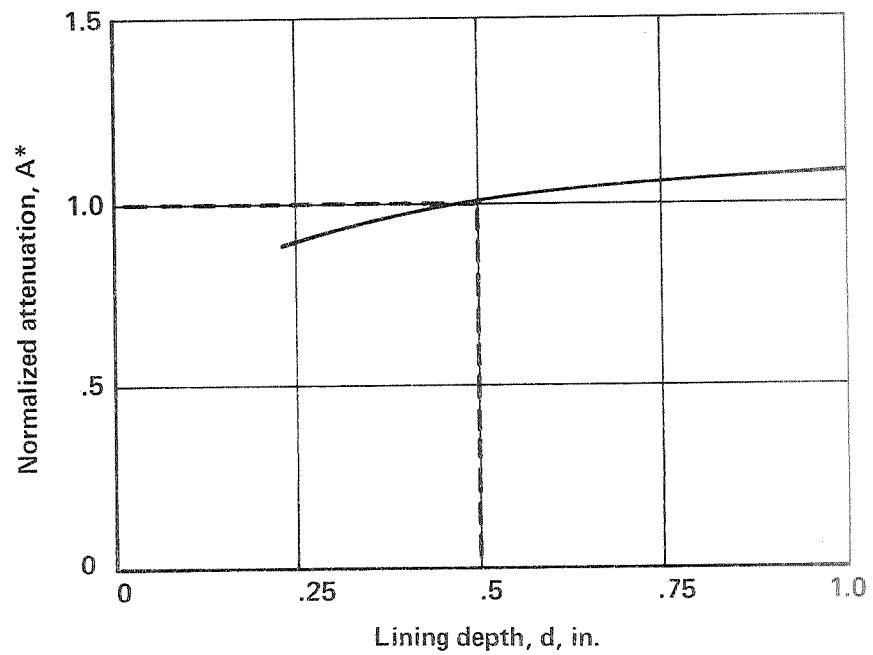


Figure 49.—Variation of Attenuation With Lining Depth for Optimum Effective Flow Resistance for High-Reactance Material

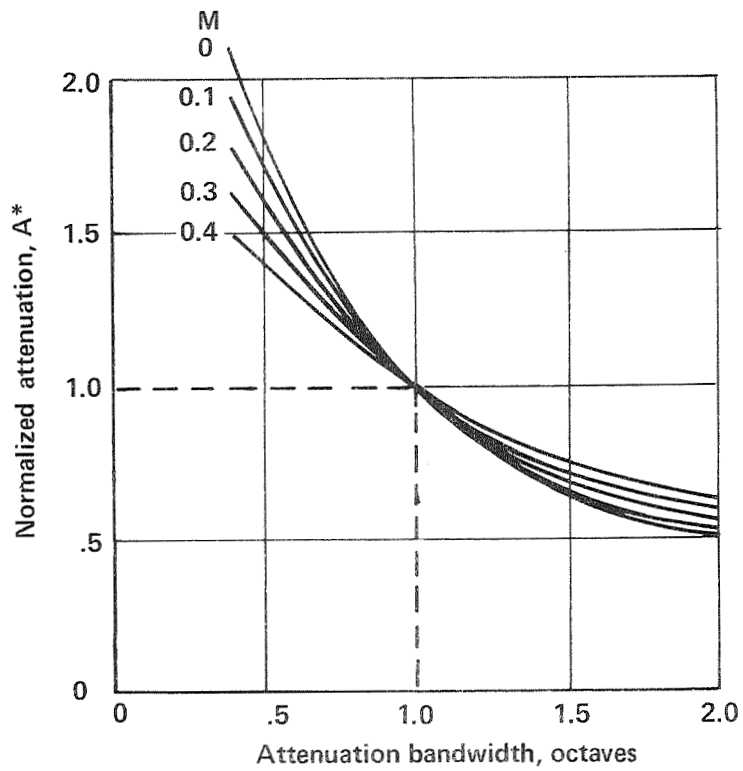


Figure 50.—Variation of Attenuation With Bandwidth and Airflow Mach Number in the Exhaust Mode

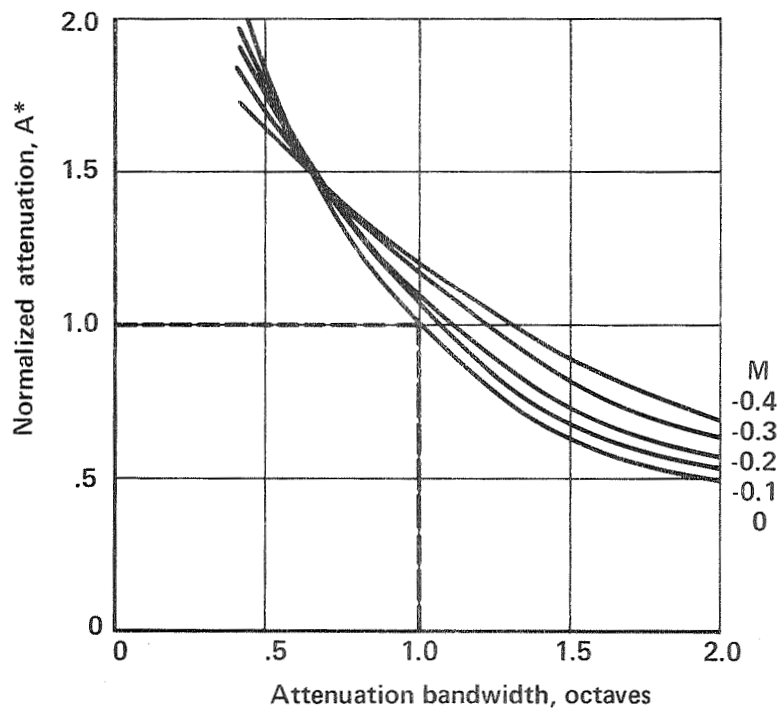


Figure 51.—Variation of Attenuation With Bandwidth and Airflow Mach Number in the Inlet Mode

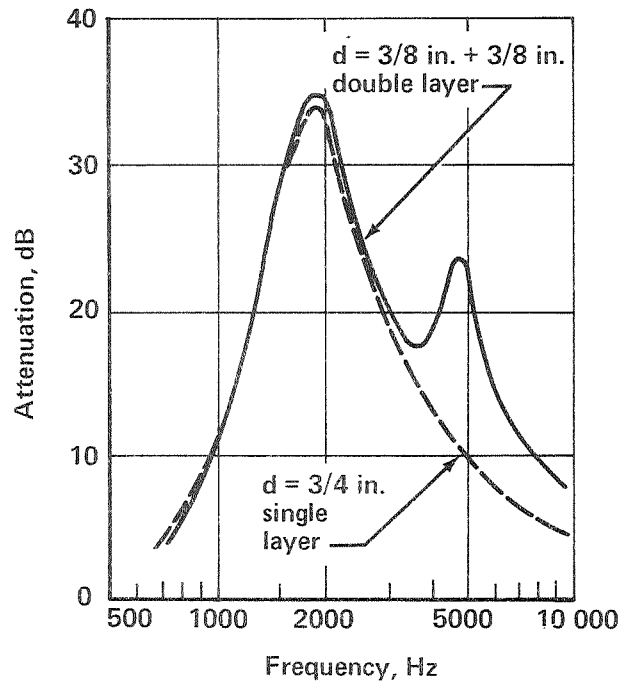


Figure 52.—Comparison of Attenuation Spectra of Typical Single- and Double-Layer Linings

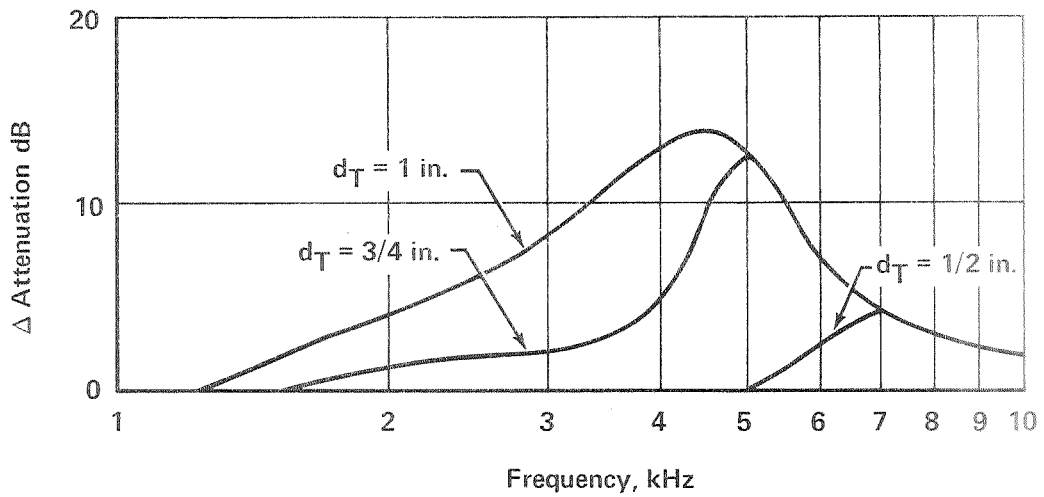


Figure 53.—Differences in Attenuation Between Double- and Single-Layer Linings of Equal Total Depth  $d_T$  in a 6-In. Duct at  $M = 0.28$



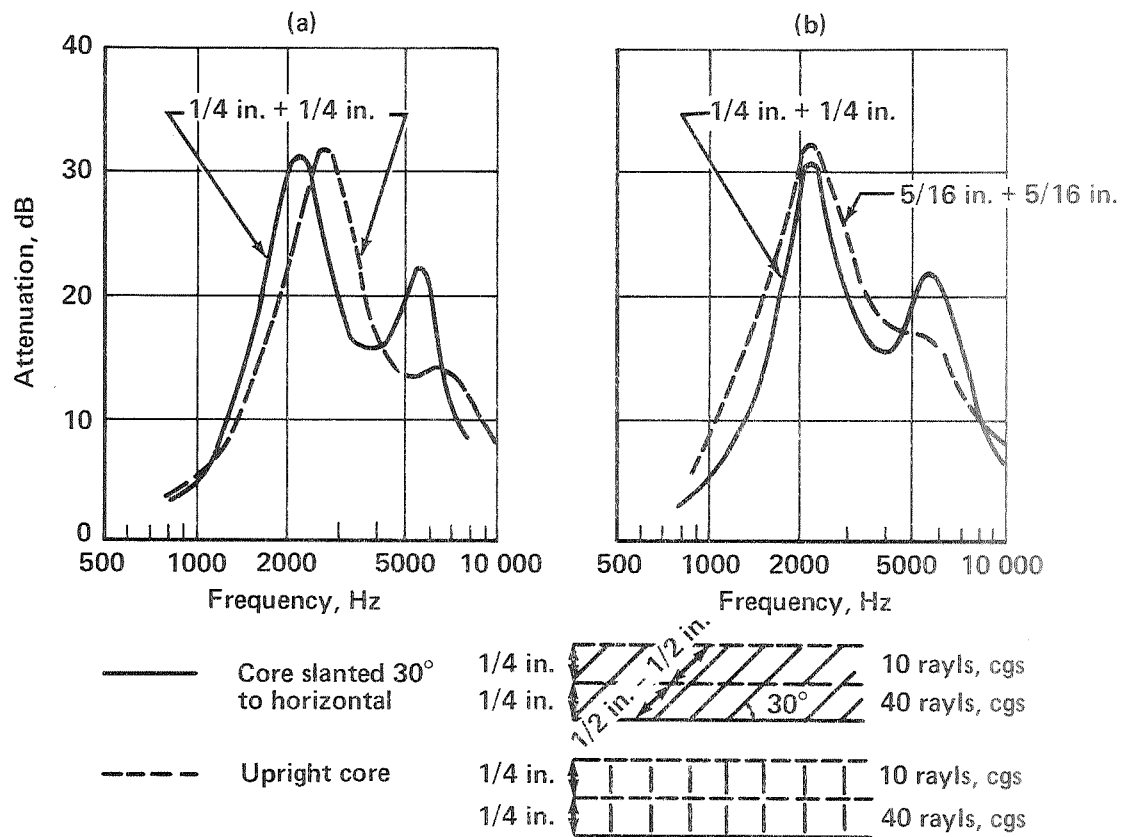


Figure 54.—Attenuation Spectra for Slanted and Upright Honeycomb Core Linings in a 6-in. Duct at  $M = 0.28$

Test No. \_\_\_\_\_  
 Duct geometry 6 x 10  
 Walls lined Two/10 in.  
 Lining length 22 in.

Lining material Polyimide  
 Flow resistance 10 + 40 rayls  
 Lining depth 1/4 in. + 1/4 in.  
 Core type 1/8-in. Hexcel, 30° slant

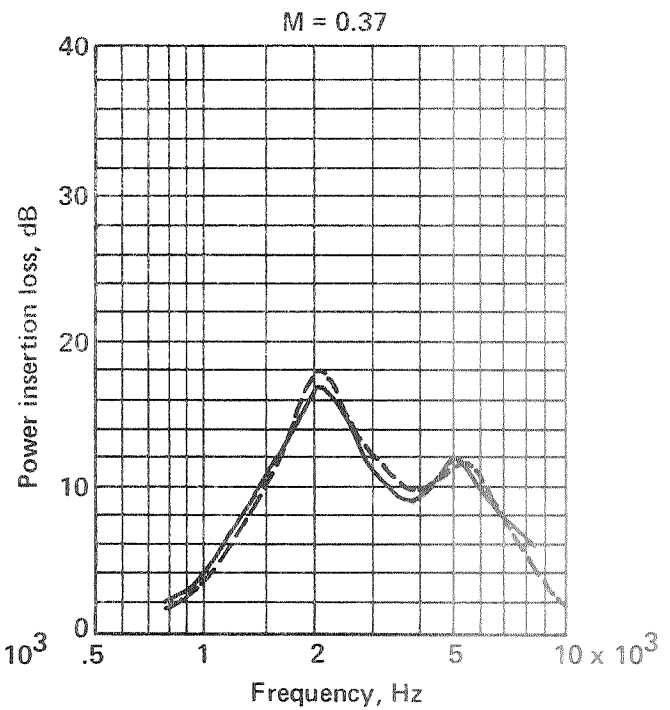
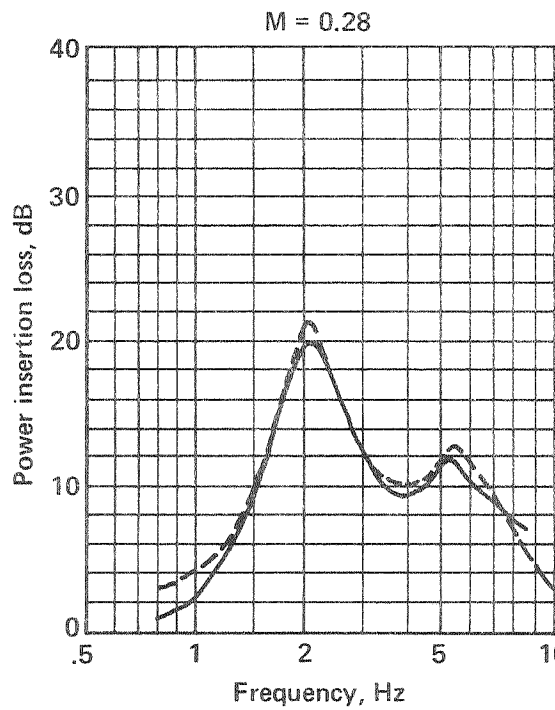
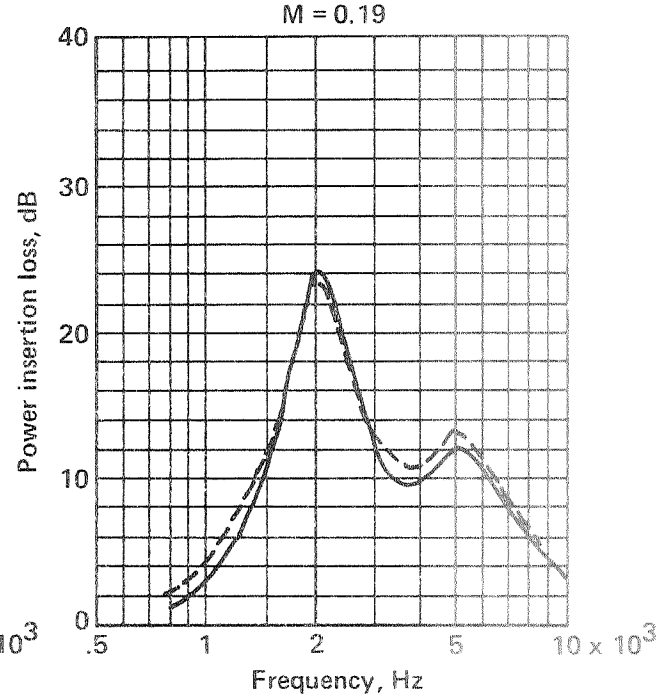
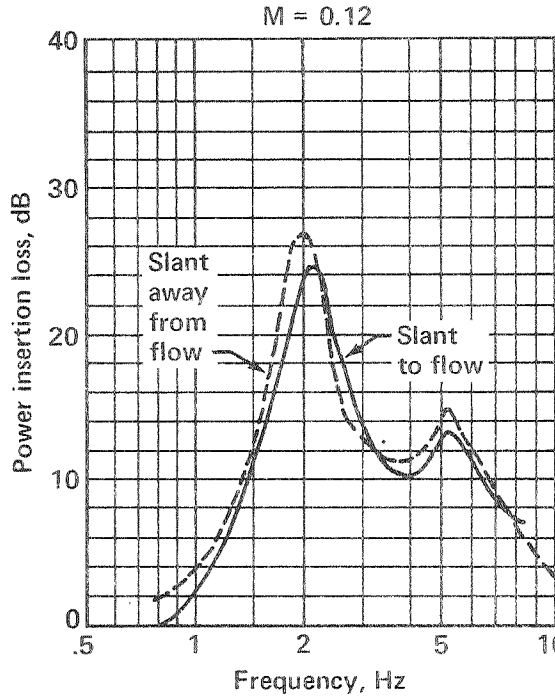


Figure 55.—Attenuation Spectra for Slanted Double-Layer Linings in a 6-In. Duct

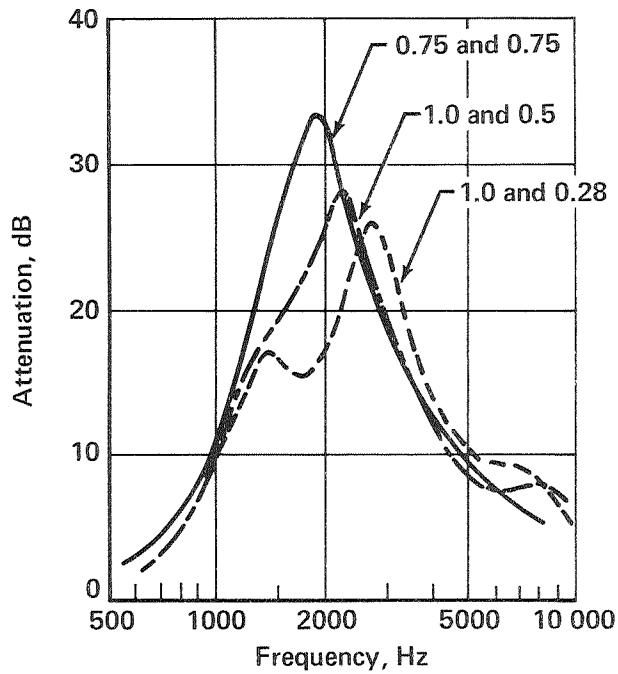


Figure 56.—Attenuation Spectra for Various Combinations of Single-Layer Lining Depths in a 6-In. Duct at  $M = 0.28$

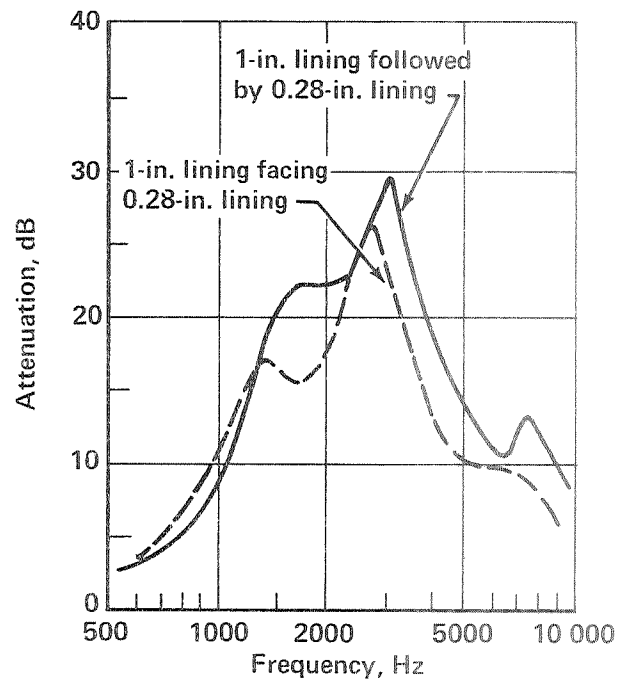
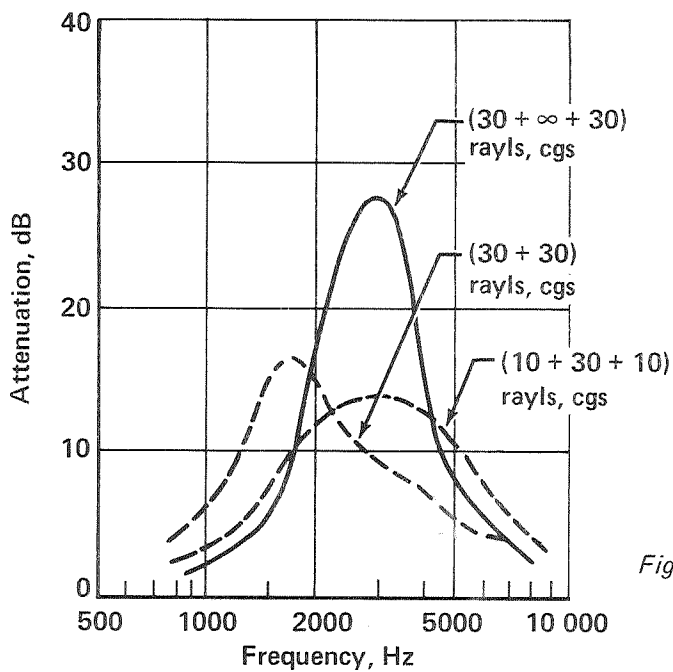


Figure 57.—Attenuation Spectra for Two Different Combinations of Single-Layer Linings of Equal Total Length in a 6-In. Duct at  $M = 0.28$

Figure 58.—Attenuation Spectra for Different Types of Duct Acoustic Splitters of the Same Total Thickness

Test No. \_\_\_\_\_  
 Duct geometry 6 x 10  
 Walls lined As shown  
 Lining length 22 in.

Lining material Polyimide  
 Flow resistance 30 rays  
 Lining depth 1/2 in.  
 Core type 3/8-in. Hexcel

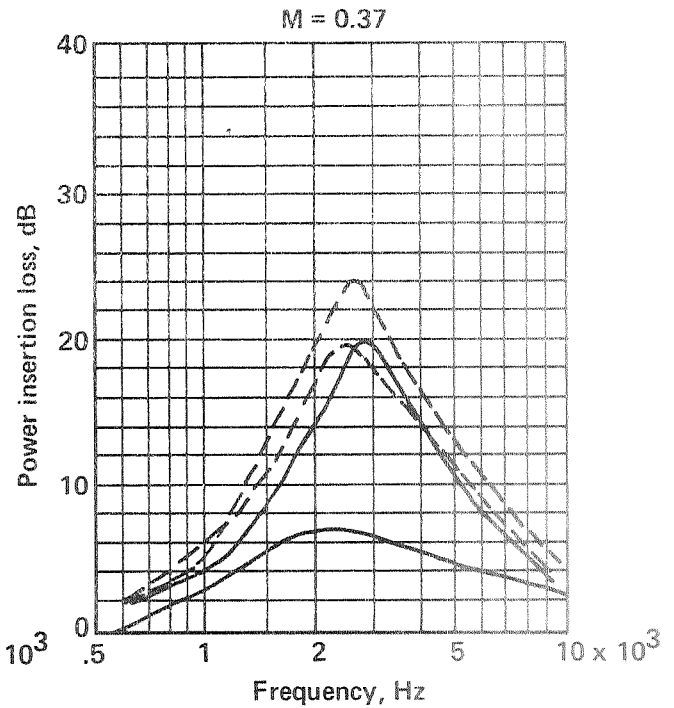
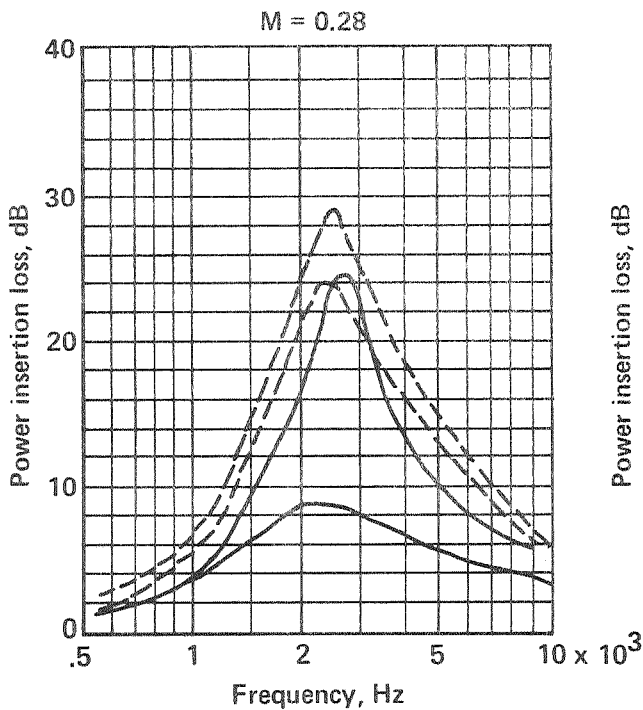
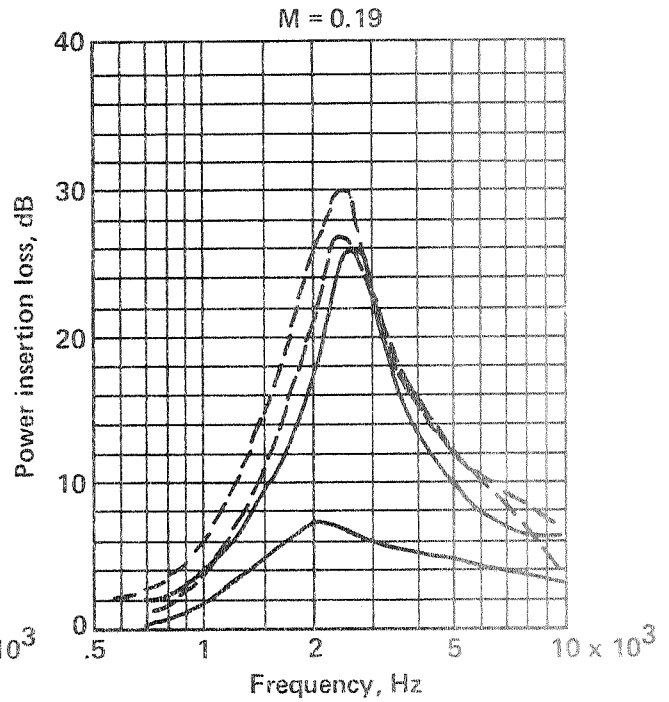
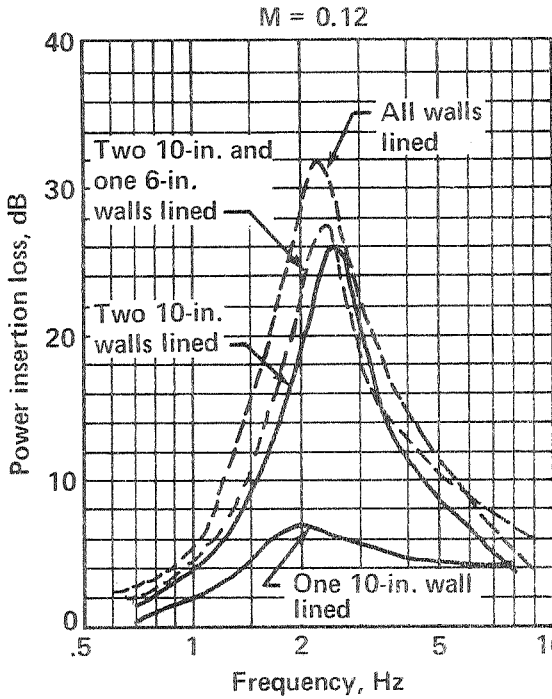


Figure 59.— Attenuation Spectra for Different Numbers of Walls Lined

Test No. \_\_\_\_\_  
 Duct geometry 6 x 10 in.  
 Walls lined Two/10 in.  
 Lining length 44 in.

Lining material As shown  
 Flow resistance As shown  
 Lining depth 1/2 in.  
 Core type As shown

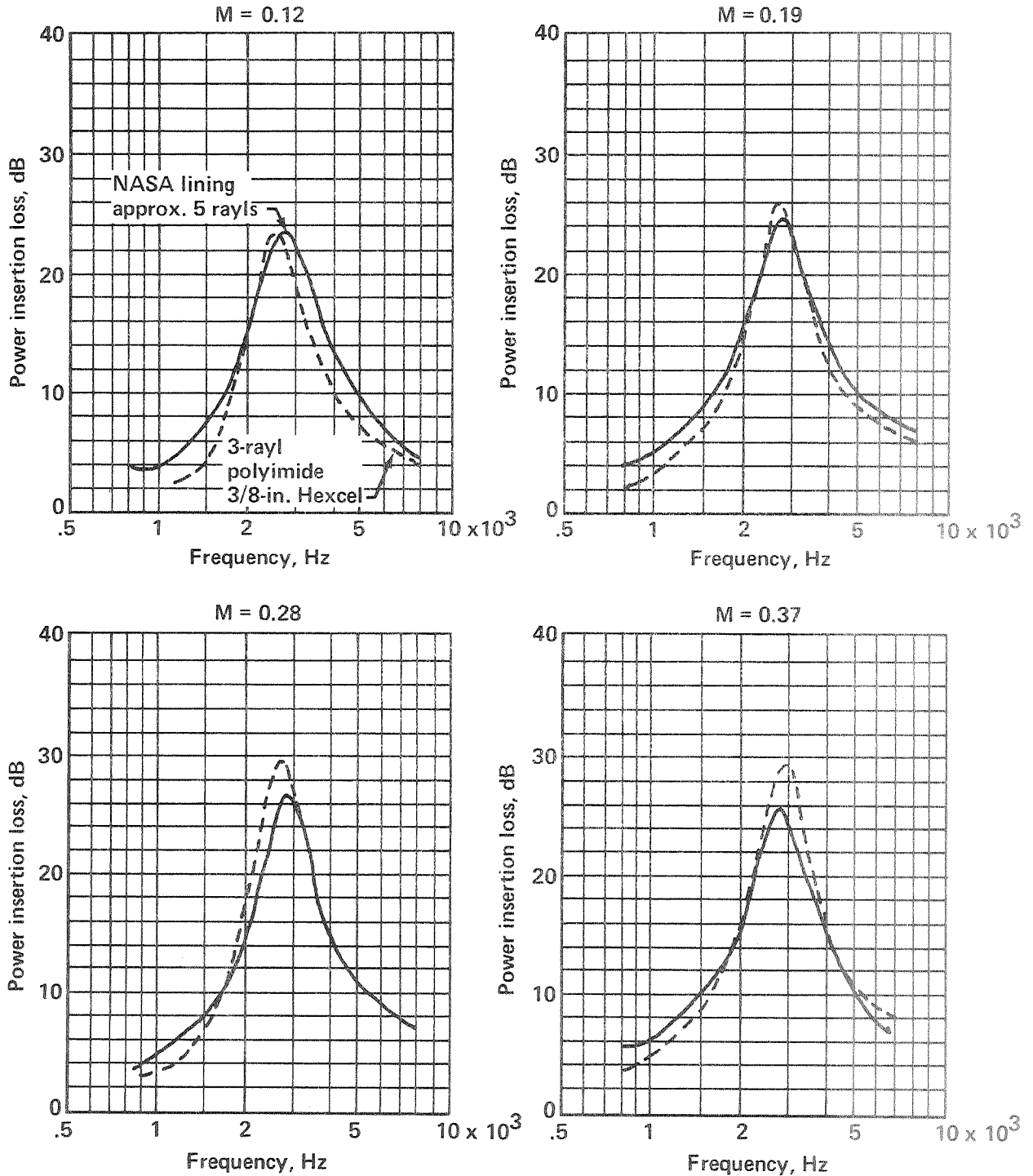


Figure 60.—Comparison of Acoustic Performance of NASA and Equivalent Polyimide Lining

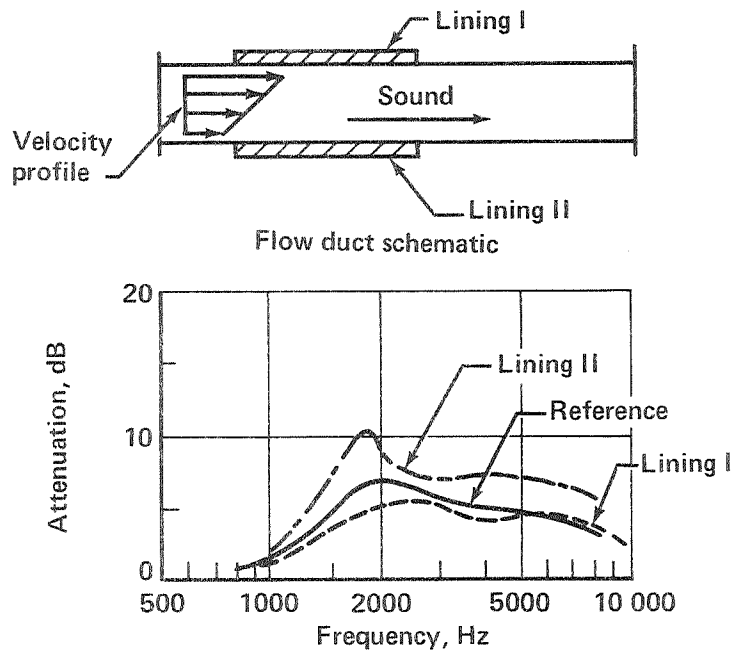


Figure 61.—Attenuation Spectra for a Fixed Length of 0.5-In.-Deep Lining Exposed to a Distorted Velocity Profile

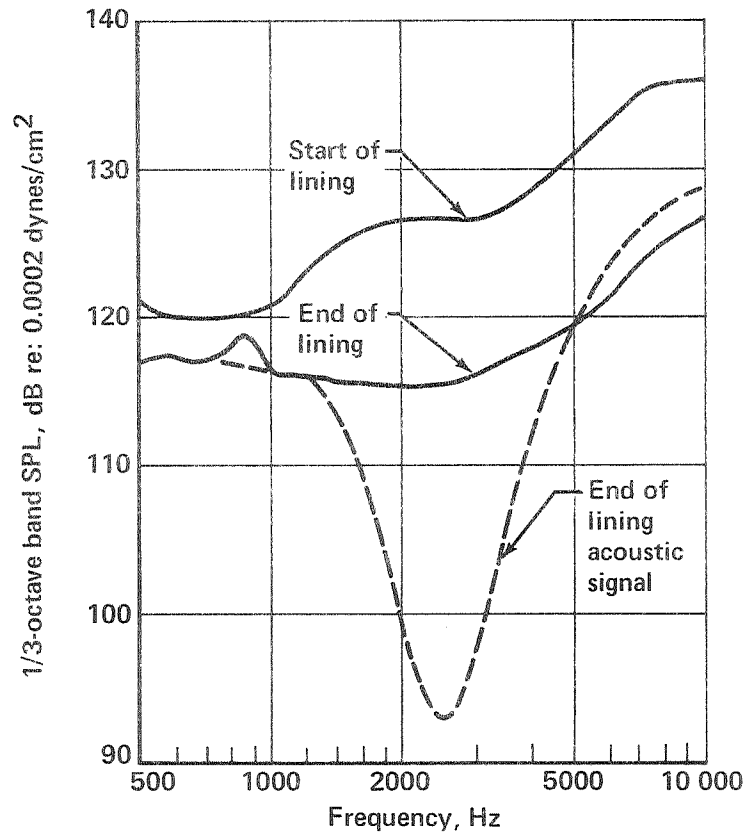


Figure 62.—Duct Wall Pressure Spectra as Measured by Flush-Mounted Microphones in a 6-In. Duct at  $M = 0.28$

## APPENDIX FLOW-DUCT TEST RESULTS

Reduced flow-duct test data in the form of power insertion loss (attenuation) spectra for a range of duct airflow Mach numbers are presented in this appendix. Table A-1, preceding the test data, summarizes all the figures for easy reference. The following additional comments will help to better understand certain blocks of data.

(1) The results shown in figures A-112 through A-115 represent identical lining configurations where the liner location inside the test section was varied in equal increments from fully forward in figure A-112 to fully aft in figure A-115.

(2) Figures A-191 through A-202 represent results obtained with flush-mounted microphones inside the test duct. The microphones were located at the beginning and end of various 44-in.-long liners. The tests recorded in figure A-197 were conducted with a siren noise source added to the regular broadband noise input.

(3) All of the results shown in this appendix represent the exhaust mode, except figures A-241 through A-263, which contain inlet mode data obtained in the Wichita flow-duct facility.





Table A-1.—Flow-Duct Test Program Data Listing

Figure number	Duct size, in.	Walls treated	Lining length, in.	Material	Number of layers	Nominal flow resistance, rayls	Core depth, in.	Core size, in.
A1	6 x 10	One/10	44	Polyimide	1	3	0.24	3/8
A2								
A3								
A4								
A5								
A6								
A7								
A8.								
A9								
A10								
A11								
A12								
A13								
A14								
A15								
A16								
A17								
A18								
A19								
A20								
A21								
A22								
A23								
A24								
A25								
A26								
A27								
A28								
A29								

Table A-1.—Continued

Figure number	Duct size, in.	Walls treated	Lining length, in.	Materials	Number of layers	Nominal flow resistance, rayls	Core depth, in.	Core size, in.	
A30	6 x 10	Two/10	22	Polyimide	1	70	0.5	3/8	
A31			44						110
A32									3
A33									9
A34									18
A35									30
A36									50
A37									70
A38		Two/10	44						110
A39		One/6	22						30
A40		One/10							
A41		Two/6							
A42		Two/6; One/10							
A43		Two/10; One/6							
A44		All	22						
A45	One/10	10							
A46	One/10	30							
A47	Two/10	10							
A48	Two/10	15							
A49	One/10	44							
A50	Two/10	22							
A51	Two/10	44							
A52	One/10								
A53									
A54									
A55									
A56	One/10	44							
A57	Two/10	22							
A58				Polyimide	1	3	1.0	3/8	

Table A-1.—Continued

Figure number	Duct size, in.	Walls treated	Lining length, in.	Material	Number of layers	Nominal flow resistance, rayls	Core depth, in.	Core size, in.	
A59	6 x 10	Two/10	22	Polyimide	1	9	0.9	3/8	
A60						18	0.98		
A61						30	1.0		
A62						50	1.0		
A63				22		70	1.0		
A64				44		3	1.0		
A65						9	0.9		
A66						18	0.98		
A67						30	1.0		
A68						50	1.0		
A69						70	1.0		
A70		Two/10			Polyimide		6		0.5
A71		One/10			Woven fiber		12		
A72							22		
A73							30		
A74							44		
A75		One/10		44			80		
A76	Two/10		22			6			
A77						12			
A78						22			
A79						30			
A80						44			
A81	Two/10		22	Woven fiber		80			
A82	One/10		44	Metallic felt		30			
A83	Two/10		22			30			
A84			44			30			
A85	One/10		44			35	0.5		
A86	Two/10		22	Metallic felt		35	0.57		
A87	One/10		44	Polyimide	1	30	0.5		

Table A-1. — Continued

Figure number	Duct size, in.	Walls treated	Lining length, in.	Material	Number of layers	Nominal flow resistance, rayls	Core depth, in.	Core size, in.
A88	6 x 10	Two/10	22	Polyimide	1	30	0.5	1/8
A89		Two/10	44		1	30	0.5	1/8
A90		One/10	22		1	30	0.5	1/2
A91		Two/10	44		2	10 + 40	1/4 + 1/4	1/2
A92		One/10	44		1	30	1/4 + 1/4	1 x 1
A93		Two/10	22		1	30	1/4 + 1/4	1 x 1
A94		Two/10	44		2	10 + 40	3/8 + 3/8	1 x 1
A95		One/10	44		1	30	3/8 + 3/8	1 x 1
A96		Two/10	22		2	10 + 40	3/8 + 3/8	3/8
A97		Two/10	44		1	30	1/2 + 1/4	↑
A98		One/10	44		1	30	1/2 + 1/4	
A99		Two/10	22		2	10 + 40	1/2 + 1/2	
A100		Two/10	44		1	30	1/2 + 1/2	
A101		Two/10	22		2	10 + 40	1/2 + 1/2	↑
A102		One/10	44		1	30	1/2 + 1/2	
A103		One/10	44		1	30	1/2 + 1/2	
A104	One/10	22	2	10 + 40	1/2 + 1/2			
A105	One/6	44	1	30	1/2 + 1/2			
A106	Two/10	44	1	30	1/2 + 1/2			
A107	Two/10	44	1	30	1/2 + 1/2			
A108	Two/6	44	1	30	1/2 + 1/2			
A109	Two/10	29.3	2	10 + 40	1/2 + 1/2			
A110	Two/10	22	1	30	1/2 + 1/2			
A111	Two/6	22	1	30	1/2 + 1/2			
A112	Two/10	14.7	1	30	1/2 + 1/2			
A113	Two/10	14.7	1	30	1/2 + 1/2			
A114	Two/10	14.7	1	30	1/2 + 1/2			
A115	One/10, Two/6	14.7	1	30	1/2 + 1/2			
A116	One/10, Two/6	44	2	10 + 40	1/2 + 1/2			

Table A-1.—Continued

Figure number	Duct size, in.	Walls treated	Lining length, in.	Material	Number of layers	Nominal flow resistance, rayls	Core depth, in.	Core size, in.	
A117	6 x 10	One/10; Two/6	22	Polyimide	2	10 + 40	1/2 + 1/2	3/8	
A118		All	22				10 + 40	1/2 + 1/2	
A119		All	44				10 + 40	1/2 + 1/2	
A120		One/10	44				10 + 40	1 + 1	
A121		Two/10	22				10 + 120	1 + 1	3/8
A122		Two/10	44				10 + 120	1 + 1	1/2
A123		One/10	44				10 + 120	1/4 + 1/2	1/2
A124		Two/10	22				10 + 140		1/2
A125		Two/10	44				10 + 140		3/8; 1/2
A126		One/10	44				10 + 140		3/8; 1/2
A127		Two/10	22				10 + 40	1/4 + 1/2	3/8; 1/2
A128		Two/10	44					1/4 + 1/4	1/8 (30°)
A129		One/10	44						
A130		Two/10	22						
A131			22						
A132		44							
A133	Two/10	44							
A134	One/10	44							
A135	Two/10	22							
A136	Two/10	44			10 + 40	1/4 + 1/4			
A137	One/10	44			10 + 20 + 20 + 20	1/8 + 1/8 + 1/8	1/8 (30°)		
A138	Two/10	22			10 + 20 + 20 + 20	1/8 + 1/8 + 1/8	3/8 (30°)		
A139	One/10	44			30	0.25	3/8 (30°)		
A140	One/10	22					3/8 (30°)		
A141	Two/10	44					3/8 (30°)		
A142	One/10	44					1/8 (30°)		
A143	One/10	44					1/8 (45°)		
A144	One/10	44					1/8 (60°)		
A145	Two/10	22		Polyimide	1	30	0.25	1/8 (30°)	

Table A-1.—Continued

Figure number	Duct size, in.	Walls treated	Lining length, in.	Material	Number of layers	Nominal flow resistance, rayls	Core depth, in.	Core size, in.	
A146	6 x 10	Two/10	22	Polyimide	1	30	0.25	1/8 (45°)	
A147			22						1/8 (60°)
A148			44						1/8 (30°)
A149			44						1/8 (45°)
A150			44						1/8 (60°)
A151		Two/10	44				1	30	3/8
A152		Splitter					1	30/30	
A153		Splitter					2	30/∞/30	
A154		Splitter					2	10/30/10	
A155		Two/10; Spt					2	30/30	1/2 + 1/2
A156		Two/10; Spt					2	30/∞/30	1/2 + 1/2
A157		Two/10; Spt					2	10/30/10	1/2 + 1/2
A158		One/10					1	30	0.5
A159		One/10				Polyimide	1	30	
A160		One/10				NASA-Met.	1	5	
A161		Two/10				NASA-Met.	1	5	0.5
A162		Two/10				Polyimide	1; 2	30; 10 + 40	1/2; 1/2 + 1/2
A163	One/10; Two/6				1; 2	30; 10 + 40	1/2; 1/2 + 1/2		
A164	Two/10; Two/6				1; 2	30; 10 + 40	3/8		
A165	Two/10		44		1	30	0.5; 0.28		
A166			22 + 22		1	30	0.5; 0.28		
A167			44		1	30	0.75; 0.28		
A168			44		1	30	1.0; 0.28		
A169			22 + 22		1	30	1.0; 0.28		
A170			44		1; 2	30; 10 + 40	0.28; 1/2 + 1/2		
A171			44; 22		1	30	1.0; 0.28		
A172	Two/10		44		1	30	1.0; 0.5		
A173	Test summary		22 + 22		1	30	1.0; 0.5		
A174	One/10		24	Polyimide	1	30	1.0; 0.5		
	S-bend duct			Metallic felt	1	30	0.5	3/8	
	6 x 10S							3/8	

Table A-1—Continued

Figure number	Duct size, in.	Walls treated	Lining length, in.	Material	Number of layers	Nominal flow resistance, rayls	Core depth, in.	Core size, in.
A175	6 x 10S	One/10	24	Metallic felt	1	30	0.5	3/8
A176		Two/10	24	Metallic felt	1	30	0.5	
A177			24 + 14.7	MF; PI	1; 2	30; 10 + 40	0.5; 1/2 + 1/2	
A178			14.7	Polyimide	2	10 + 40	1/2 + 1/2	
A179			24	Metallic felt	1	30	0.5	
A180			24 + 14.7	MF; PI	1; 2	30; 10 + 40	0.5; 1/2 + 1/2	
A181	6 x 10S	Two/10	14.7	Polyimide	2	10 + 40	1/2 + 1/2	3/8
A182	6 x 10	One/10	22	Woven fiber	1	30	0.5	Distorted airflow
A183		One/10	22	Woven fiber	1	30	0.5	
A184		Two/10	44; 22	Polyimide	1; 2	30; 4 + 25	1/2; 1/2 + 1/2	
A185			44		1	30	0.49	1700 Hz
A186							0.49	2500 Hz
A187							0.49	3600 Hz
A188							0.24	3600 Hz
A189							1.01	1700 Hz
A190							0.47	2500 Hz
A191							0.49	3/8
A192							0.49	
A193							0.5	
A194								
A195								
A196								
A197								
A198								
A199								
A200								
A201	6 x 10	Two/10						
A202	4 x 10	One/10						
A203			44	Polyimide	1	3	0.5	3/8

Table A-1.—Continued

Figure number	Duct size, in.	Walls treated	Lining length, in.	Material	Number of layers	Nominal flow resistance, rayls	Core depth, in.	Core size, in.
A204	4 x 10	One/10	44	Polyimide	1	9	0.5	3/8
A205		One/10	44					
A206	4 x 10	One/10	44	Polyimide	1	30	0.5	3/8
A207		Two/10	44					
A208	4 x 10	One/10	22	Polyimide	1	3	0.5	3/8
A209		Two/10	22					
A210	4 x 10	One/10	22	Polyimide	1	9	0.5	3/8
A211		Two/10	22					
A212	4 x 10	One/10	22	Polyimide	1	18	0.5	3/8
A213		Two/10	22					
A214	4 x 10	One/10	22	Polyimide	1	30	0.5	3/8
A215		Two/10	22					
A216	4 x 10	One/10	44	Polyimide	1	30	0.28	3/8
A217		One/10	44					
A218	4 x 10	One/10	44	Polyimide	1	30	0.75	3/8
A219		Two/10	44					
A220	4 x 10	One/10	22	Polyimide	1	50	1.0	3/8
A221		Two/10	22					
A222	4 x 10	One/10	22	Polyimide	1	30	0.28	3/8
A223		Two/10	22					
A224	4 x 10	One/10	44	Polyimide	1	30	0.5	3/8
A225		Two/10	44					
A226	4 x 10	One/10	44	Polyimide	1	30	0.5	3/8
A227		Two/10	44					
A228	4 x 10	One/10	44	Woven fiber	1	30	0.5	3/8
A229		Two/10	44					
A230	4 x 10	One/10	44	Woven fiber	1	30	0.5	3/8
A231		Two/10	44					
A232	4 x 10	One/10	22	Metallic felt	1	30	0.5	3/8
A232		Two/10	44					
A232	4 x 10	One/10	44	Metallic felt	2	10 + 40	3/8 + 3/8	3/8
A232		Two/10	44					



Table A-1.—Concluded

Figure number	Duct size, in.	Walls treated	Lining length, in.	Material	Number of layers	Nominal flow resistance, rayls	Core depth, in.	Core size, in.
A233	4 x 10	Two/10	22	Polyimide	2	10 + 40	3/8 + 3/8	3/8
A234		One/10	44		2	10 + 40	1/2 + 1/2	
A235		Two/10	14.7		2	10 + 40	1/2 + 1/2	
A236		Two/10	22		1	30	1; 0.5	
A237		Two/10	22		1	30	1; 0.28	
A238		One/7	44		2	10 + 40	1/2 + 1/2	
A239		Two/7			1	30	0.5	
A240		All			2	10 + 40	1/2 + 1/2	
A241		One/10			1	3	0.5	
A242						9		
A243	6 x 7							
A244								
A245								
A246								
A247								
A248								
A249								
A250								
A251								
A252								
A253	6 x 10	Two/10	22	Polyimide	2	10 + 40	3/8 + 3/8	3/8
A254		Two/10	44		2	10 + 40	1/2 + 1/2	
A255		Two/10	22		1	30	1; 0.5	
A256		One/10	44		2	10 + 40	1/2 + 1/2	
A257		One/10			1	3	0.5	
A258		One/10				9		
A259		Two/10				18		
A260						30		
A261						70		
A262						3		
A263				9				

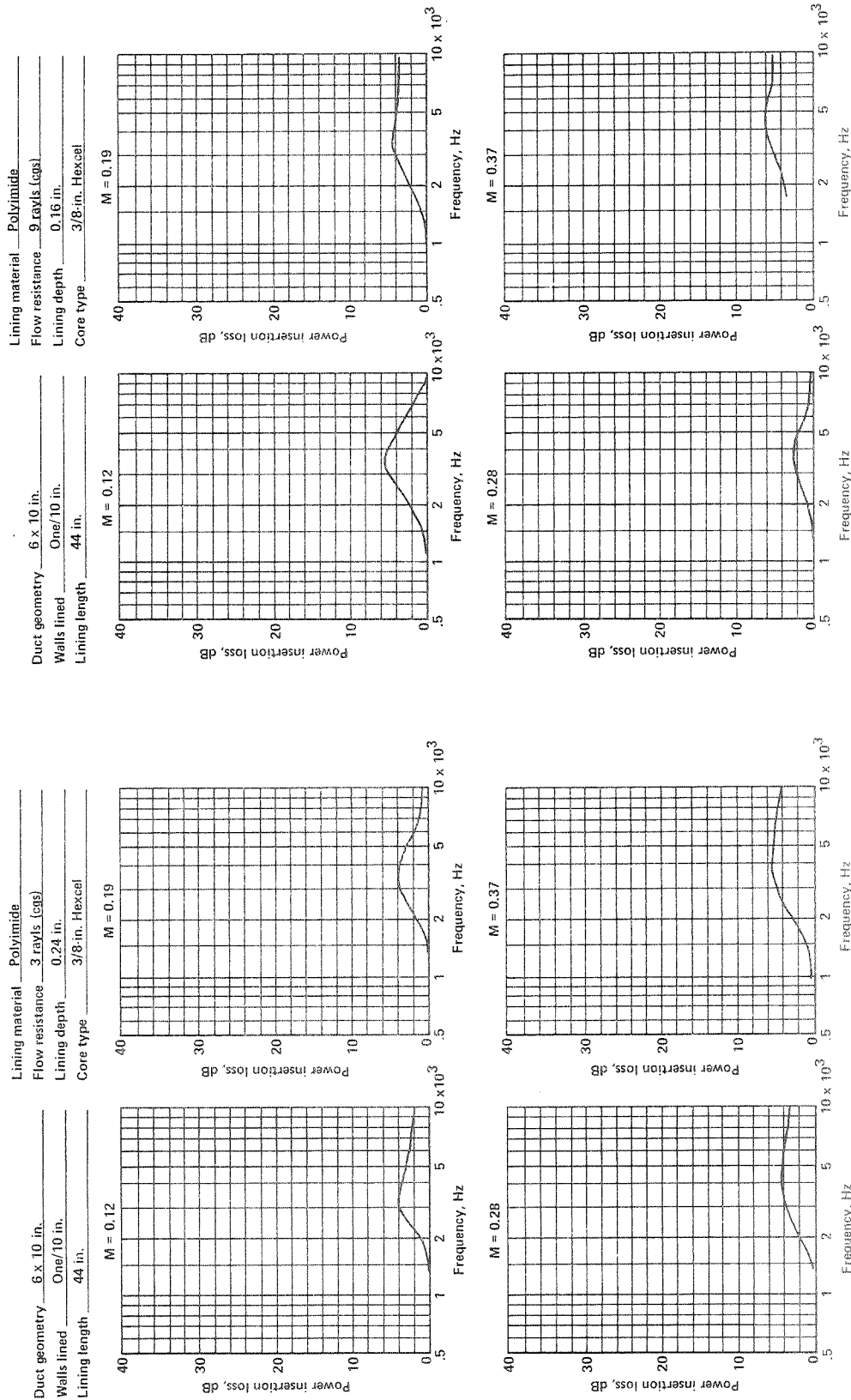


Figure A-1.

Figure A-2.

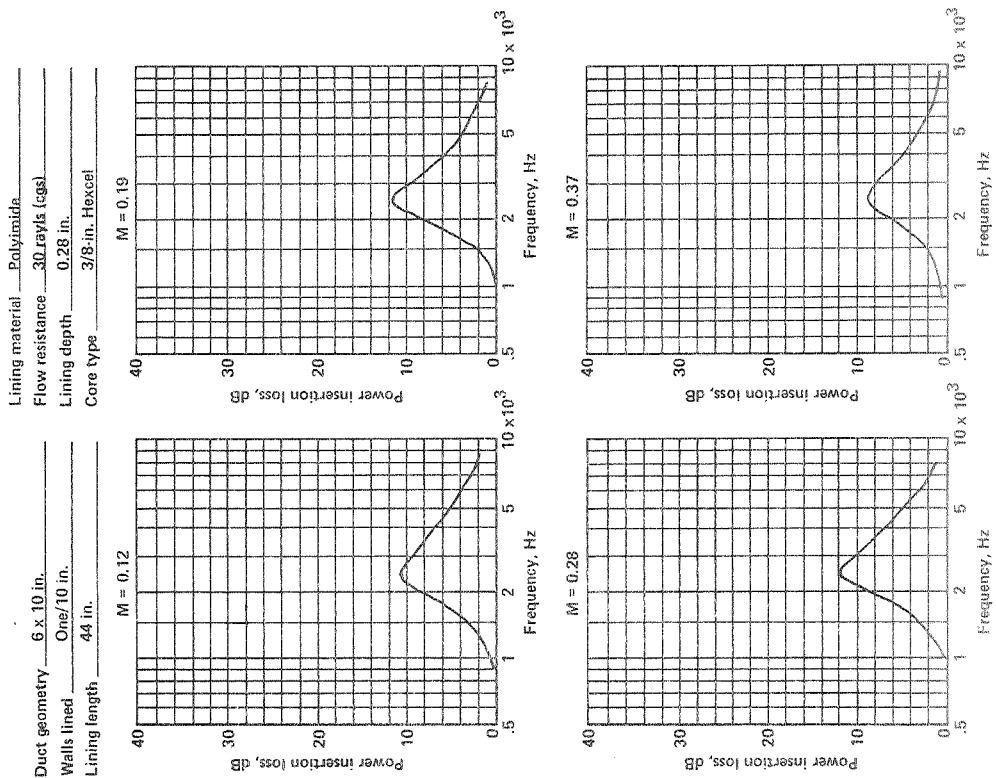


Figure A-4.

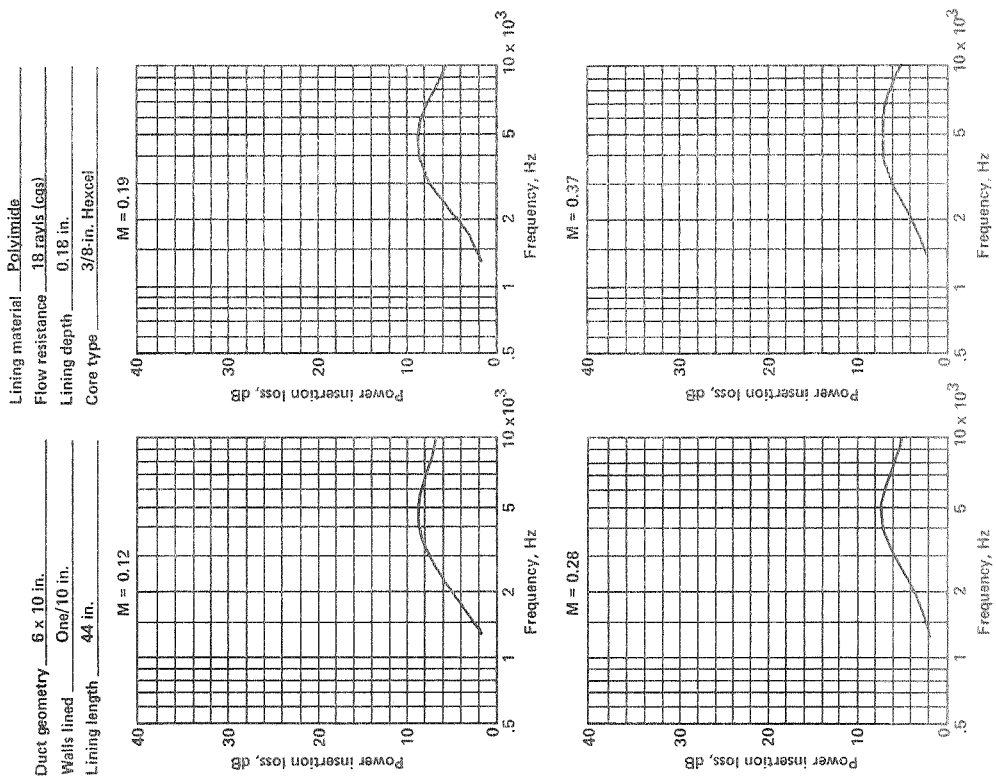


Figure A-3.

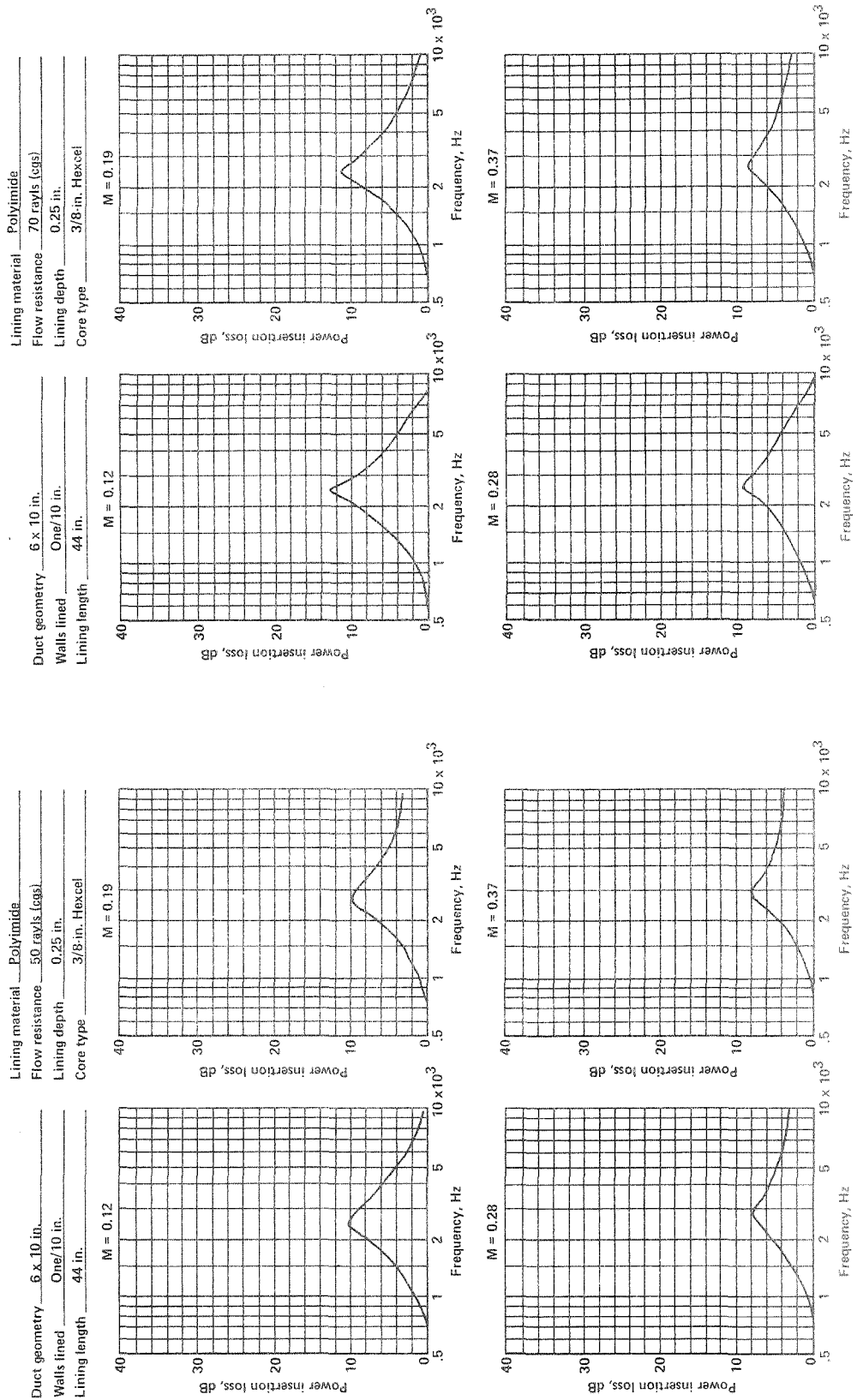


Figure A-5.

Figure A-6.

Lining material Polyimide  
 Flow resistance 9 rays (cgs)  
 Lining depth 0.16 in.  
 Core type 3/8-in. Hexcel

Duct geometry 6 x 10 in.  
 Walls lined Two/10 in.  
 Lining length 22 in.

Lining material Polyimide  
 Flow resistance 3 rays (cgs)  
 Lining depth 0.24 in.  
 Core type 3/8-in. Hexcel

Duct geometry 6 x 10 in.  
 Walls lined Two/10 in.  
 Lining length 22 in.

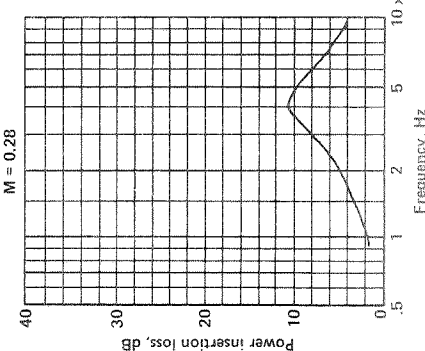
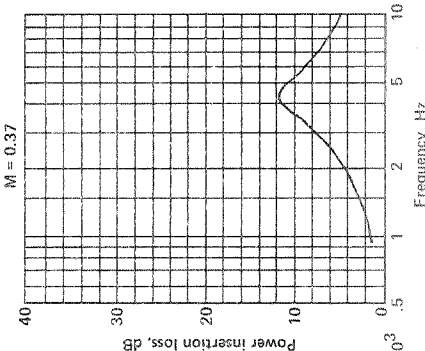
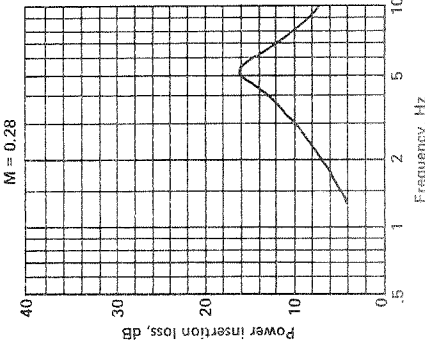
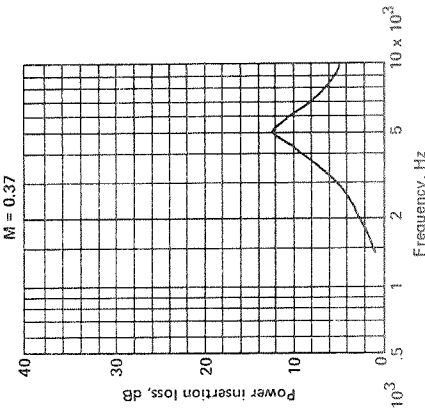
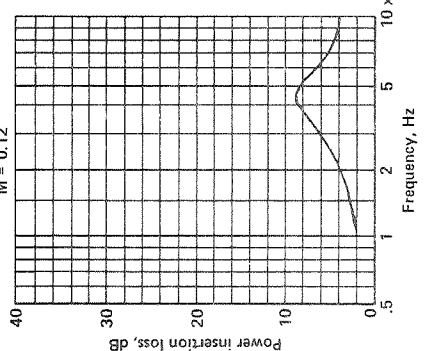
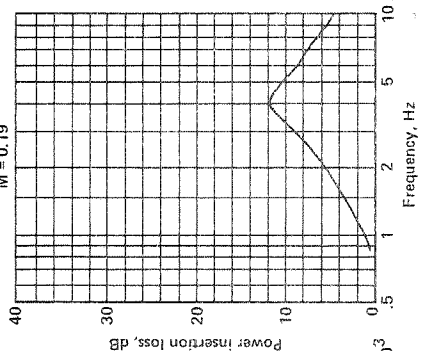
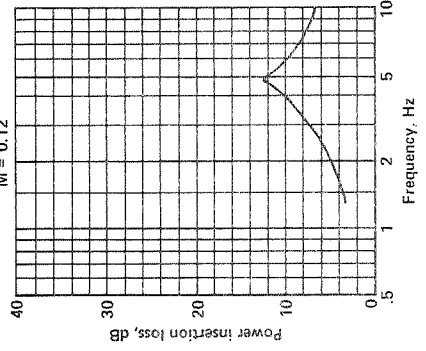
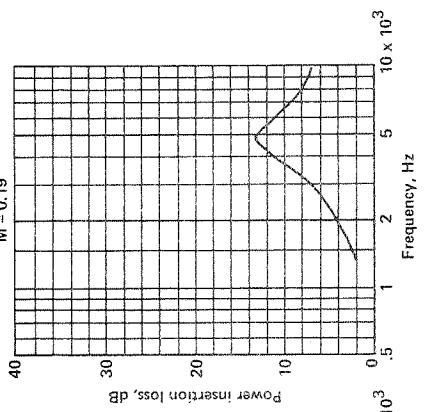


Figure A-8.

Figure A-7.

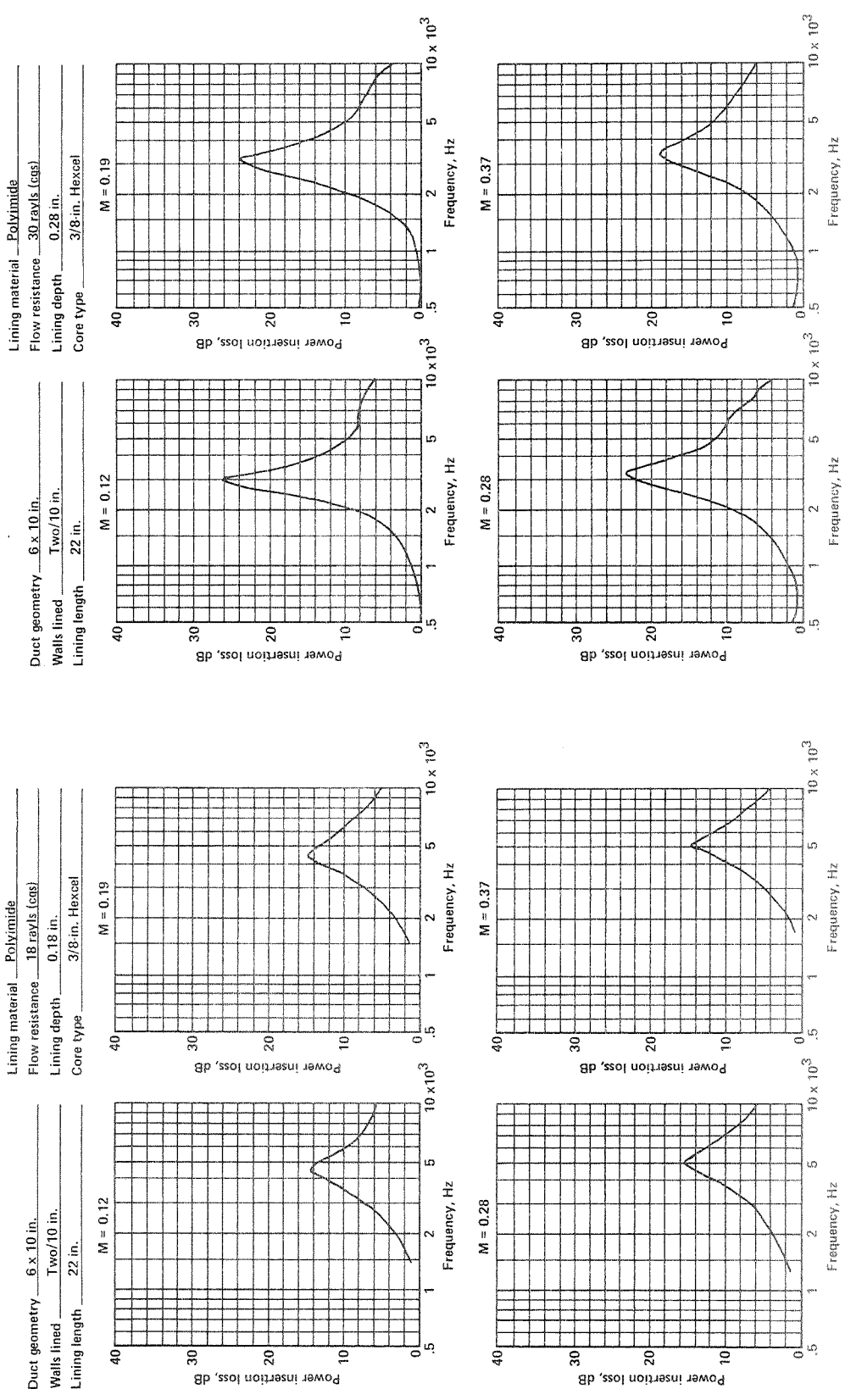


Figure A-9.

Figure A-10.

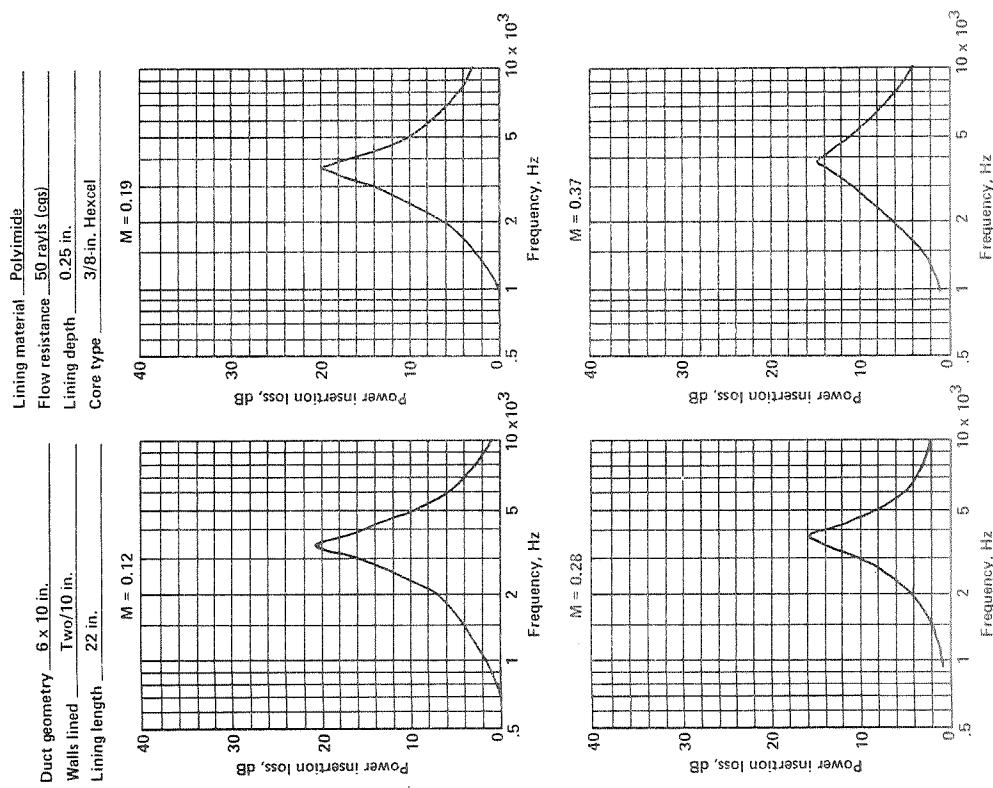
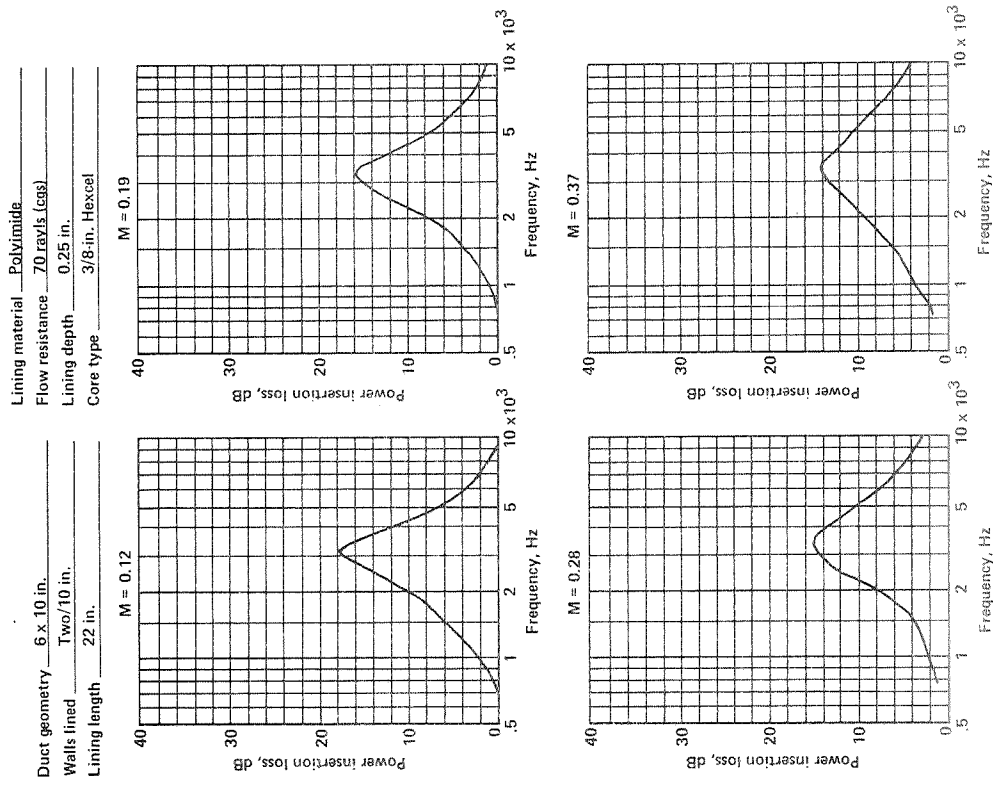


Figure A-12.

Figure A-11.

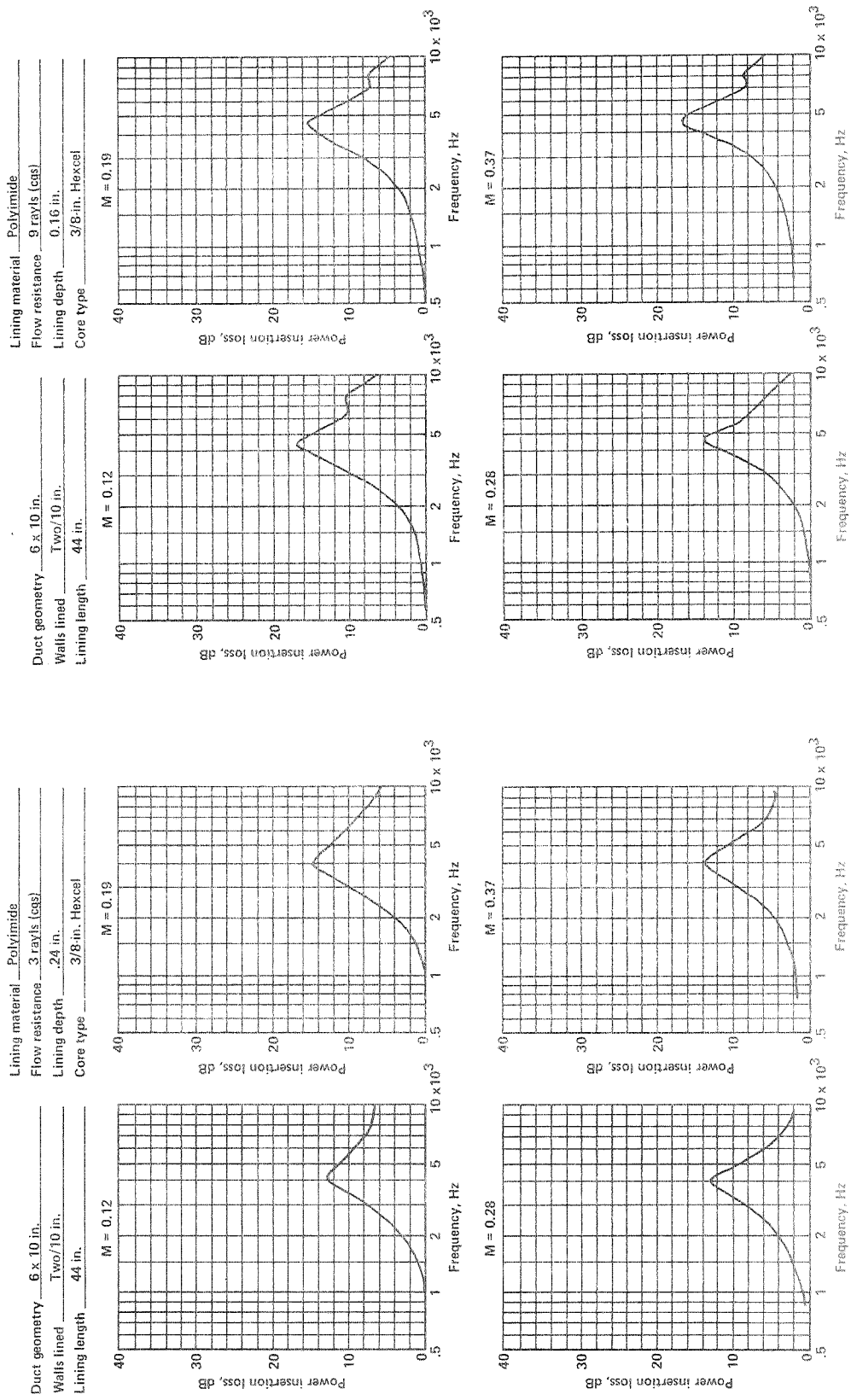


Figure A-14.

Figure A-13.



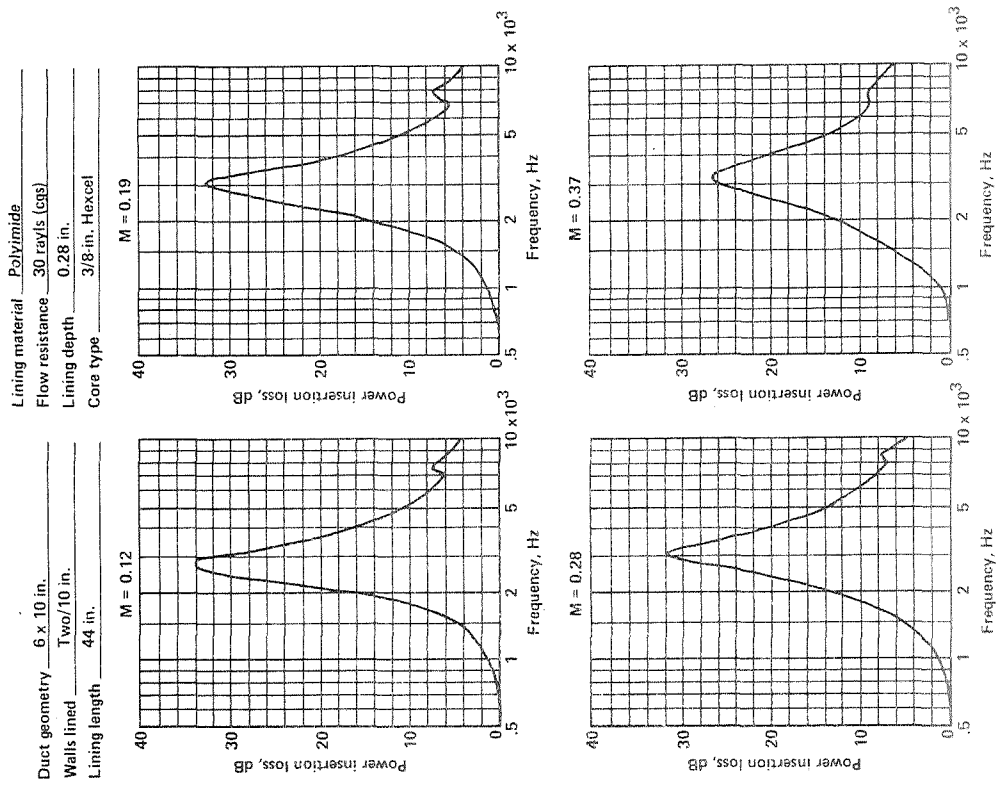


Figure A-16.

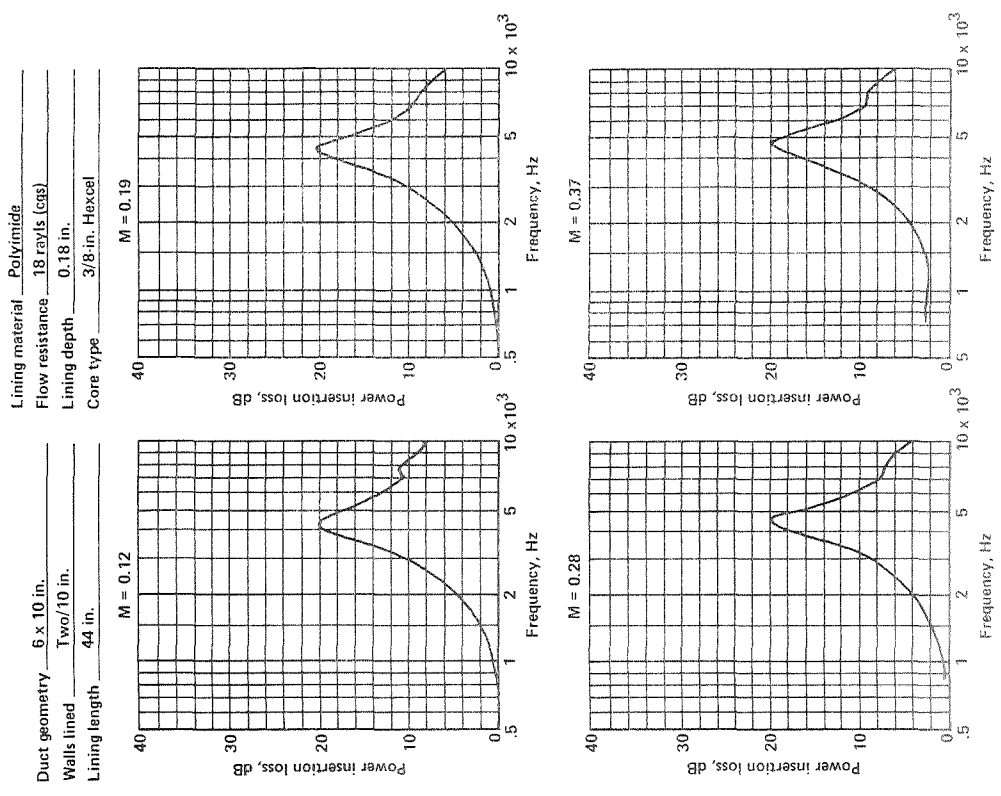


Figure A-15.

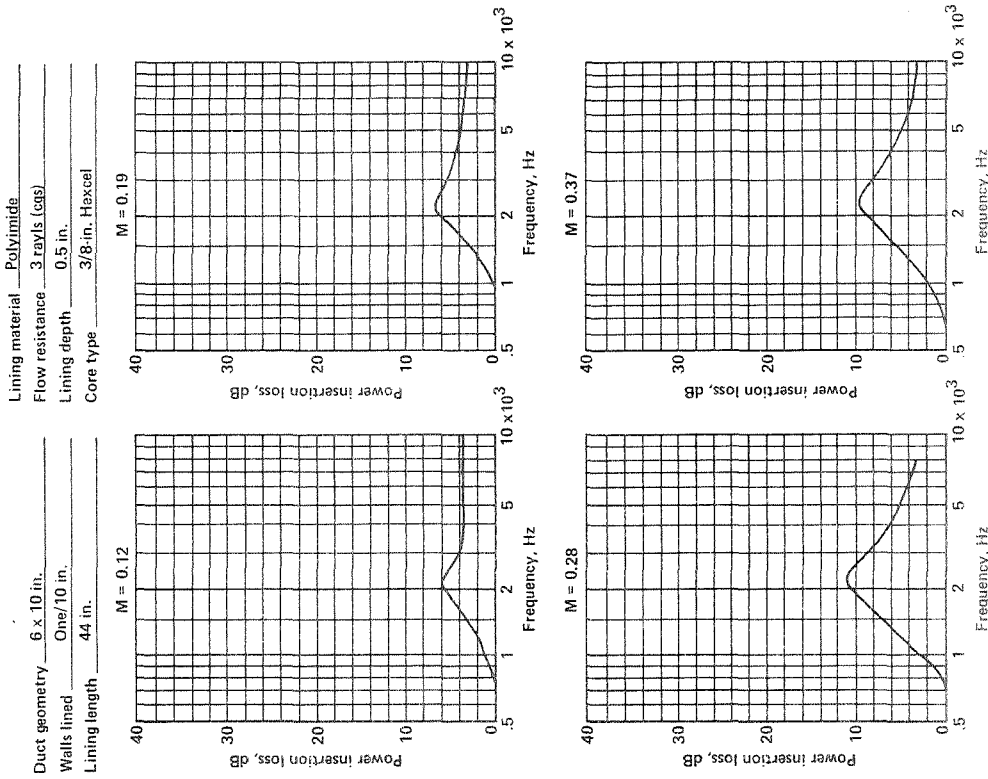


Figure A-18.

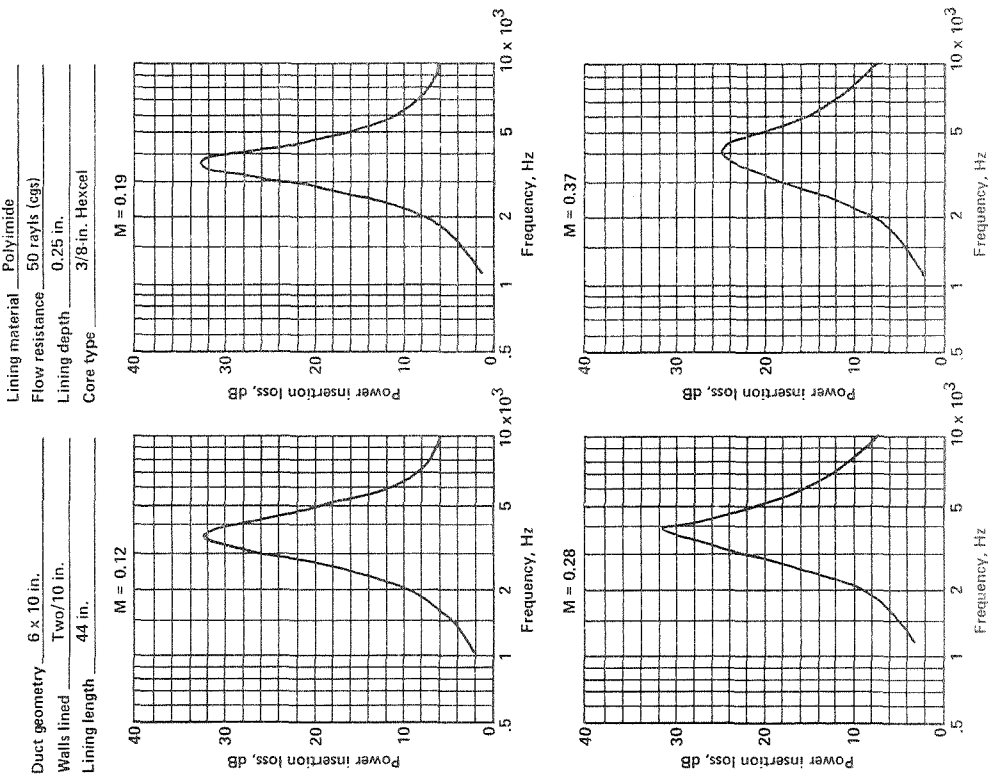


Figure A-17.

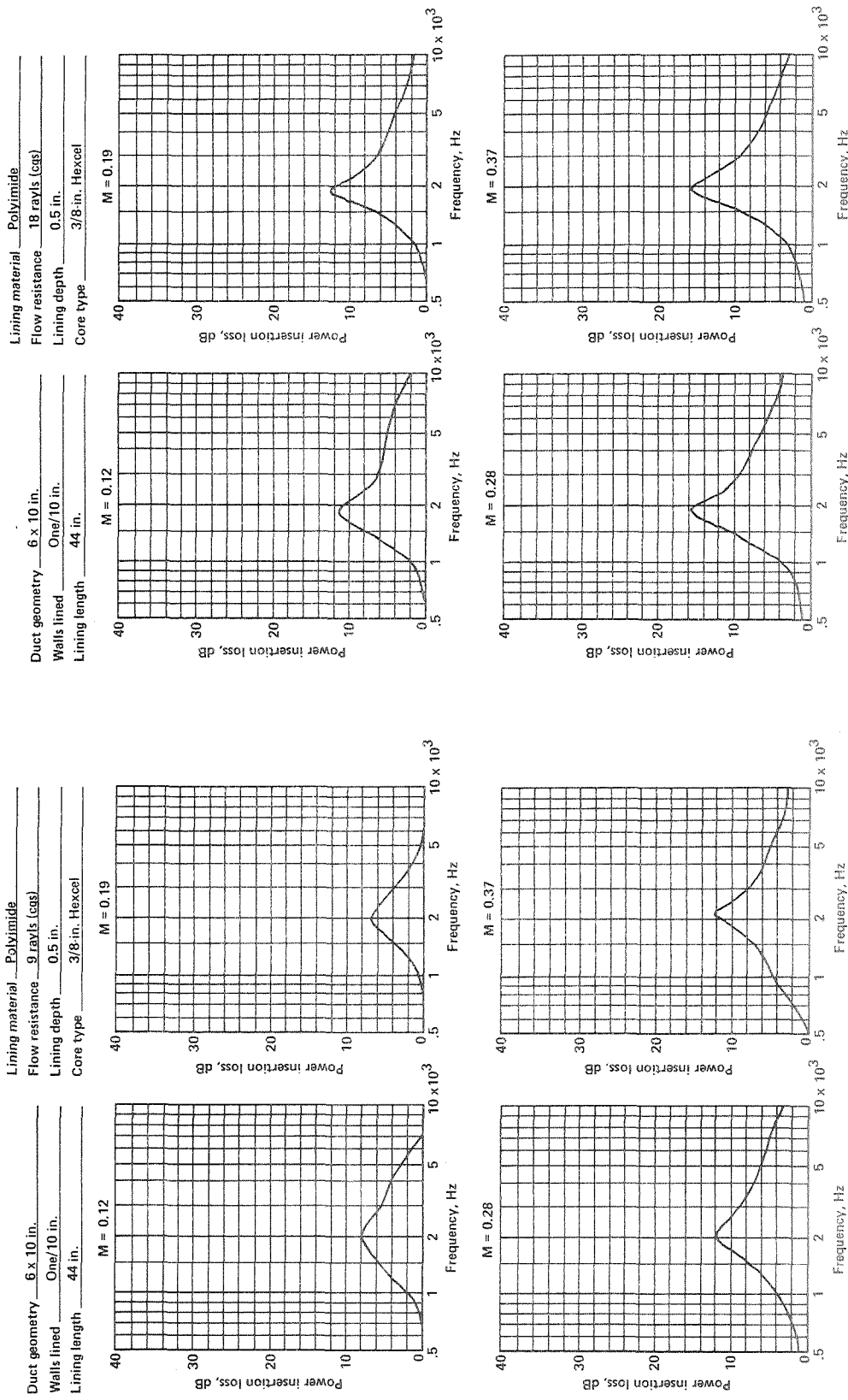


Figure A-19.

Figure A-20.

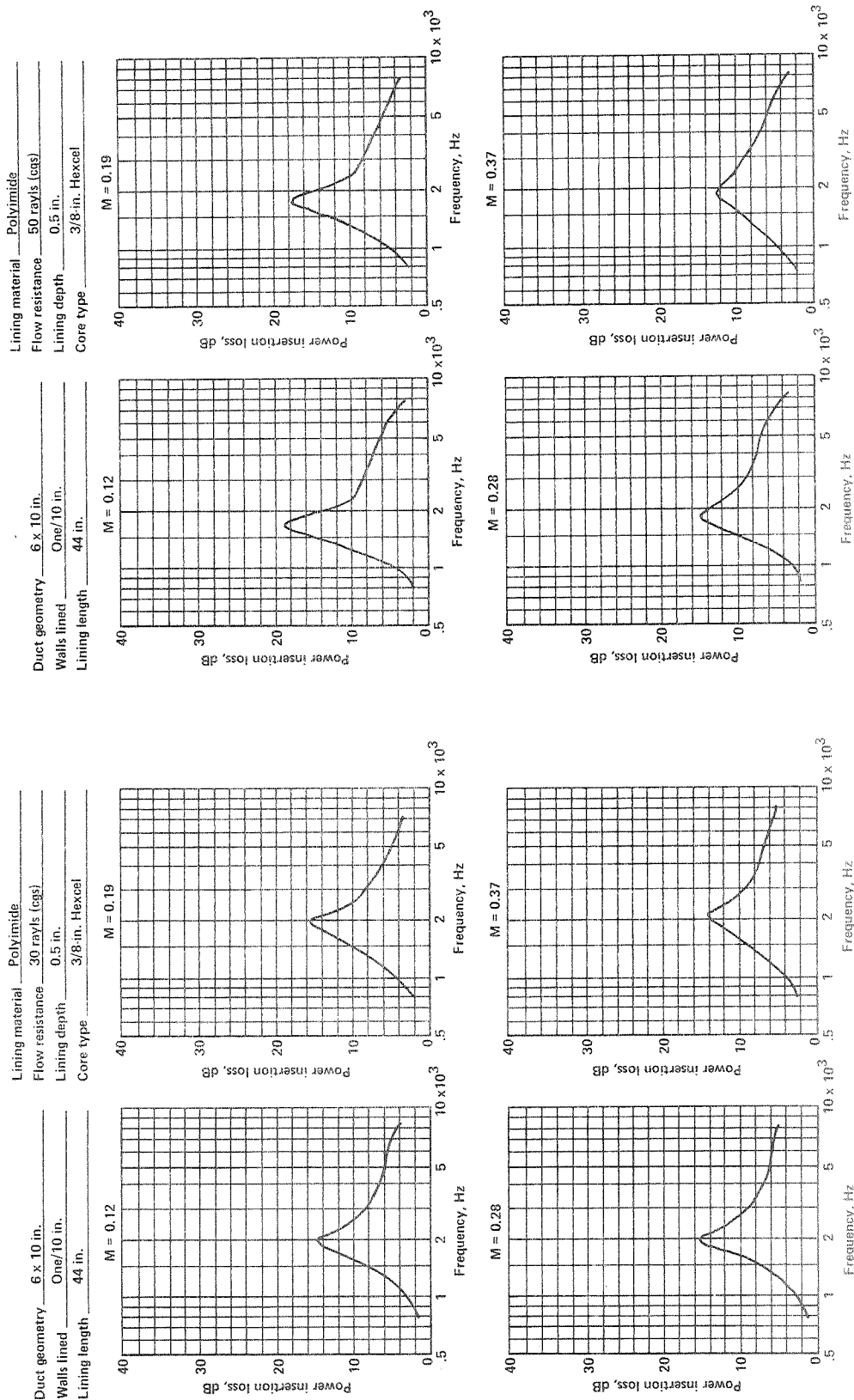


Figure A-21.

Figure A-22.

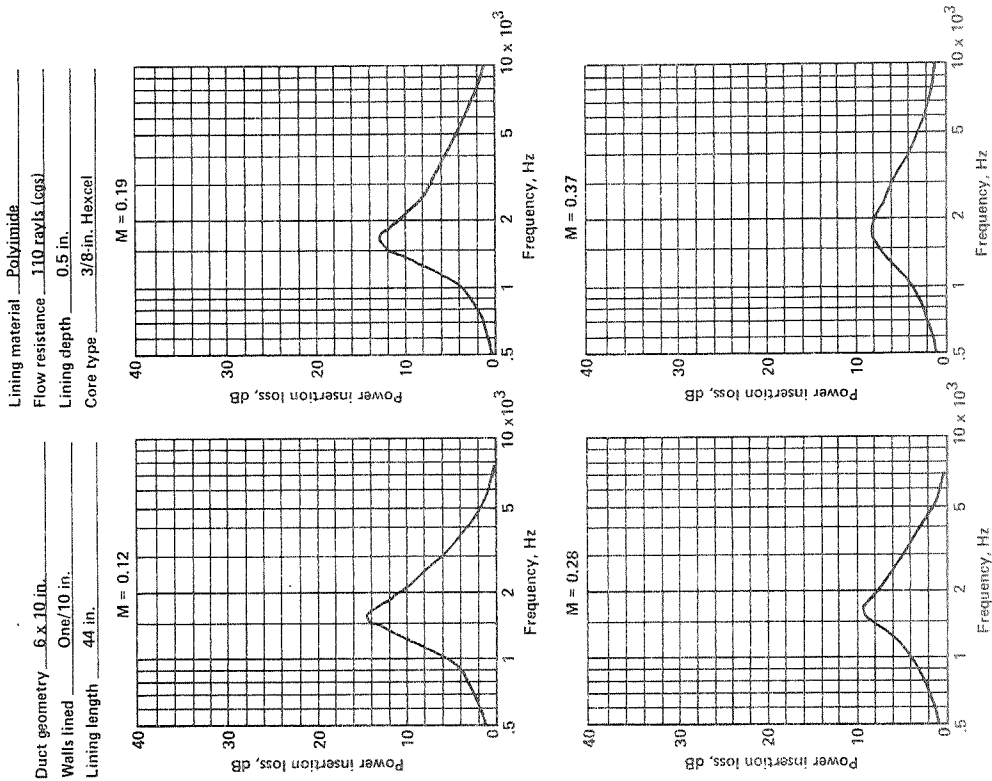


Figure A-24.

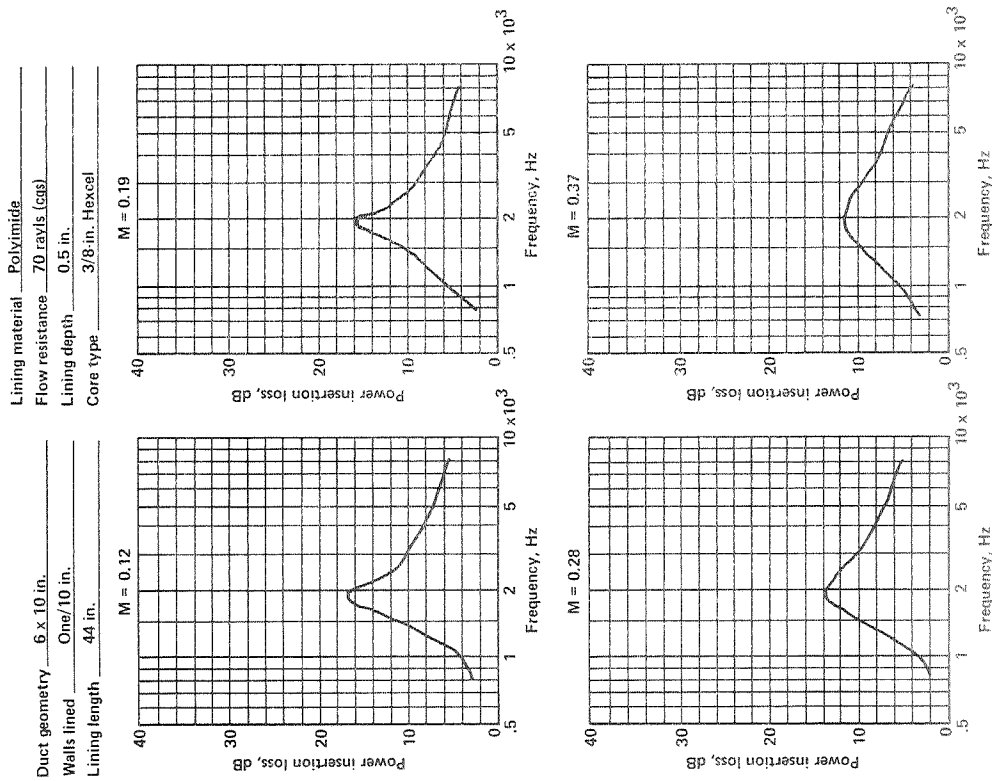


Figure A-23.

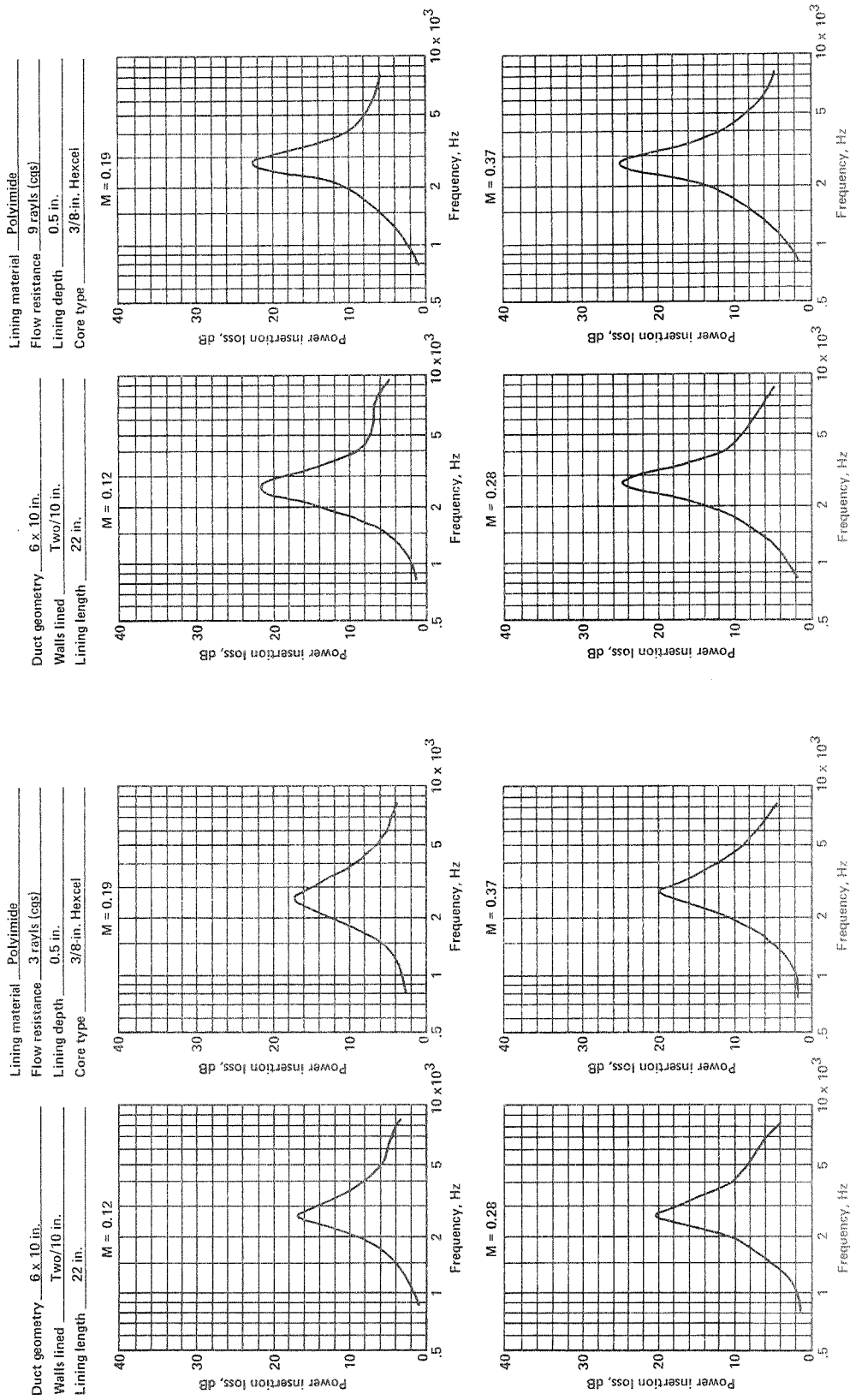


Figure A-26.

Figure A-25.

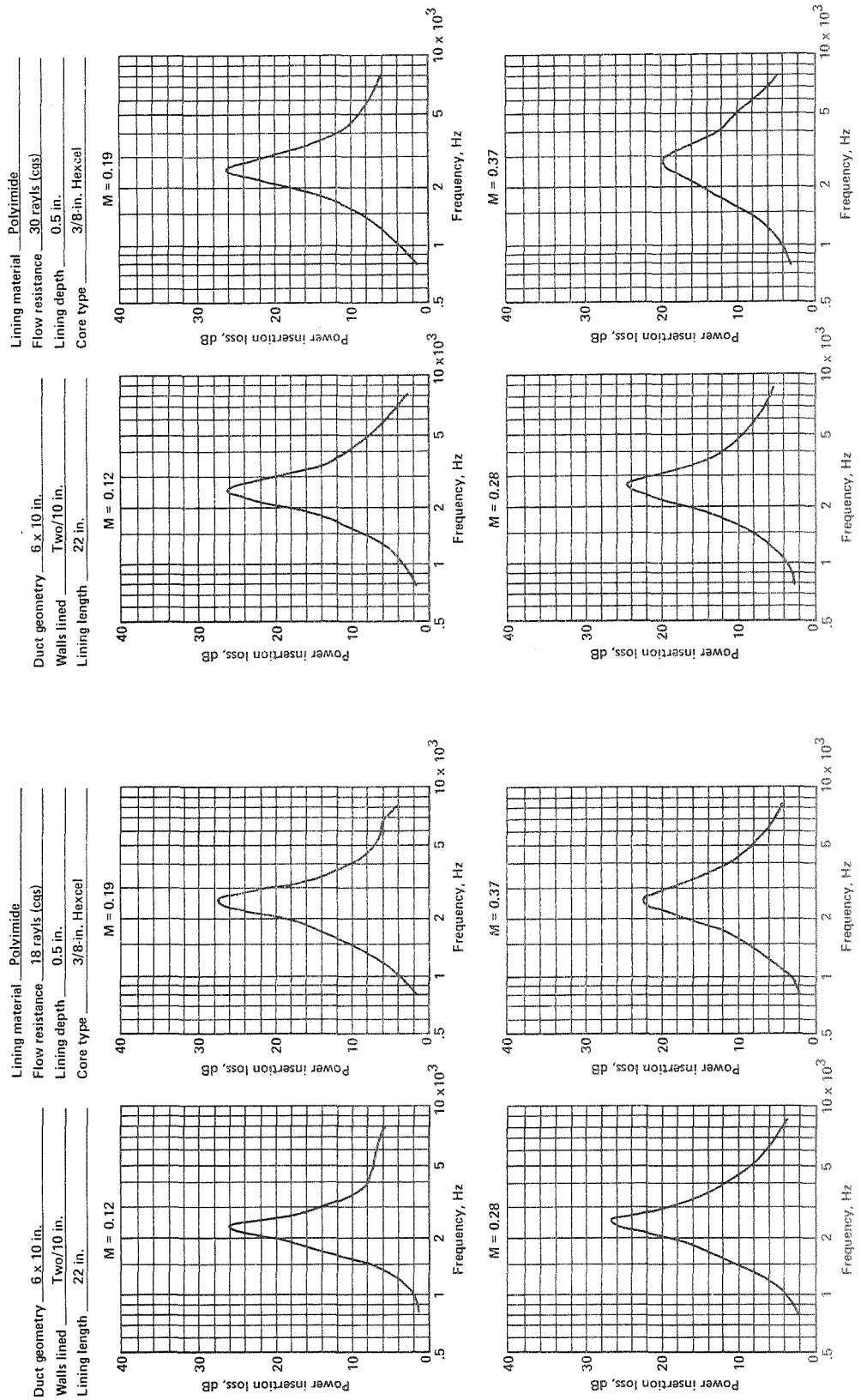


Figure A-27.

Figure A-28.

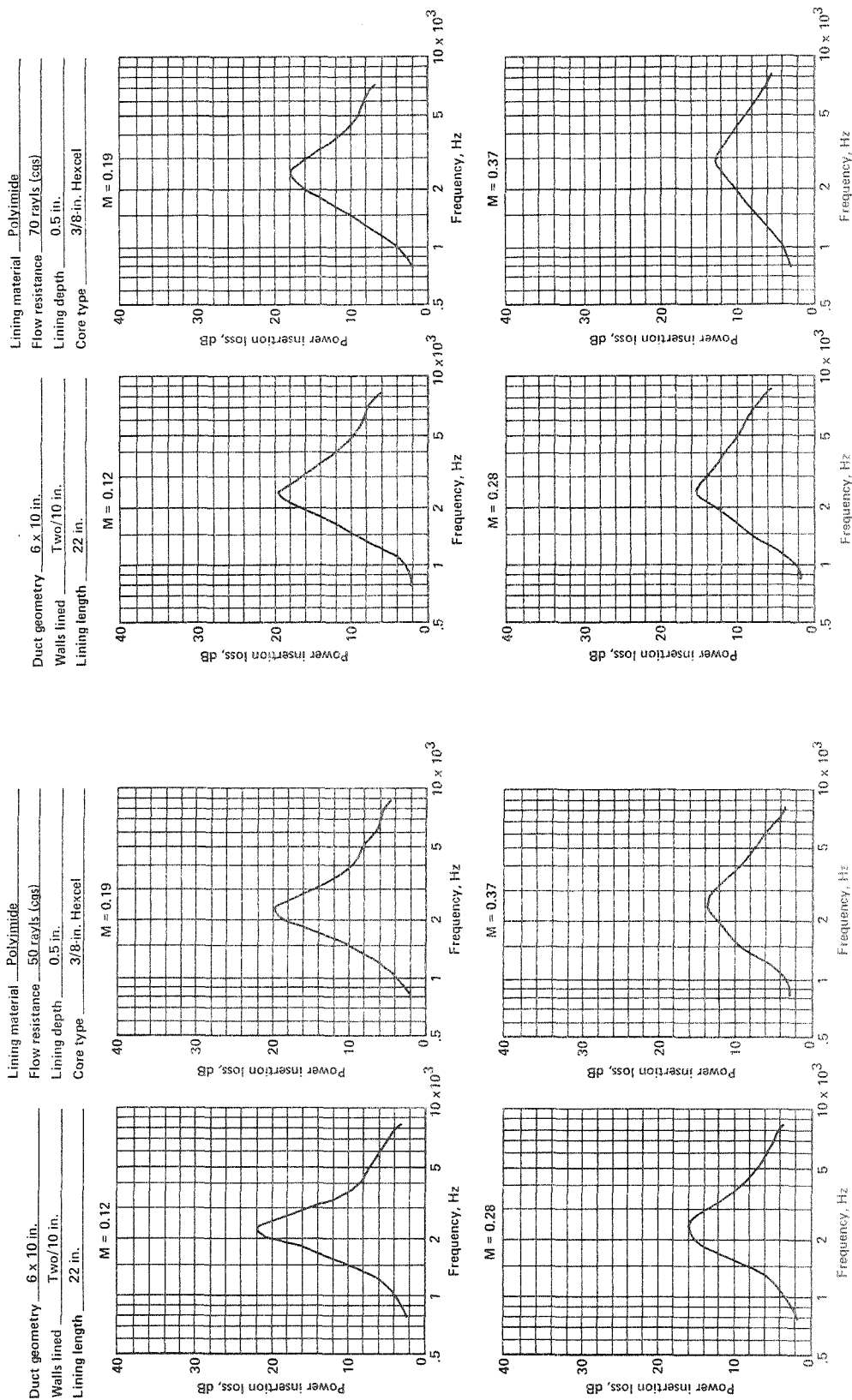


Figure A 29.

Figure A-30.



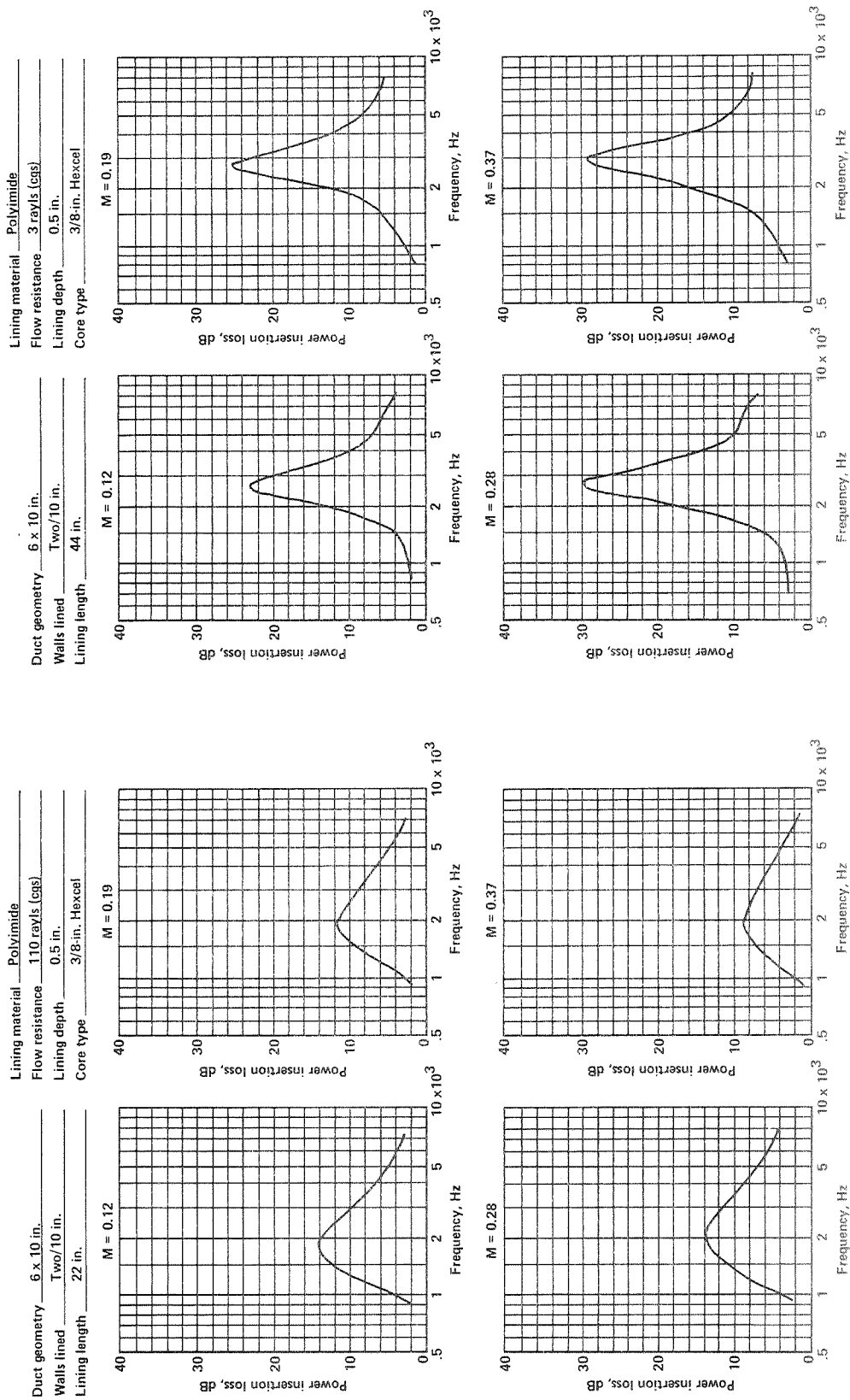


Figure A-31.

Figure A-32.

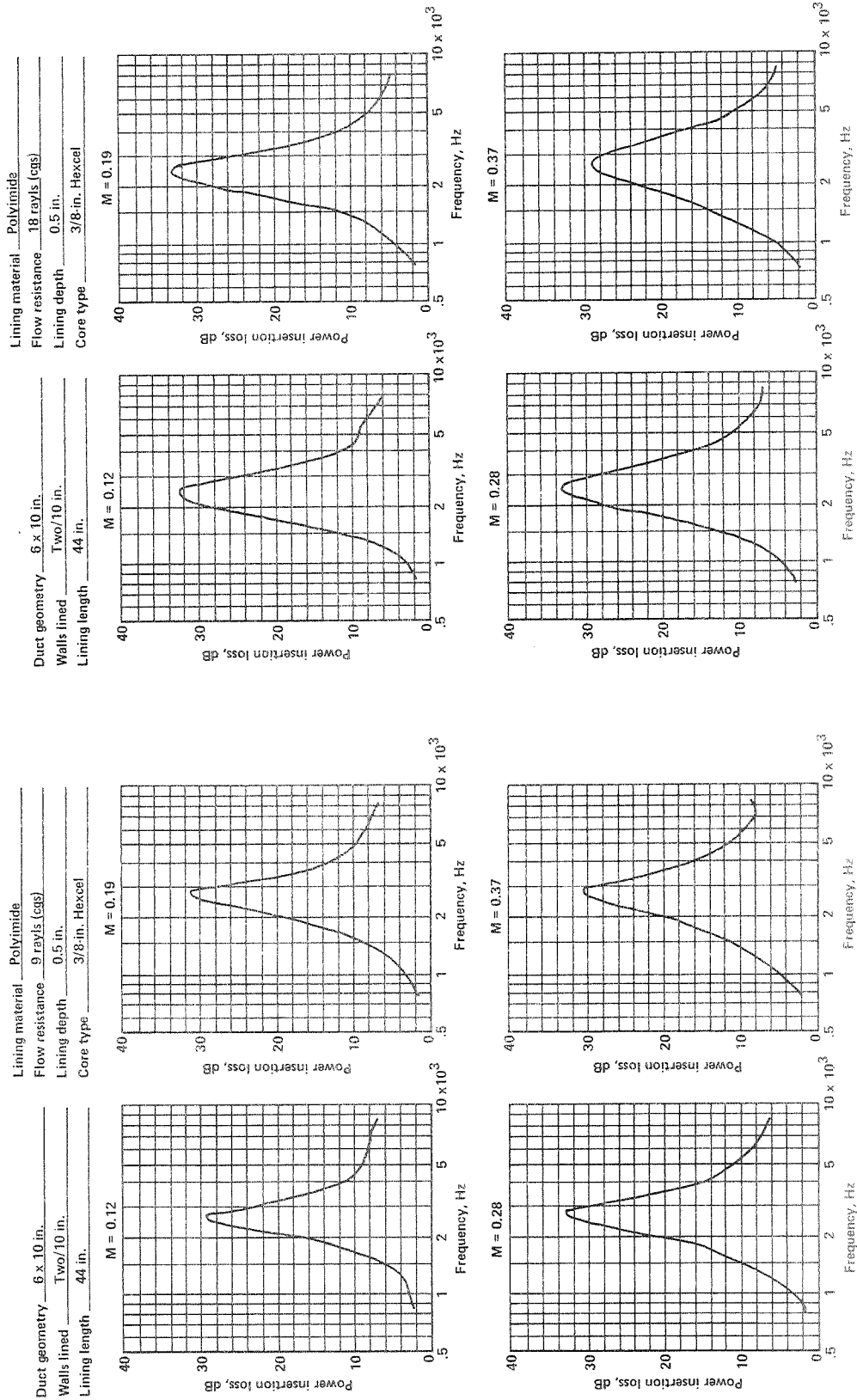
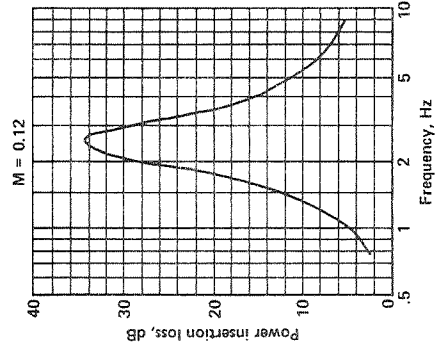
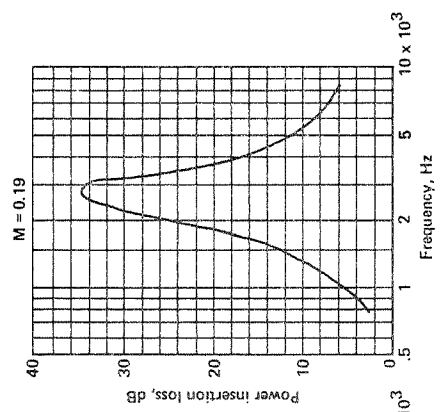


Figure A-33.

Figure A-34.

Lining material Polyimide  
 Flow resistance 30 rays (ags)  
 Lining depth 0.5 in.  
 Core type 3/8-in. Hexcel

Duct geometry 6 x 10 in.  
 Walls lined Two/10 in.  
 Lining length 44 in.



Lining material Polyimide  
 Flow resistance 50 rays (ags)  
 Lining depth 0.5 in.  
 Core type 3/8-in. Hexcel

Duct geometry 6 x 10 in.  
 Walls lined Two/10 in.  
 Lining length 44 in.

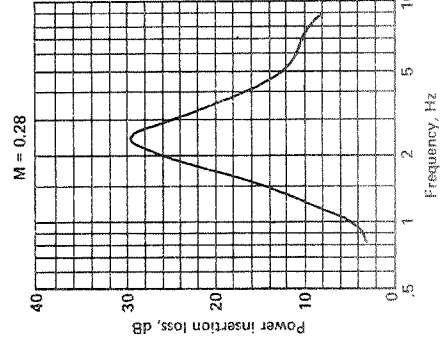
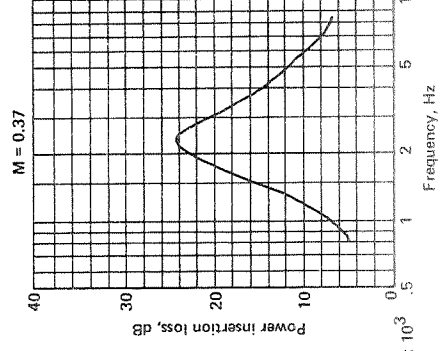
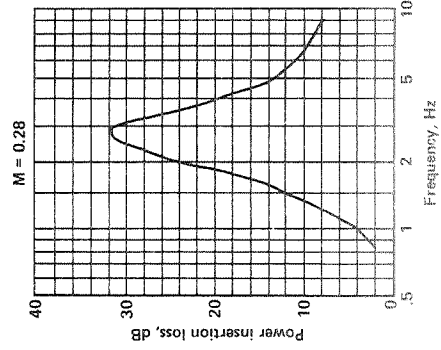
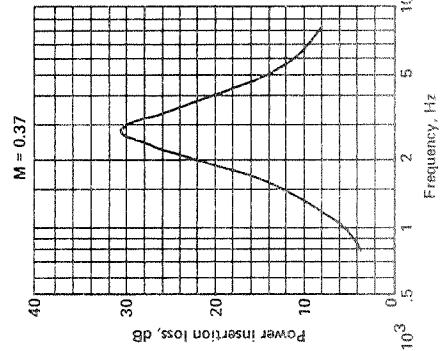
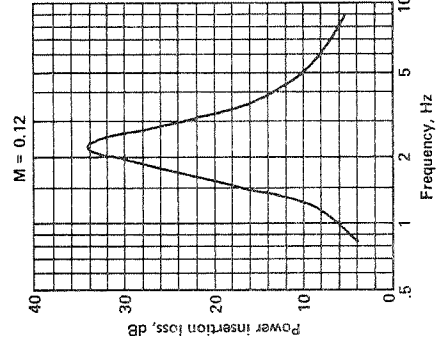
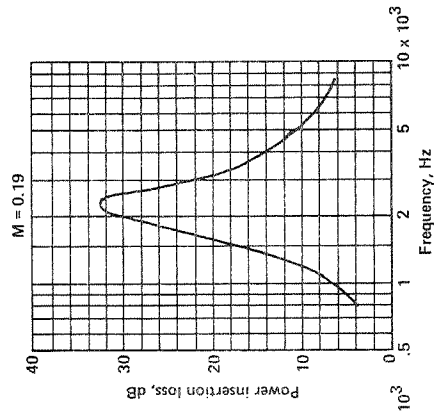


Figure A-35.

Figure A-36.

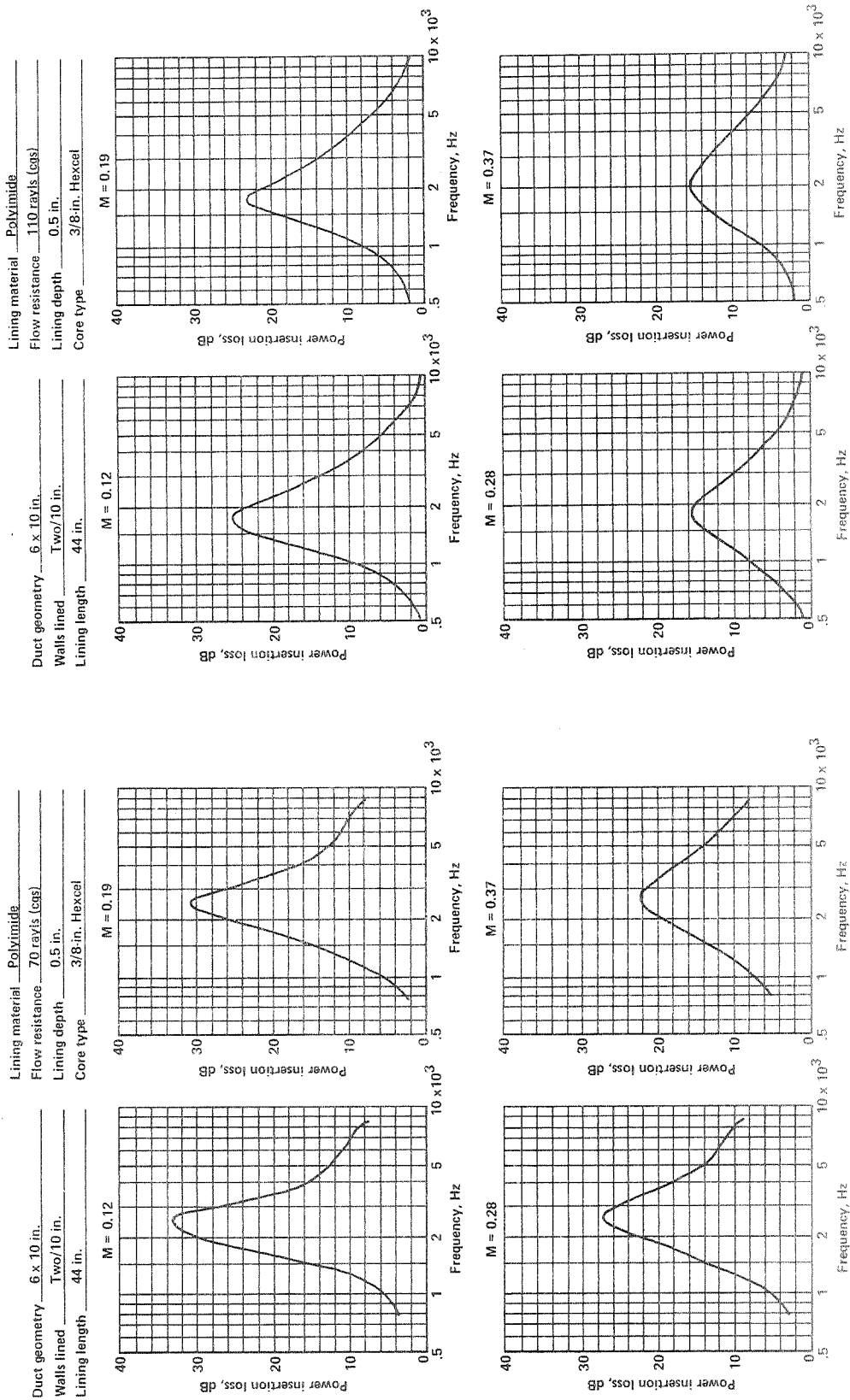


Figure A-37.

Figure A-38.

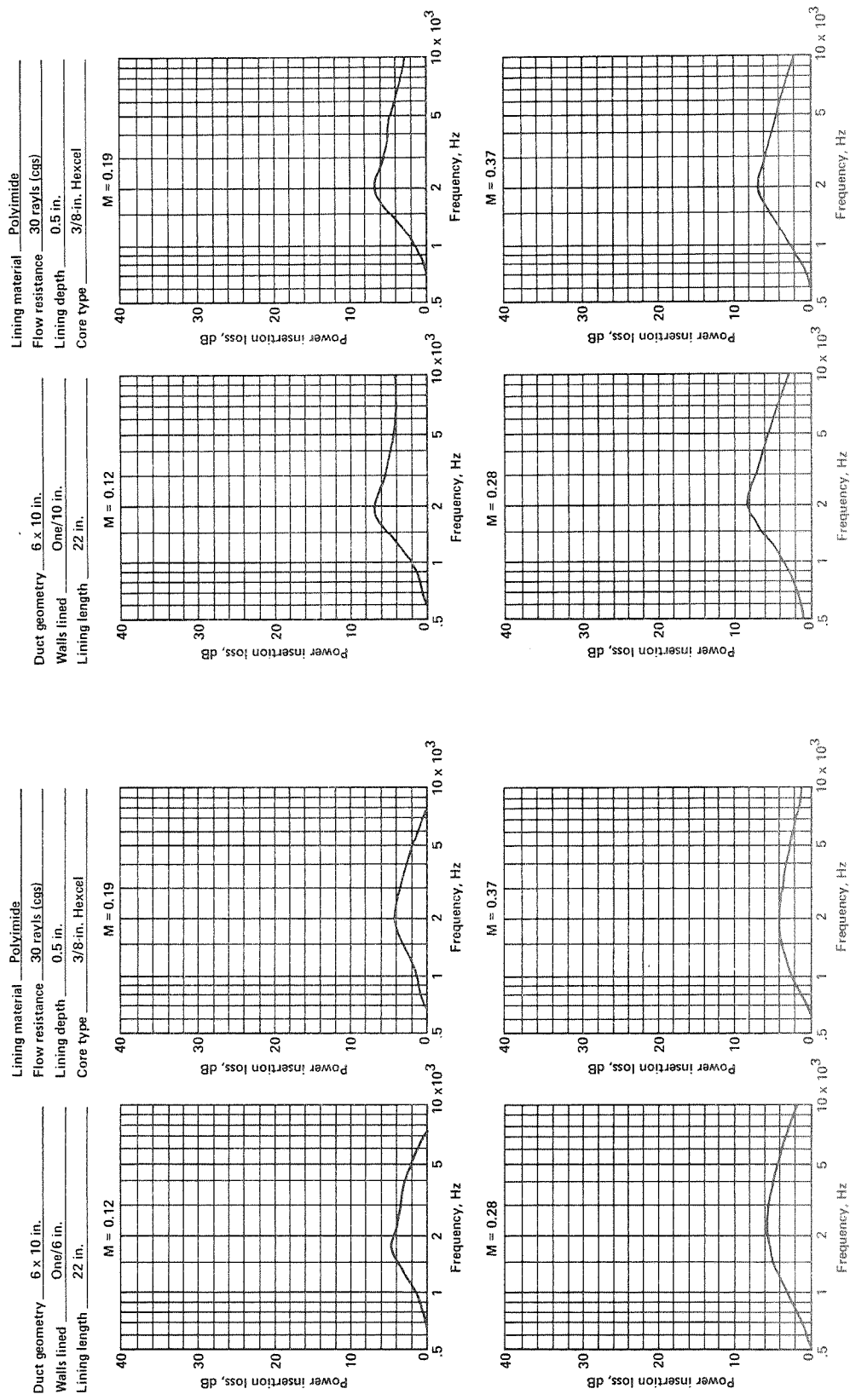


Figure A-39.

Figure A-40.

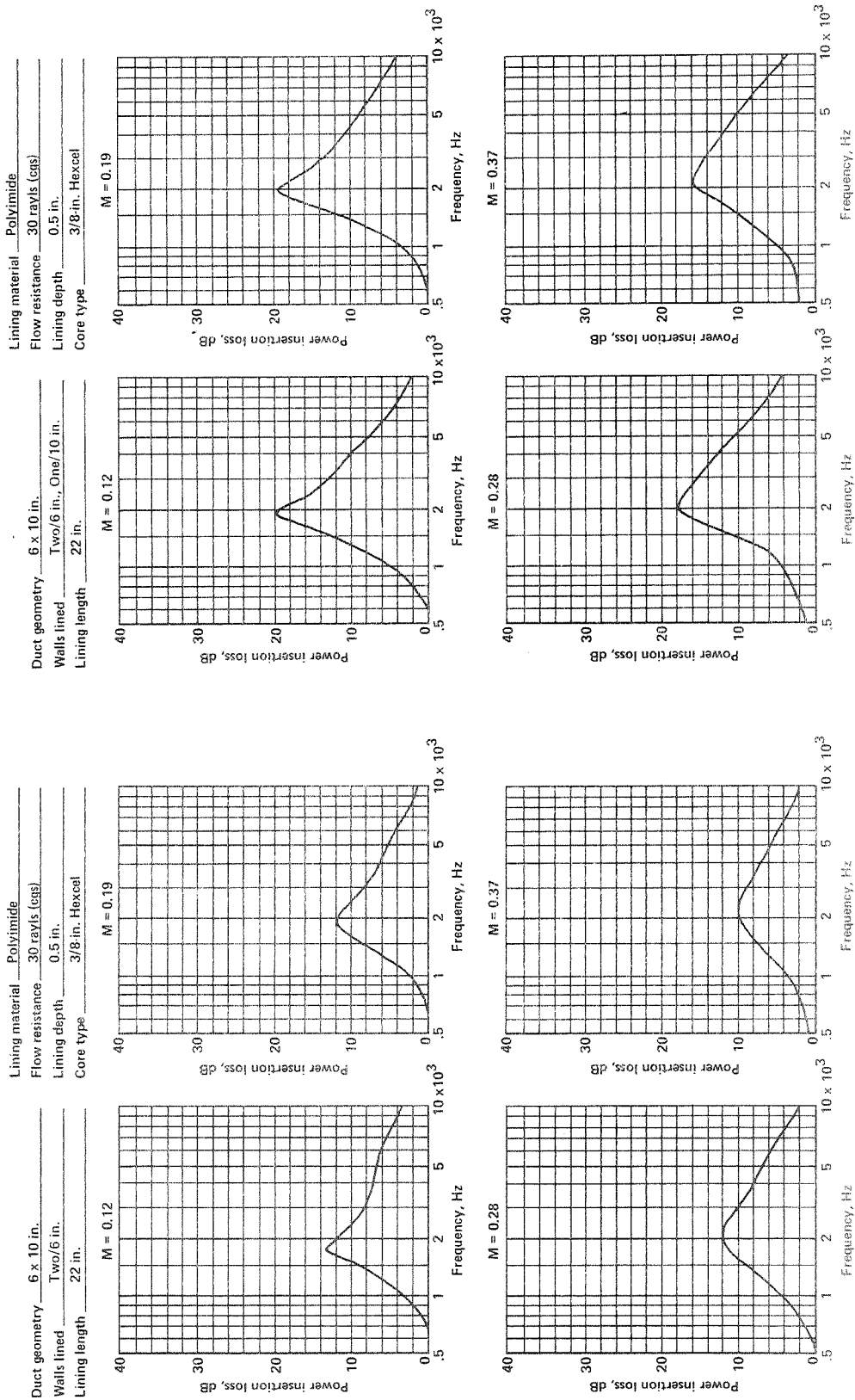


Figure A-41.

Figure A-42.

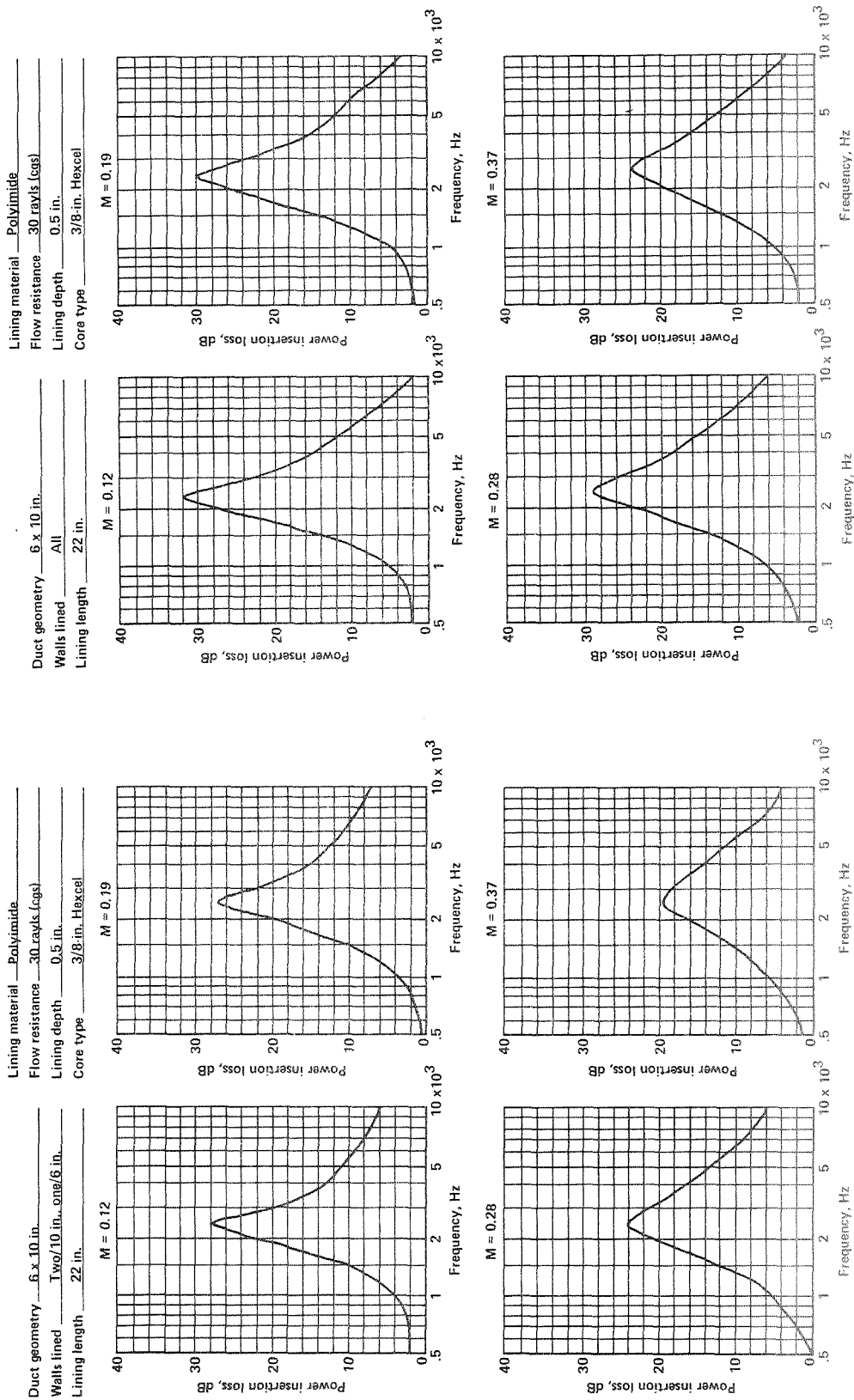


Figure A-43.

Figure A-44.

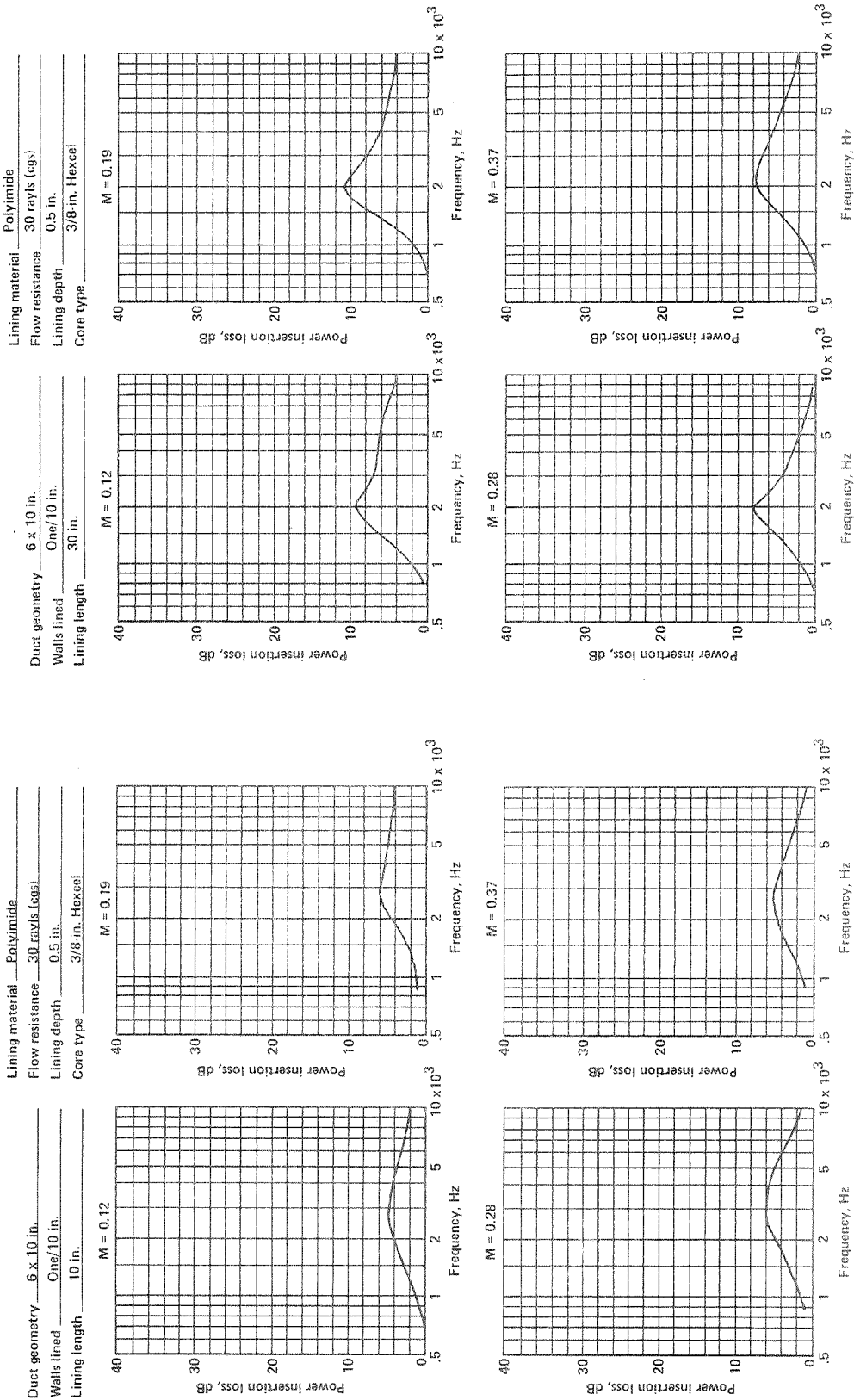


Figure A-46.

Figure A-45.



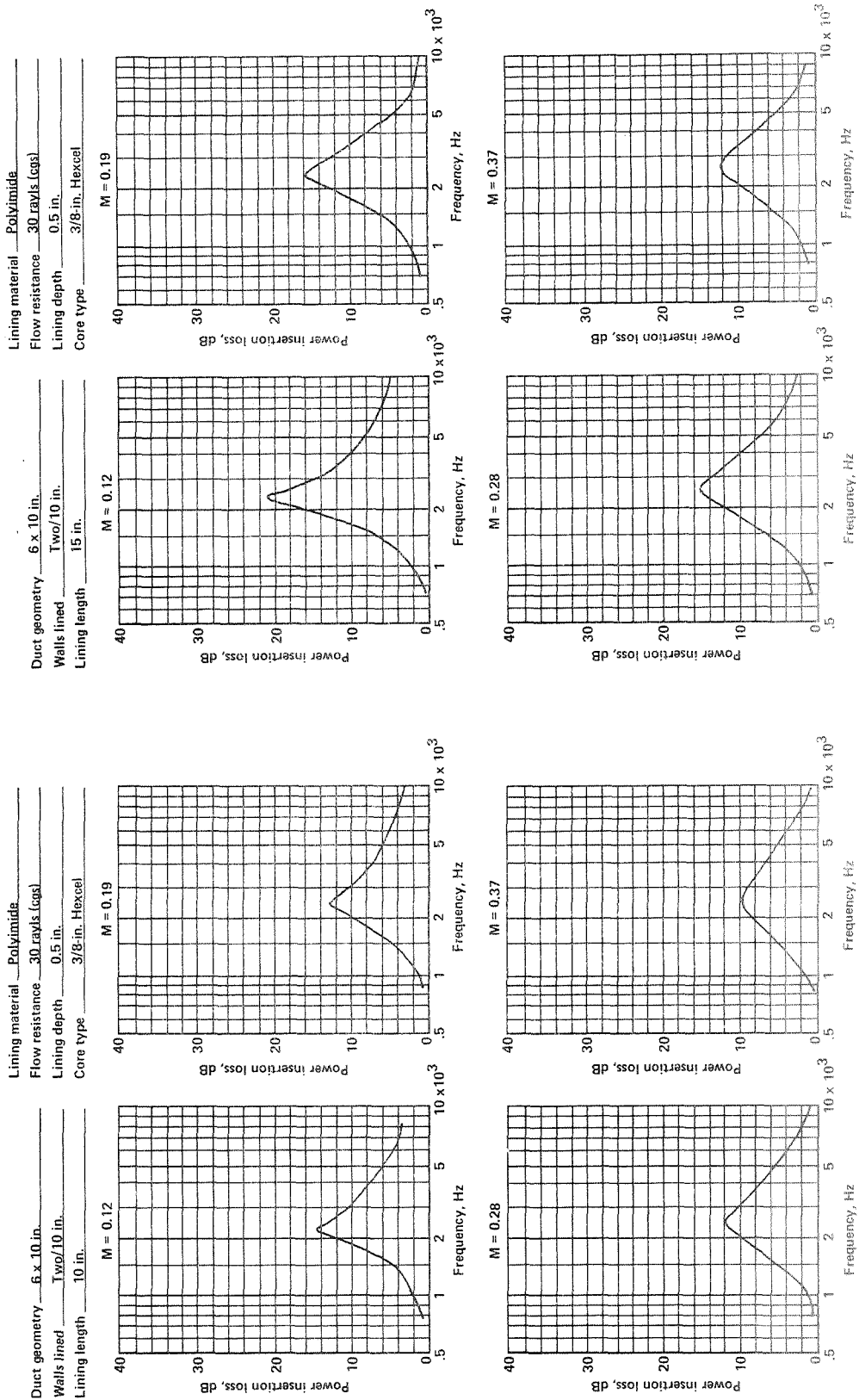


Figure A-47.

Figure A-48.

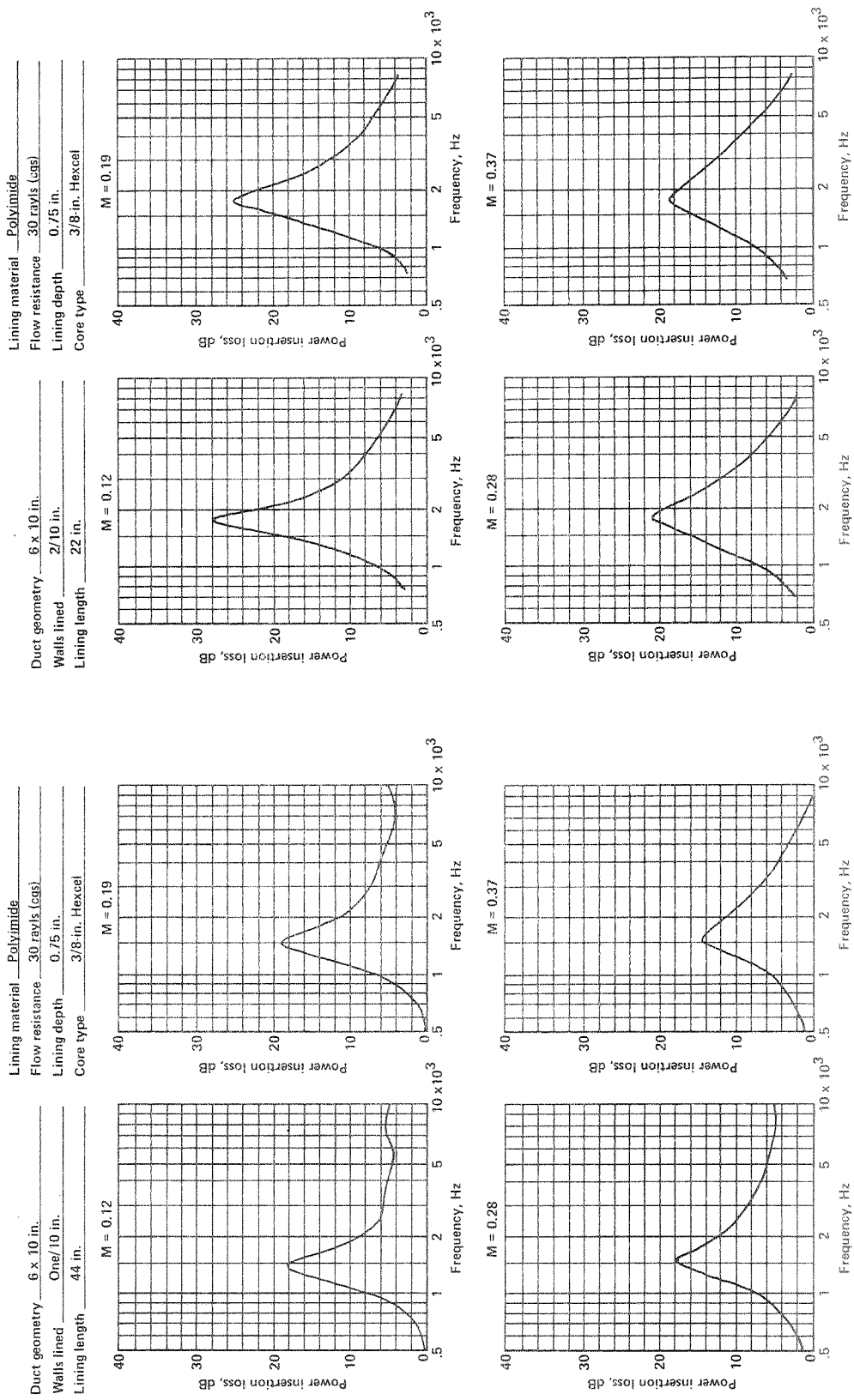


Figure A-49.

Figure A-50.

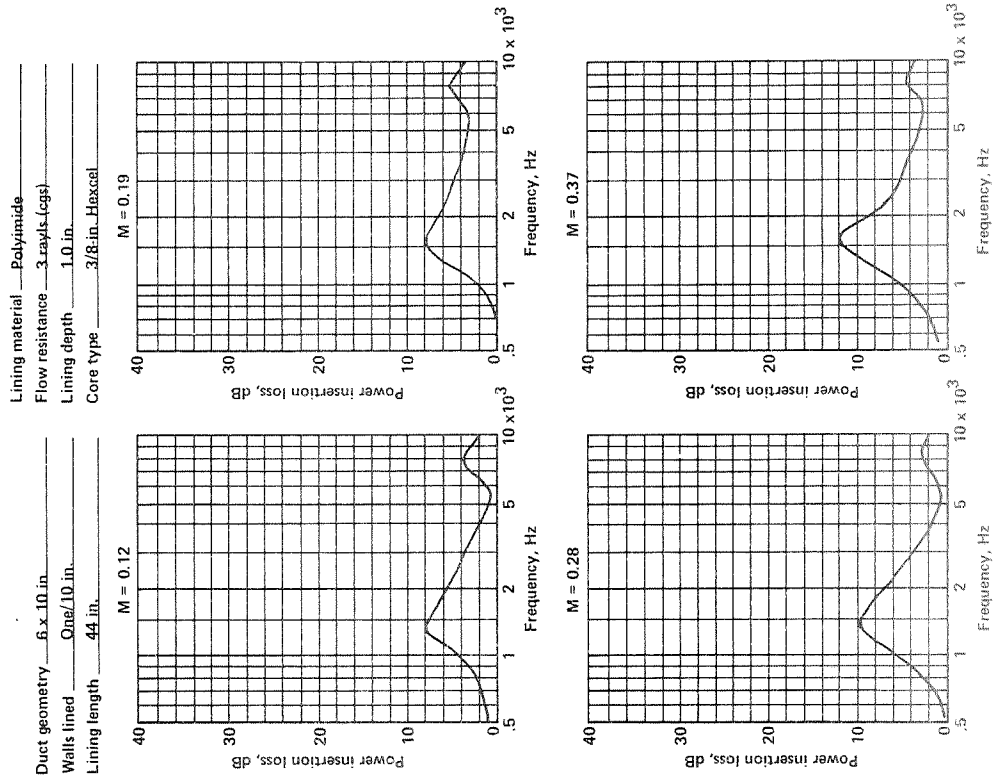


Figure A-52.

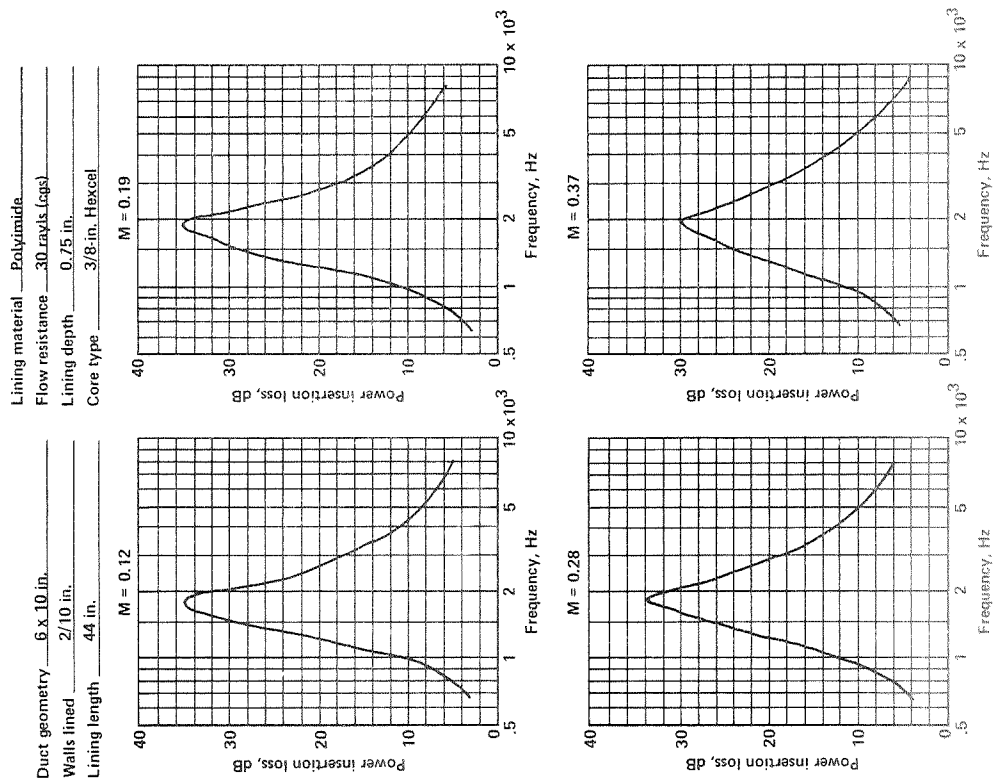


Figure A-51.

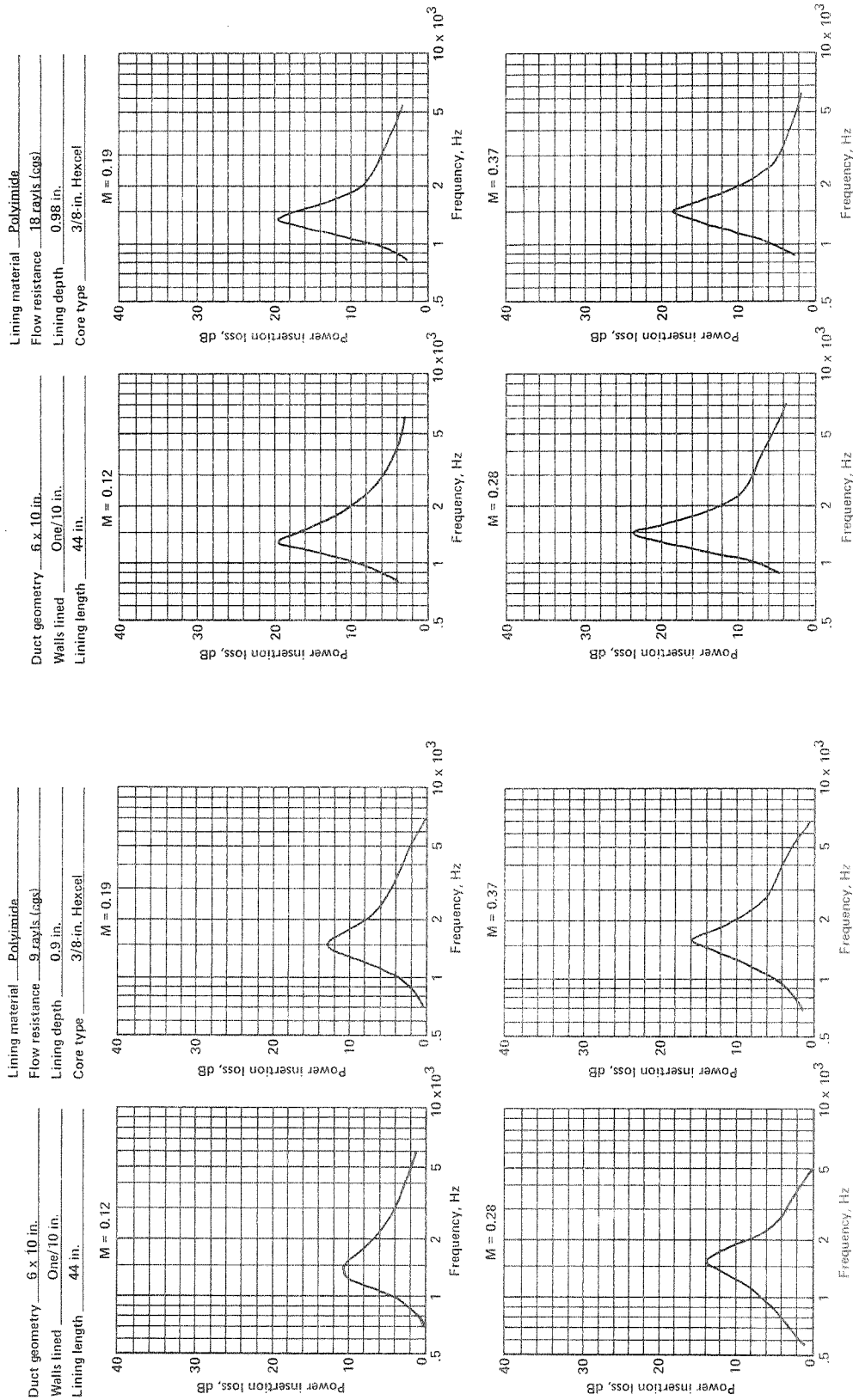


Figure A-54.

Figure A-53.

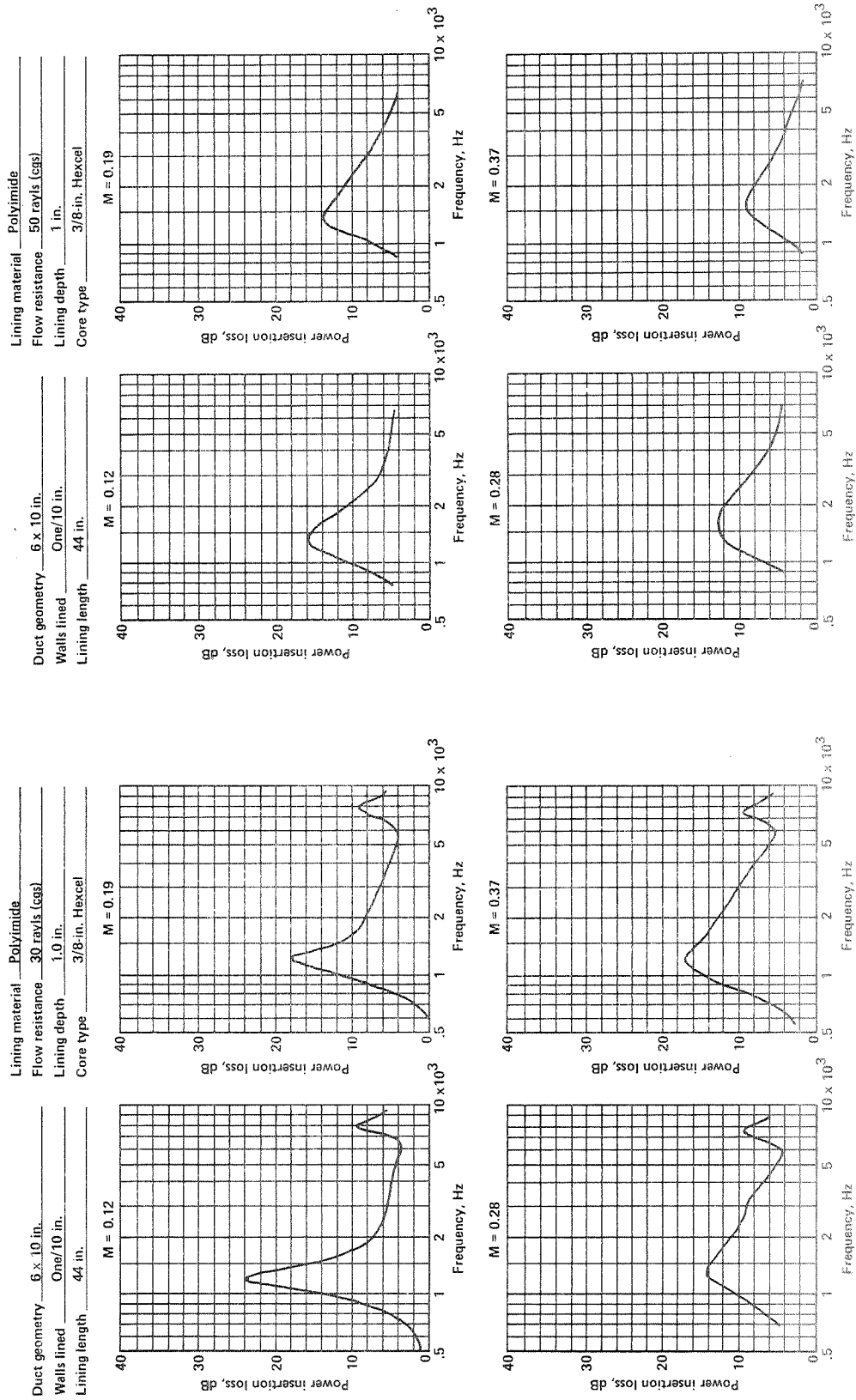


Figure A-55.

Figure A-56.

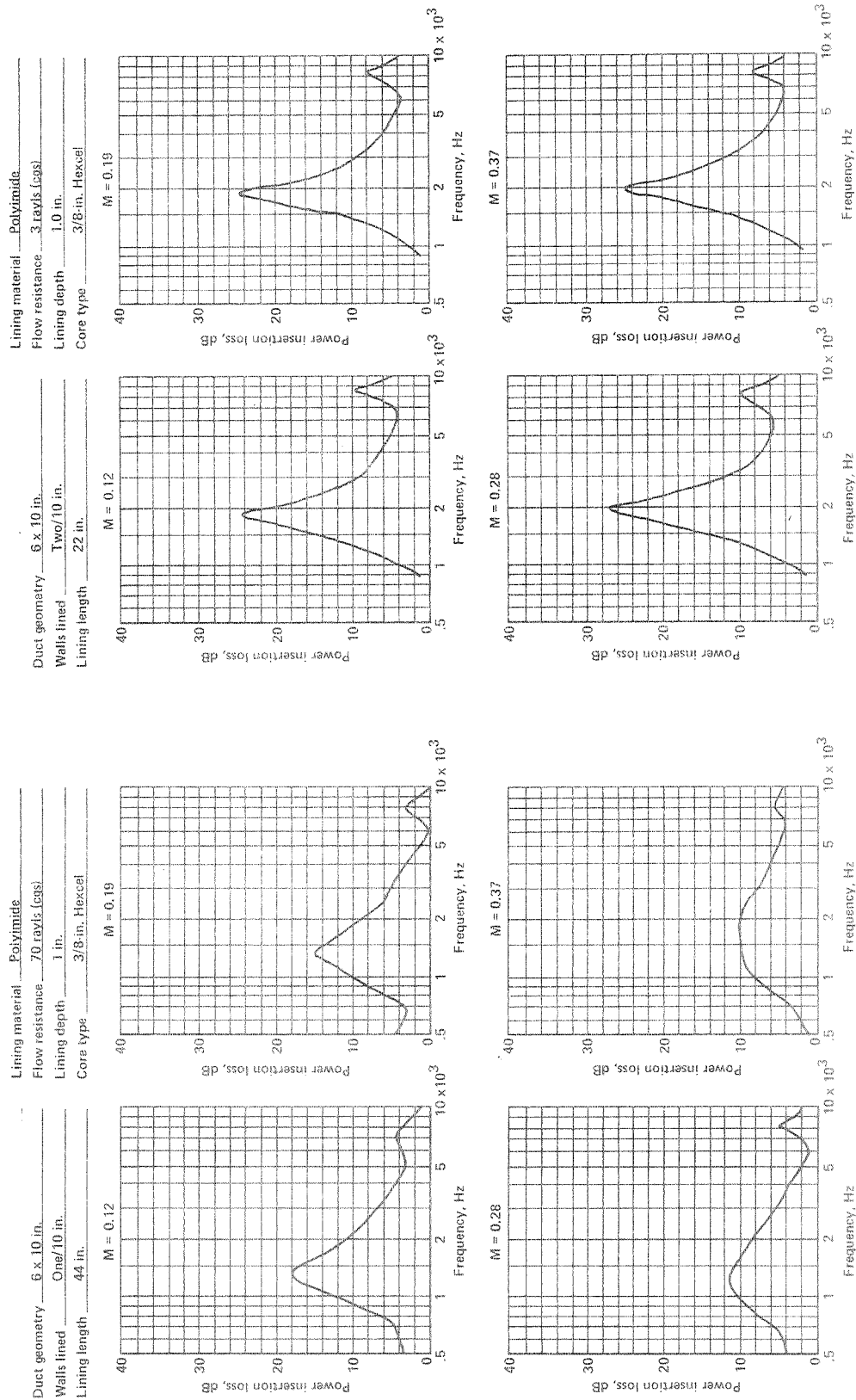


Figure A-57.

Figure A-58.

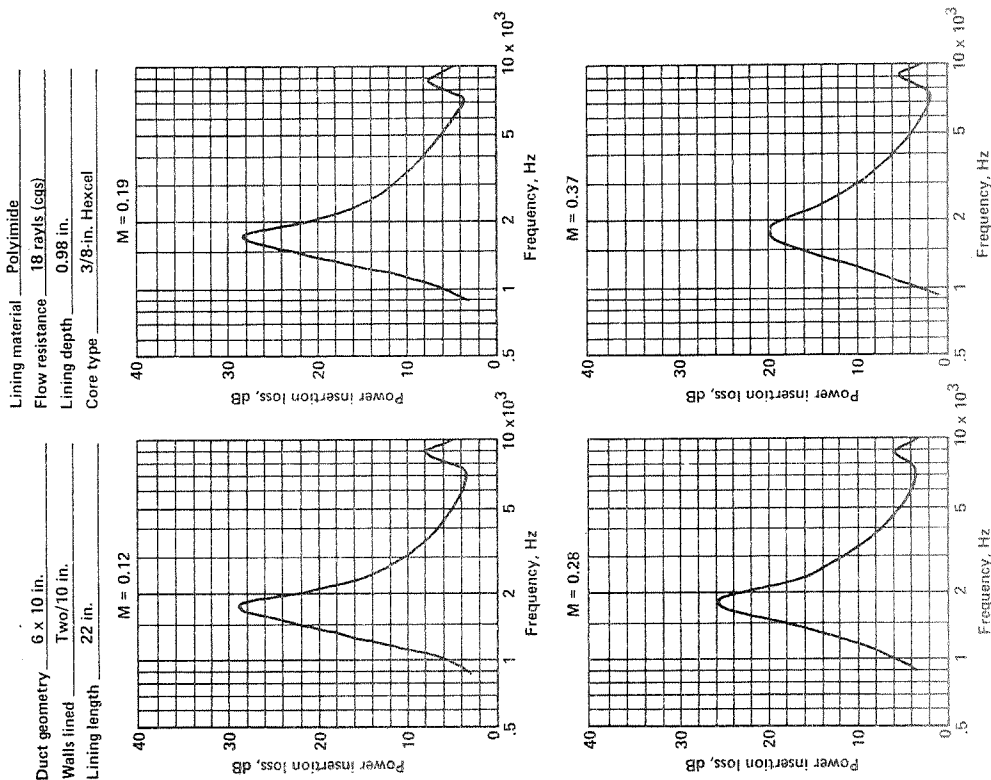


Figure A-60.

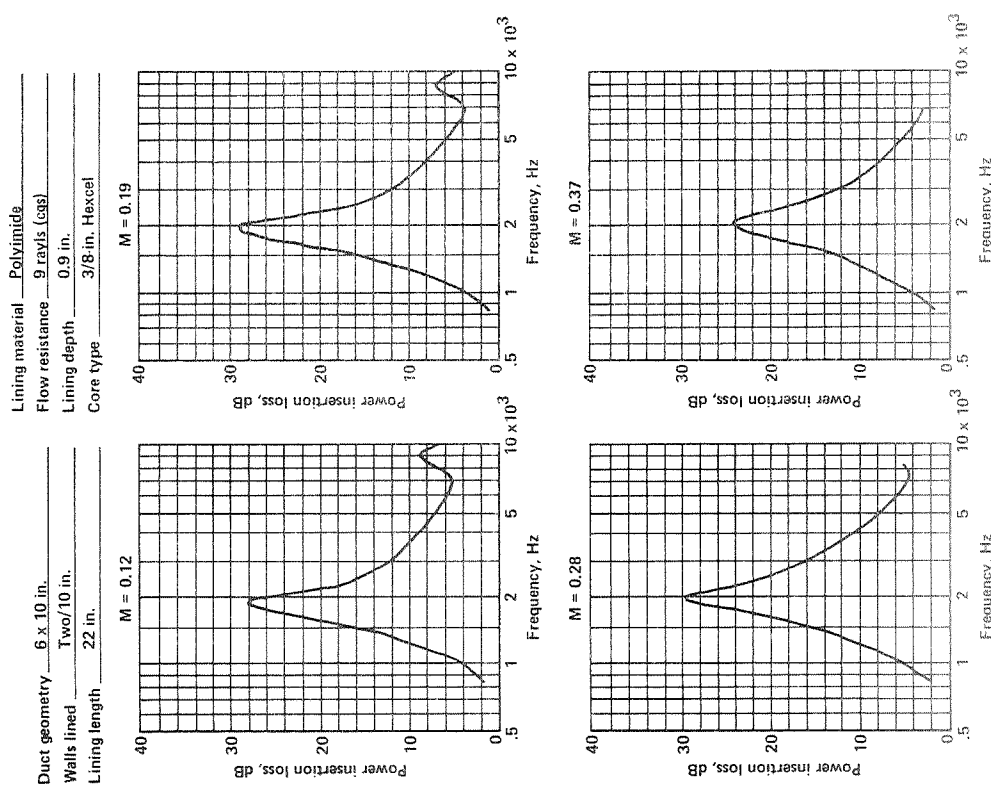


Figure A-59.

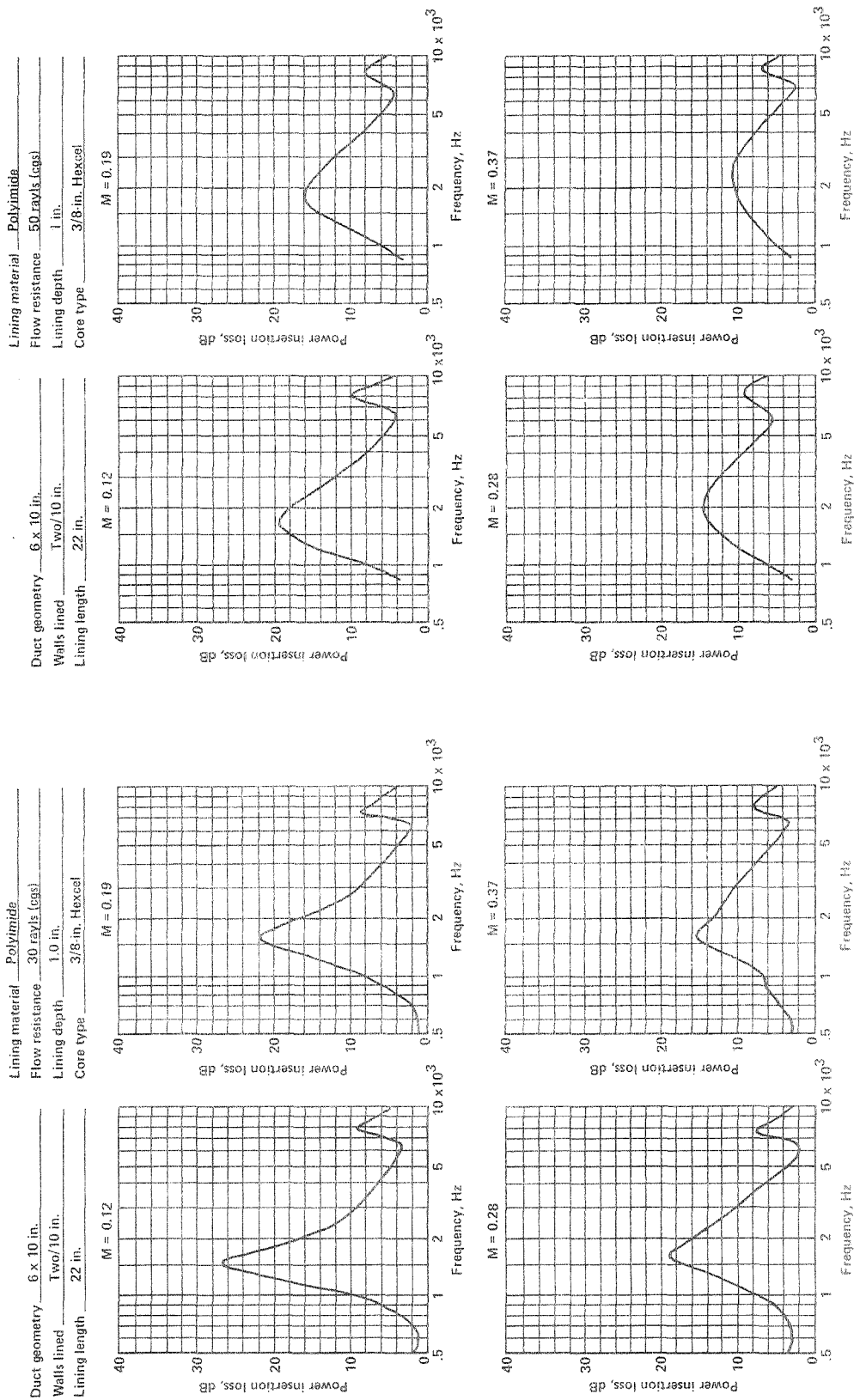


Figure A-62.

Figure A-61.



Lining material Polyimide  
 Flow resistance 3 rays (ags)  
 Lining depth 1.0 in.  
 Core type 3/8-in. Hexcel

Duct geometry 6 x 10 in.  
 Walls lined Two/10 in.  
 Lining length 44 in.

Lining material Polyimide  
 Flow resistance 70 rays (ags)  
 Lining depth 1 in.  
 Core type 3/8-in. Hexcel

Duct geometry 6 x 10 in.  
 Walls lined Two/10 in.  
 Lining length 22 in.

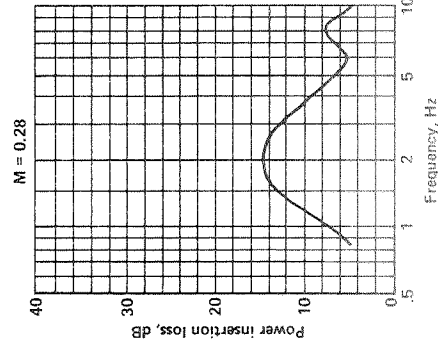
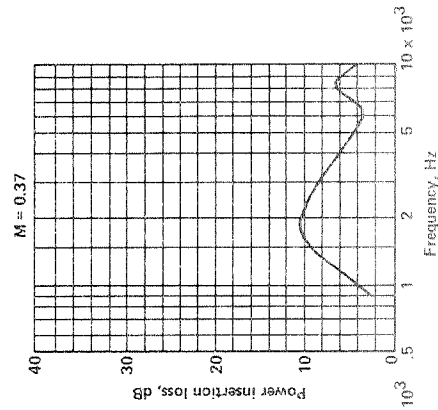
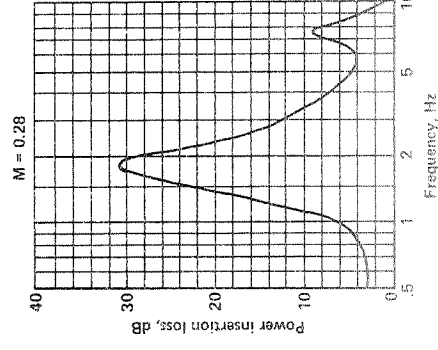
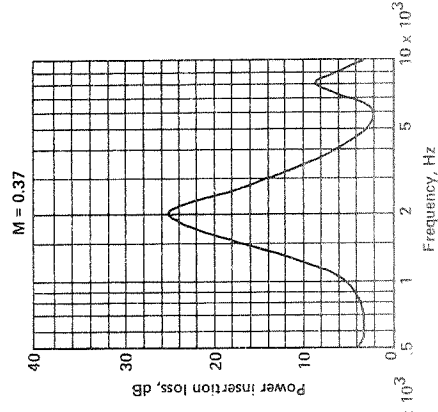
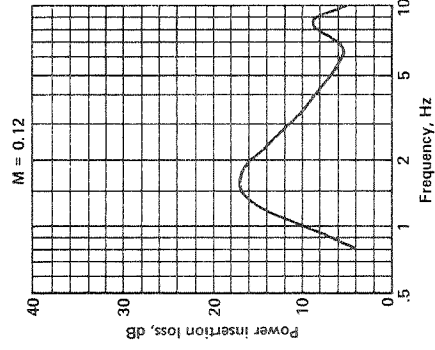
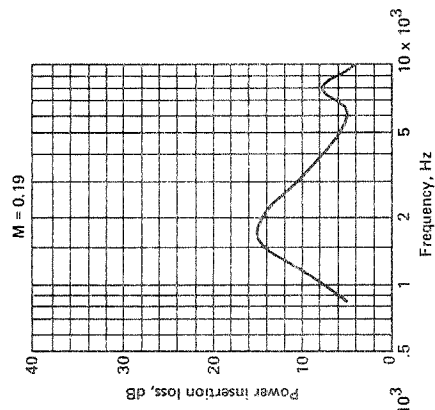
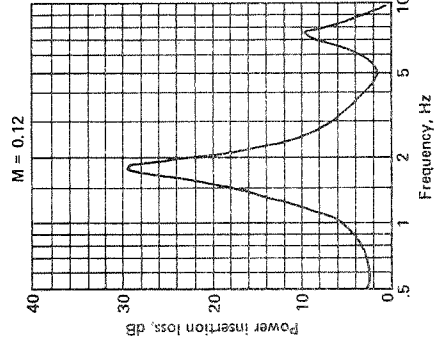
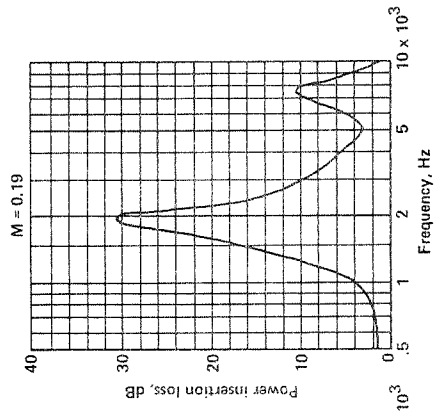


Figure A-64.

Figure A-63.

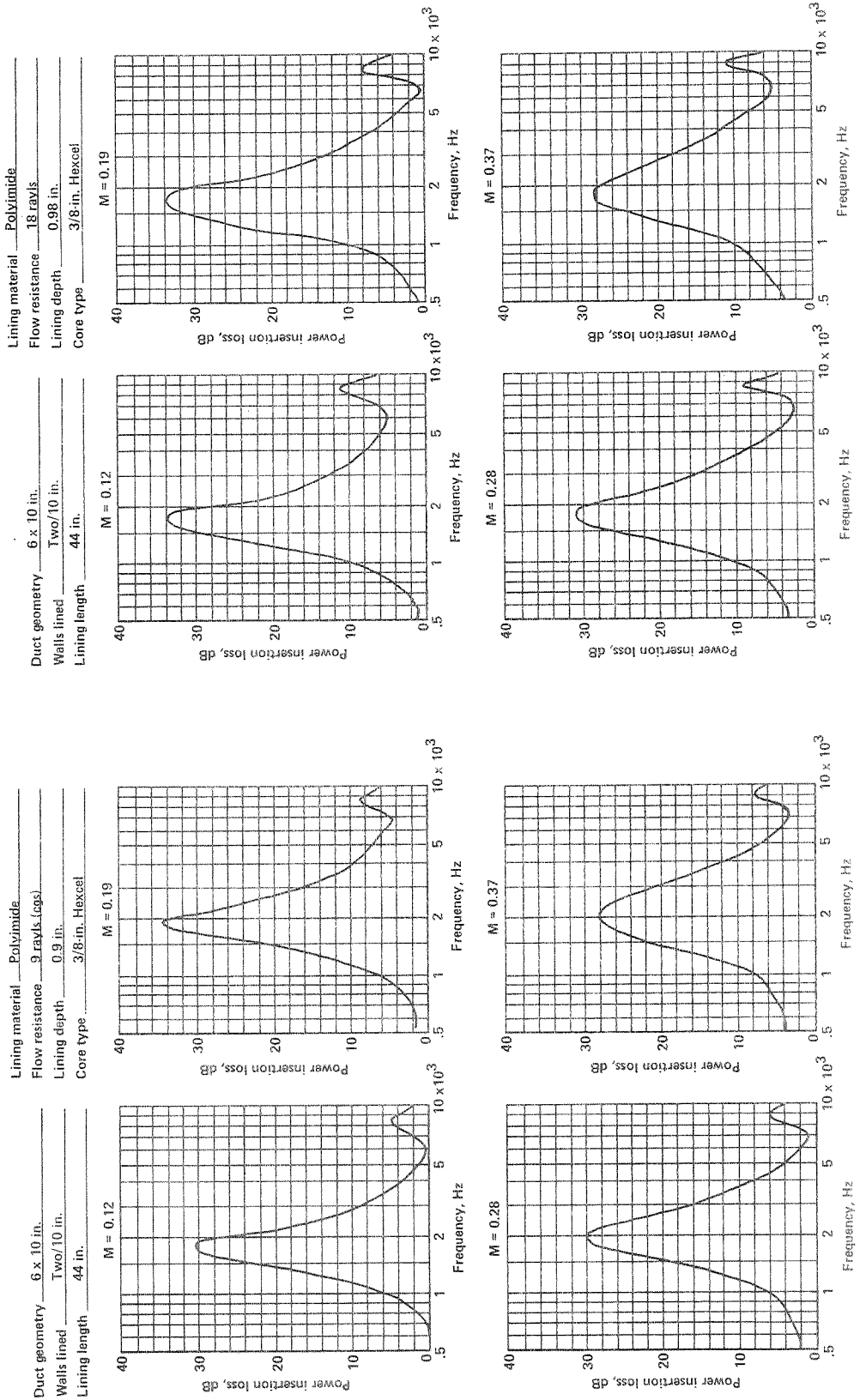


Figure A-66.

Figure A-65.

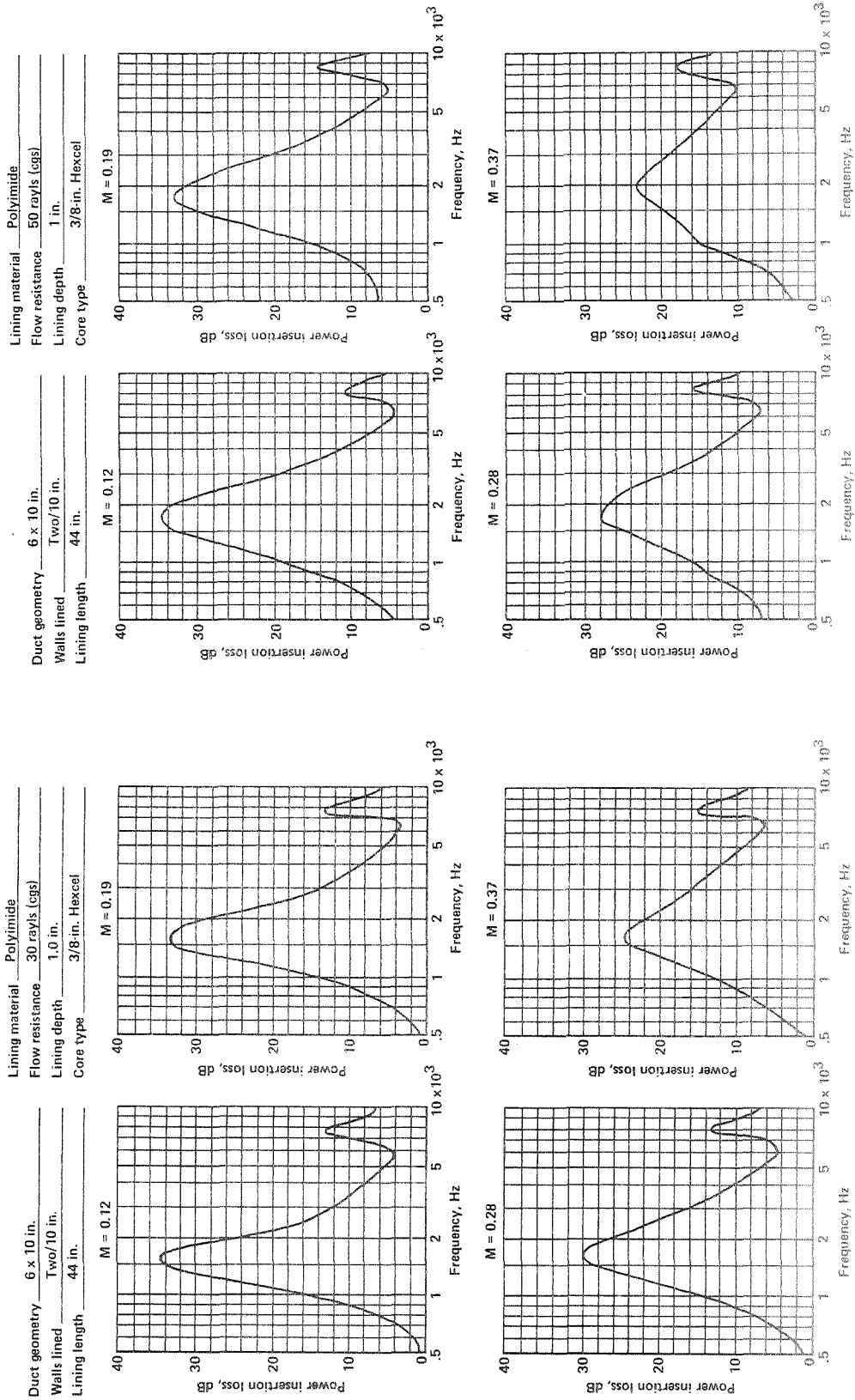


Figure A-68.

Figure A-67.

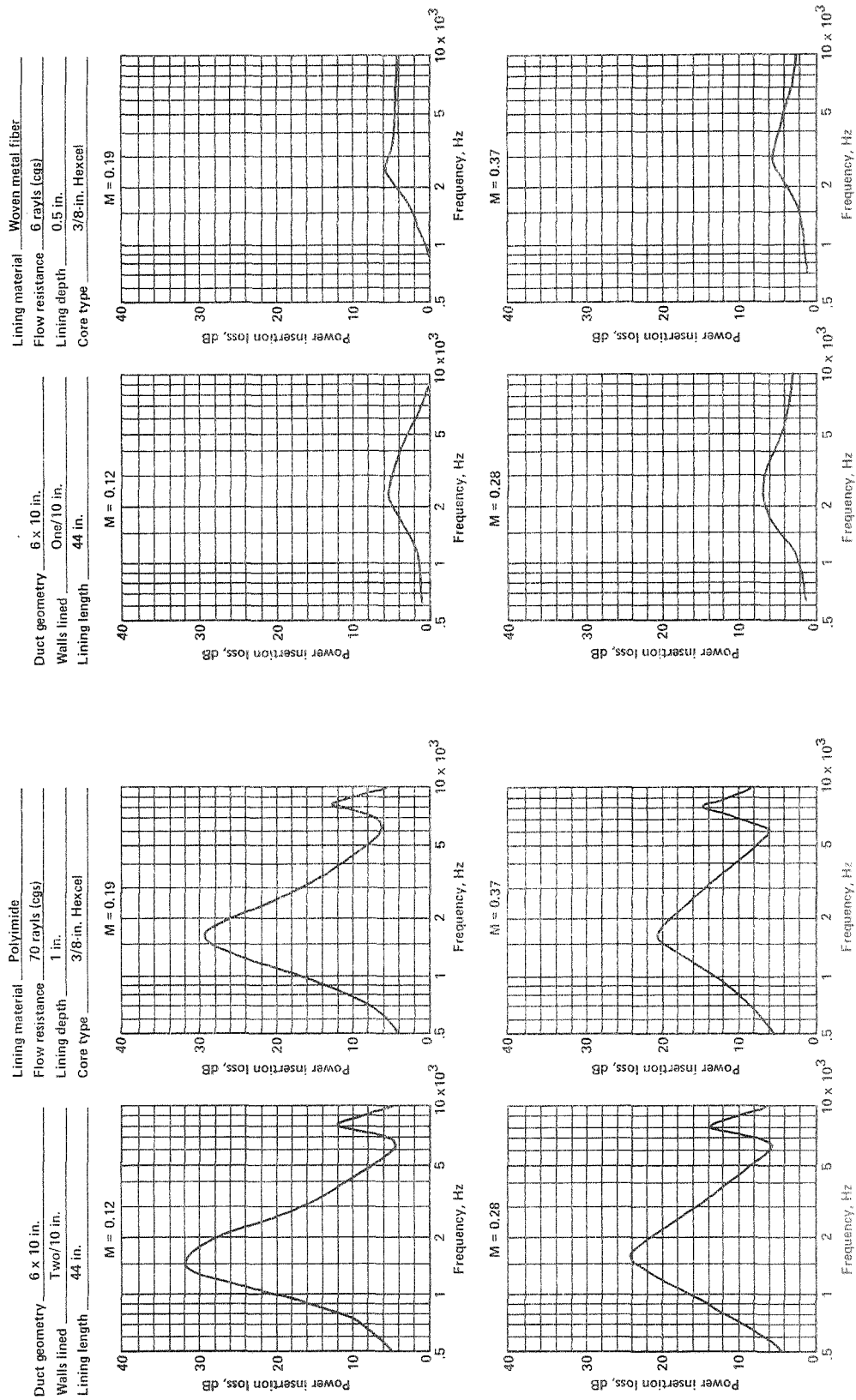


Figure A-70.

Figure A-69.

Lining material Woven metal fiber  
 Flow resistance 22 rays/ls (cgs)  
 Lining depth 0.5 in.  
 Core type 3/8-in. Hexcel

Duct geometry 6 x 10 in.  
 Walls lined One/10 in.  
 Lining length 44 in.

Lining material Woven metal fiber  
 Flow resistance 12 rays/ls (cgs)  
 Lining depth 0.5 in.  
 Core type 3/8-in. Hexcel

Duct geometry 6 x 10 in.  
 Walls lined One/10 in.  
 Lining length 44 in.

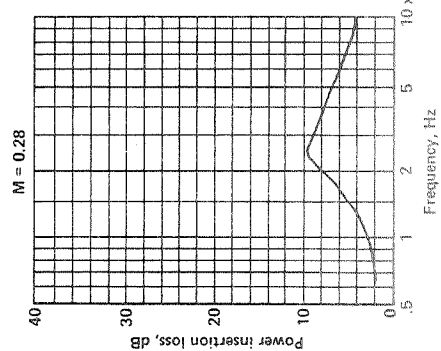
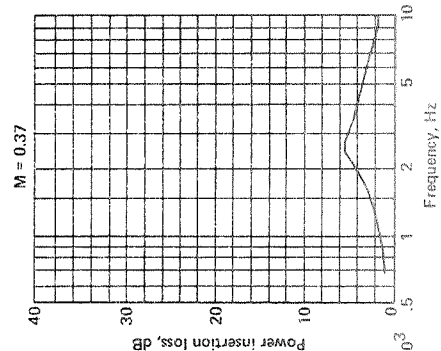
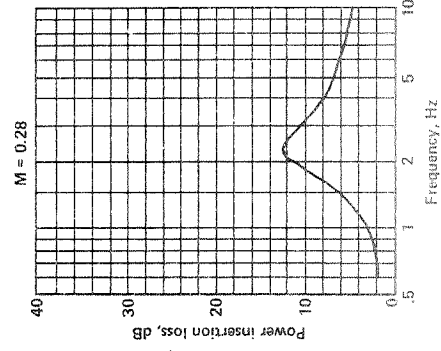
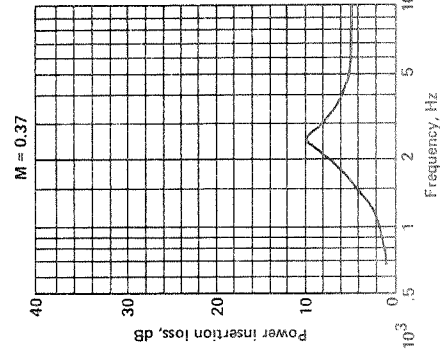
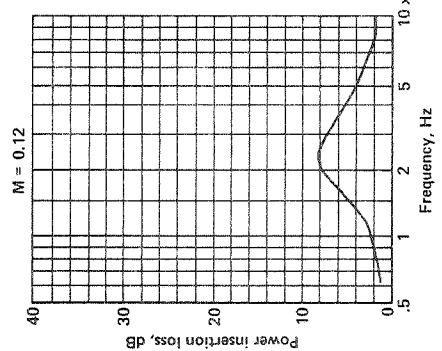
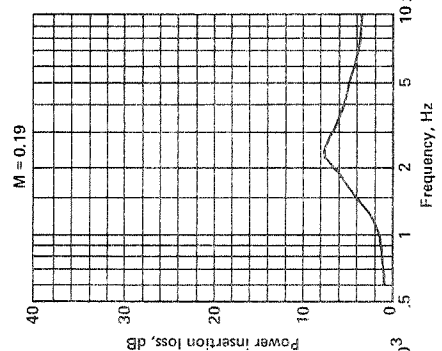
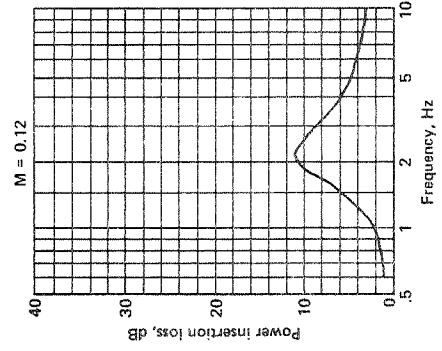
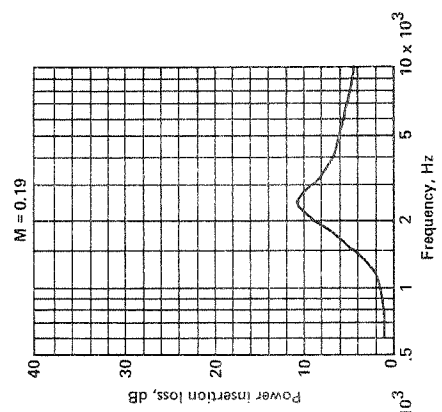


Figure A-72.

Figure A-71.

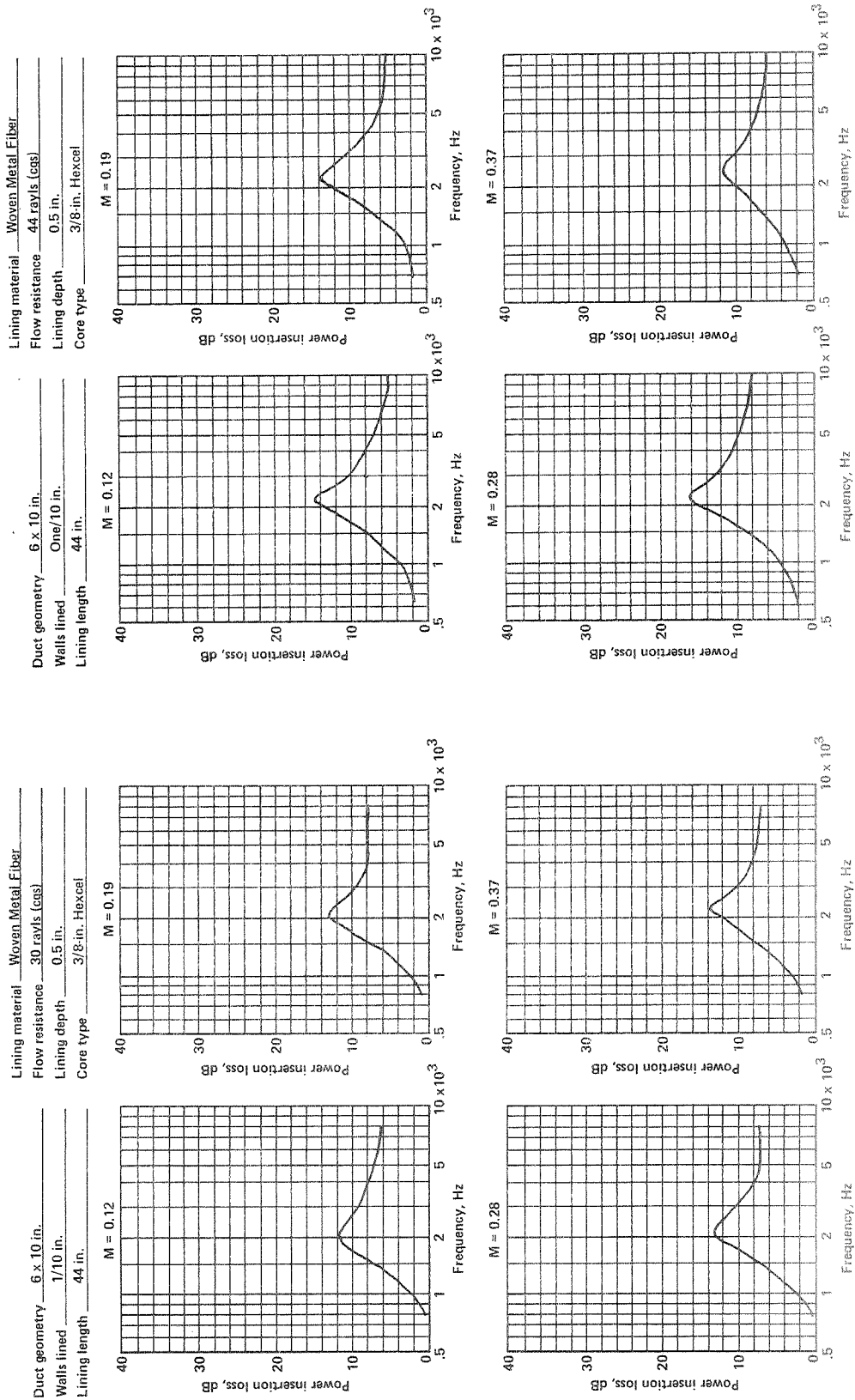


Figure A-73.

Figure A-74.

Lining material Woven Metal Fiber  
 Flow resistance 6 rays (cgs)  
 Lining depth 0.5 in.  
 Core type 3/8-in. Hexcel

Duct geometry 6 x 10 in.  
 Walls lined Two/10 in.  
 Lining length 22 in.

Lining material Woven Metal Fiber  
 Flow resistance 80 rays (cgs)  
 Lining depth 0.5 in.  
 Core type 3/8-in. Hexcel

Duct geometry 6 x 10 in.  
 Walls lined One/10 in.  
 Lining length 44 in.

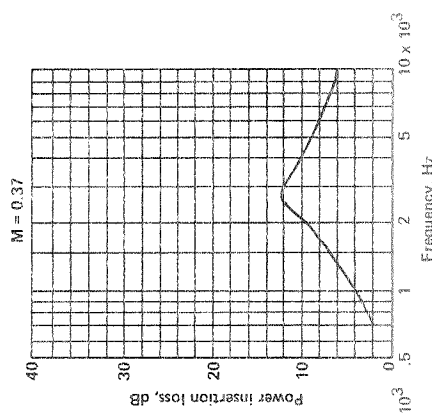
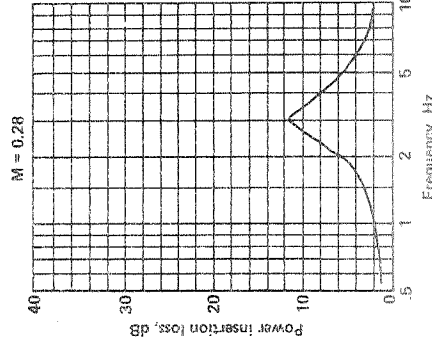
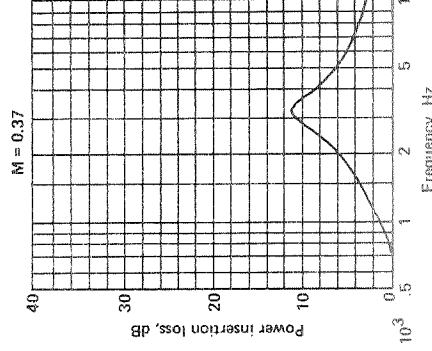
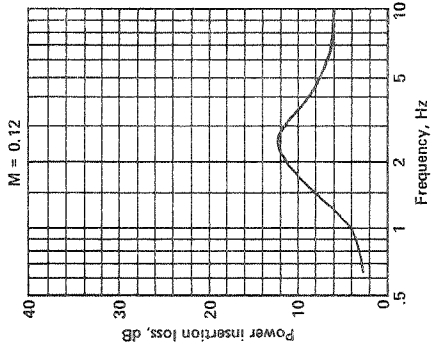
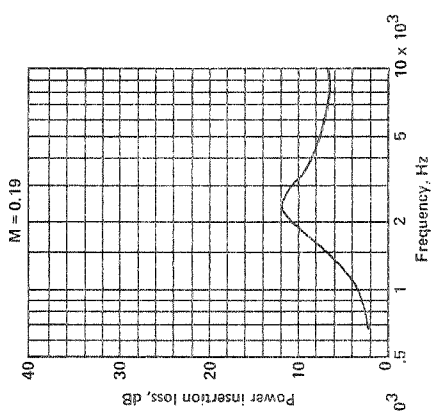
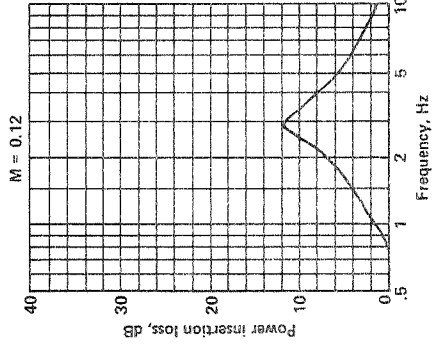
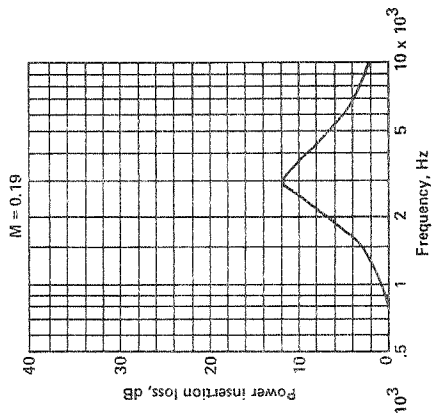


Figure A-76.

Figure A-75.

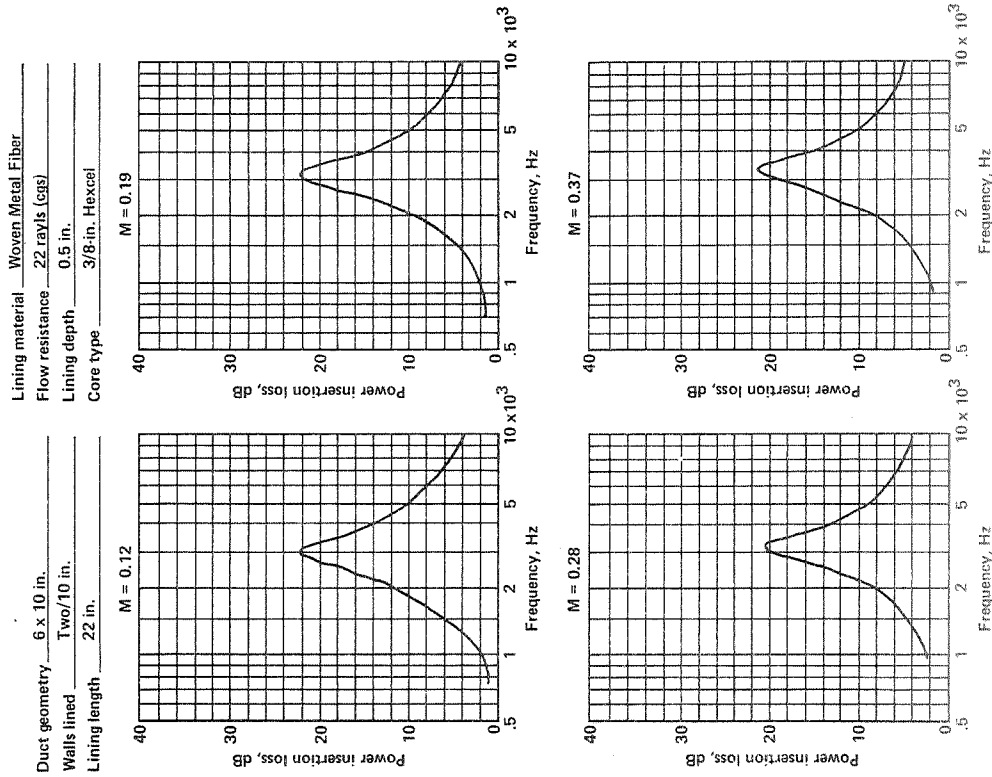


Figure A-78.

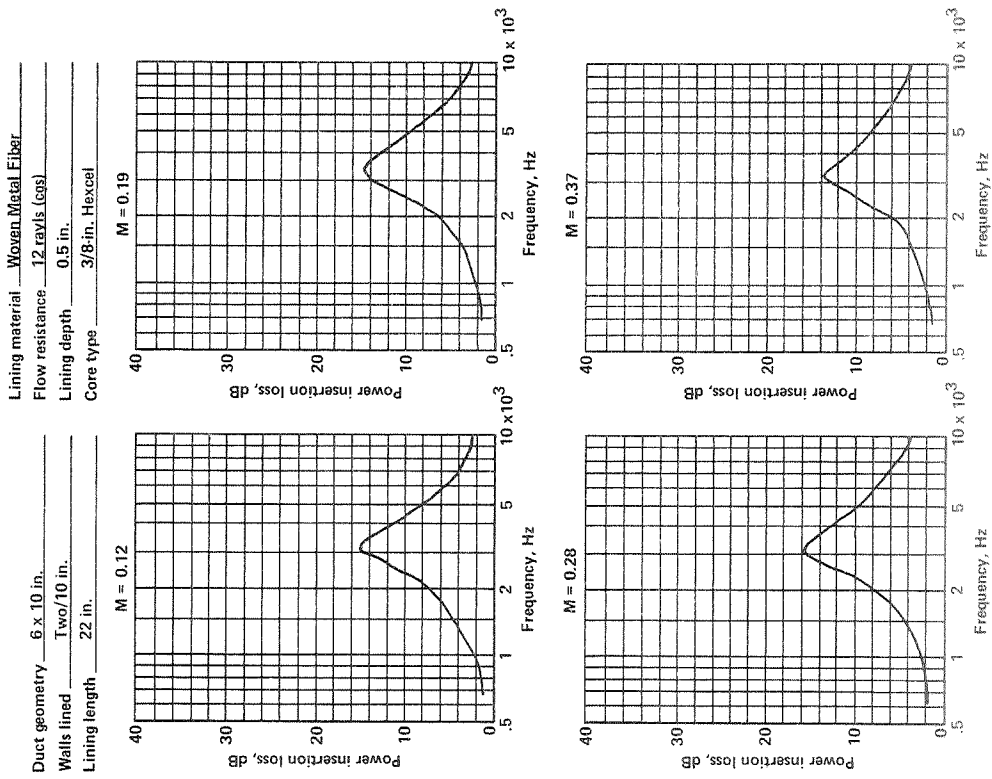


Figure A-77.



Lining material Woven Metal Fibar  
 Flow resistance 44 rays/ls (cgs)  
 Lining depth 0.5 in.  
 Core type 3/8-in. Hexcel

Duct geometry 6 x 10 in.  
 Walls lined Two/10 in.  
 Lining length 22 in.

Lining material Woven Metal Fibar  
 Flow resistance 30 rays/ls (cgs)  
 Lining depth 0.5 in.  
 Core type 3/8-in. Hexcel

Duct geometry 6 x 10 in.  
 Walls lined Two/10 in.  
 Lining length 22 in.

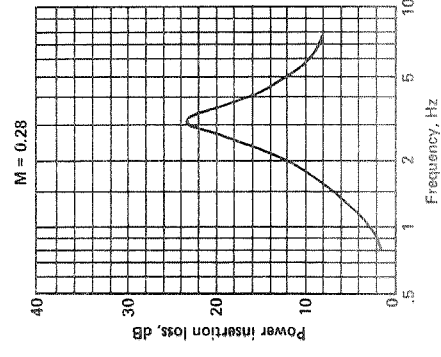
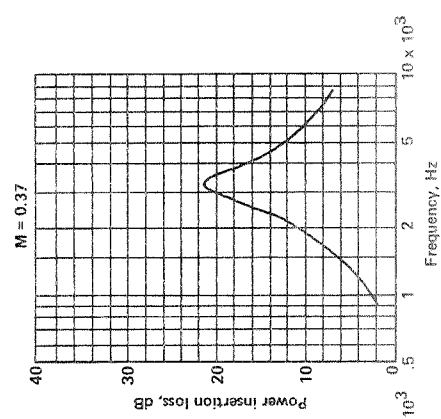
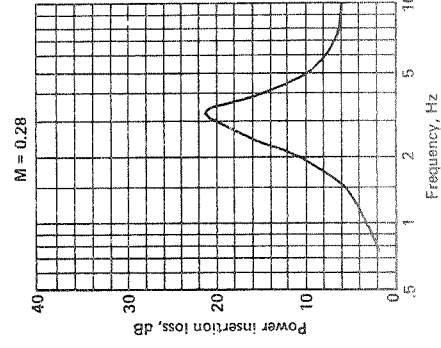
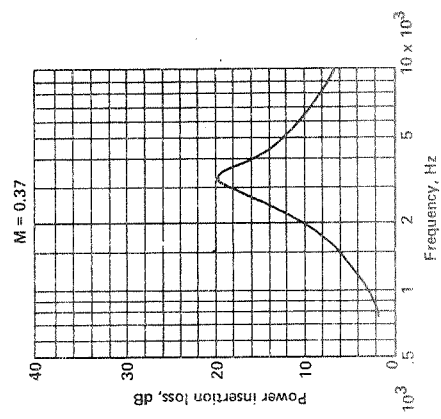
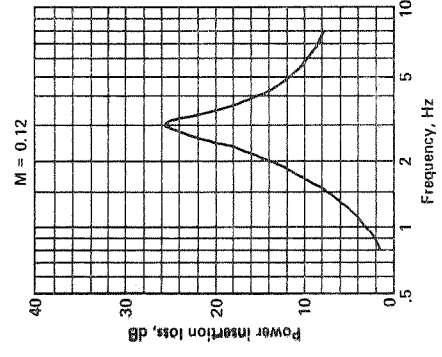
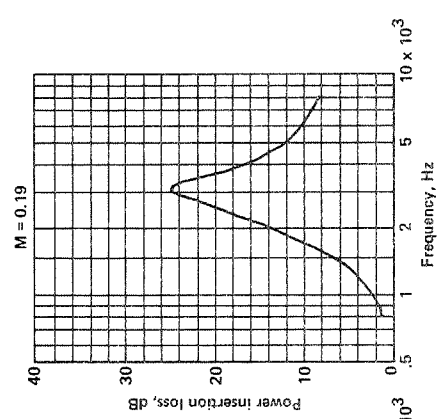
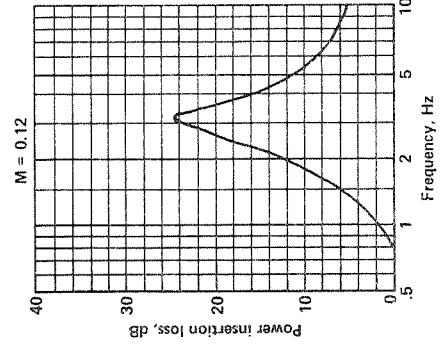
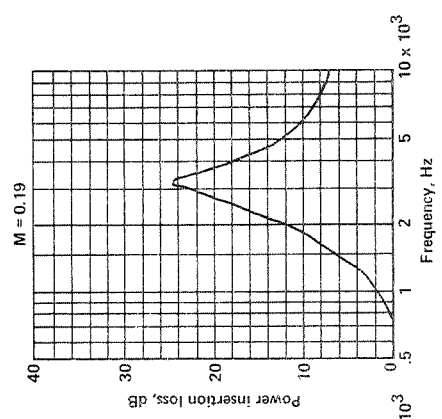
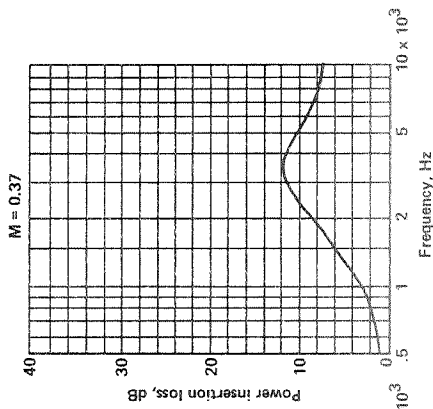
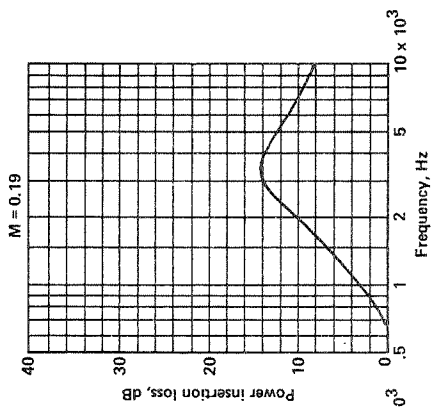


Figure A-80.

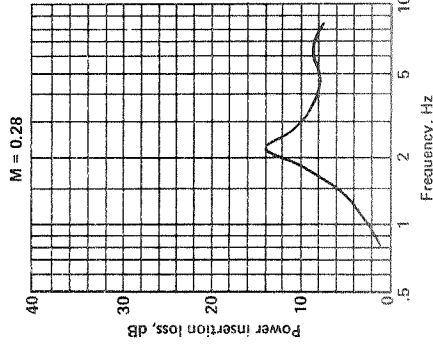
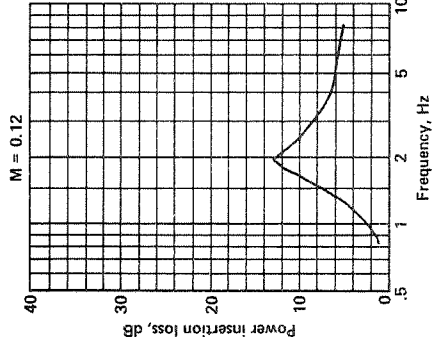
Figure A-79.

Lining material Woven Metal Fiber  
 Flow resistance 80 rayls (cgs)  
 Lining depth 0.5 in.  
 Core type 3/8-in. Hexcel

Duct geometry 6 x 10 in.  
 Walls lined Two/10 in.  
 Lining length 22 in.



Duct geometry 6 x 10 in.  
 Walls lined One/10 in.  
 Lining length 44 in.



Lining material Metallic Felt  
 Flow resistance 30 rayls (cgs)  
 Lining depth 0.5 in.  
 Core type 3/8-in. Hexcel

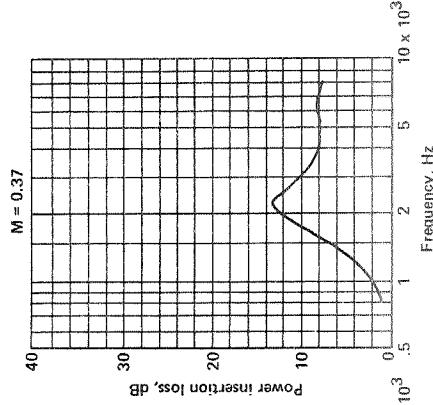
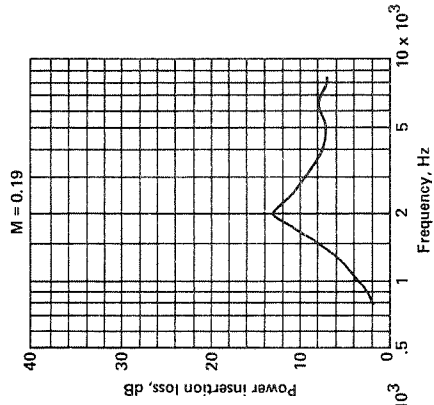


Figure A-81.

Figure A-82.

Lining material     Metallic Felt      
 Flow resistance     30 rays (cgs)      
 Lining depth     0.5 in.      
 Core type     3/8-in. Hexcel    

Duct geometry     6 x 10 in.      
 Walls lined     Two/10 in.      
 Lining length     44 in.    

Lining material     Metallic Felt      
 Flow resistance     30 rays (cgs)      
 Lining depth     0.5 in.      
 Core type     3/8-in. Hexcel    

Duct geometry     6 x 10 in.      
 Walls lined     Two/10 in.      
 Lining length     22 in.    

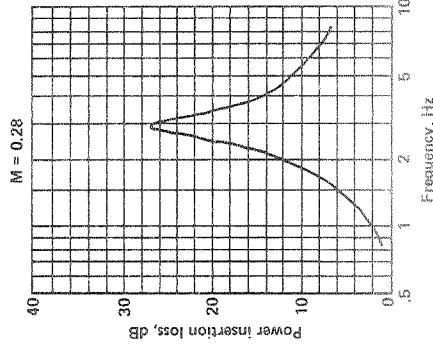
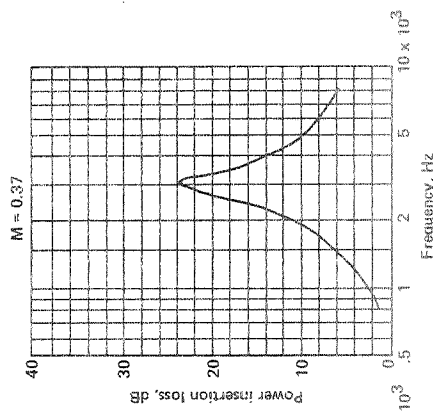
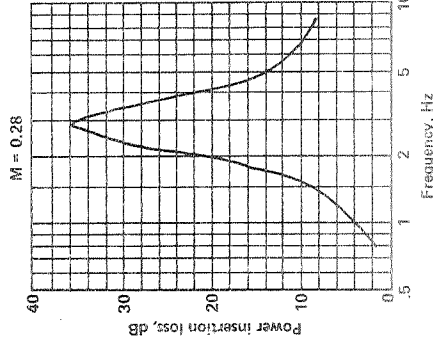
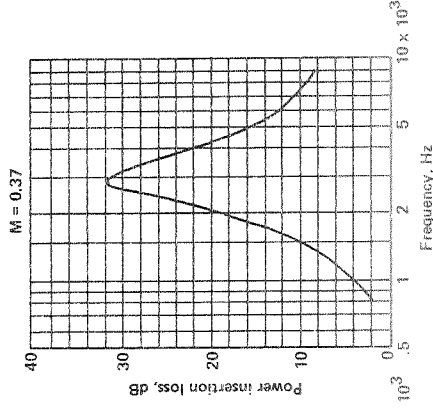
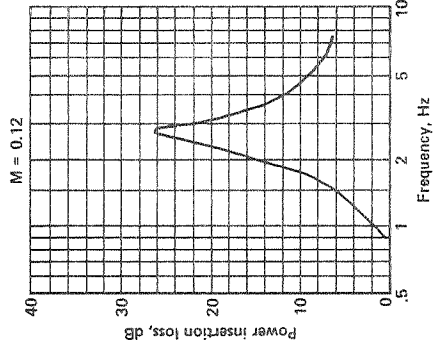
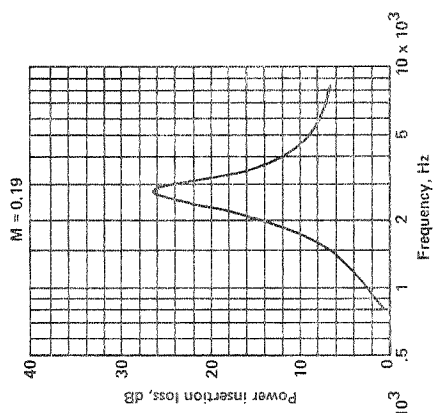
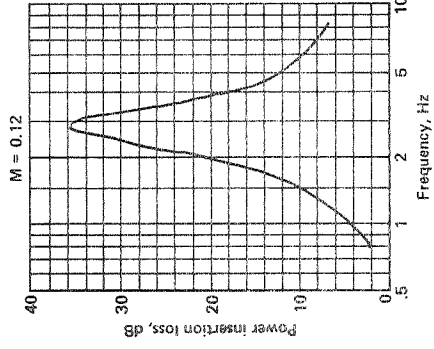
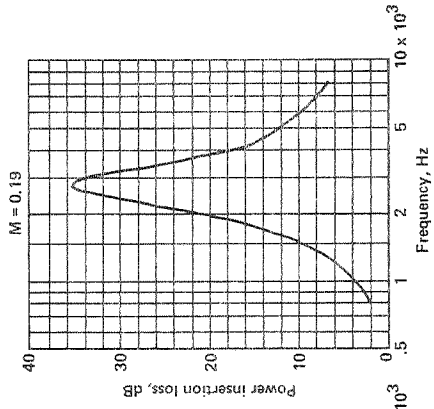


Figure A-84.

Figure A-83.

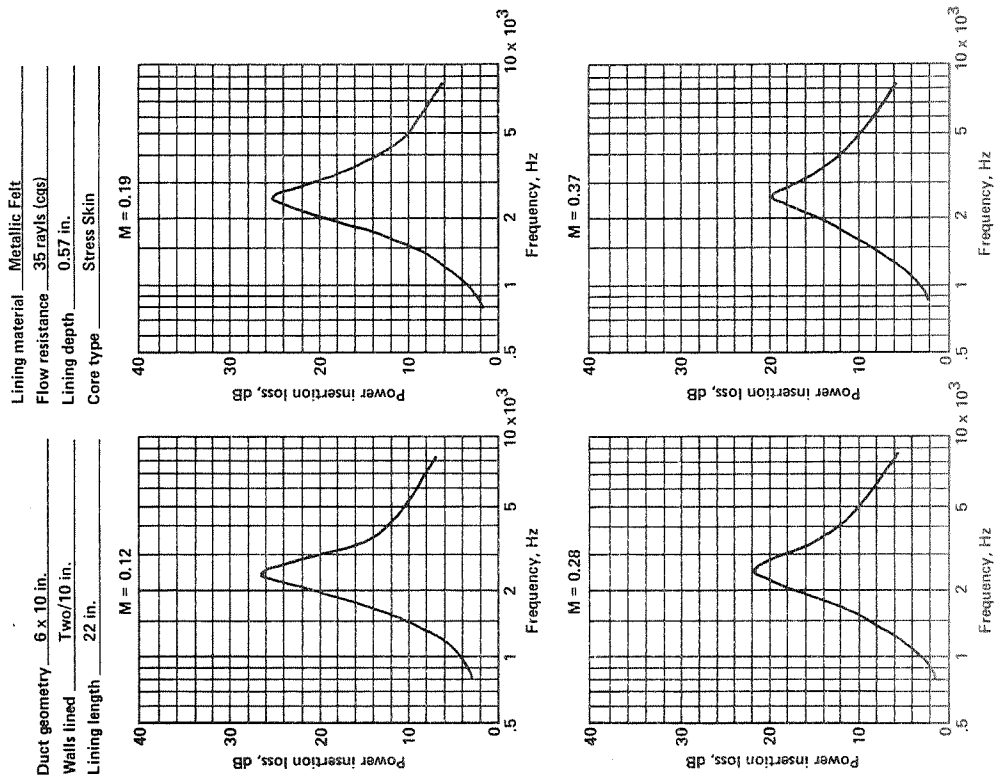


Figure A-86.

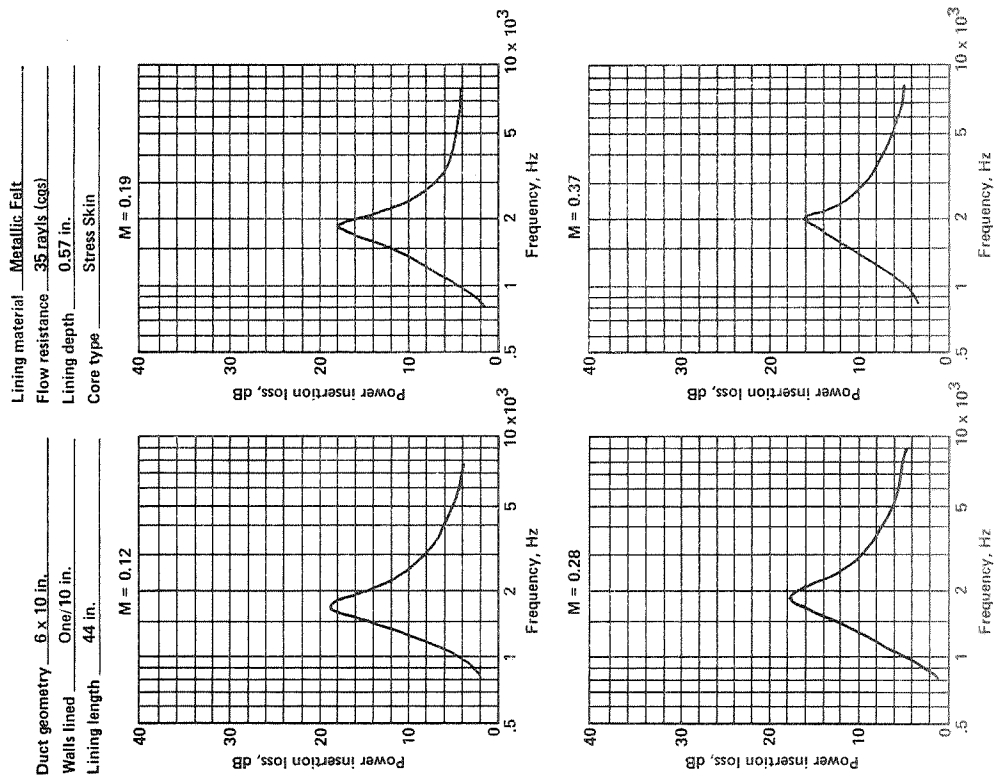


Figure A-85.

Lining material Polyimide  
 Flow resistance 30 raysls (cgs)  
 Lining depth 0.5 in.  
 Core type 1/8-in. Hexcel

Duct geometry 6 x 10 in.  
 Walls lined Two/10 in.  
 Lining length 22 in.

Lining material Polyimide  
 Flow resistance 30 raysls (cgs)  
 Lining depth 0.5 in.  
 Core type 1/8-in. Hexcel

Duct geometry 6 x 10 in.  
 Walls lined One/10 in.  
 Lining length 44 in.

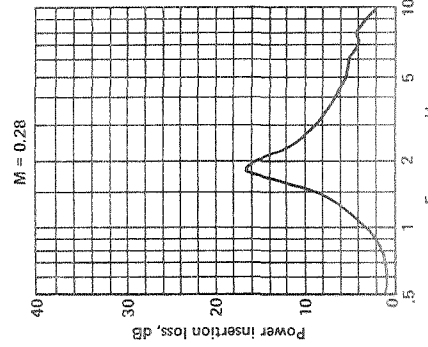
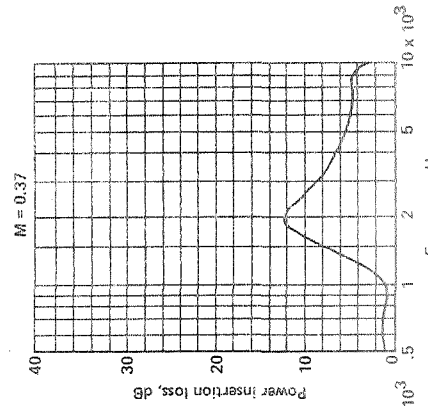
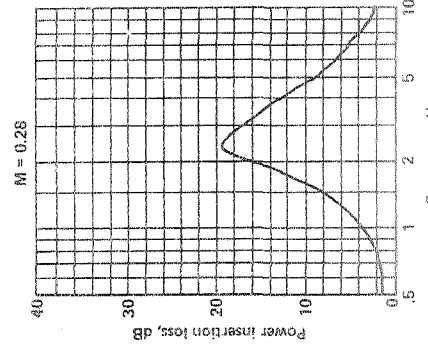
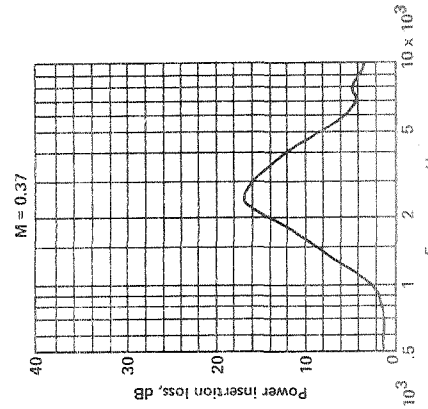
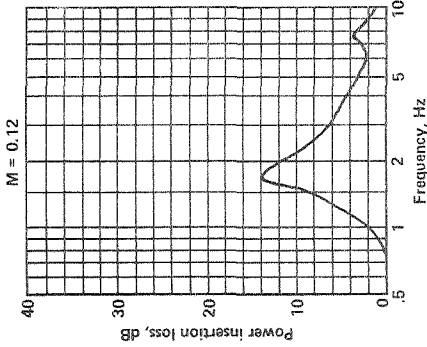
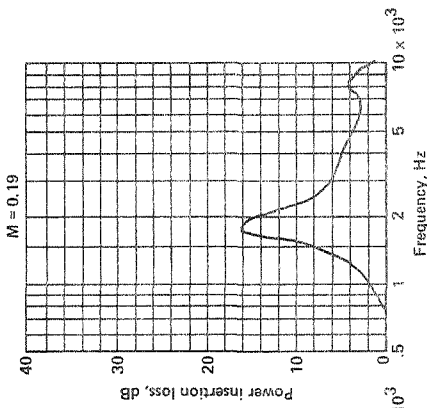
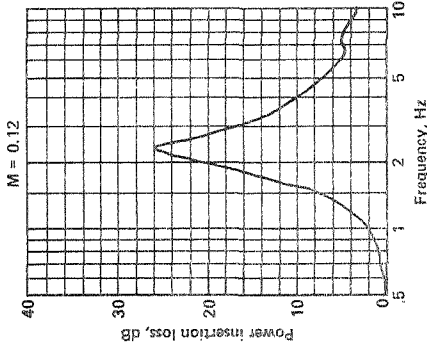
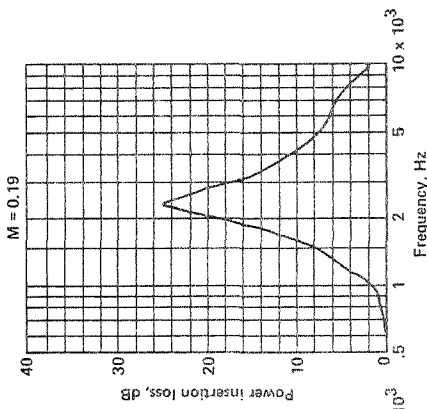


Figure A-88.

Figure A-87.

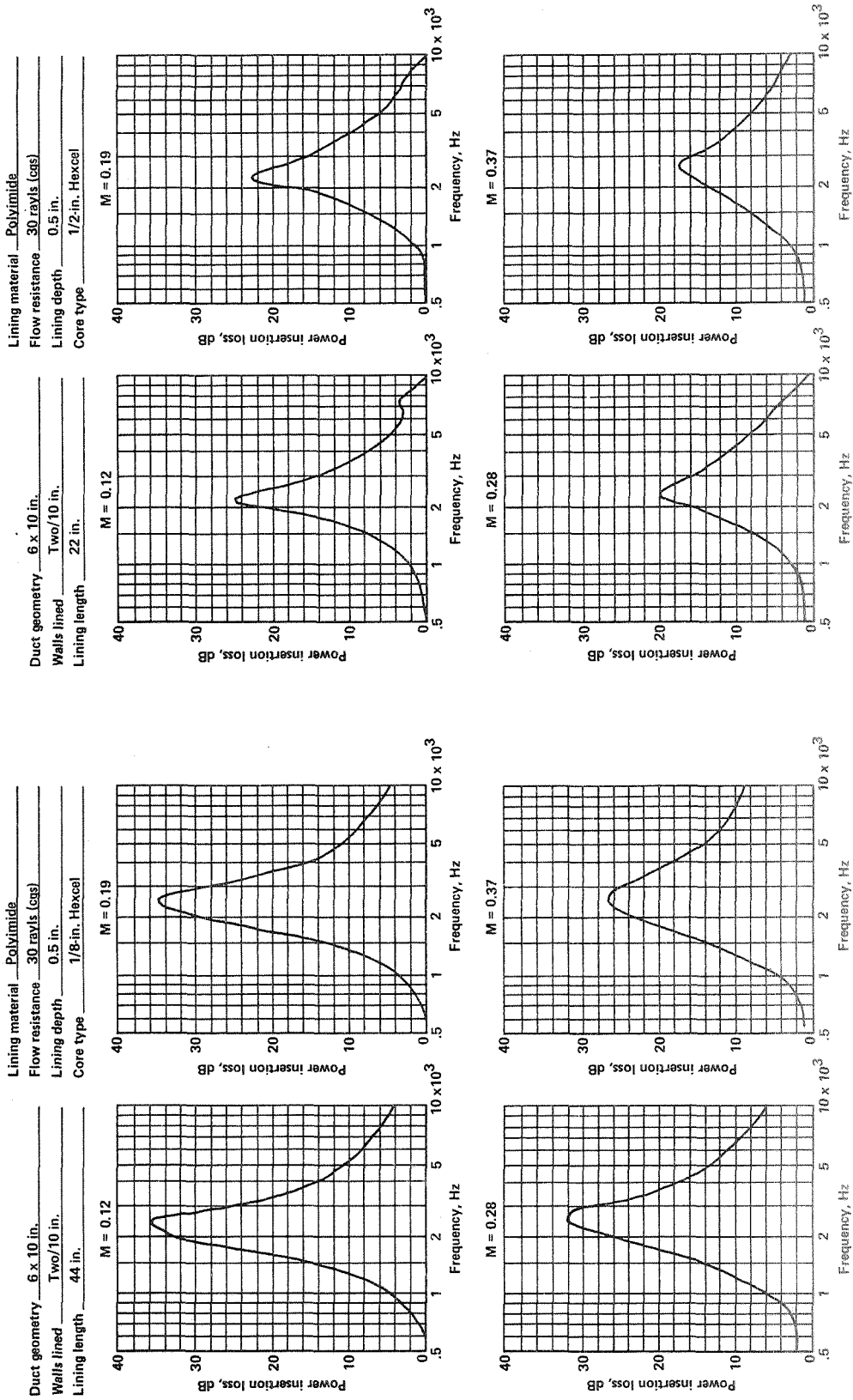


Figure A-89.

Figure A-90.

Lining material Polyimide  
 Flow resistance 30 rays (cgs)  
 Lining depth 0.5 in.  
 Core type 1-in. Eggcrate

Duct geometry 6 x 10 in.  
 Walls lined One/10 in.  
 Lining length 44 in.

Lining material Polyimide  
 Flow resistance 30 rays (cgs)  
 Lining depth 0.5 in.  
 Core type 1/2-in. Hexcel

Duct geometry 6 x 10 in.  
 Walls lined Two/10 in.  
 Lining length 44 in.

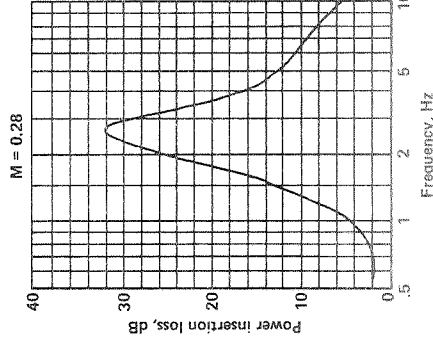
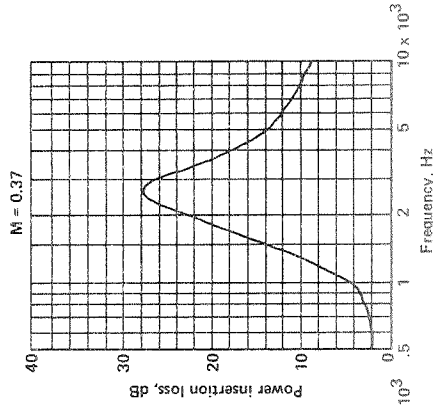
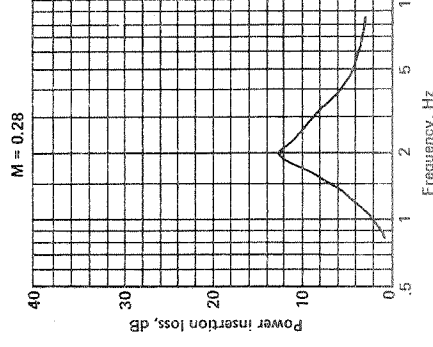
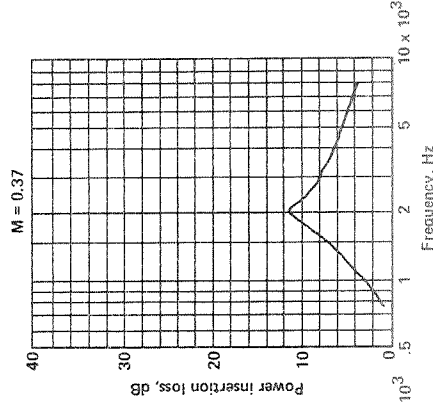
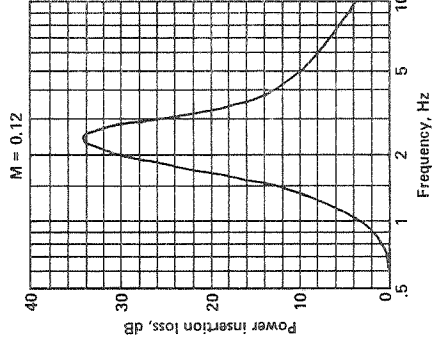
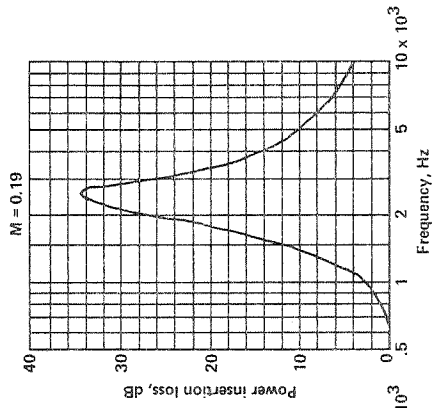
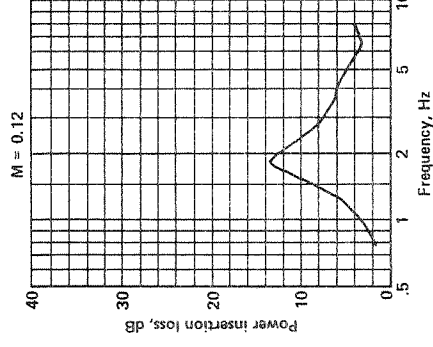
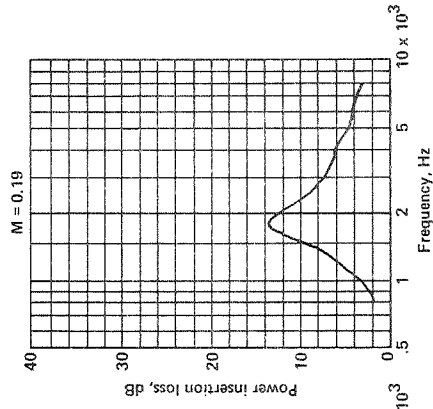
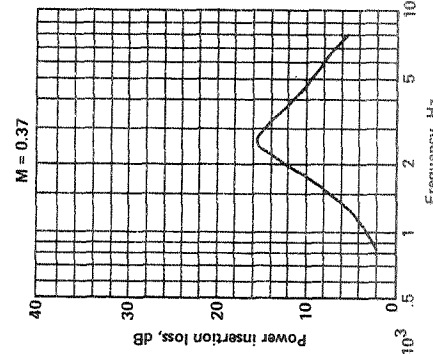
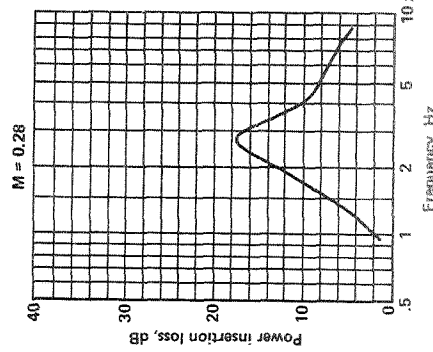
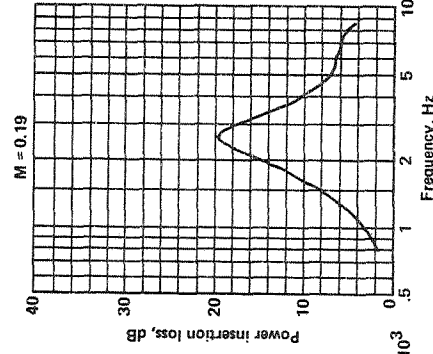
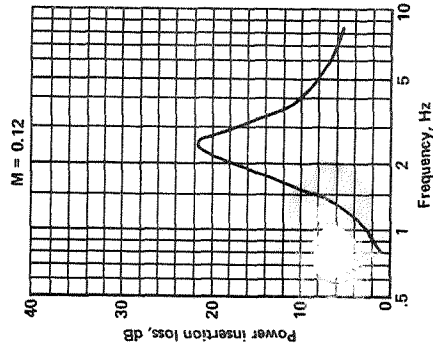


Figure A-92.

Figure A-91.

Test No. 4C  
 Duct geometry 6 x 10 in.  
 Walls lined Two/10 in.  
 Lining length 22 in.

Lining material Polyimide  
 Flow resistance 30 rays/lcs  
 Lining depth 0.5 in.  
 Core type 1-in. Eggcrate



Duct geometry 6 x 10 in.  
 Walls lined Two/10 in.  
 Lining length 44 in.

Lining material Polyimide  
 Flow resistance 30 rays/lcs  
 Lining depth 0.5 in.  
 Core type 1-in. Eggcrate

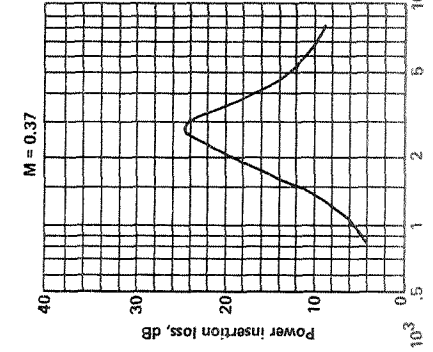
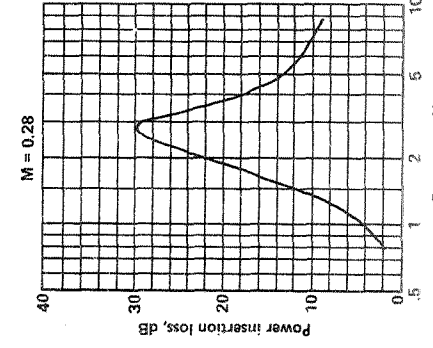
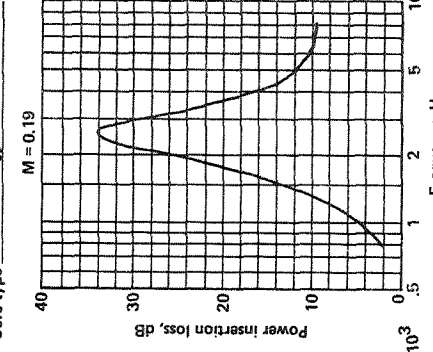
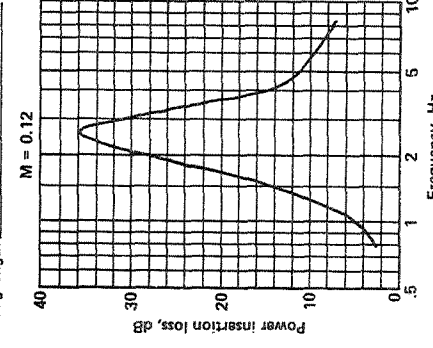


Figure A-93.

Figure A-94.



Lining material Polyimide  
 Flow resistance 10 + 40 rays (cgs)  
 Lining depth 1/4 in. + 1/4 in.  
 Core type 3/8-in. Hexcel

Duct geometry 6 x 10 in.  
 Walls lined Two/10 in.  
 Lining length 22 in.

Lining material Polyimide  
 Flow resistance 10 + 40 rays (cgs)  
 Lining depth 1/4 in. + 1/4 in.  
 Core type 3/8-in. Hexcel

Duct geometry 6 x 10 in.  
 Walls lined One/10 in.  
 Lining length 44 in.

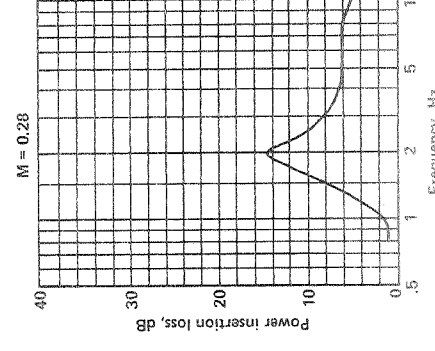
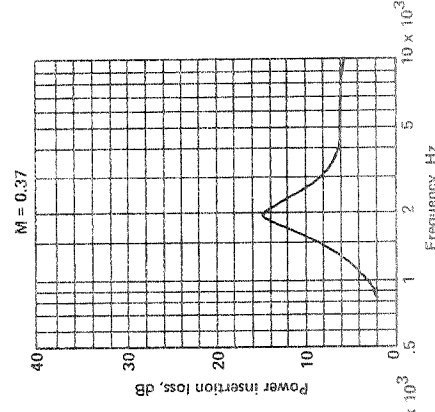
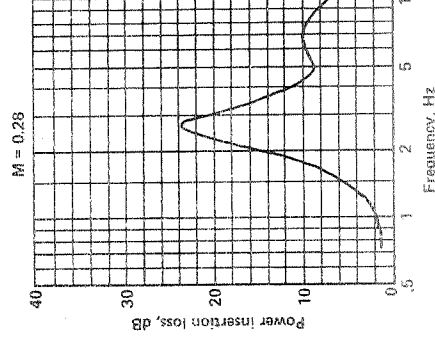
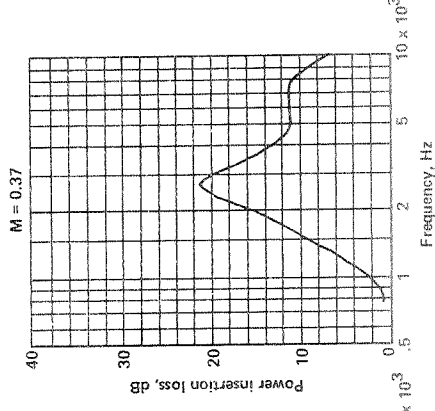
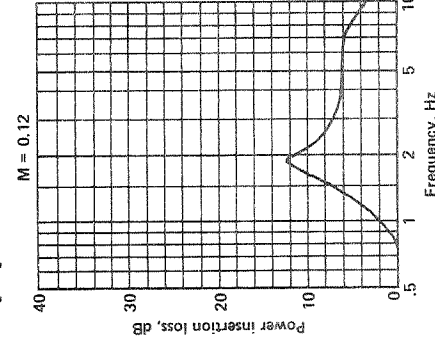
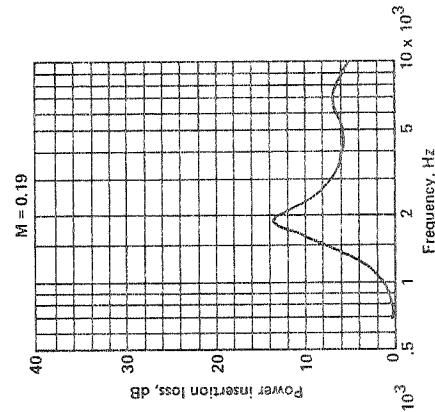
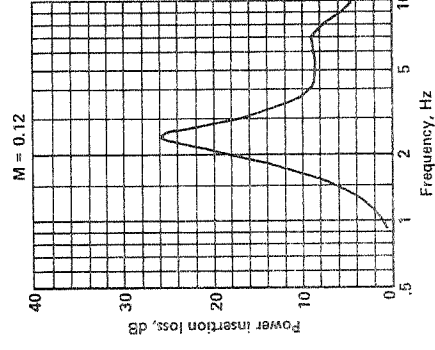
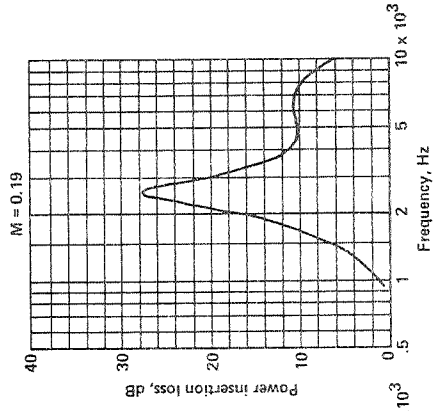


Figure A-96.

Figure A-95.

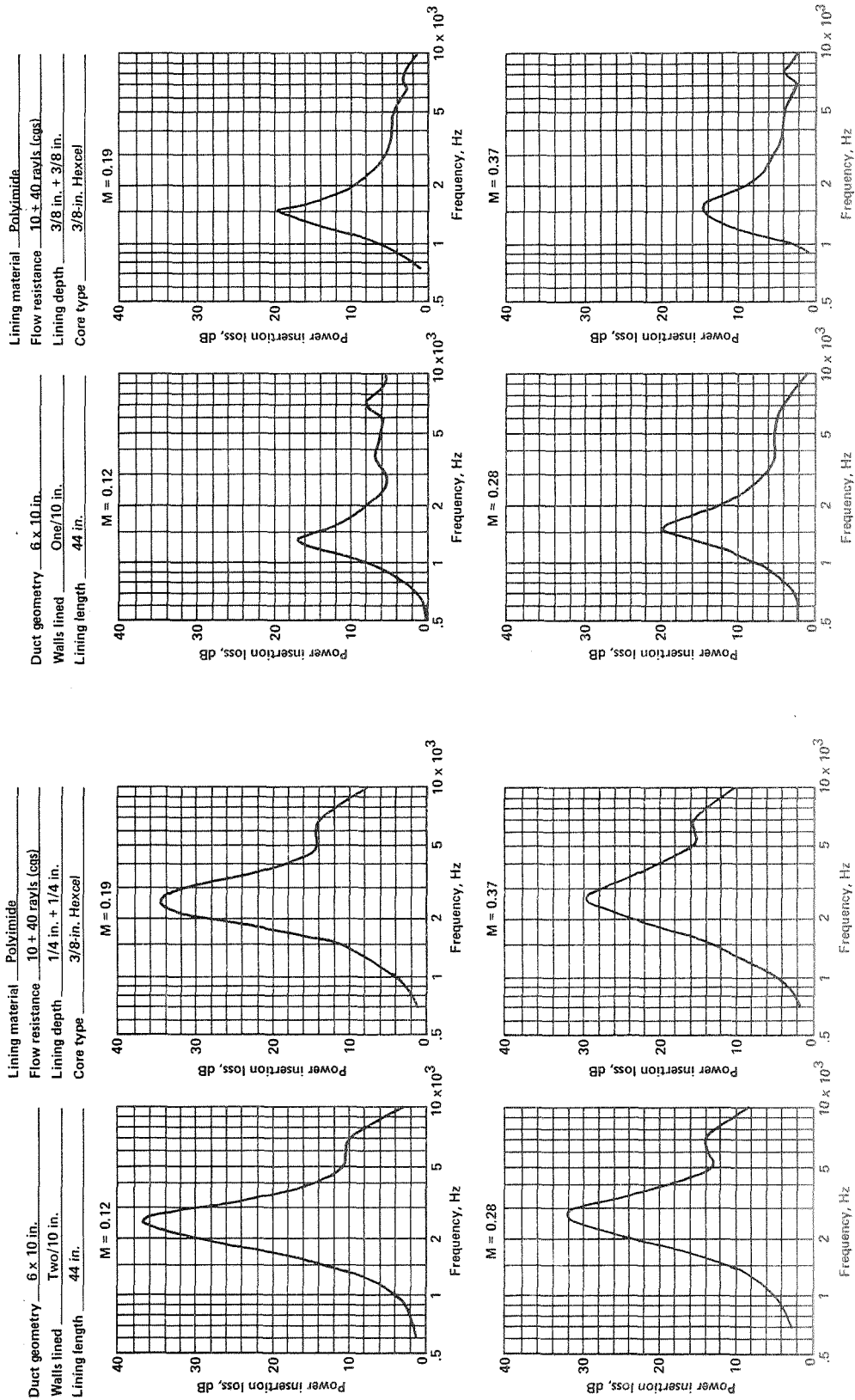


Figure A-97.

Figure A-98.

Lining material   Polyimide    
 Flow resistance   10 + 40 rays/ls. (egs)    
 Lining depth   3/8 in. + 3/8 in.    
 Core type   3/8-in. Hexcel  

Duct geometry   6 x 10 in.    
 Walls lined   2/10 in.    
 Lining length   44 in.  

Lining material   Polyimide    
 Flow resistance   10 + 40 rays/ls. (egs)    
 Lining depth   3/8 in. + 3/8 in.    
 Core type   3/8-in. Hexcel  

Duct geometry   6 x 10 in.    
 Walls lined   2/10 in.    
 Lining length   22 in.  

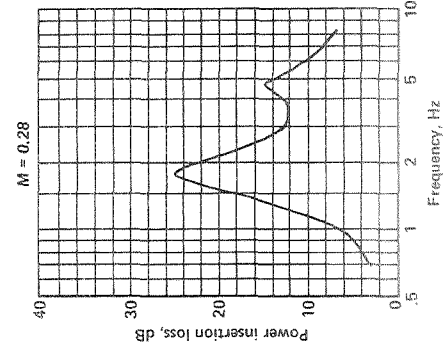
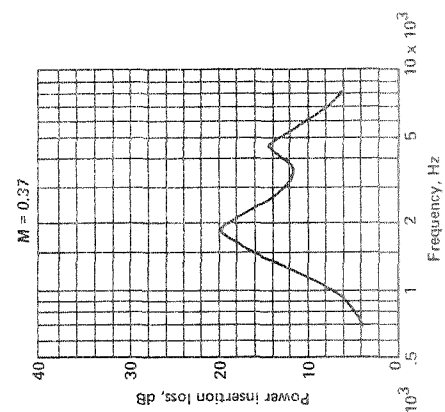
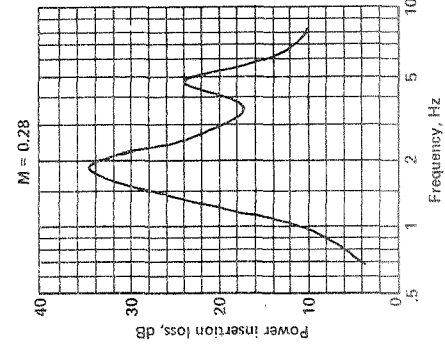
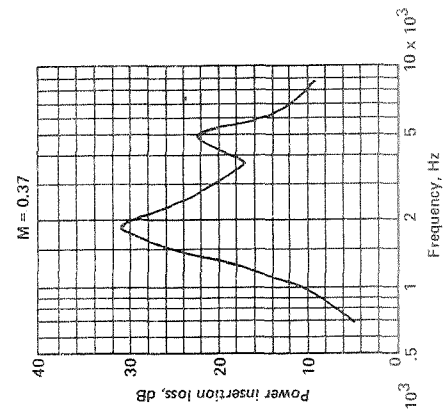
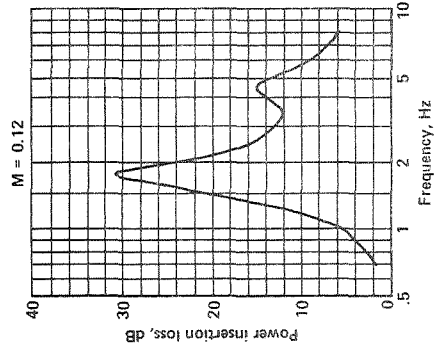
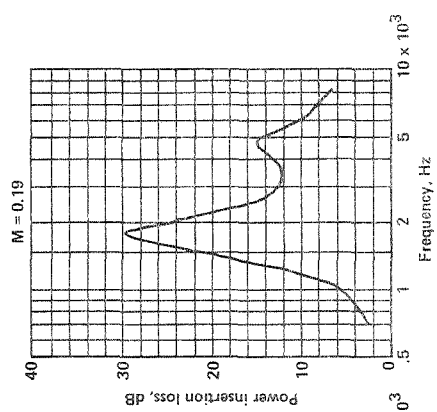
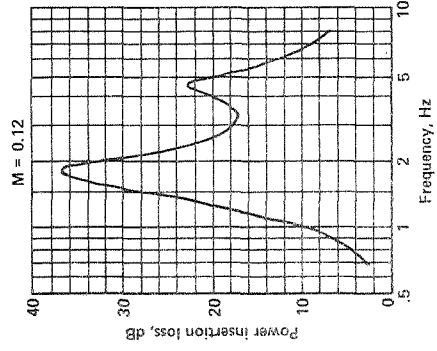
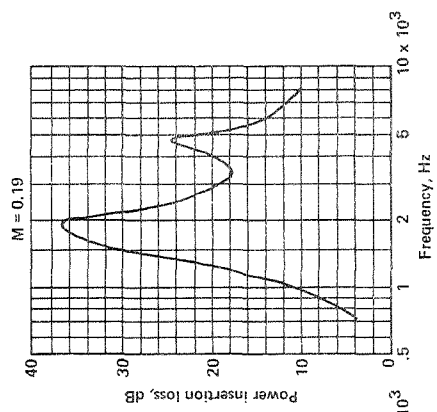


Figure A-100.

Figure A-99.

Lining material Polyimide  
 Flow resistance 10 + 40 rays (cgs)  
 Lining depth 1/2 in. + 1/4 in.  
 Core type 3/8-in. Hexcel

Duct geometry 6 x 10 in.  
 Walls lined Two/10 in.  
 Lining length 44 in.

Lining material Polyimide  
 Flow resistance 10 + 40 rays (cgs)  
 Lining depth 1/2 in. + 1/4 in.  
 Core type 3/8-in. Hexcel

Duct geometry 6 x 10 in.  
 Walls lined Two/10 in.  
 Lining length 22 in.

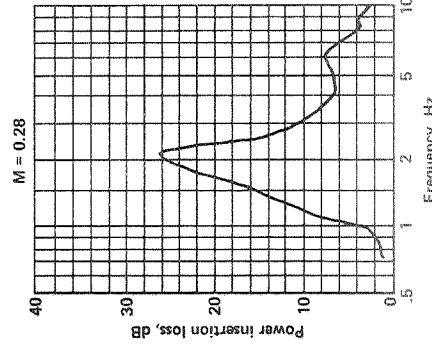
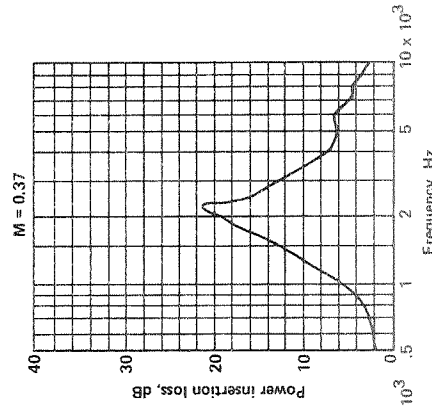
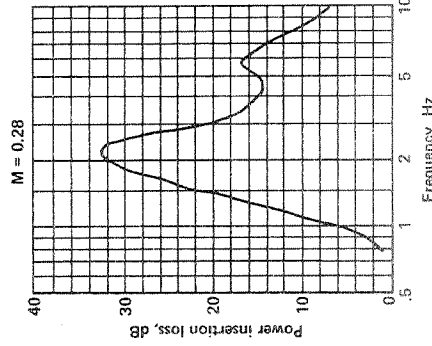
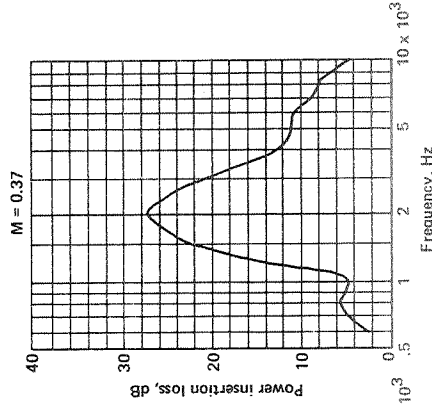
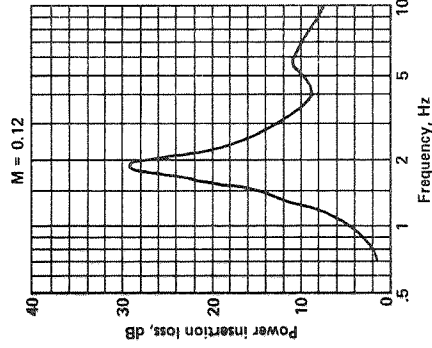
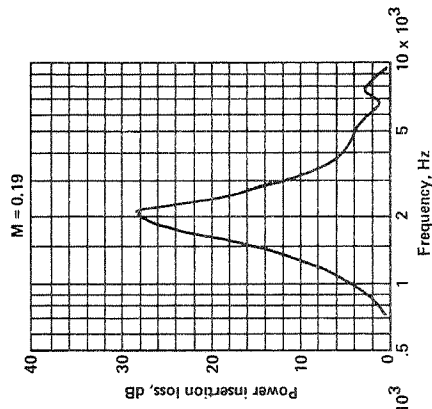
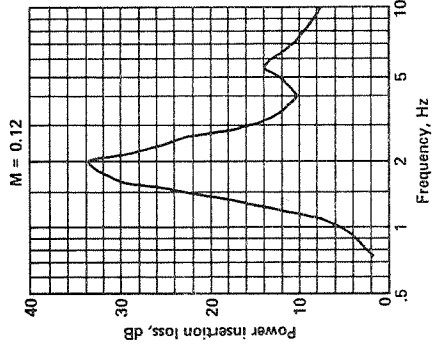
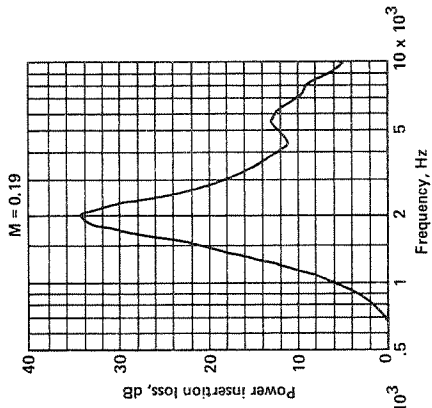


Figure A-102.

Figure A-101.

Duct geometry 6 x 10 in.  
 Walls lined One/10 in.  
 Lining length 44 in.

Lining material Polyimide  
 Flow resistance 10 + 40 rayls (cgs)  
 Lining depth 1/2 in. + 1/2 in.  
 Core type 3/8-in. Hexcel

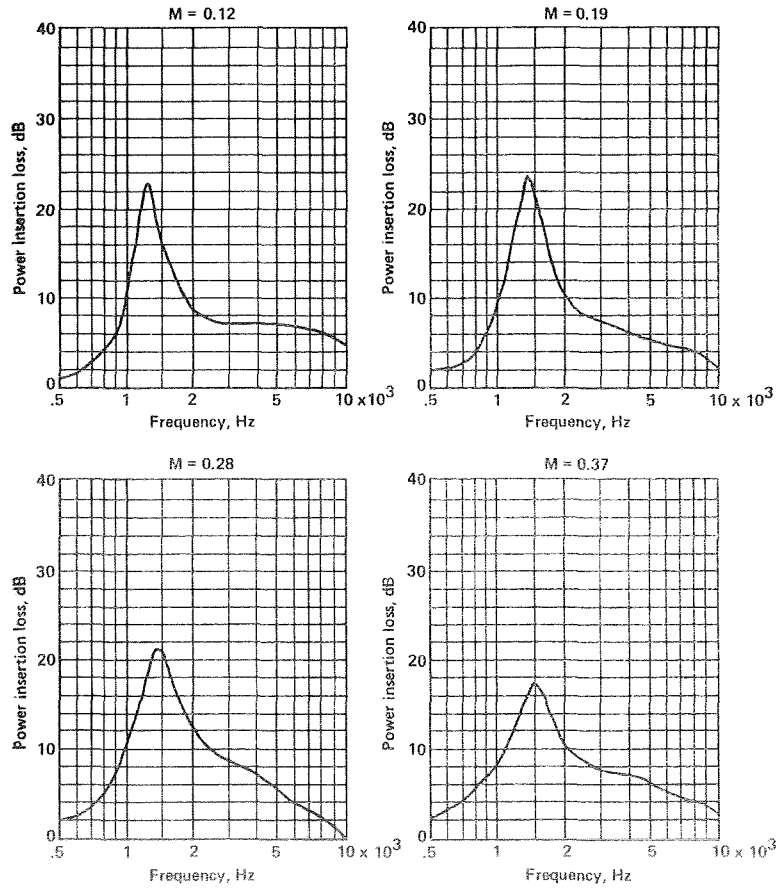


Figure A-103.

Duct geometry 6 x 10 in.  
 Walls lined One/10 in.  
 Lining length 22 in.

Lining material Polyimide  
 Flow resistance 10 + 40 rayls (cgs)  
 Lining depth 1/2 in. + 1/2 in.  
 Core type 3/8-in. Hexcel

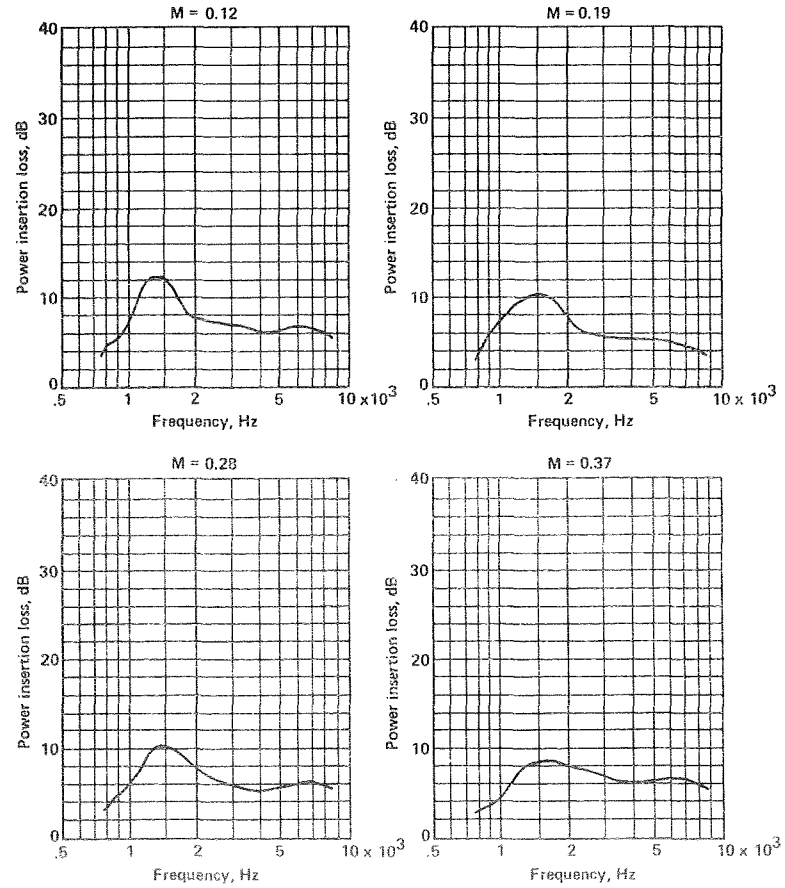


Figure A-104.

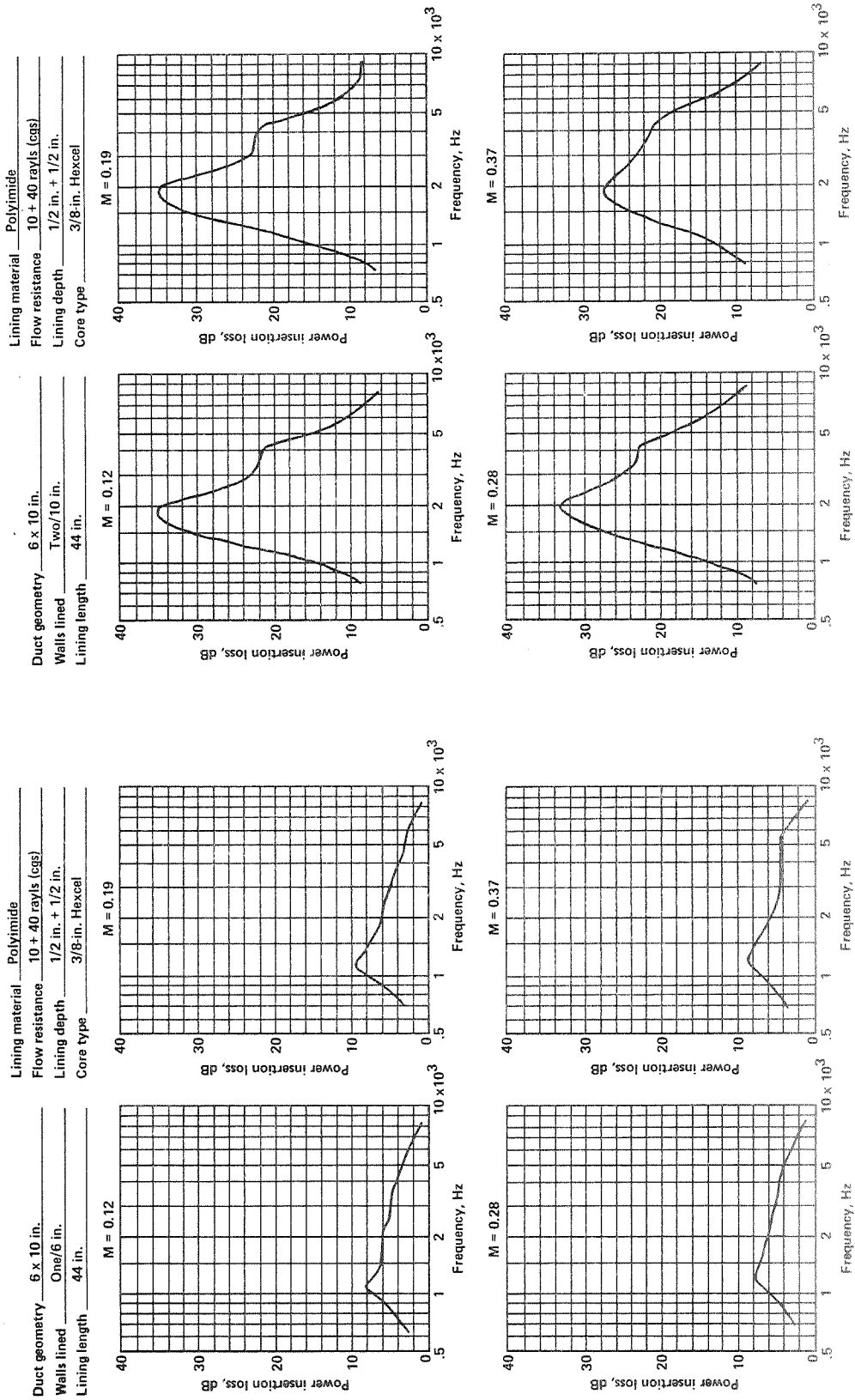


Figure A-106.

Figure A-105.

Lining material Polyimide  
 Flow resistance 10 + 40 rays (cgs)  
 Lining depth 1/2 in. + 1/2 in.  
 Core type 3/8-in. Hexcel

Duct geometry 6 x 10 in.  
 Walls lined Two/6 in.  
 Lining length 44 in.

Lining material Polyimide  
 Flow resistance 10 + 40 rays (cgs)  
 Lining depth 1/2 in. + 1/2 in.  
 Core type 3/8-in. Hexcel  
 (Siren at 1800 Hz & 150 dB in Plenum)

Duct geometry 6 x 10 in.  
 Walls lined Two/10 in.  
 Lining length 44 in.

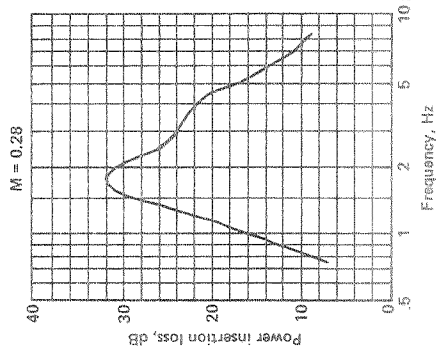
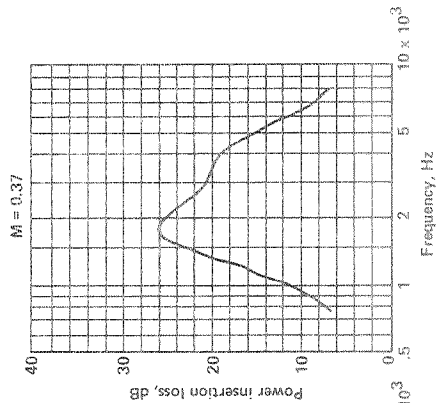
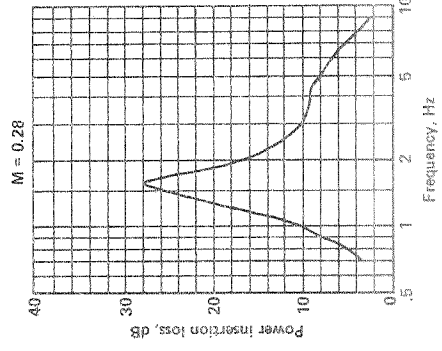
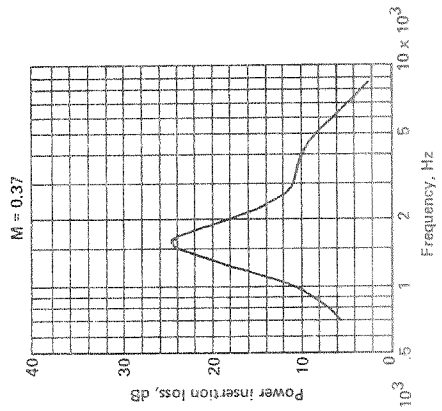
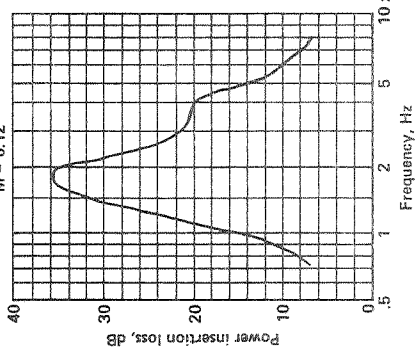
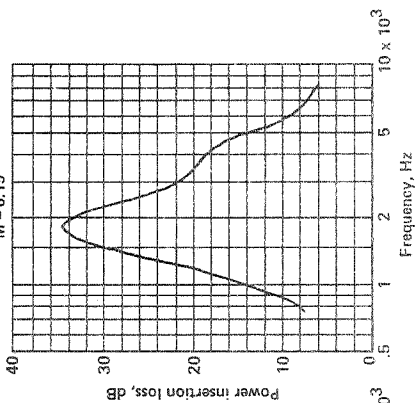
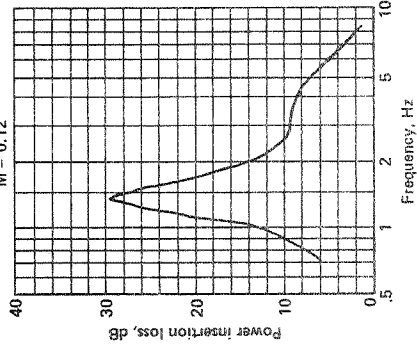
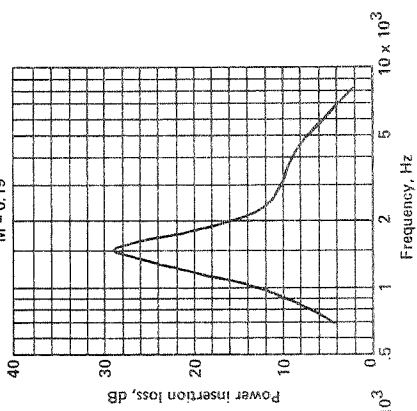


Figure A-108.

Figure A-107.

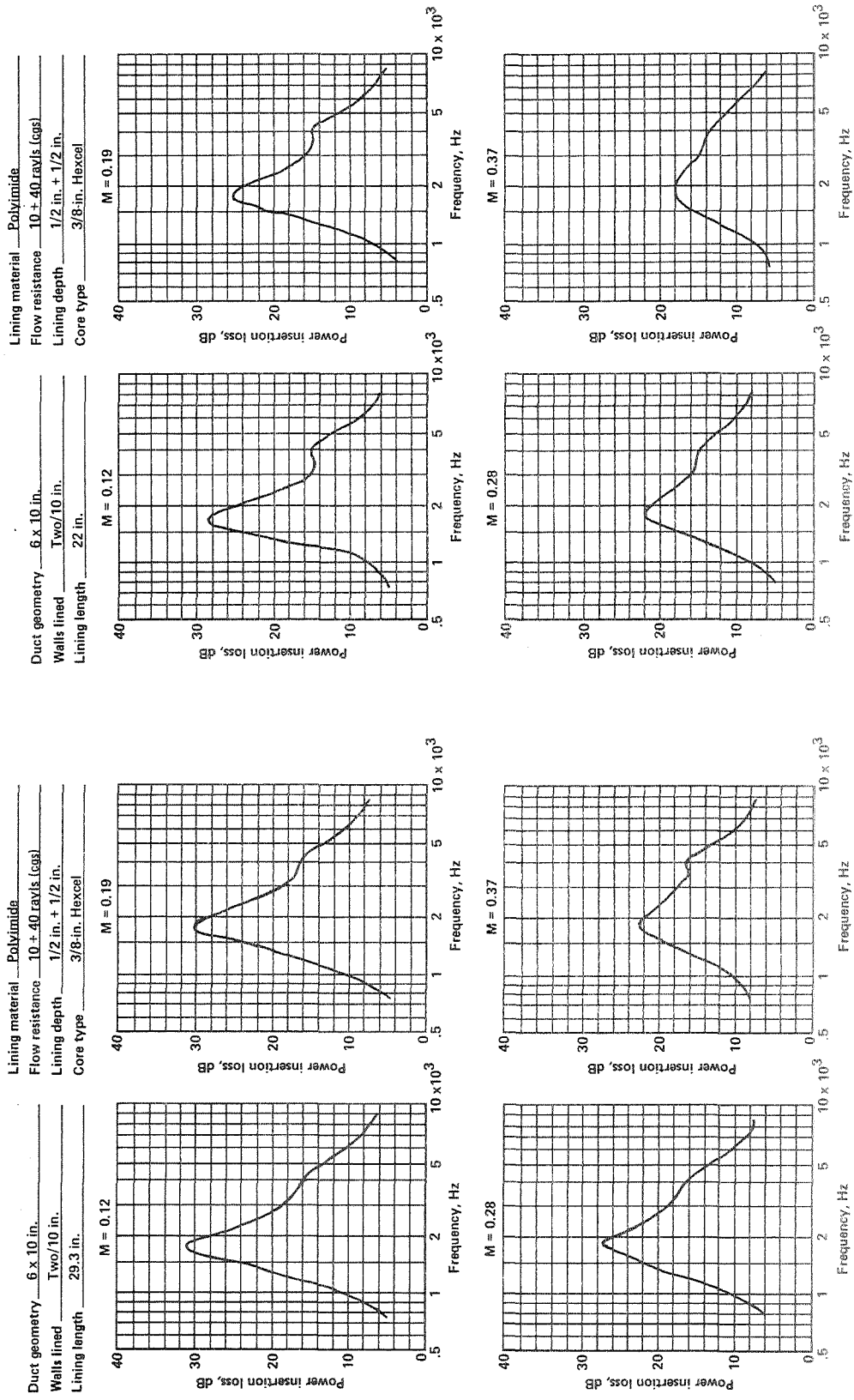


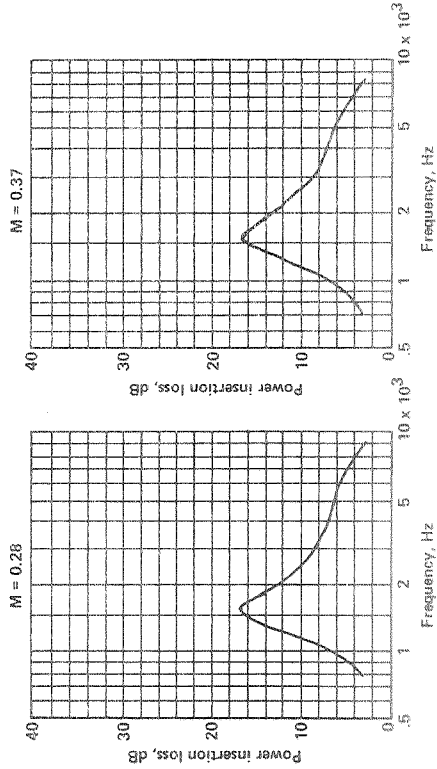
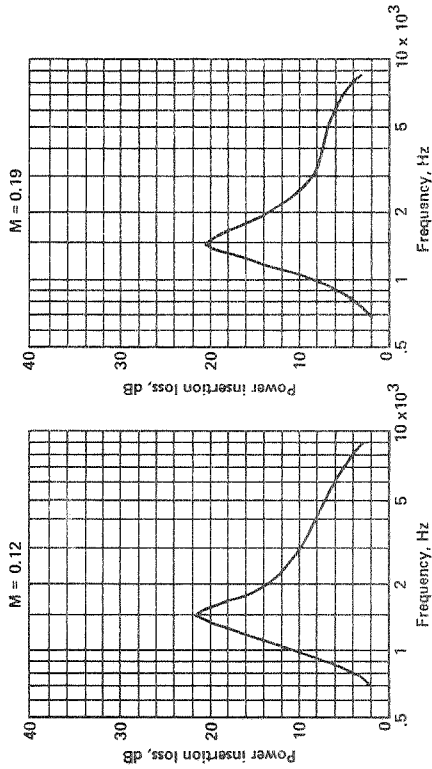
Figure A-109.

Figure A-110.



Lining material Polyimide  
 Flow resistance 10 + 40 rays (cgs)  
 Lining depth 1/2 in. + 1/2 in.  
 Core type 3/8-in. Hexcel

Duct geometry 6 x 10 in.  
 Walls lined Two/6 in.  
 Lining length 22 in.



Duct geometry 6 x 10 in.  
 Walls lined Two/10 in.  
 Lining length 14.7 in.

Lining material Polyimide  
 Flow resistance 10 + 40 rays (cgs)  
 Lining depth 1/2 in. + 1/2 in.  
 Core type 3/8-in. Hexcel

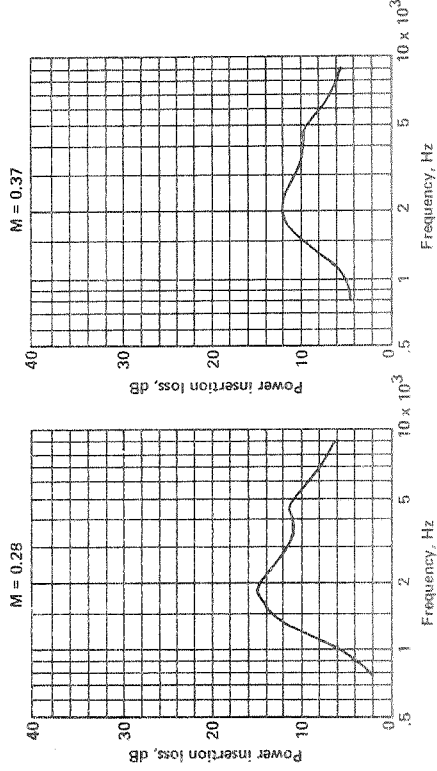
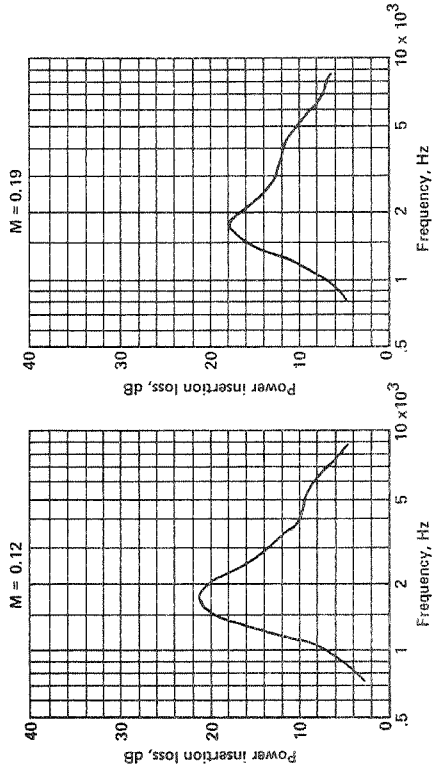


Figure A-111.

Figure A-112.

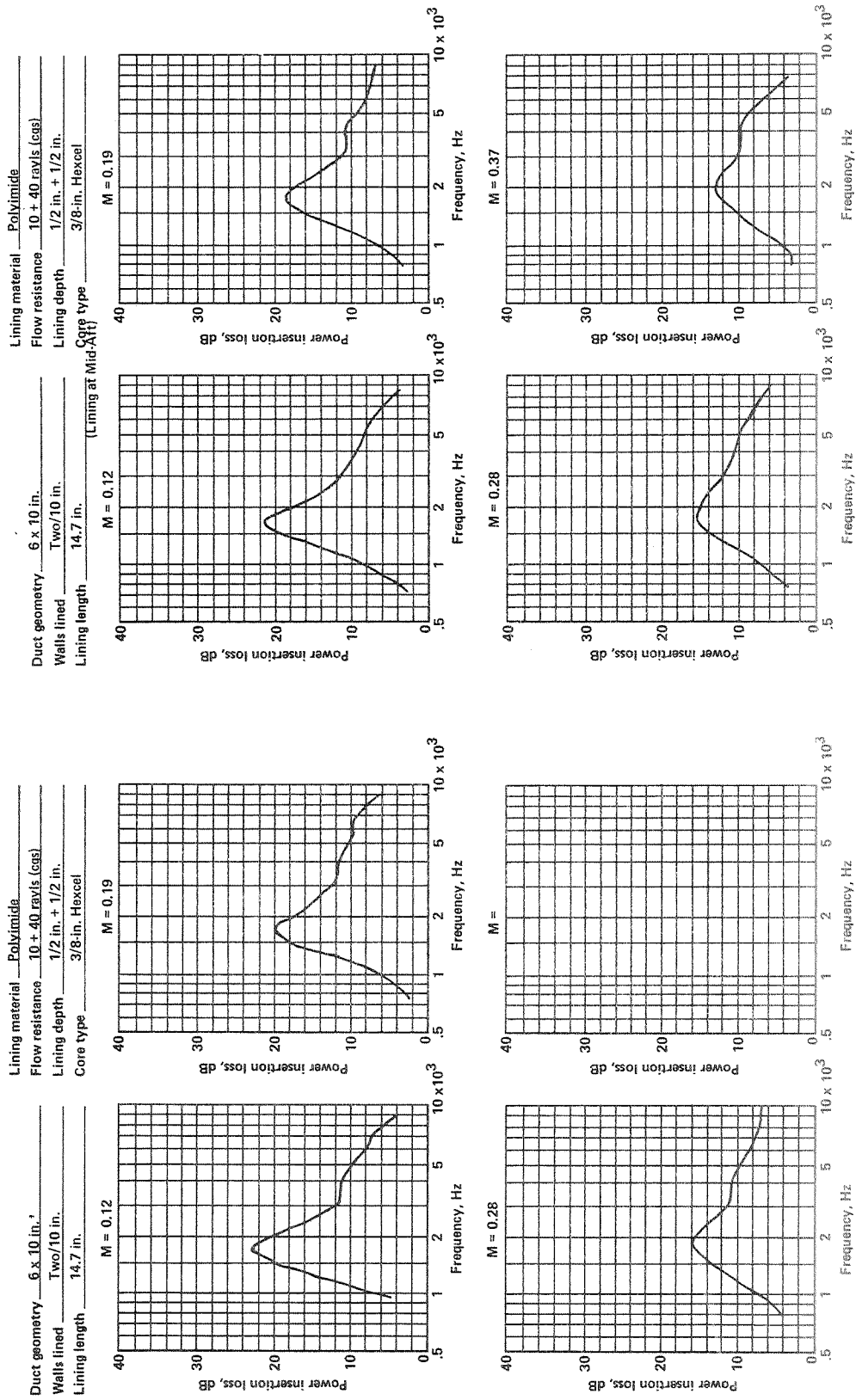


Figure A.114.

Figure A.113.

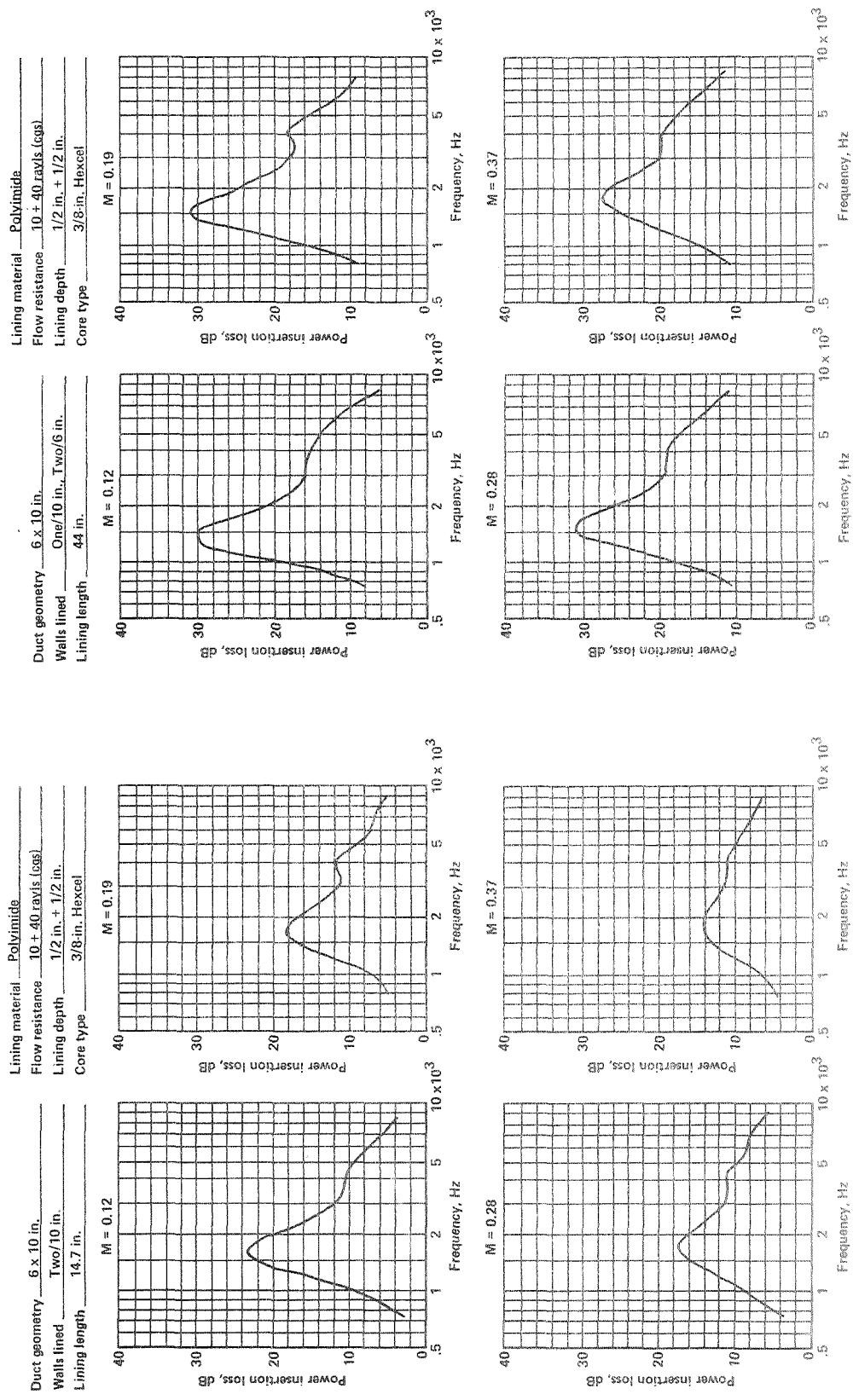


Figure A-116.

Figure A-115.

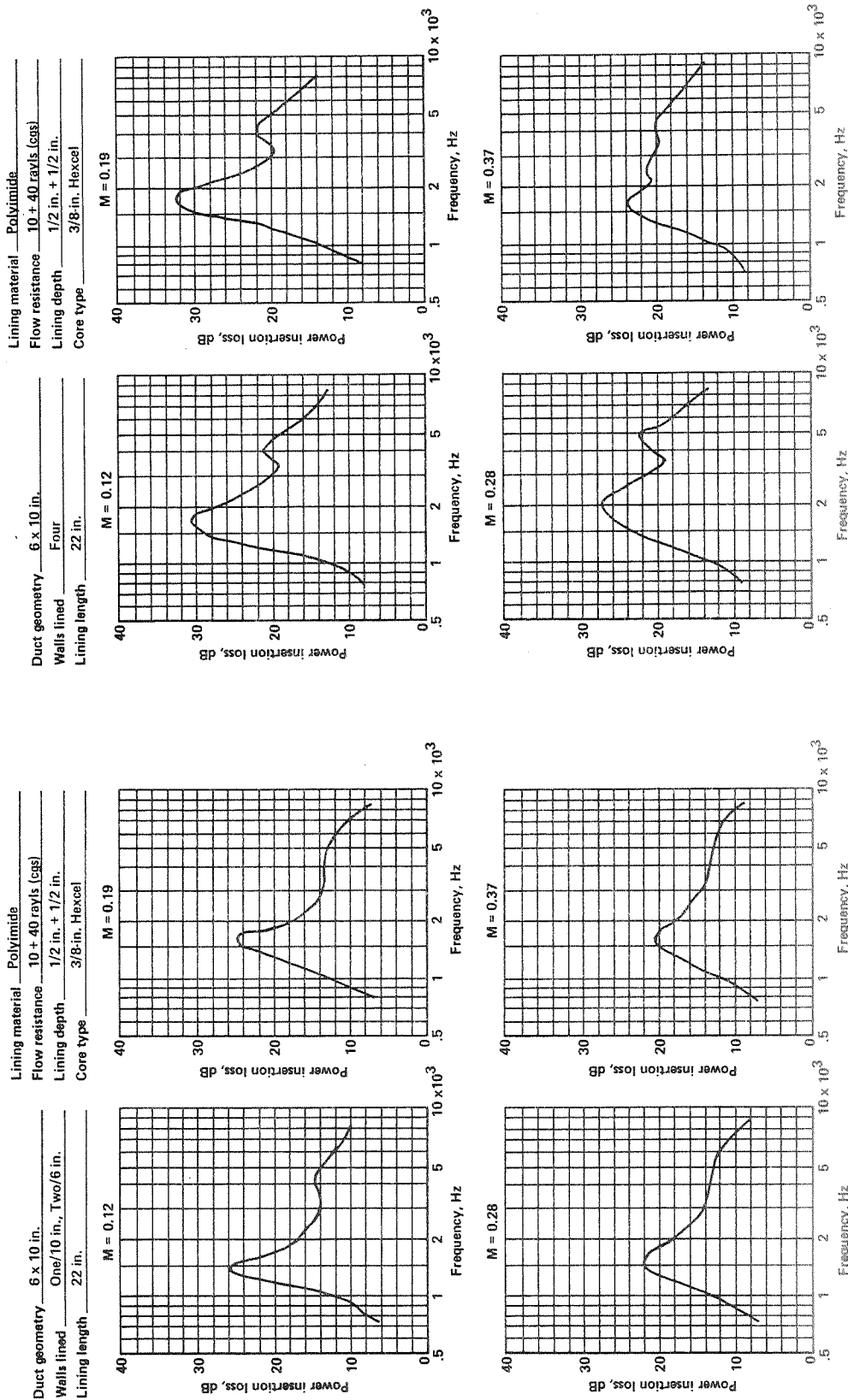
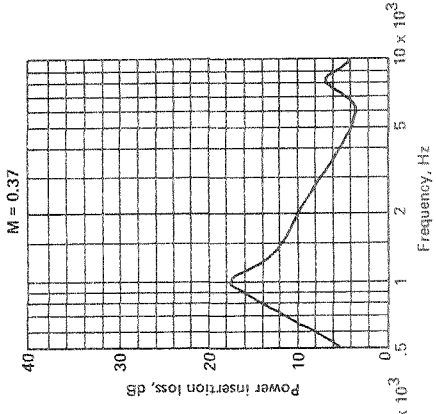
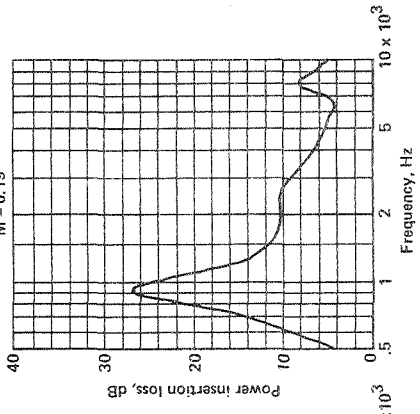


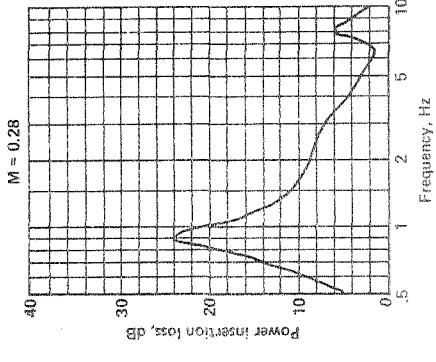
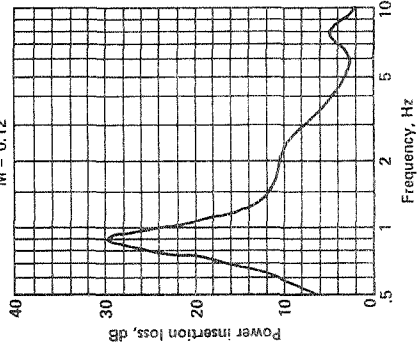
Figure A-117.

Figure A-118.

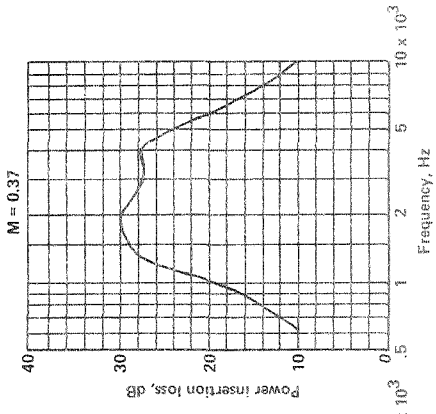
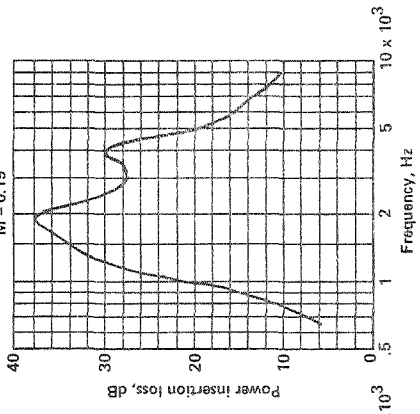
Lining material   Polyimide    
 Flow resistance   10 ± 40 ray/s. (cgs)    
 Lining depth   1 in. + 1 in.    
 Core type   3/8-in. Hexcel  



Duct geometry   6 x 10 in.    
 Walls lined   One/10 in.    
 Lining length   44 in.  



Lining material   Polyimide    
 Flow resistance   10 ± 40 ray/s. (cgs)    
 Lining depth   1/2 in. + 1/2 in.    
 Core type   3/8-in. Hexcel  



Duct geometry   6 x 10 in.    
 Walls lined   Four    
 Lining length   44 in.  

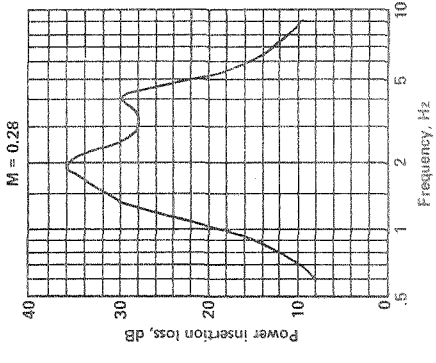
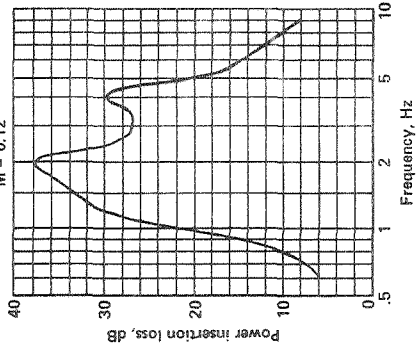


Figure A-120.

Figure A-119.

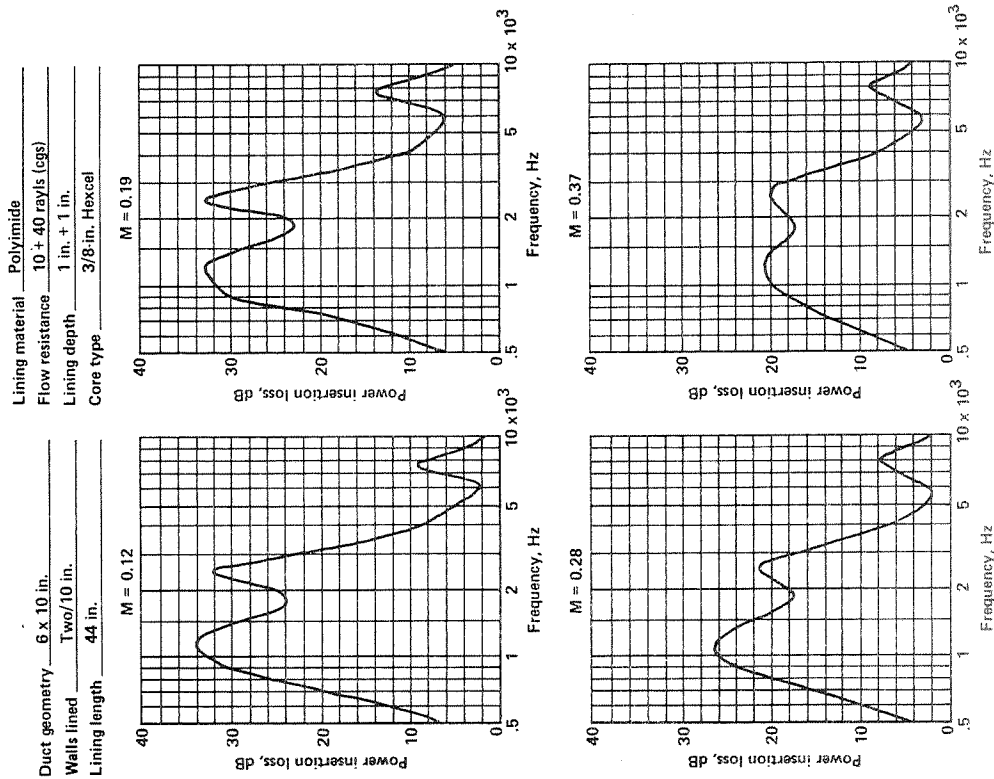


Figure A-121.

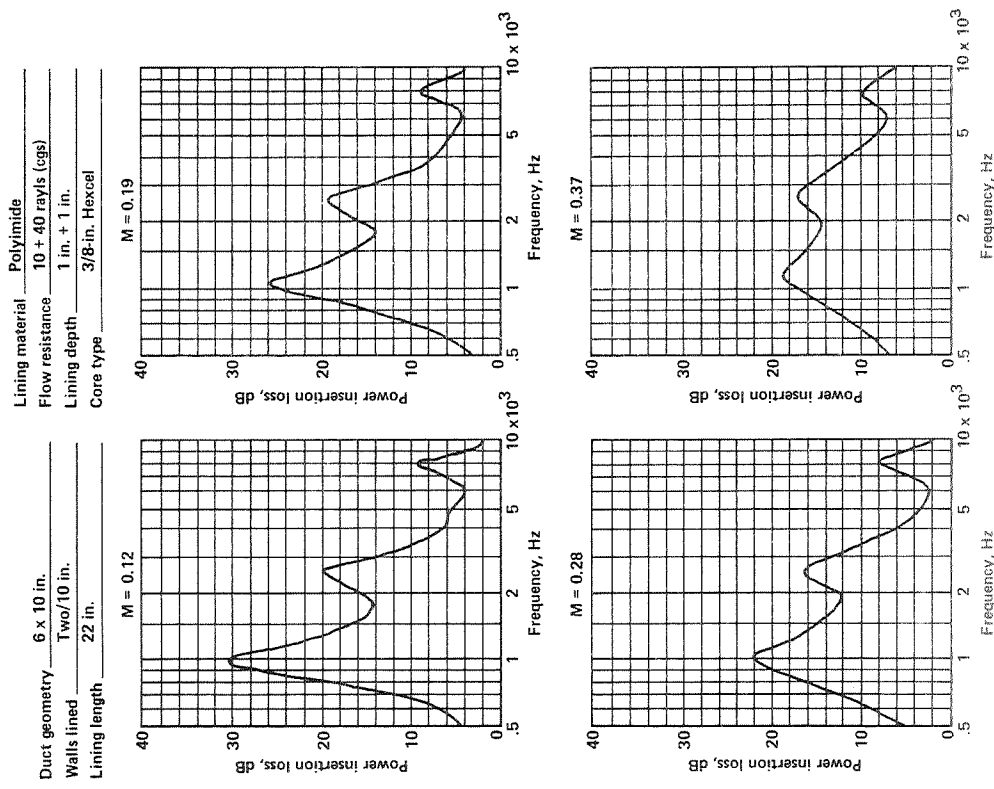


Figure A-122.

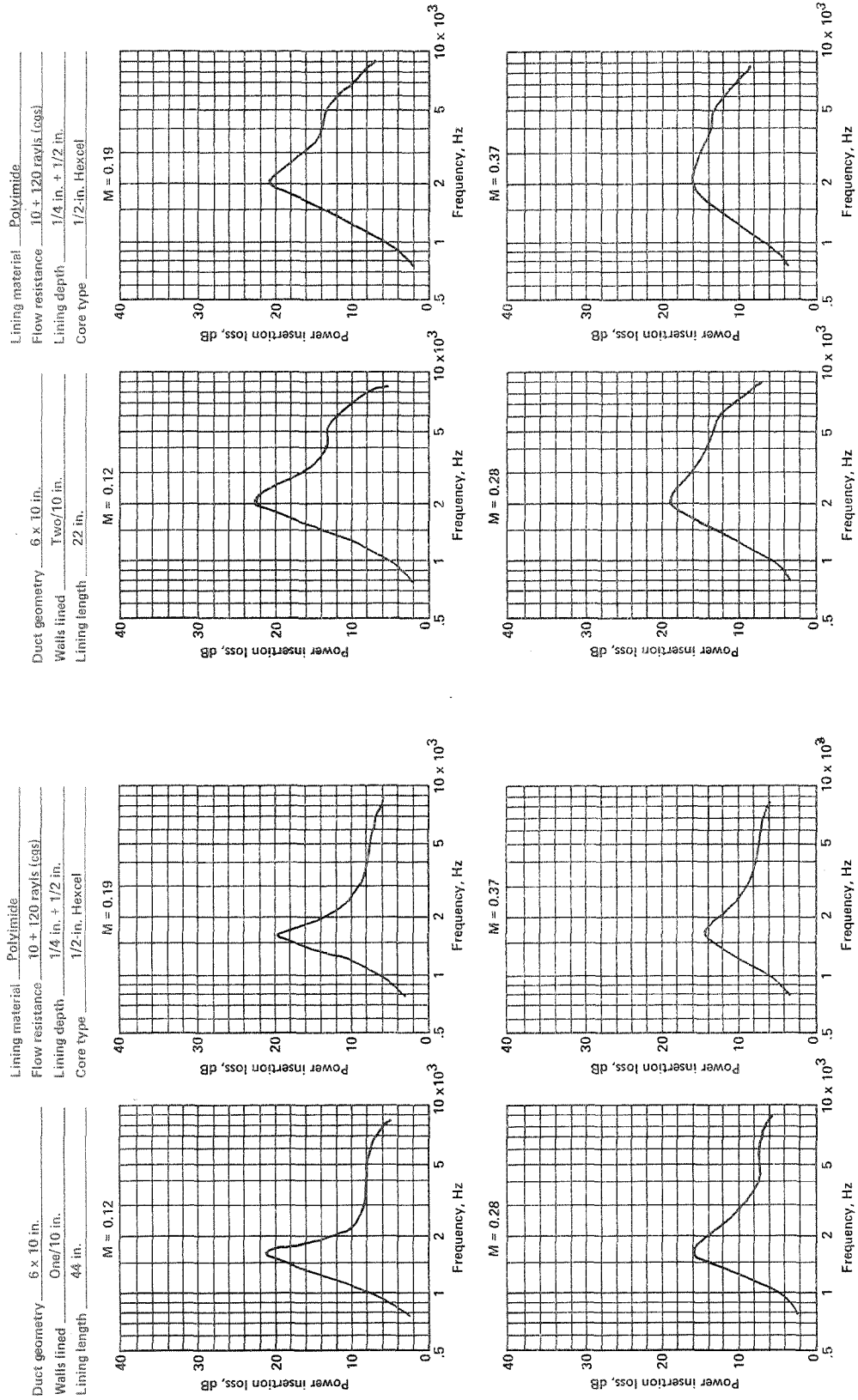


Figure A-124.

Figure A-123.

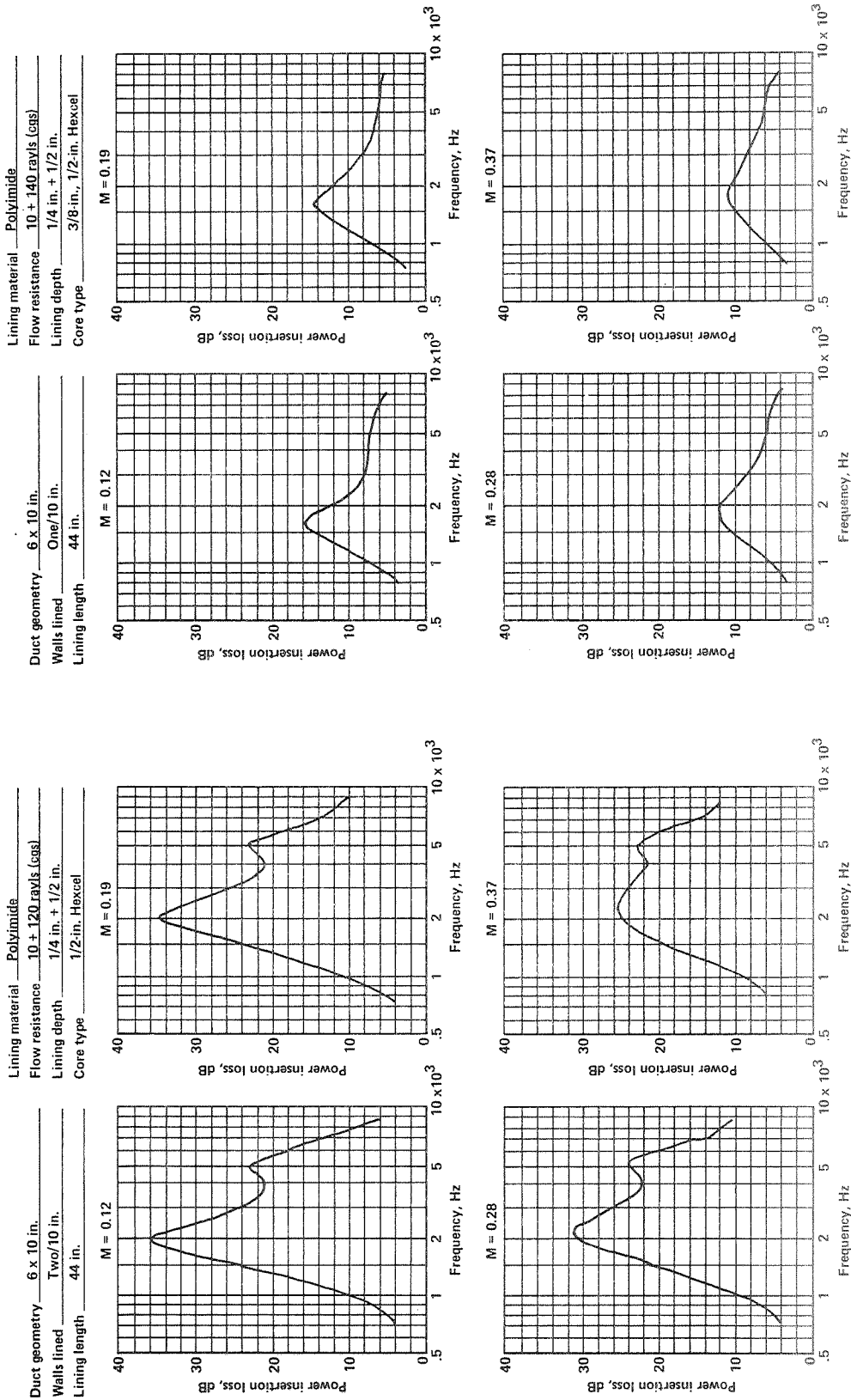


Figure A-125.

Figure A-126.



Lining material Polyimide  
 Flow resistance 10 + 140 rays (cgs)  
 Lining depth 1/4 in. + 1/2 in.  
 Core type 3/8-in., 1/2-in. Hexcel

Duct geometry 6 x 10 in.  
 Walls lined Two/10 in.  
 Lining length 44 in.

Lining material Polyimide  
 Flow resistance 10 + 140 rays (cgs)  
 Lining depth 1/4 in. + 1/2 in.  
 Core type 3/8-in., 1/2-in. Hexcel

Duct geometry 6 x 10 in.  
 Walls lined Two/10 in.  
 Lining length 22 in.

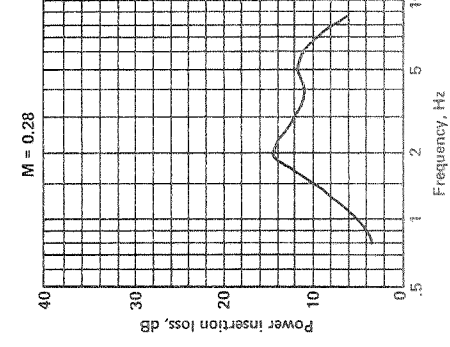
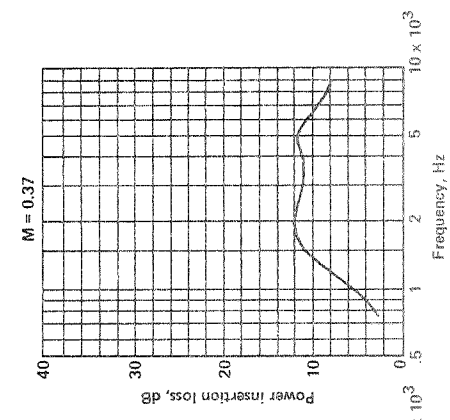
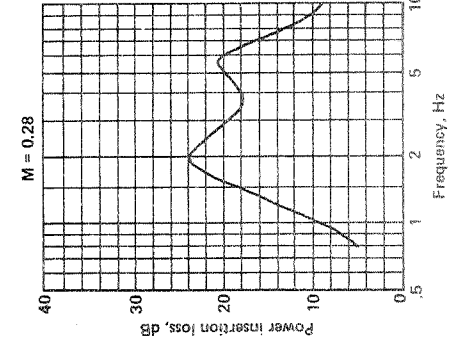
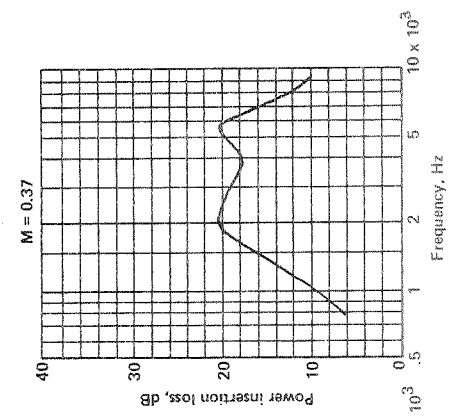
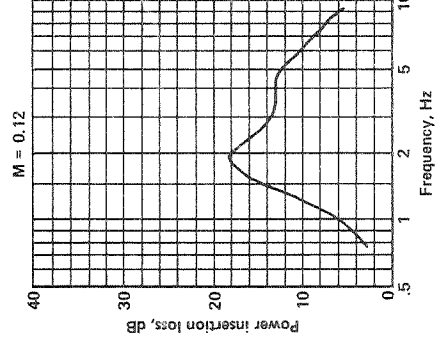
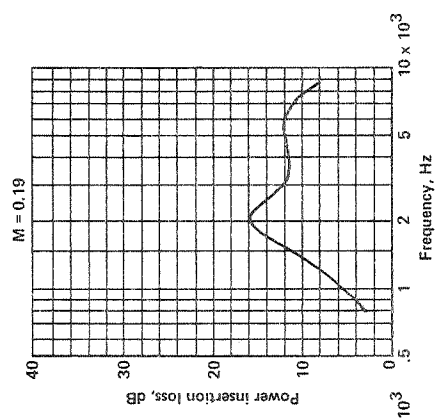
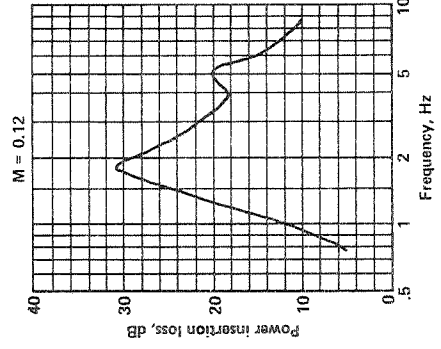
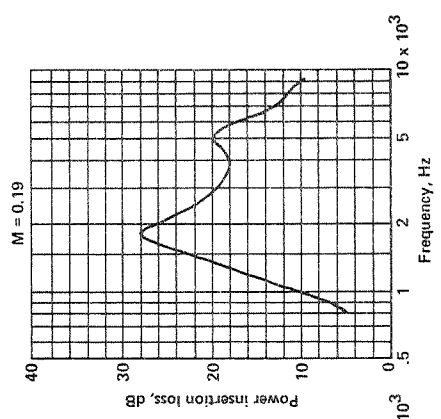


Figure A-128.

Figure A-127.

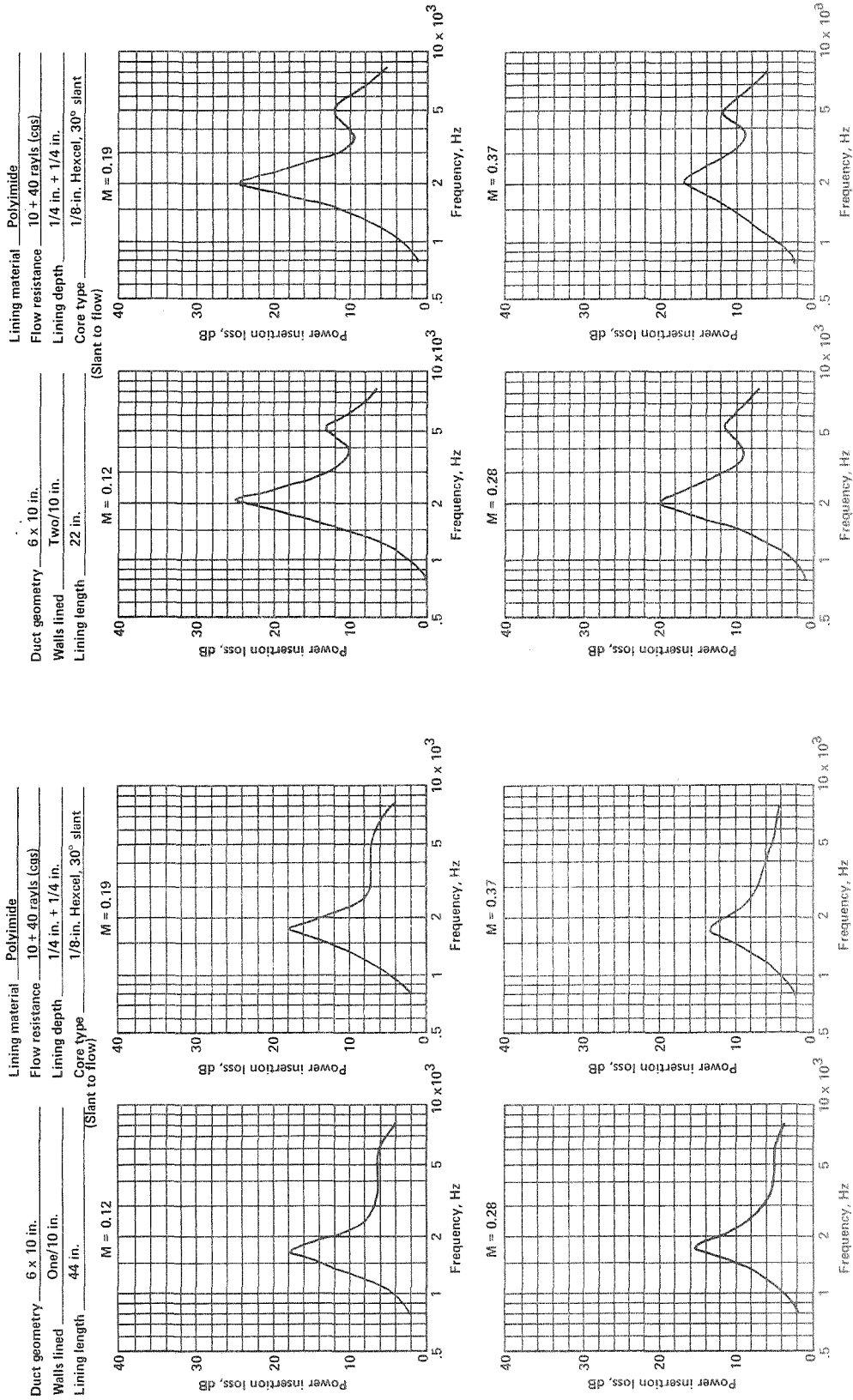


Figure A-129.

Figure A-130.

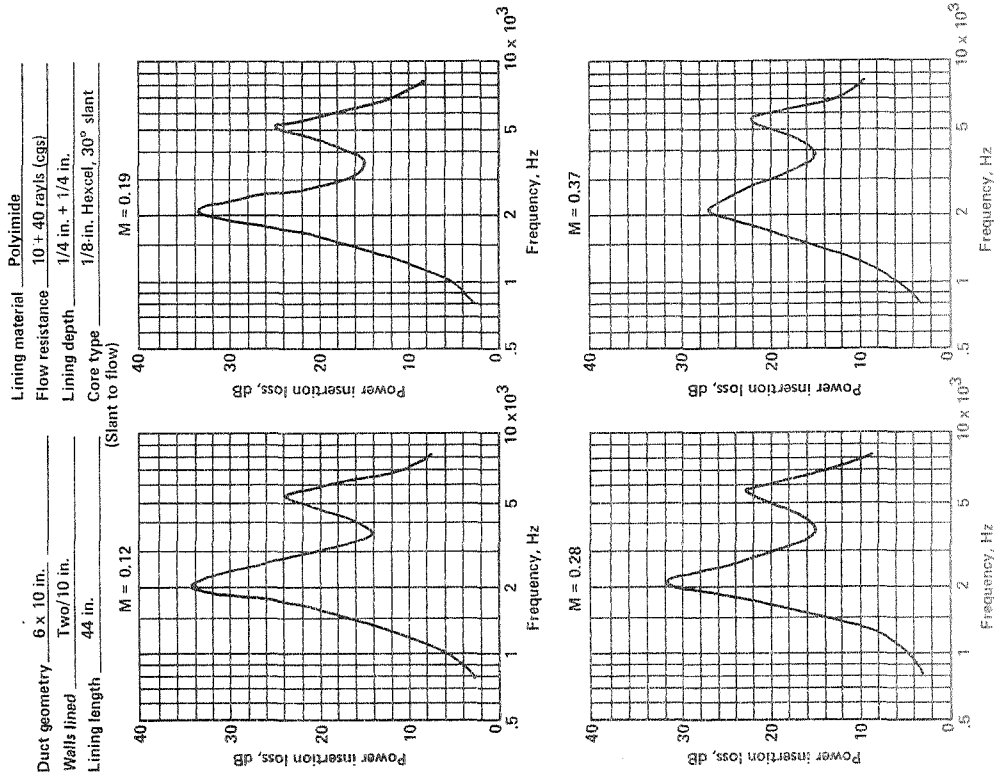


Figure A-132.

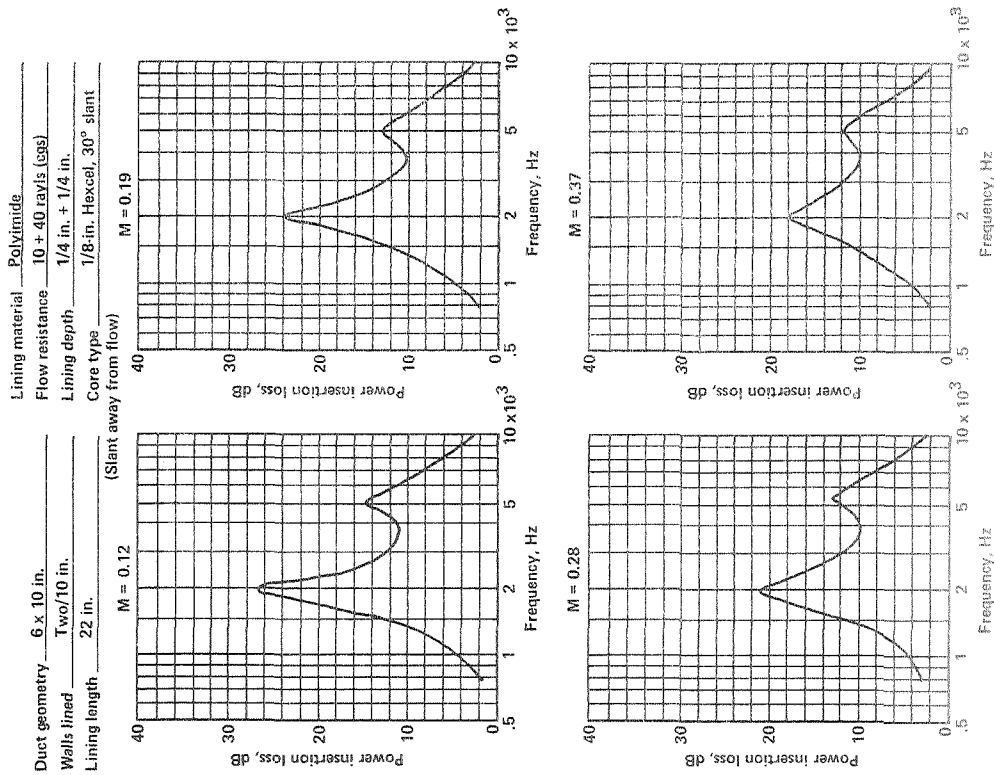


Figure A-131.

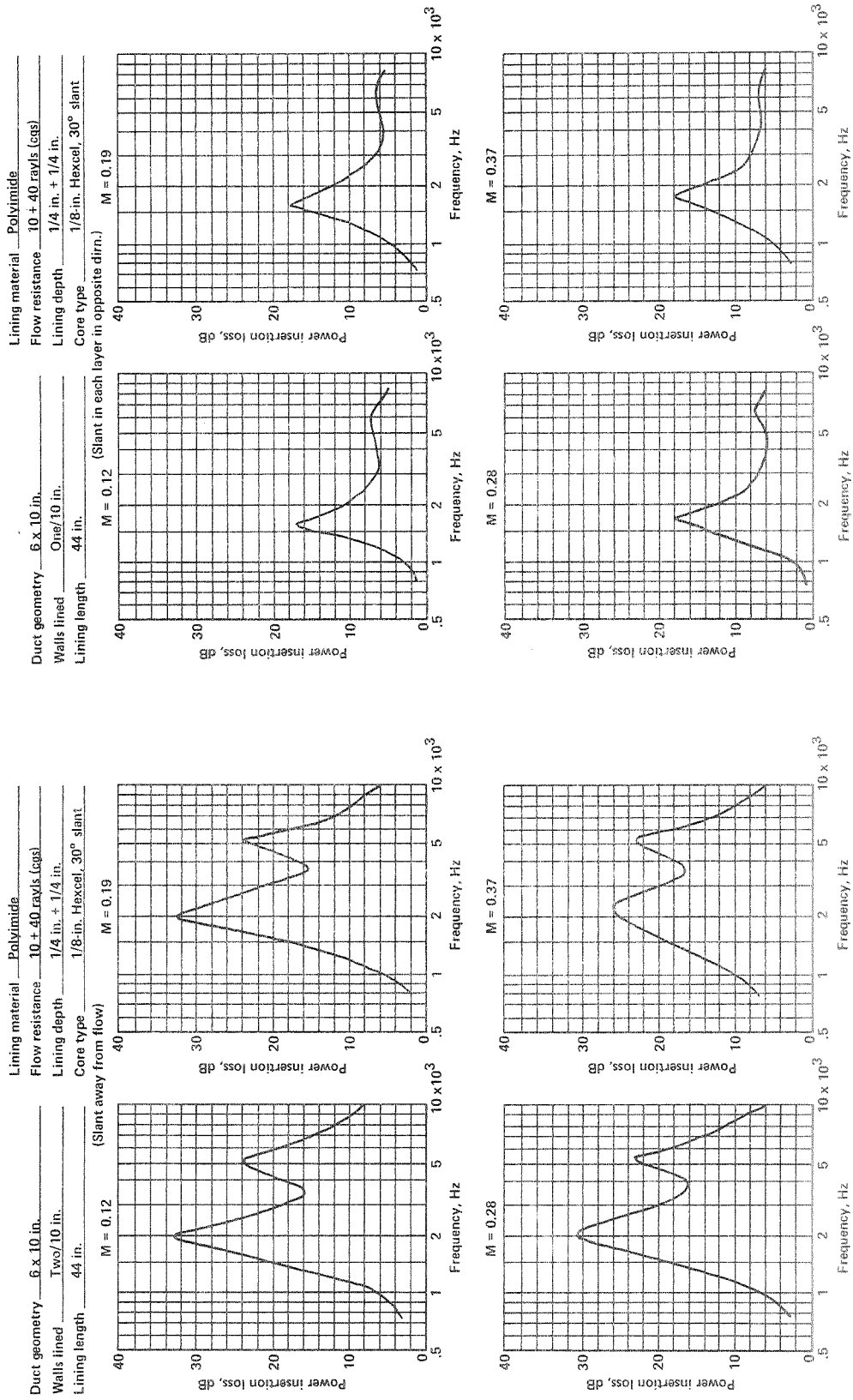


Figure A-134.

Figure A-133.

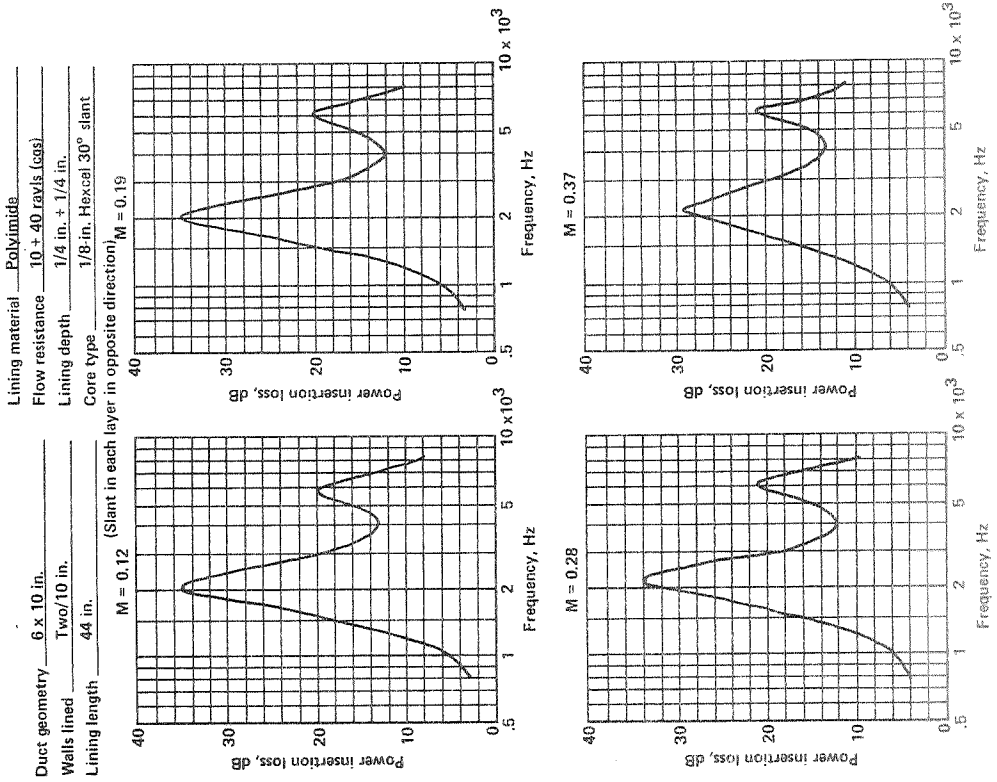


Figure A-136.

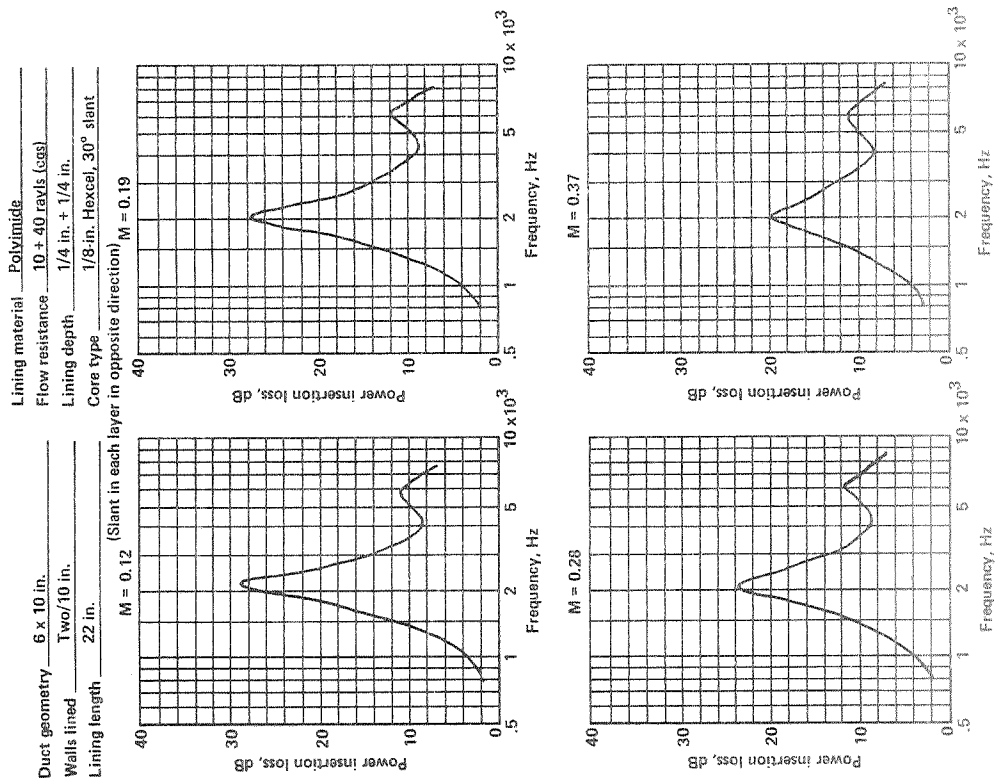


Figure A-135.

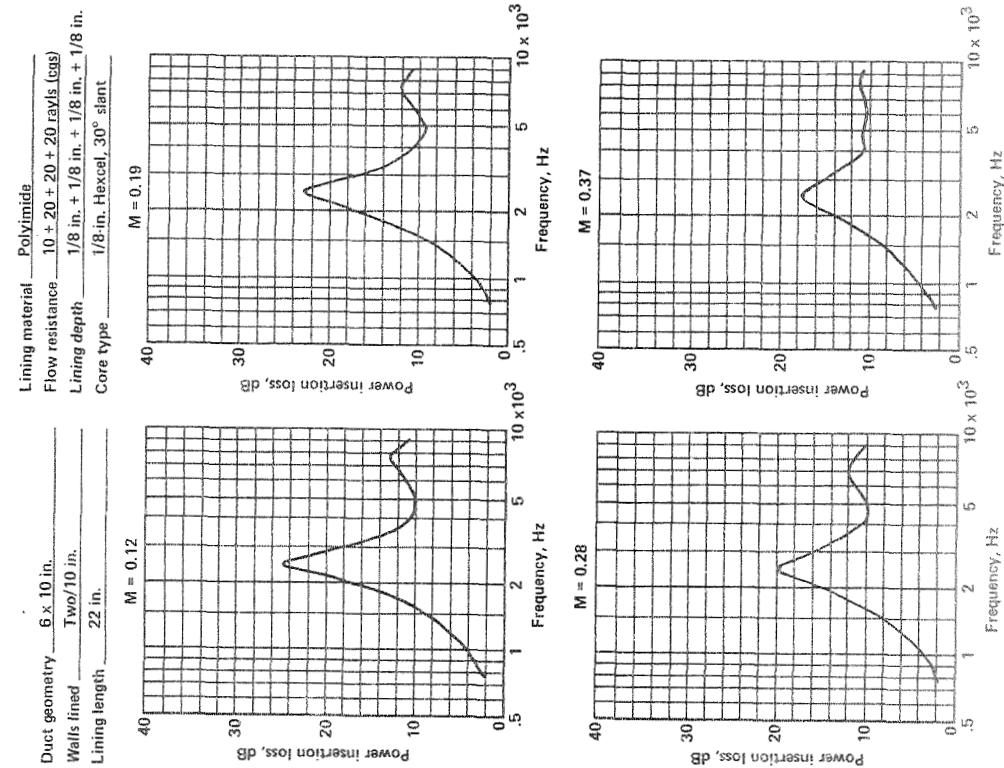


Figure A-138.

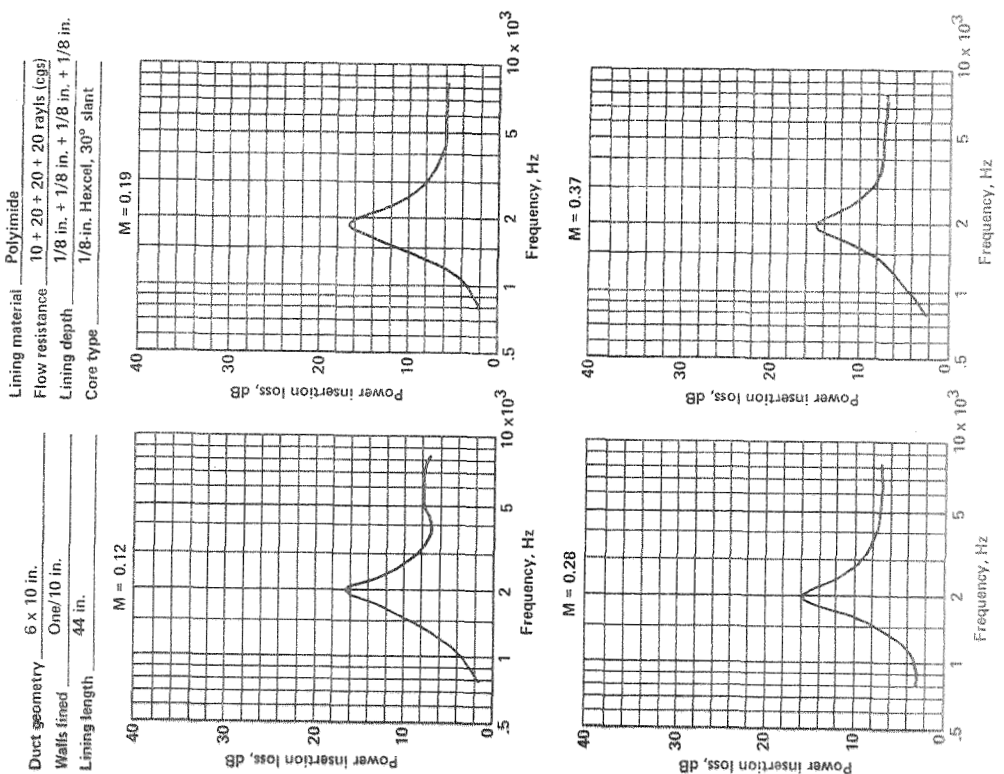


Figure A-137.

Lining material Polyimide  
 Flow resistance 30 rays (cgs)  
 Lining depth 0.25 in.  
 Core type 3/8-in. Hexcel, 30° slant

Duct geometry 6 x 10 in.  
 Walls lined Two/10 in.  
 Lining length 22 in.

Lining material Polyimide  
 Flow resistance 30 rays (cgs)  
 Lining depth 0.25 in.  
 Core type 3/8-in. Hexcel, 30° slant

Duct geometry 6 x 10 in.  
 Walls lined One/10 in.  
 Lining length 44 in.

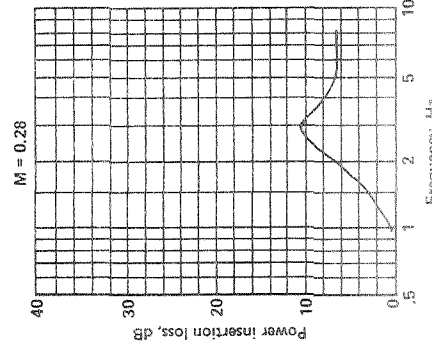
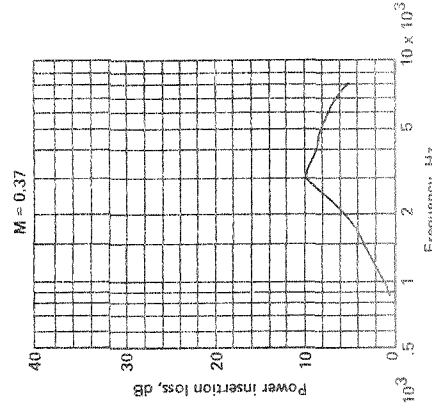
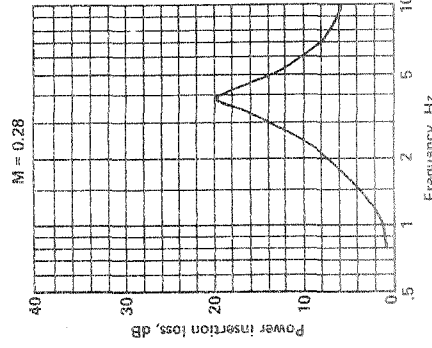
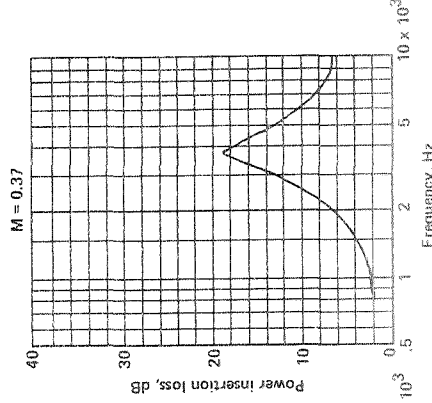
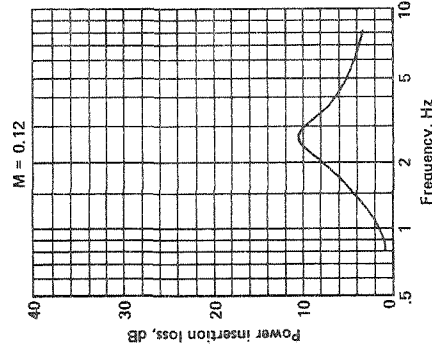
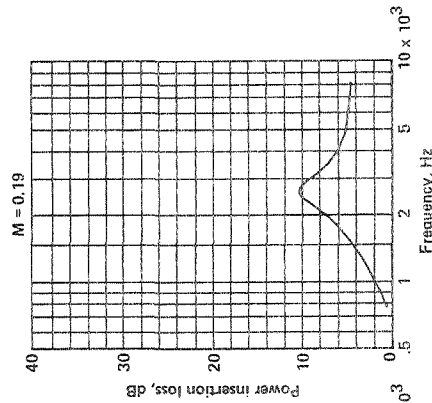
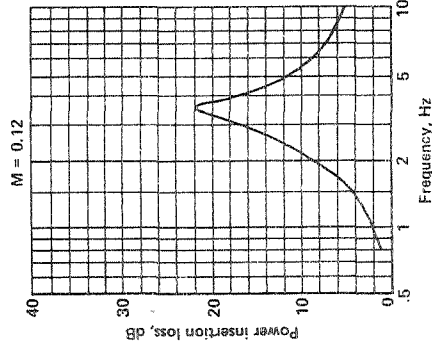
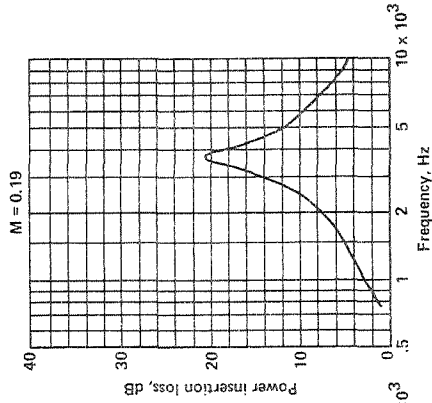


Figure A-140.

Figure A-139.

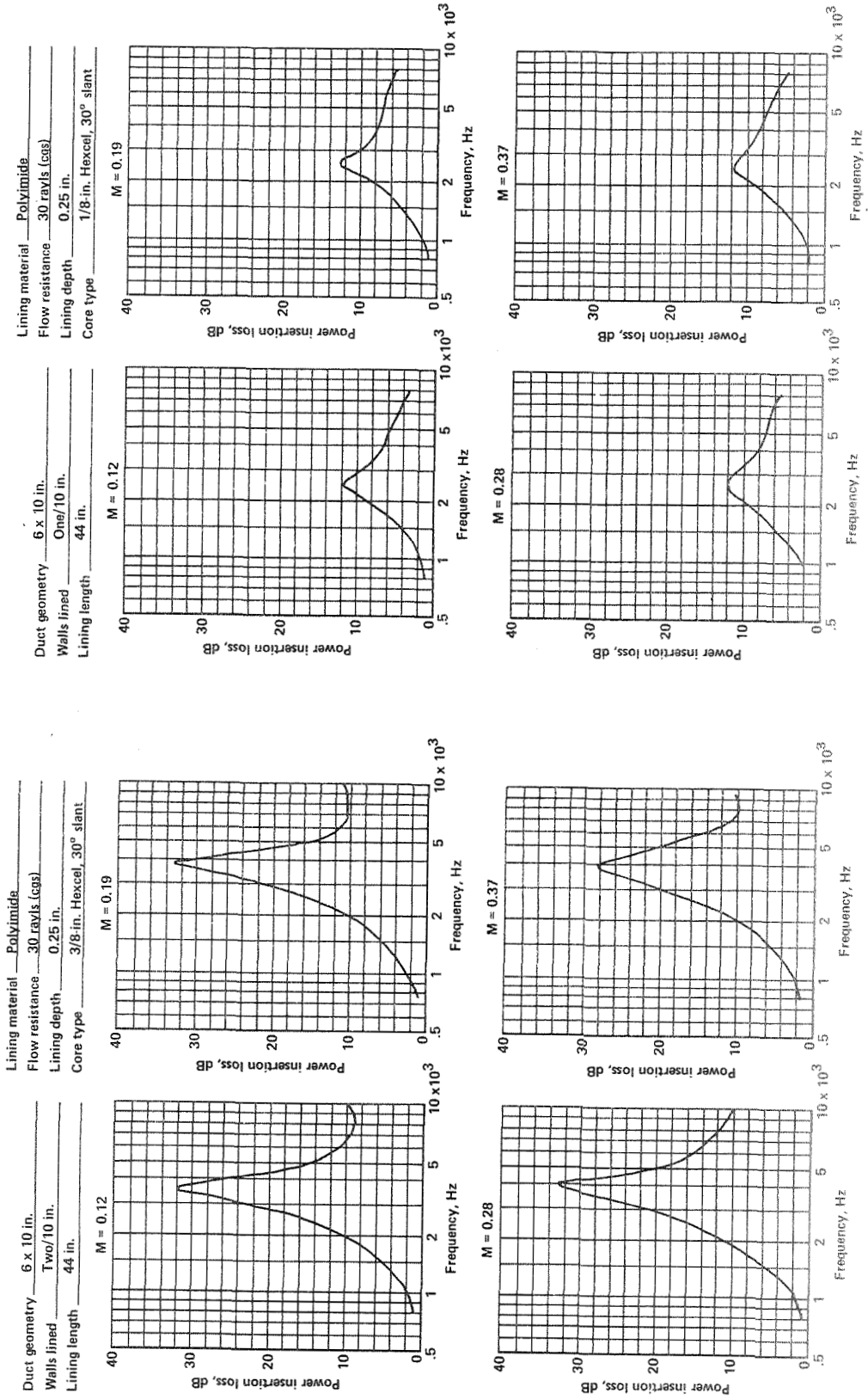


Figure A-141.

Figure A-142.



Lining material Polyimide  
 Flow resistance 30 rays (cgs)  
 Lining depth 0.25 in.  
 Core type 1/8-in. Hexcel, 60° slant

Duct geometry 6 x 10 in.  
 Walls lined One/10 in.  
 Lining length 44 in.

Lining material Polyimide  
 Flow resistance 30 rays (cgs)  
 Lining depth 0.25 in.  
 Core type 1/8-in. Hexcel, 45° slant

Duct geometry 6 x 10 in.  
 Walls lined One/10 in.  
 Lining length 44 in.

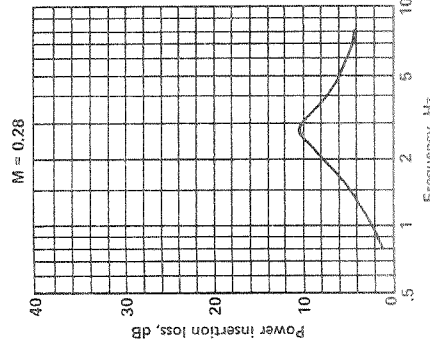
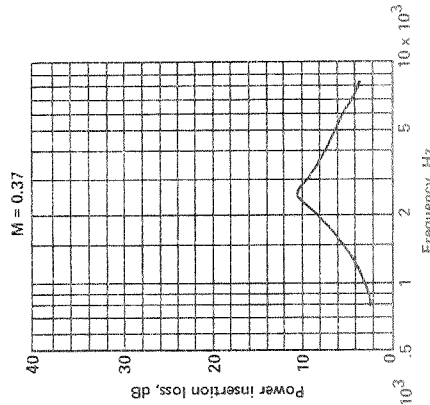
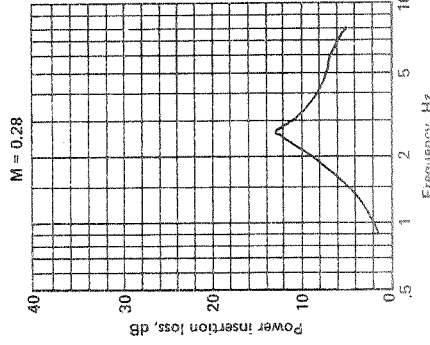
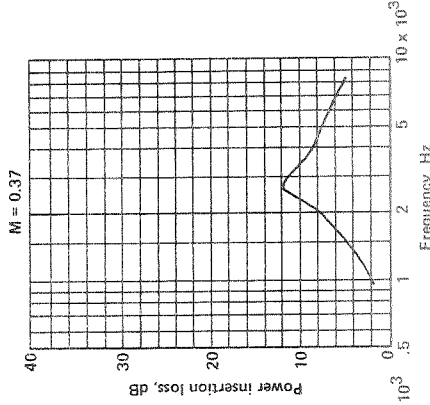
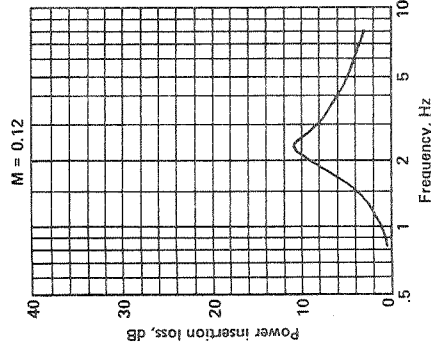
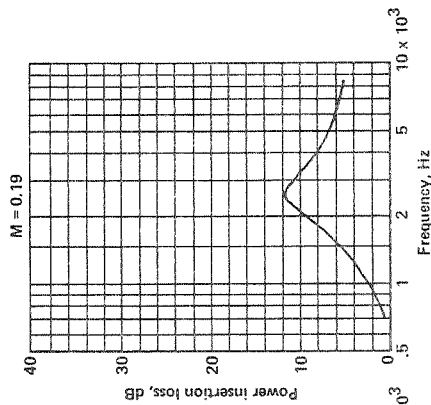
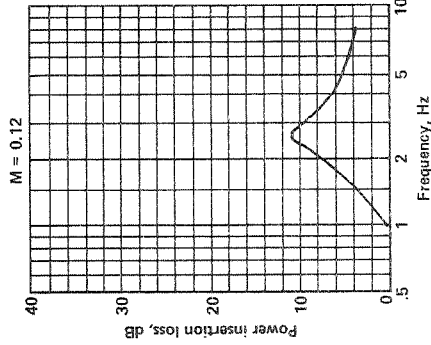
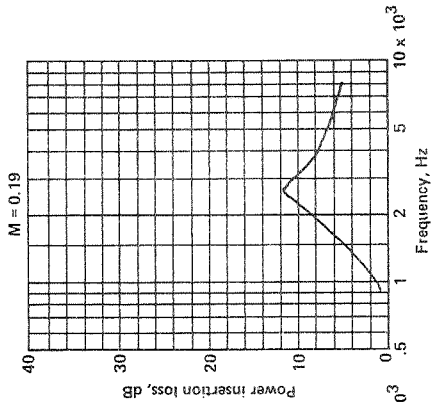


Figure A-144.

Figure A-143.

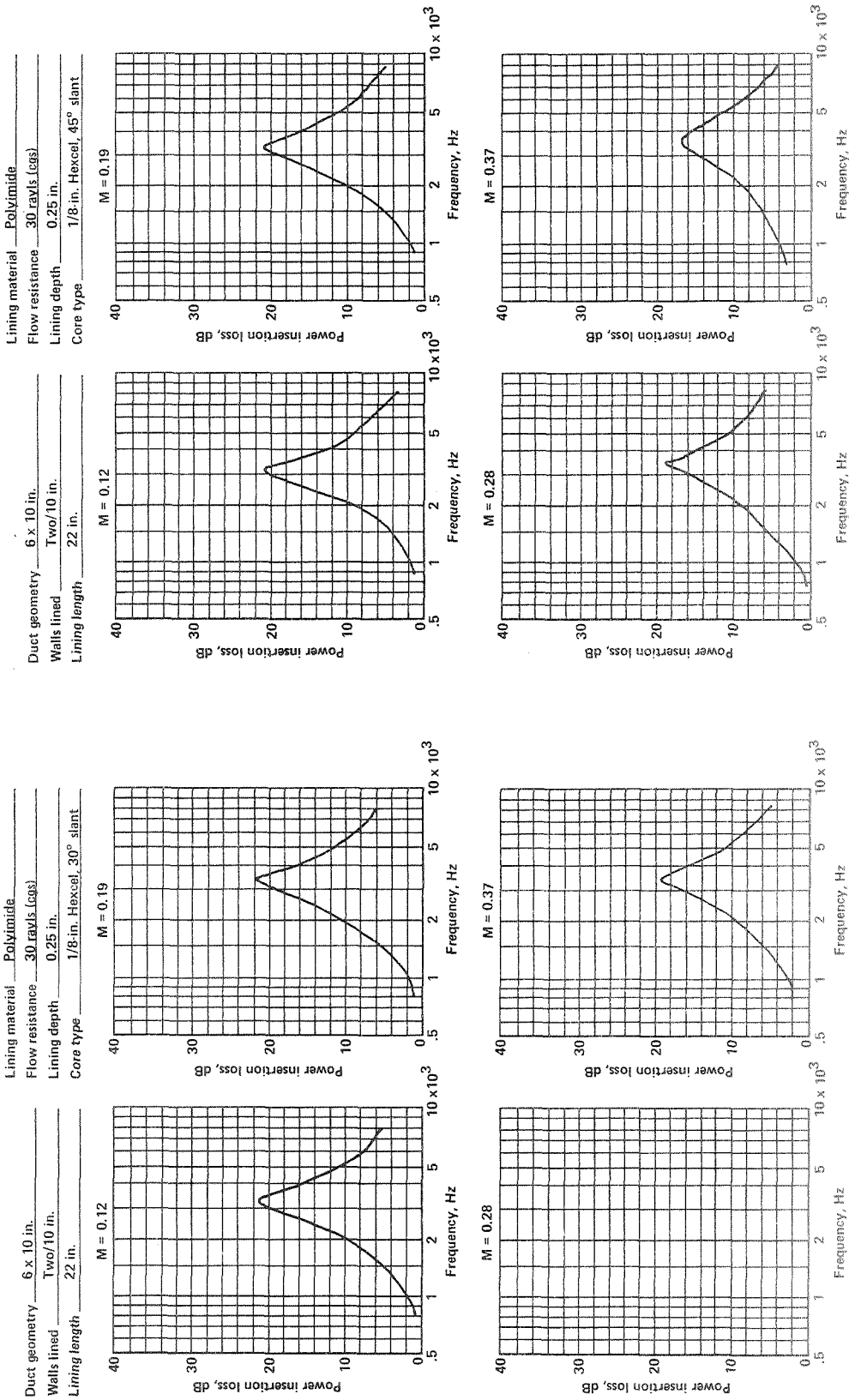


Figure A-145.

Figure A-146.

Lining material Polyimide  
 Flow resistance 30 rays/s (cgs)  
 Lining depth 0.25 in.  
 Core type 1/8-in. Hexcel, 30° slant

Duct geometry 6 x 10 in.  
 Walls lined Two/10 in.  
 Lining length 44 in.

Lining material Polyimide  
 Flow resistance 30 rays/s (cgs)  
 Lining depth 0.25 in.  
 Core type 1/8-in. Hexcel, 60° slant

Duct geometry 6 x 10 in.  
 Walls lined Two/10 in.  
 Lining length 22 in.

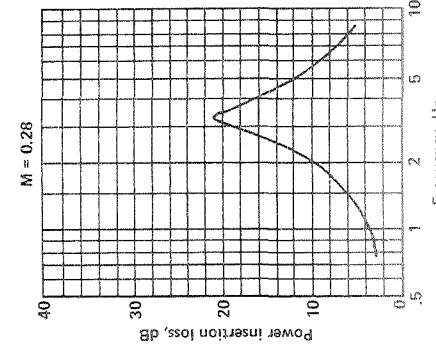
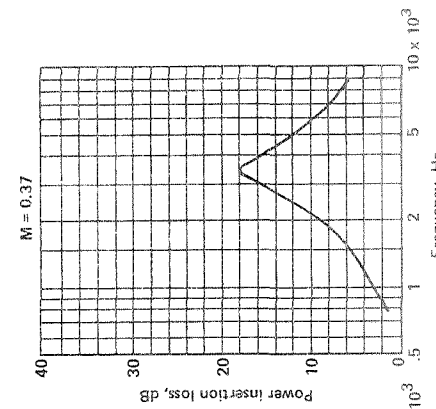
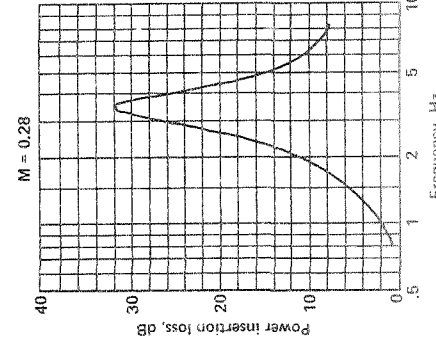
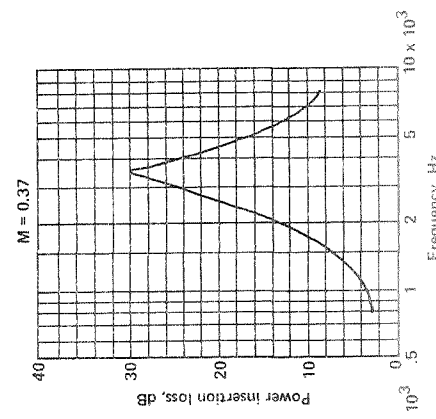
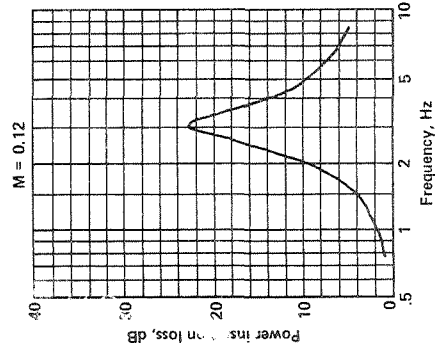
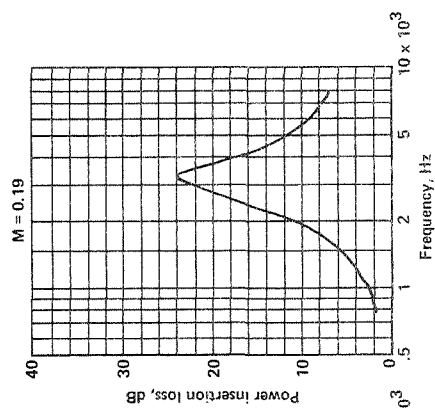
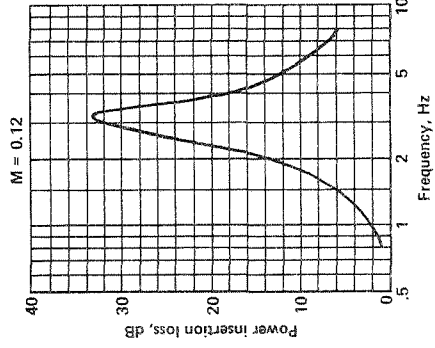
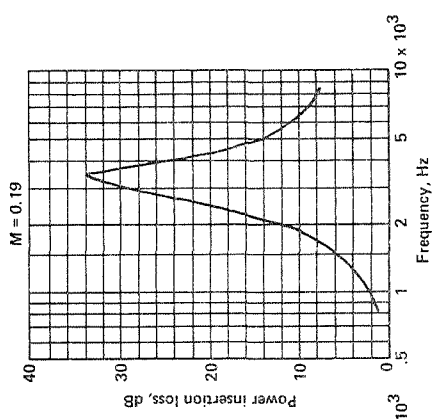


Figure A-148.

Figure A-147.

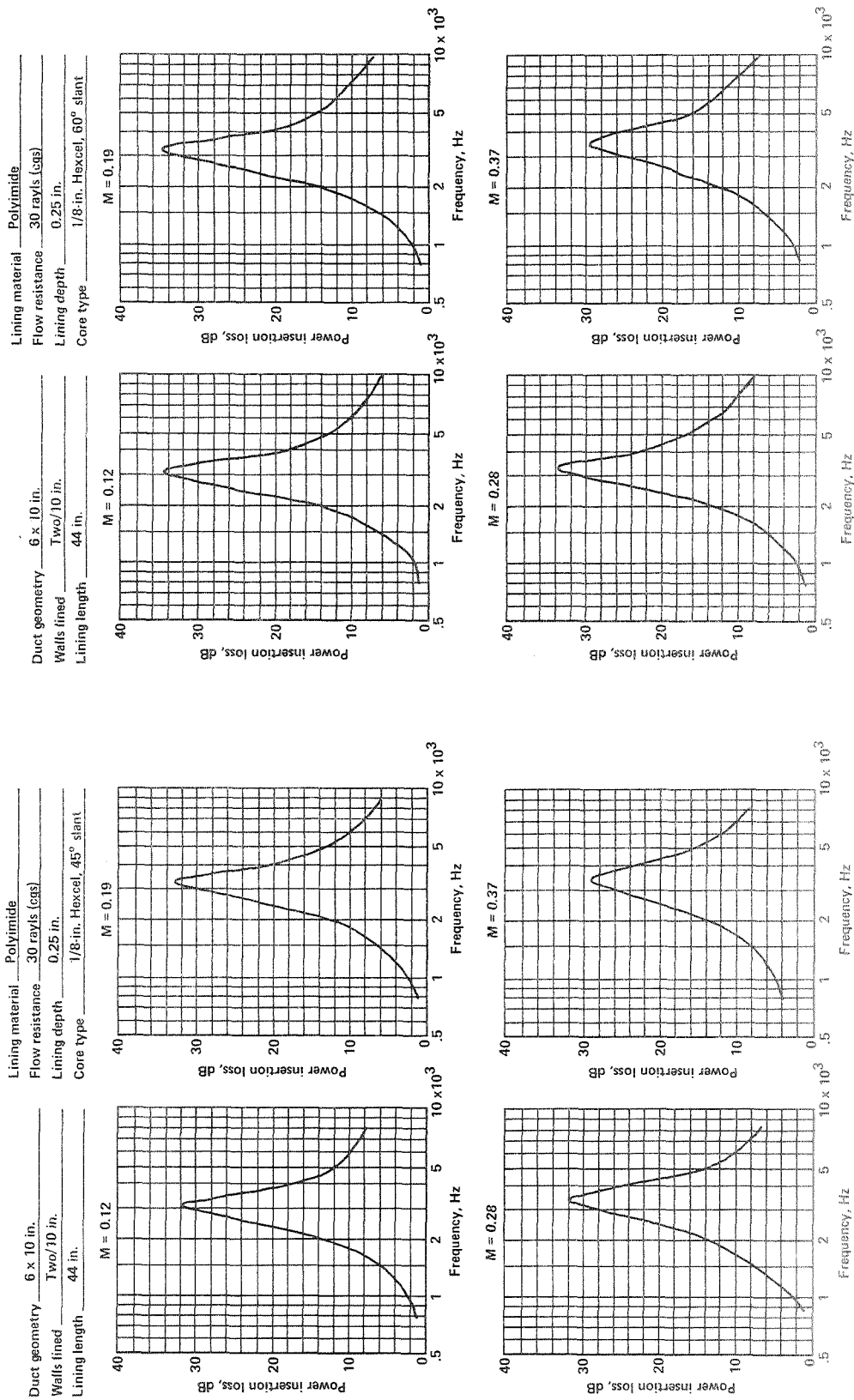


Figure A-149.

Figure A-150.

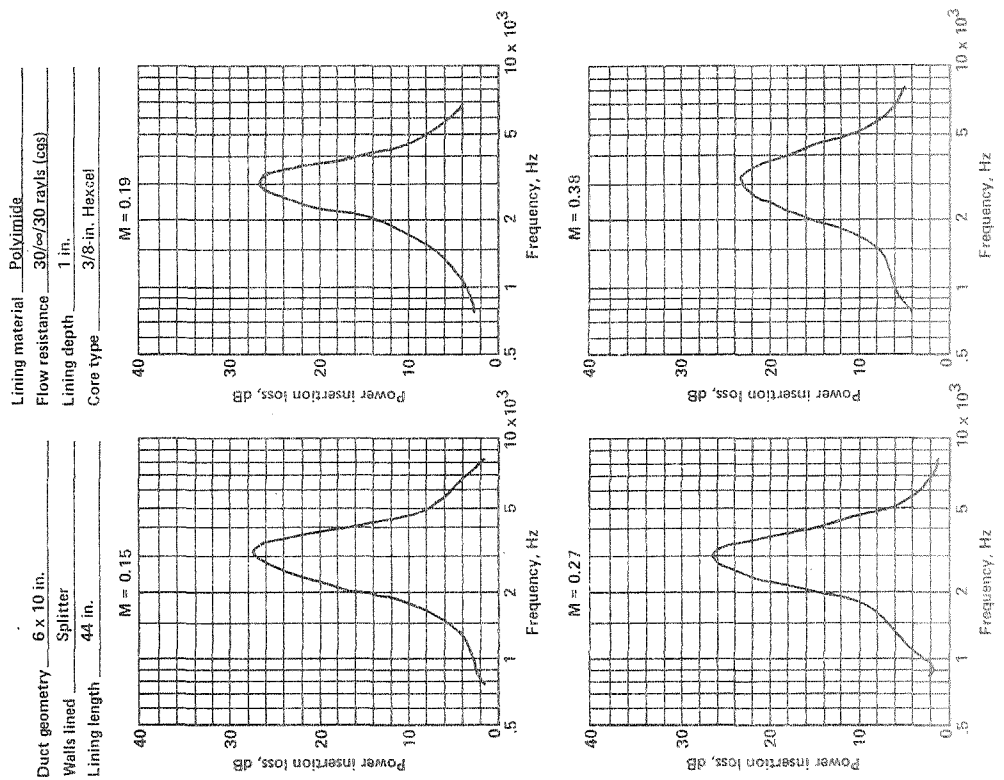


Figure A-152.

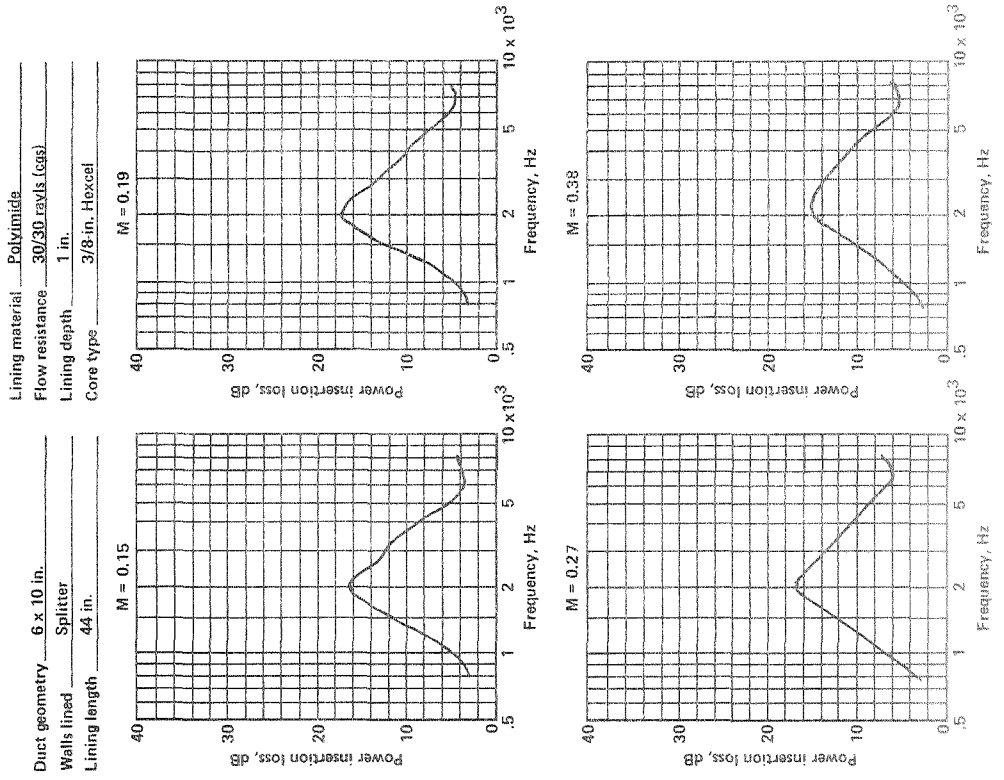
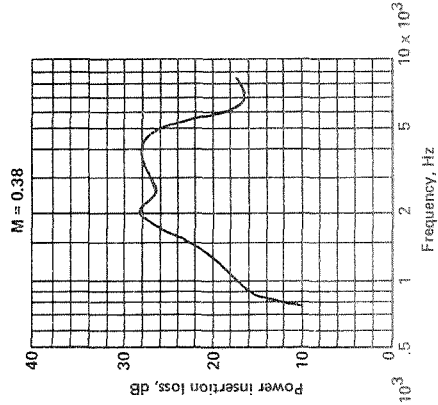
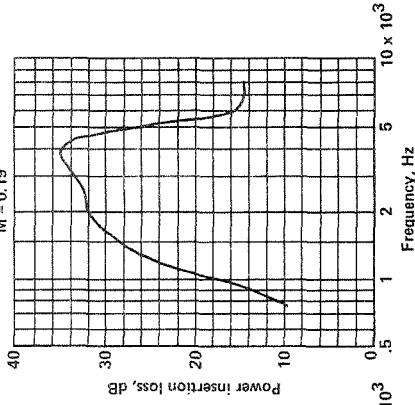
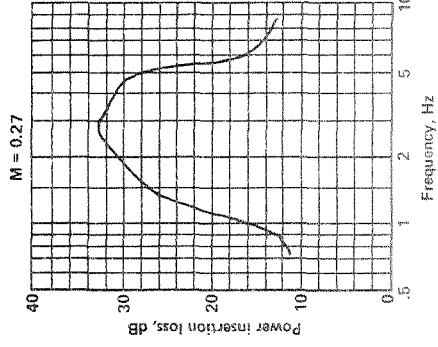
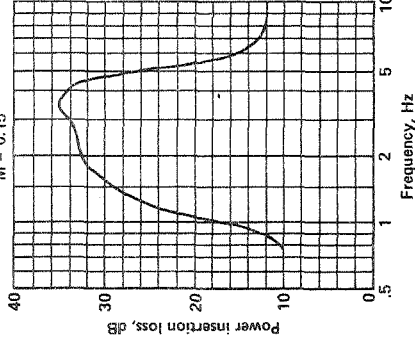


Figure A-151.

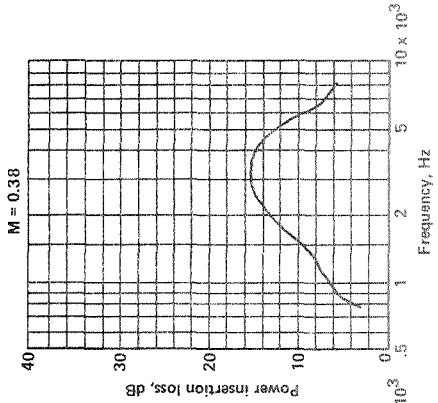
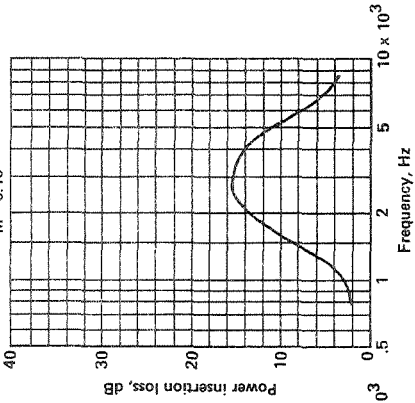
Lining material Polyimide  
 Flow resistance 10 ± 40 rays (cgs), 30 ± 30 rays (cgs)  
 Lining depth 1/2 in. + 1/2 in., 1 in.  
 Core type 3/8-in. Hexcel



Duct geometry 6 x 10 in.  
 Walls lined Two/10 in., splitter  
 Lining length 44 in.



Lining material Polyimide  
 Flow resistance 10/30/10 rays (cgs)  
 Lining depth 1 in.  
 Core type 3/8-in. Hexcel



Duct geometry 6 x 10 in.  
 Walls lined Splitter  
 Lining length 44 in.

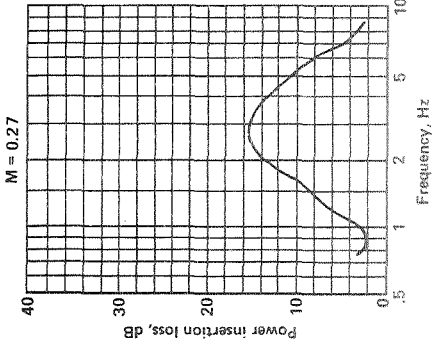
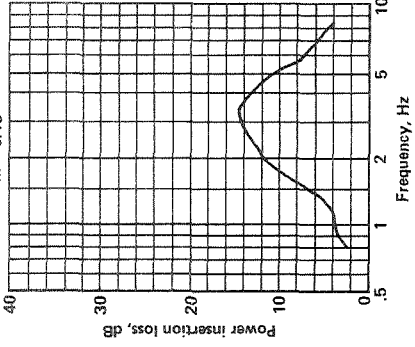
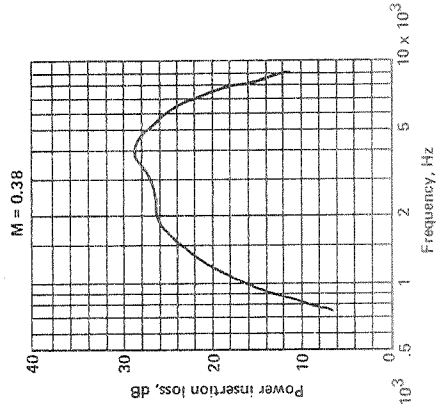
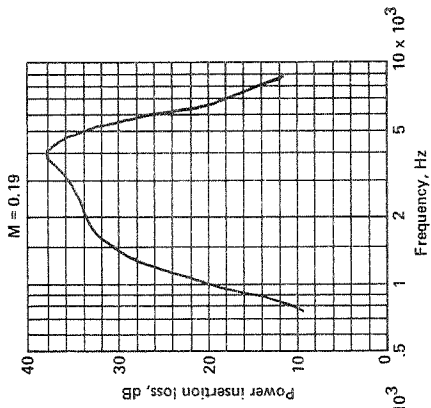
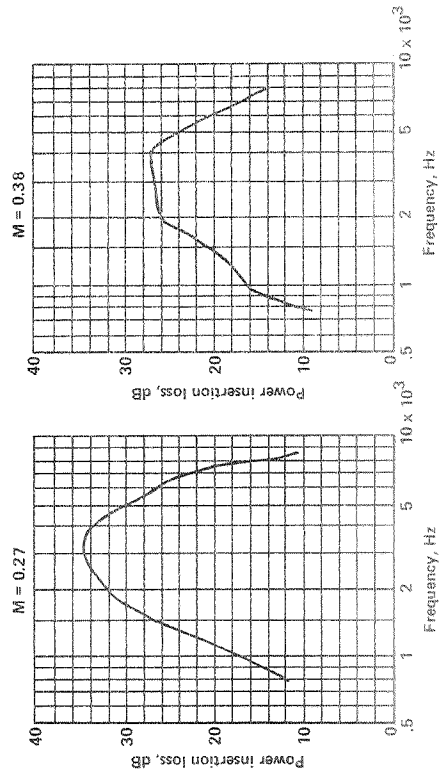
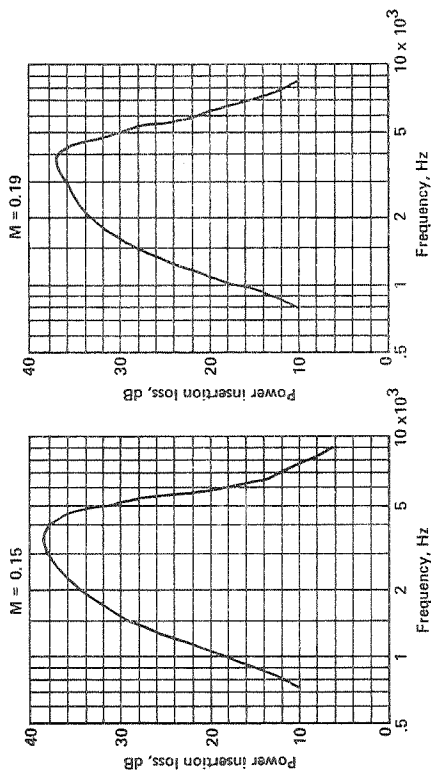


Figure A-154.

Figure A-153.

Lining material Polyimide  
 Flow resistance 10 + 40 rays (cgs), 30/( $\omega$ /30) rays (cgs)  
 Lining depth 1/2 in. + 1/2 in., 1/2 in. + 1/2 in.  
 Core type 3/8-in. Hexcel

Duct geometry 6 x 10 in.  
 Walls lined Two/10 in., splitter  
 Lining length 44 in.



Lining material Polyimide  
 Flow resistance 10 + 40 rays (cgs), 10/(30/10) rays (cgs)  
 Lining depth 1/2 in. + 1/2 in., 1/2 in. + 1/2 in.  
 Core type 3/8-in. Hexcel

Duct geometry 6 x 10 in.  
 Walls lined Two/10 in., splitter  
 Lining length 44 in.

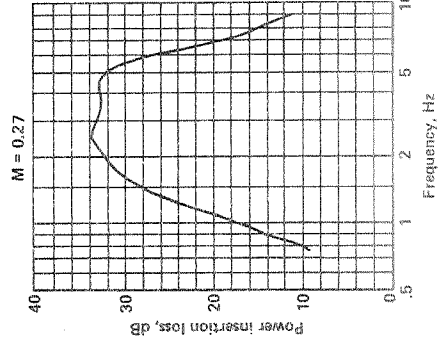
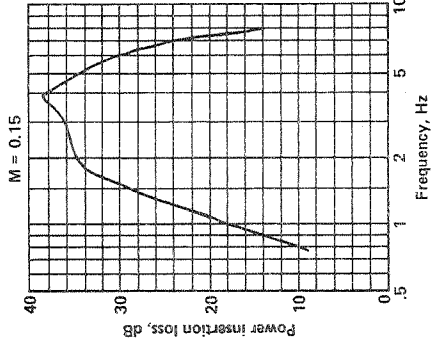


Figure A-155.

Figure A-156.

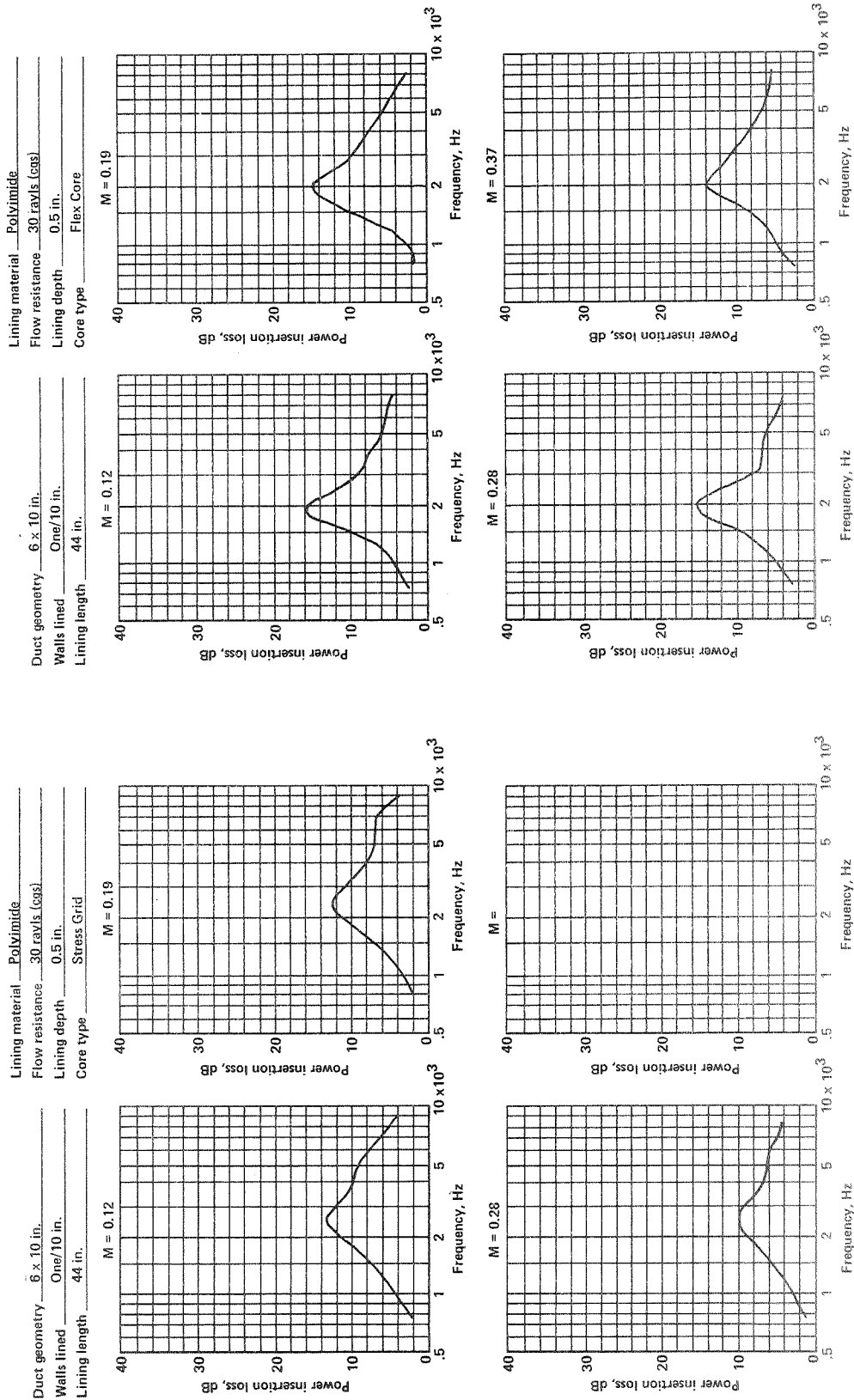


Figure A-157.

Figure A-158.



Lining material "NASA" Metal Mesh  
 Flow resistance Approx. 5 rays/ls Legs  
 Lining depth 0.5 in.  
 Core type Aluminum

Duct geometry 6 x 10 in.  
 Walls lined One/10 in.  
 Lining length 44 in.

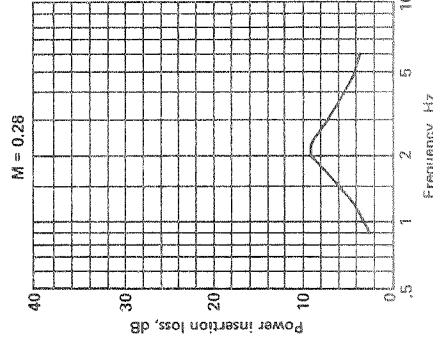
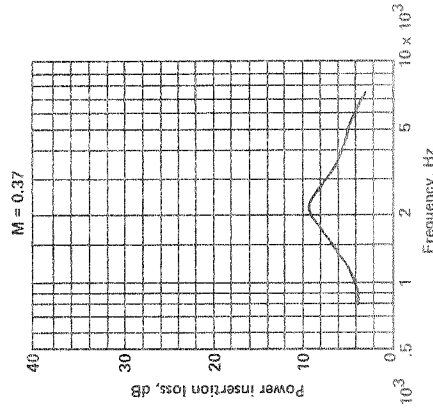
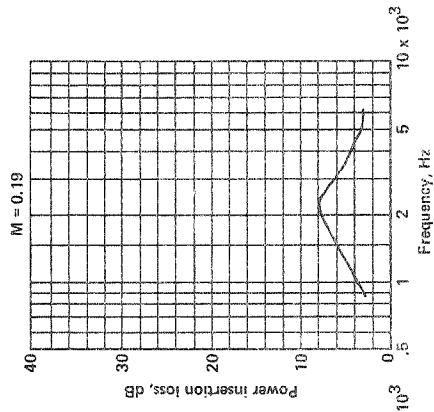


Figure A-159.

Lining material "NASA" Metal Mesh  
 Flow resistance Approx. 5 rays/ls Legs  
 Lining depth 0.5 in.  
 Core type Aluminum

Duct geometry 6 x 10 in.  
 Walls lined Two/10 in.  
 Lining length 44 in.

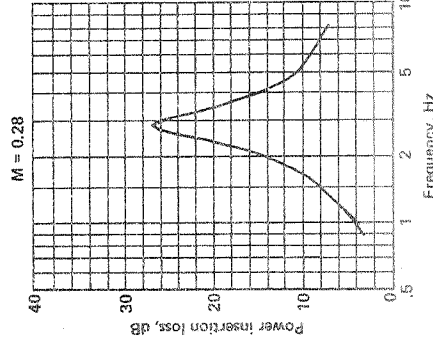
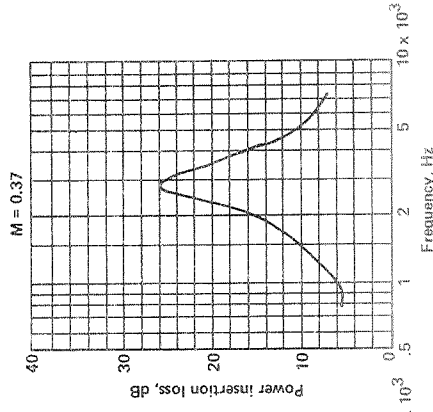
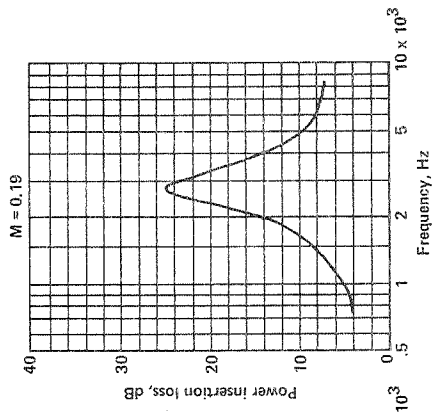


Figure A-160.

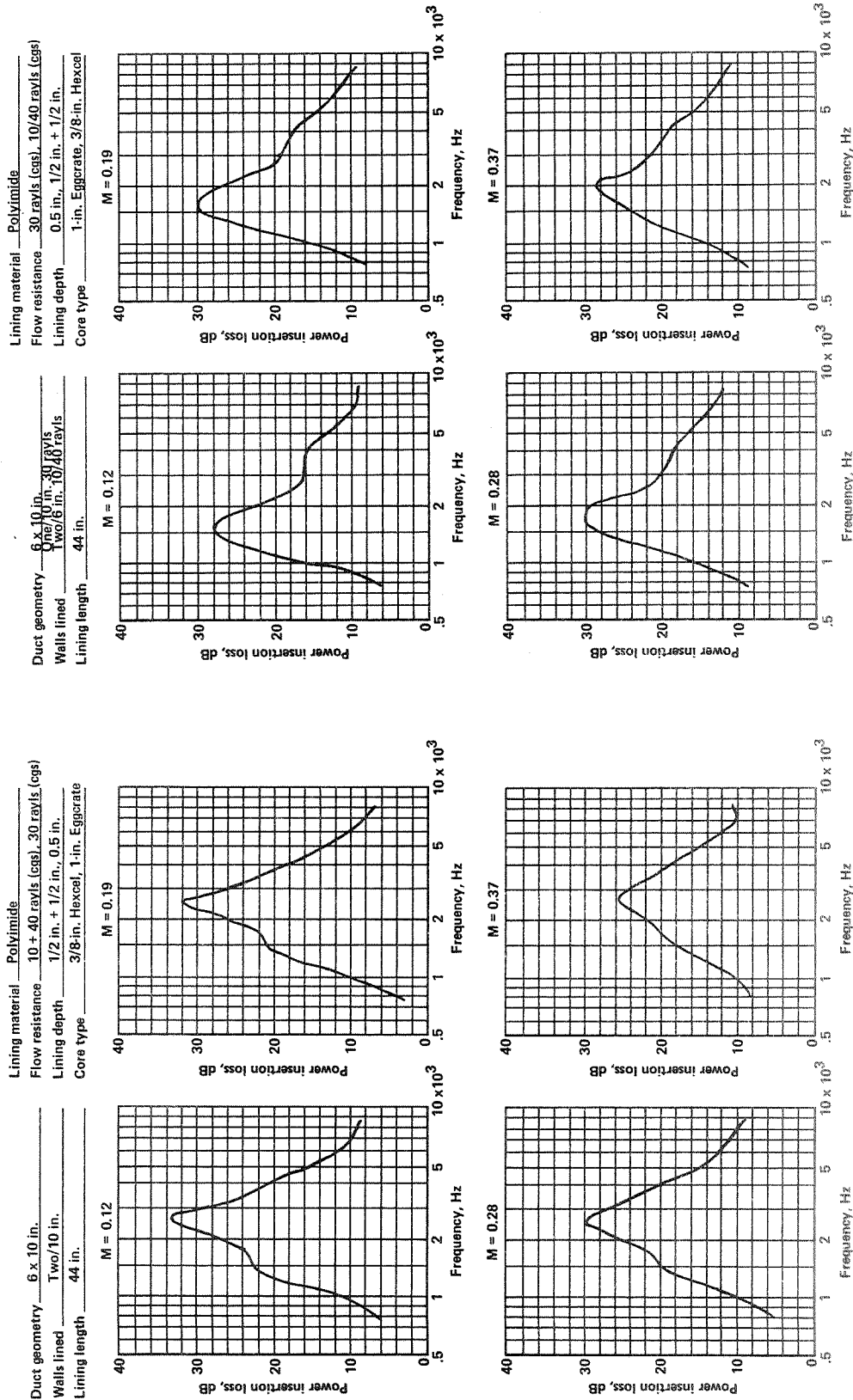


Figure A-161.

Figure A-162.

Lining material: Polyimide  
 Flow resistance: 10 rays (cgs)/6 in. walls  
 Lining depth: 1/2 in. + 1/2 in., 0.5 in.  
 Core type: 3/8-in. Hexcel

Lining material: Polyimide  
 Flow resistance: 30 rays (cgs)  
 Lining depth: 0.5 in. & 0.28 in.  
 Core type: 1/2-in. + 3/8-in. Hexcel

Duct geometry: 6 x 10 in.  
 Walls lined: Four  
 Lining length: 44 in.

Duct geometry: 6 x 10 in.  
 Walls lined: Two/10 in.  
 Lining length: 44 in.

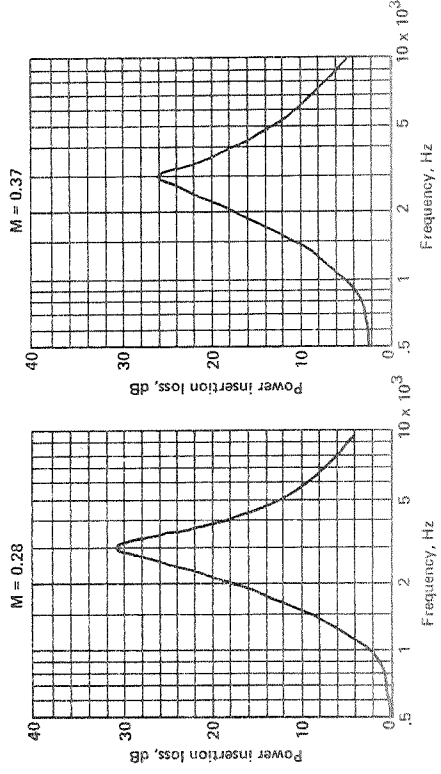
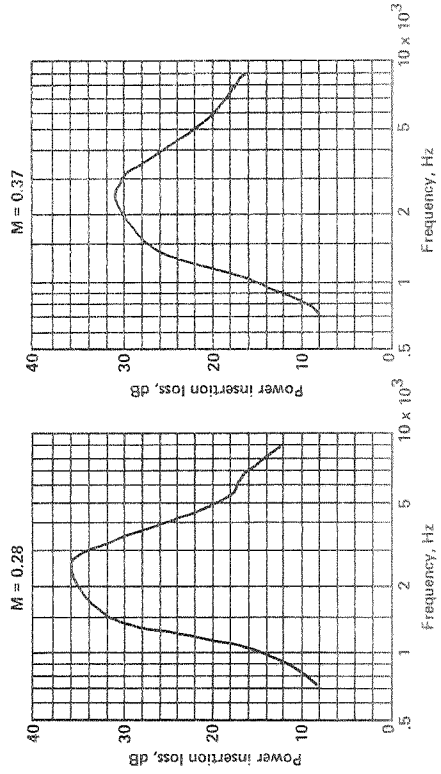
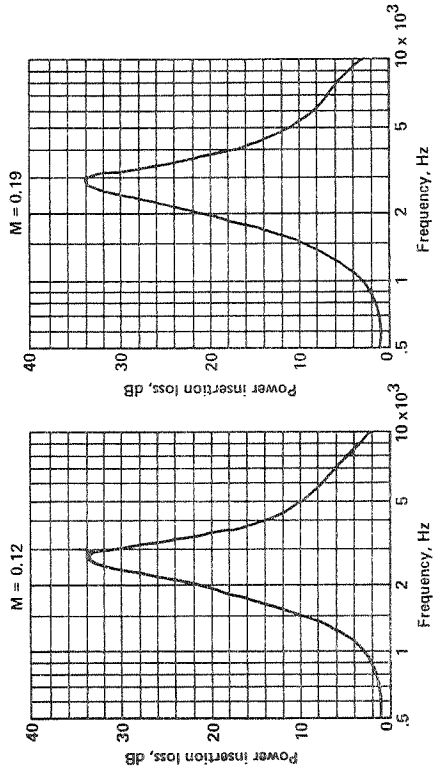
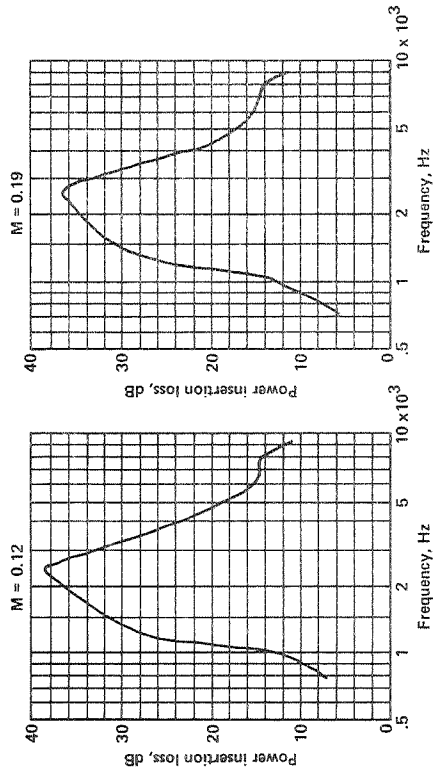


Figure A-164.

Figure A-163.

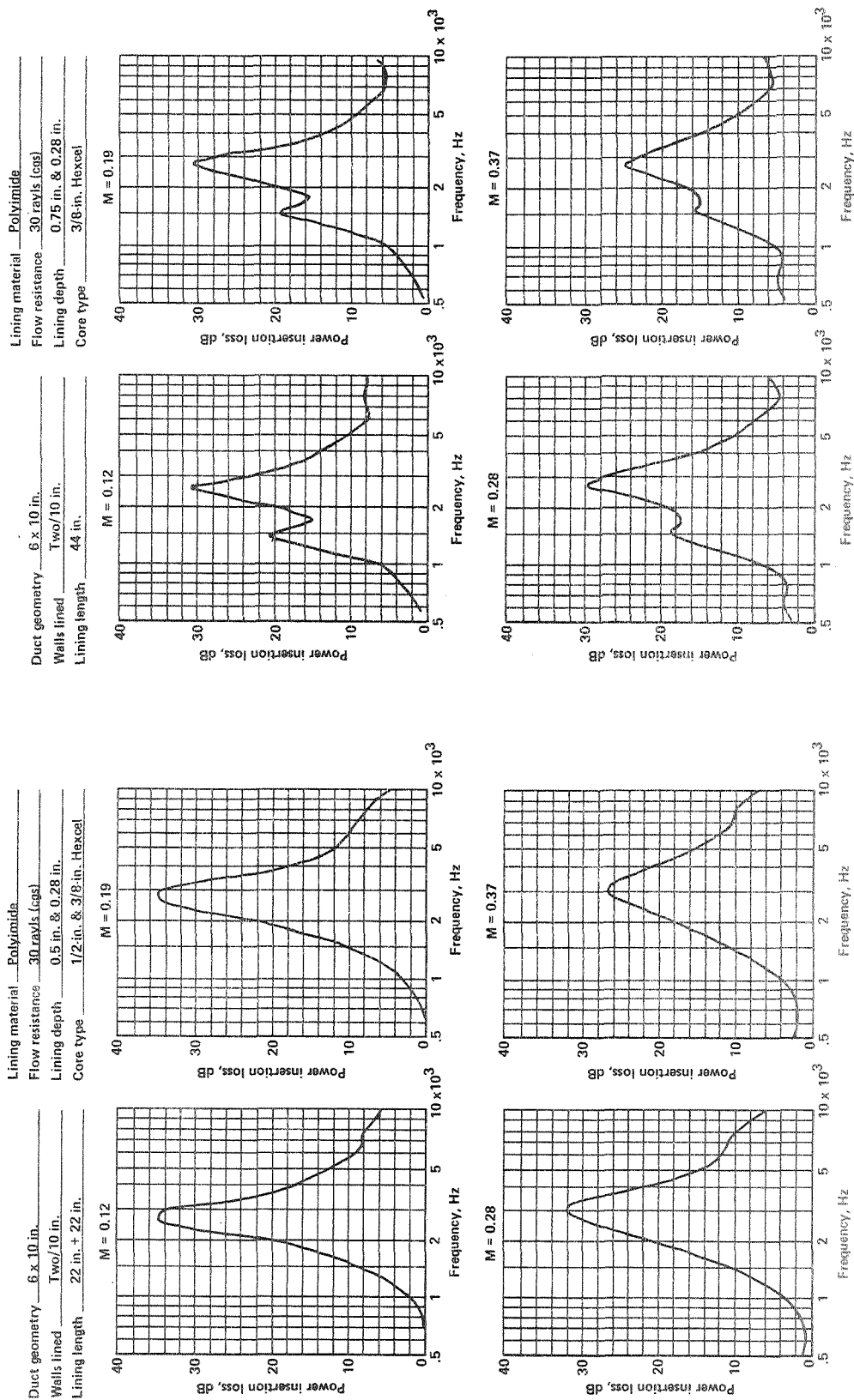


Figure A-165.

Figure A-166.

Lining material Polyimide  
 Flow resistance 30 rays (cgs)  
 Lining depth 1 in. & 0.28 in.  
 Core type 3/8-in. Hexcel

Duct geometry 6 x 10 in.  
 Walls lined Two/10 in.  
 Lining length 22 in. + 22 in.

Lining material Polyimide  
 Flow resistance 30 rays (cgs)  
 Lining depth 1.0 in. & 0.28 in.  
 Core type 3/8-in. Hexcel

Duct geometry 6 x 10 in.  
 Walls lined Two/10 in.  
 Lining length 44 in.

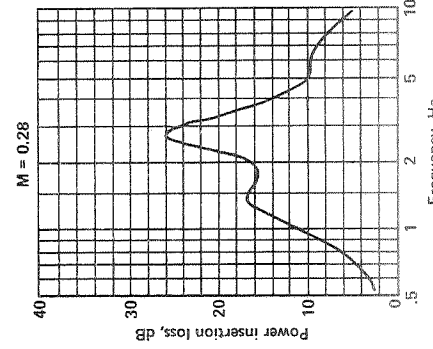
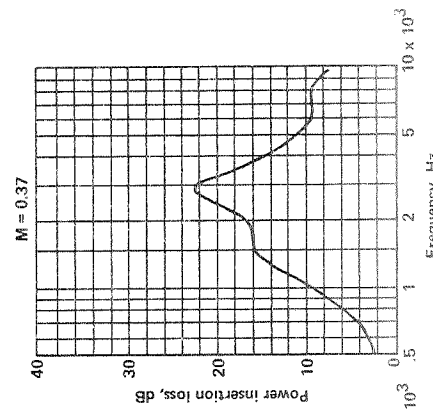
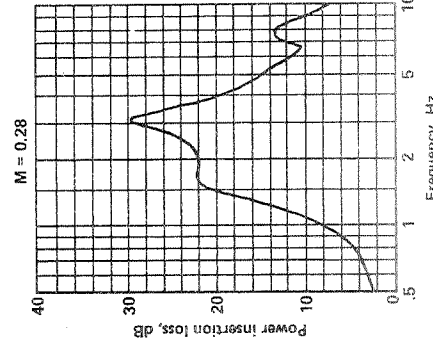
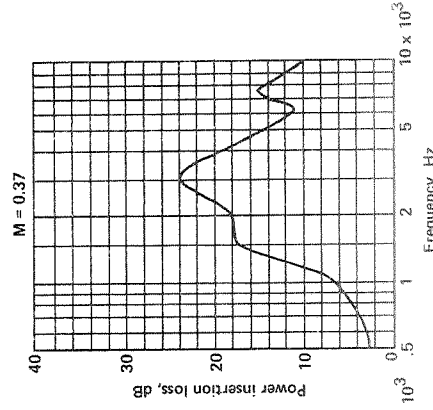
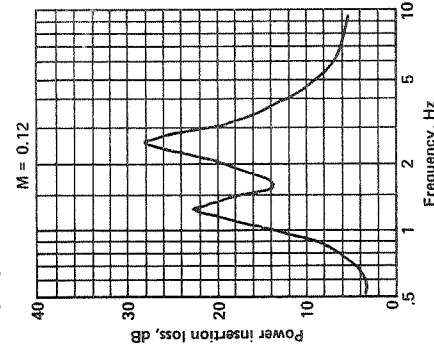
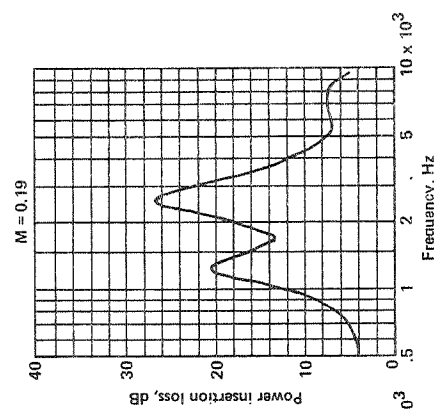
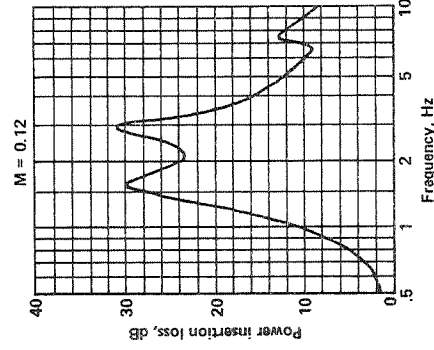
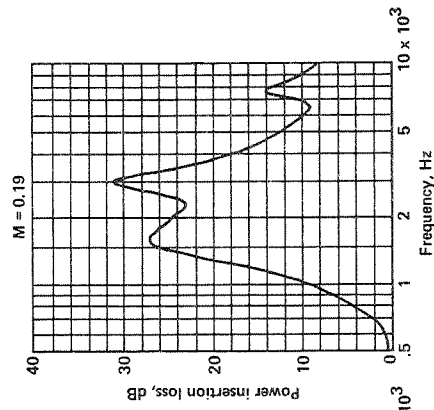


Figure A-168.

Figure A-167.

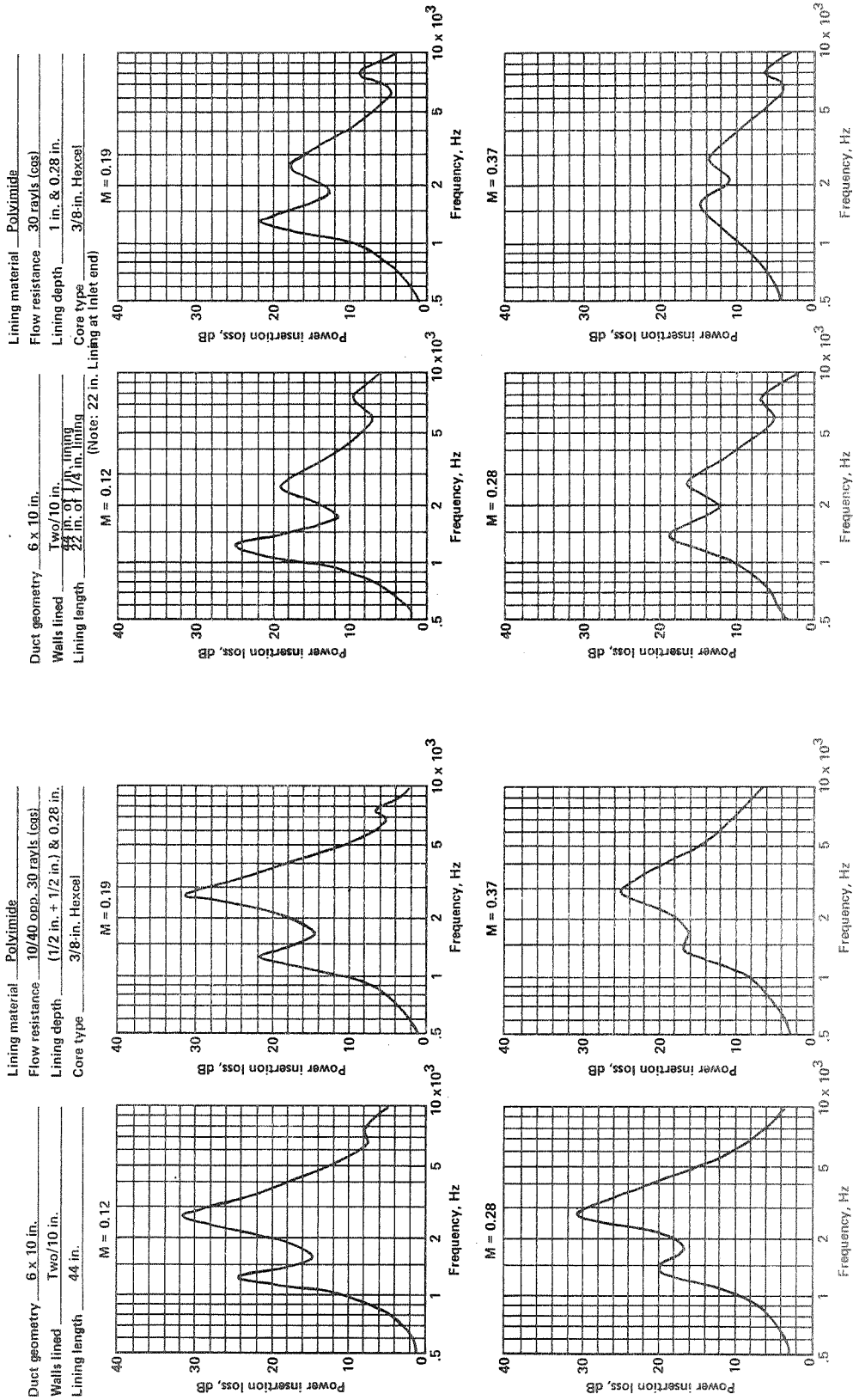


Figure A-170.

Figure A-169.

Lining material Polymide  
 Flow resistance 30 rays (logs)  
 Lining depth 1 in. & 0.5 in.  
 Core type 3/8-in. Hexcel

Duct geometry 6 x 10 in.  
 Walls lined Two/10 in.  
 Lining length 22 + 22

Lining material Polymide  
 Flow resistance 30 rays (logs)  
 Lining depth 1.0 in. & 0.5 in.  
 Core type 3/8-in. & 1/2-in. Hexcel

Duct geometry 6 x 10 in.  
 Walls lined Two/10 in.  
 Lining length 44 in.

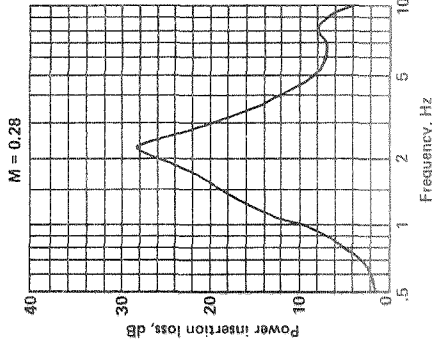
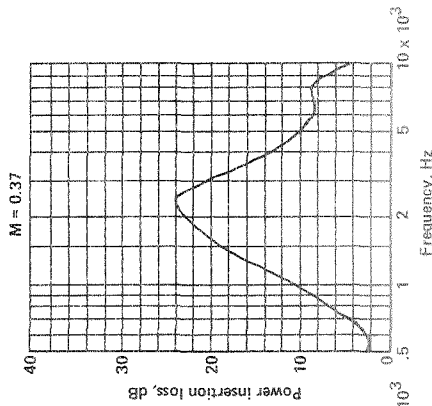
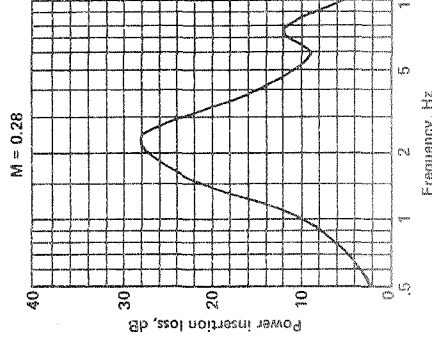
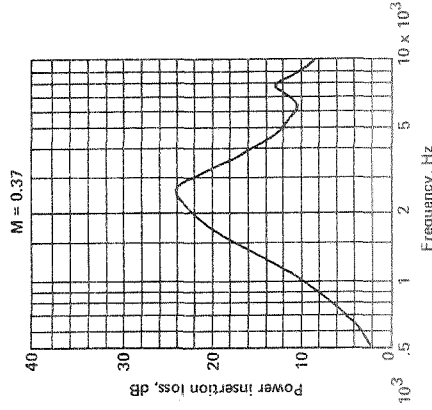
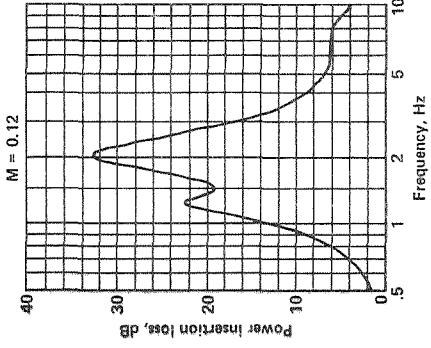
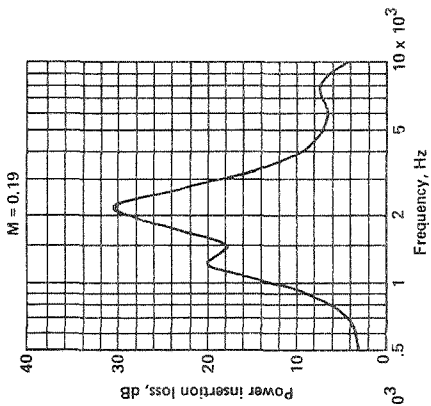
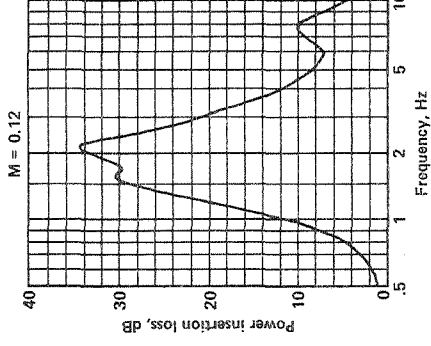
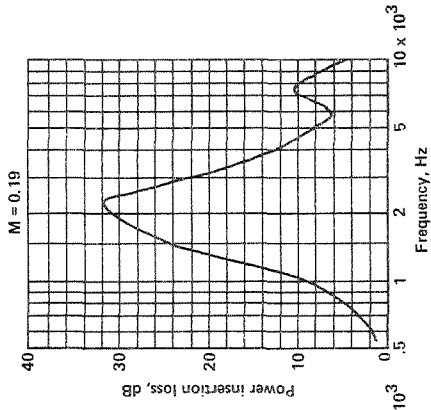


Figure A-172.

Figure A-171.

### S-BEND DUCT TEST SUMMARY






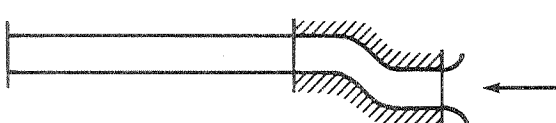
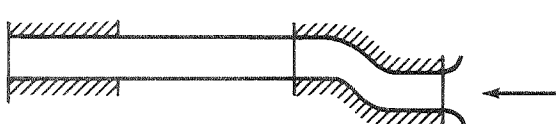
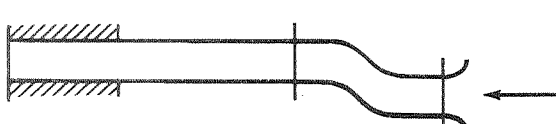
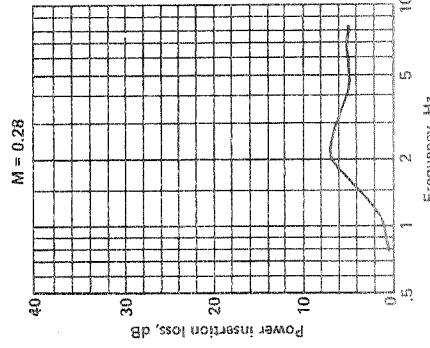
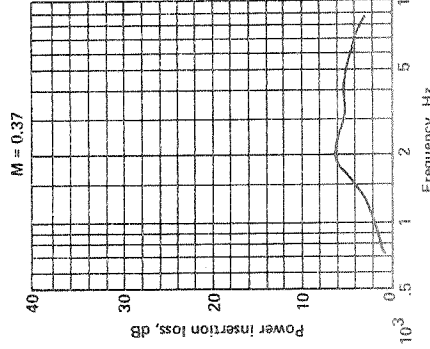
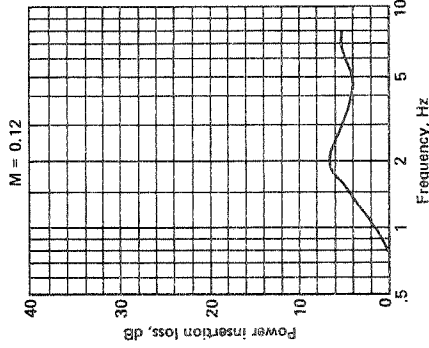
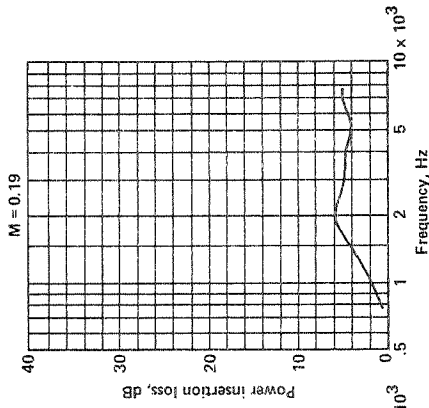
Configuration	Description
	Upper wall, 30 rays Metallic felt, 1/2 in. thick, 25 in. long
	Lower wall, 30 rays Metallic felt 1/2 in. thick, 25 in. long
	Both walls, 30 rays Metallic felt 1/2 in. thick, 25 in. long
	S-bend: 2 walls, 30 rays Metallic felt 1/2 in. thick, 25 in. long Str duct: 2 walls, 10/40 rays polyimide 1/2 in. + 1/2 in. thick, 14.7 in. long
	Str duct: 2 walls, 10/40 rays polyimide 1/2 in. + 1/2 in. thick, 14.7 in. long
	Two walls, 30 rays Metallic felt 1/2 in. thick, 25 in. long
	S-bend: 2 walls, 30 rayl Metallic felt 1/2 in. thick, 25 in. long Str duct: 2 walls, 10/40 rays polyimide 1/2 in. + 1/2 in. thick, 14.7 in. long
	Str duct: 2 walls, 10/40 polyimide 1/2 in. + 1/2 in. thick 14.7 in. long

Figure A-173.



Lining material Metallic felt  
 Flow resistance 30 rays (cgs)  
 Lining depth 0.5 in.  
 Core type 3/8-in. Hexcel

Duct geometry 6 x 10 in. S.  
 Walls lined One/10 in. S. bottom  
 Lining length 24 in.



Lining material Metallic Felt  
 Flow resistance 30 rays (cgs)  
 Lining depth 0.5 in.  
 Core type 3/8-in. Hexcel

Duct geometry 6 x 10  
 Walls lined One/10 in. S. top  
 Lining length 24 in.

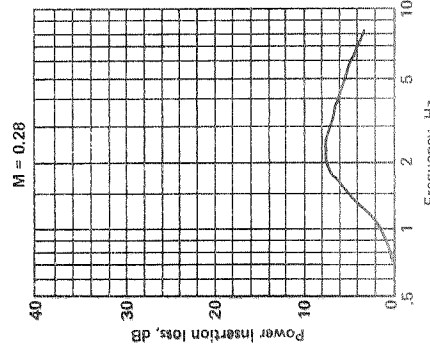
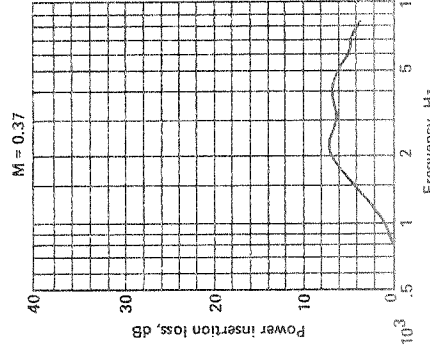
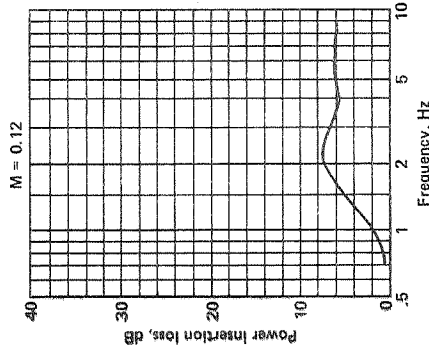
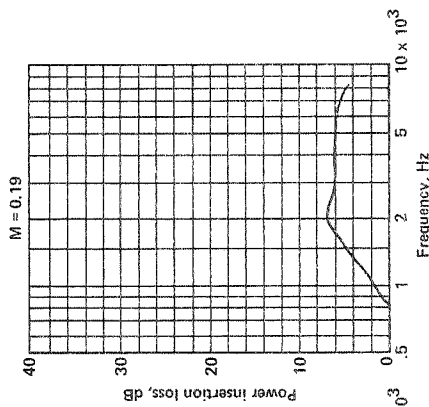


Figure A.175.

Figure A.174.

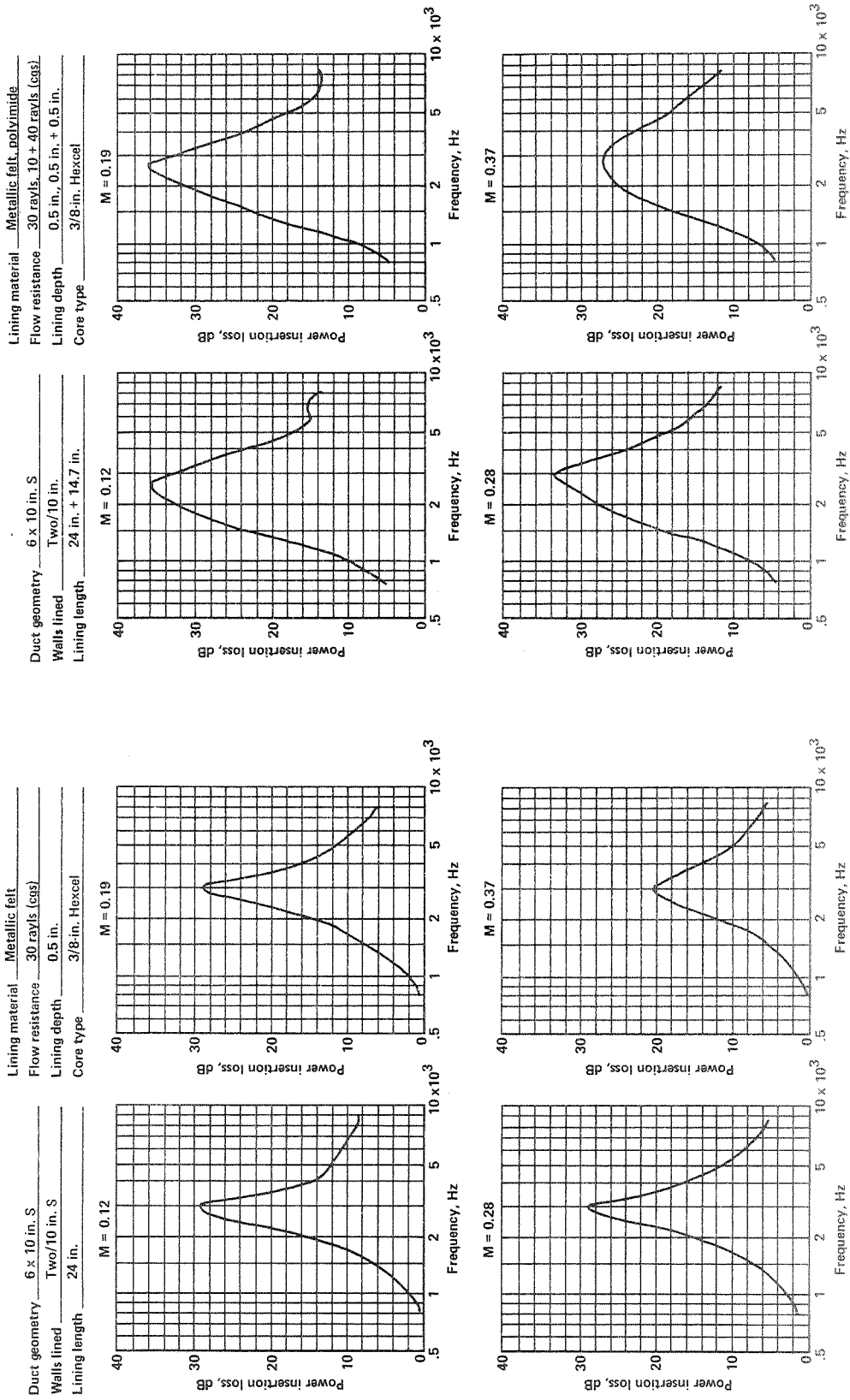
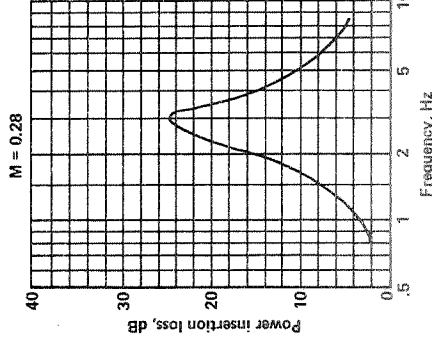
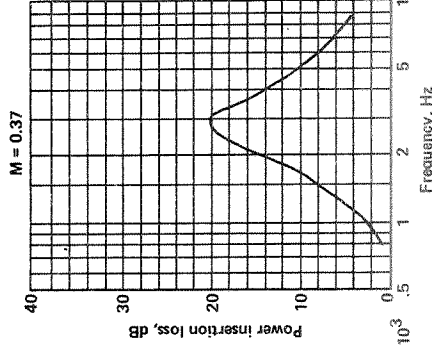
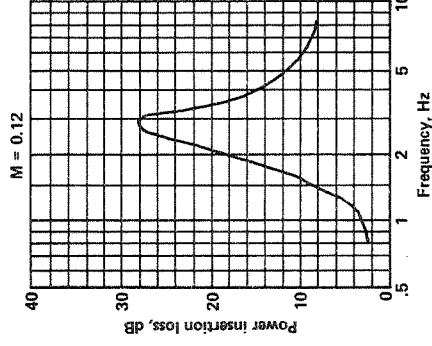


Figure A-176.

Figure A-177.

Lining material Metallic felt  
 Flow resistance 30 rays (gas)  
 Lining depth 0.5 in.  
 Core type 3/8-in. Hexcel

Duct geometry 6 x 10 in. S  
 Walls lined Two/10 in. S  
 Lining length 24 in.



Lining material Polyimide  
 Flow resistance 10 + 40 rays (gas)  
 Lining depth 1/2 in. + 1/2 in.  
 Core type 3/8-in. Hexcel

Duct geometry 6 x 10 in. S  
 Walls lined Two/10 in.  
 Lining length 14.7 in.

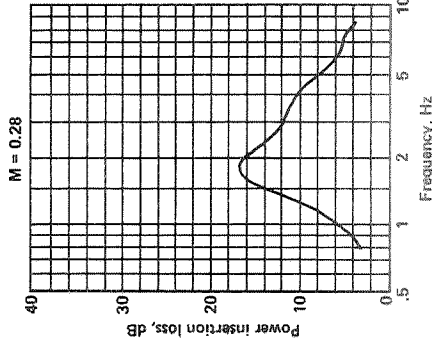
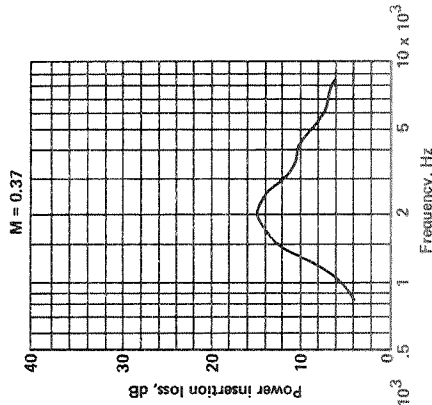
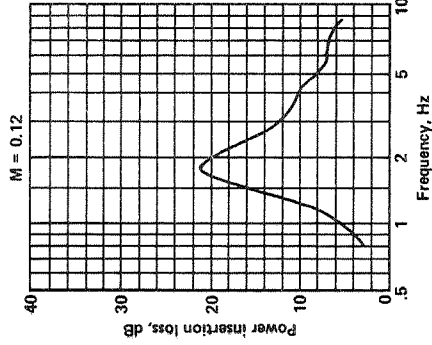
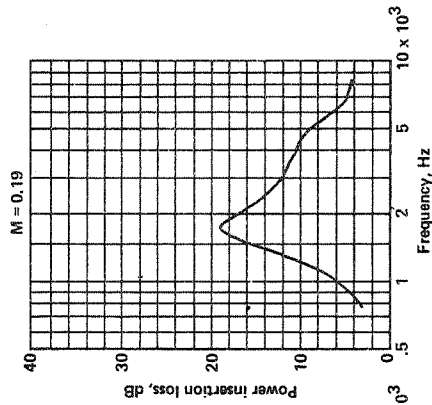
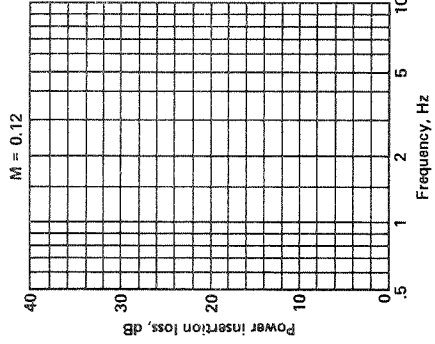
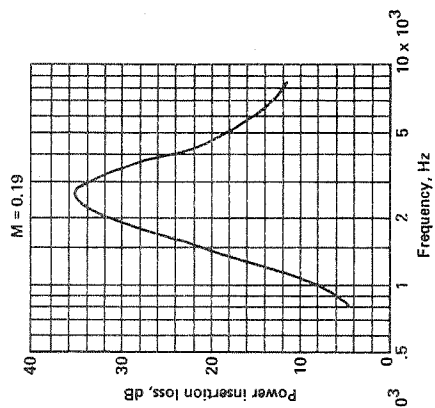


Figure A-179.

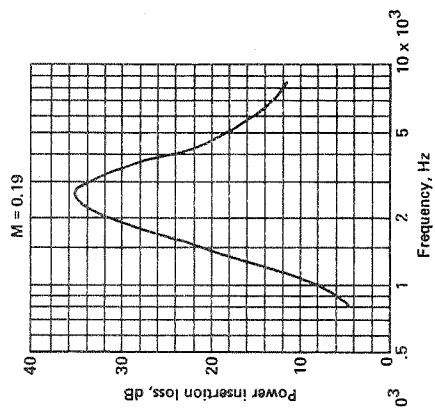
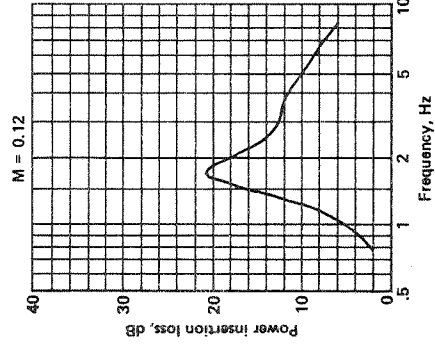
Figure A-178.

Lining material Metallic falt., polyimide  
 Flow resistance 30 rayls, 10 + 40 rayls (cgs)  
 Lining depth 0.5 in., 1/2 in. + 1/2 in.  
 Core type 3/8-in. Hexcel

Duct geometry 6 x 10 in. S  
 Walls lined Two/10 in.  
 Lining length 24 in. + 14.7 in.



Duct geometry 6 x 10 in. S  
 Walls lined Two/10 in.  
 Lining length 14.7 in.



Lining material Polyimide  
 Flow resistance 10 + 40 rayls (cgs)  
 Lining depth 1/2 in. + 1/2 in.  
 Core type 3/8-in. Hexcel

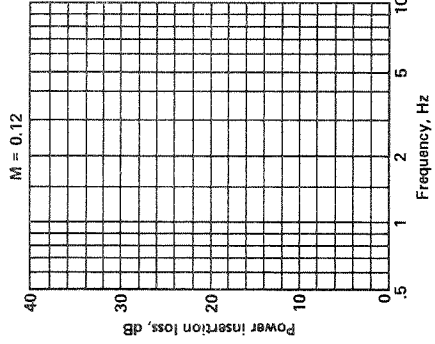
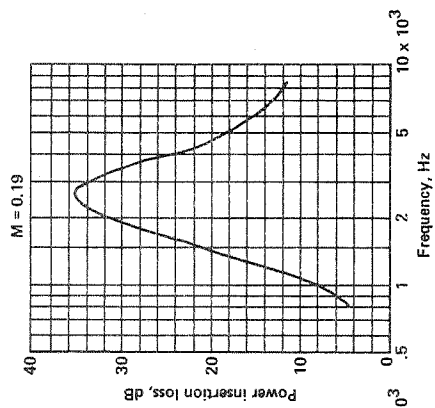
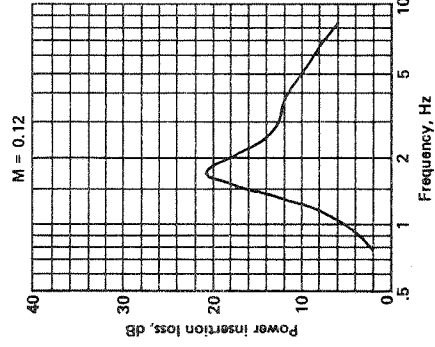
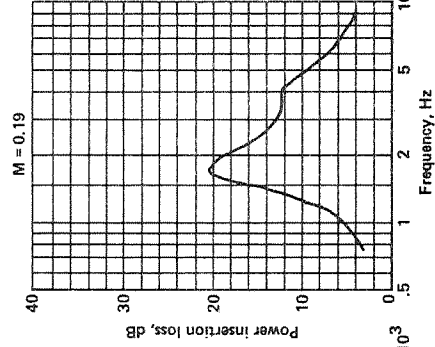
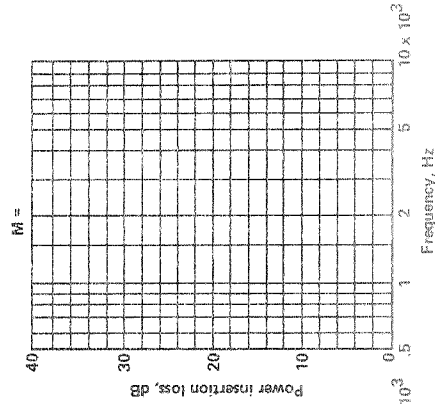
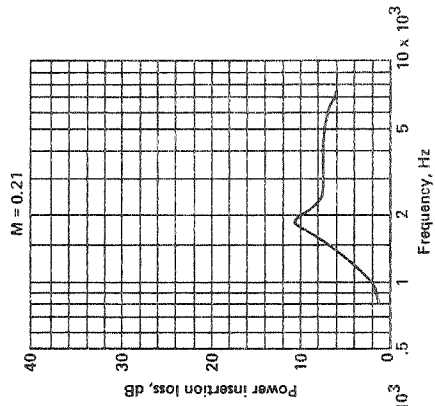


Figure A-180.

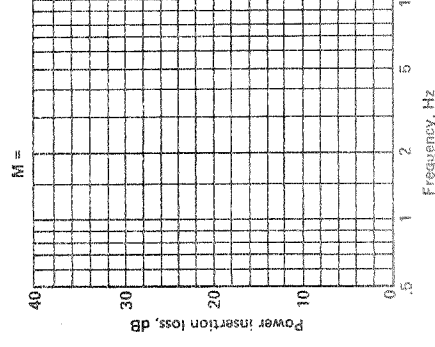
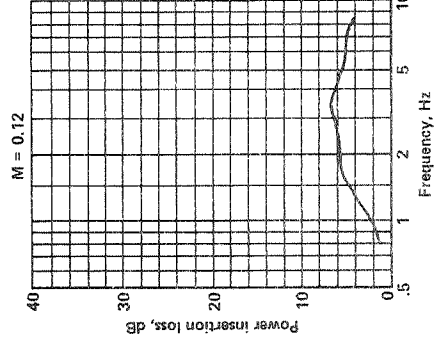
Figure A-181.

Lining material Woven Metal Fiber  
 Flow resistance 30 rays (cgs)  
 Lining depth 0.5 in.  
 Core type 3/8-in. Hexcel

Duct geometry 6 x 10 in.  
 Walls lined One/10 in. (Bottom)  
 Lining length 22 in.



Duct geometry 6 x 10 in.  
 Walls lined One/10 in. (Top)  
 Lining length 22 in.



Lining material Woven Metal Fiber  
 Flow resistance 30 rays (cgs)  
 Lining depth 0.5 in.  
 Core type 3/8-in. Hexcel

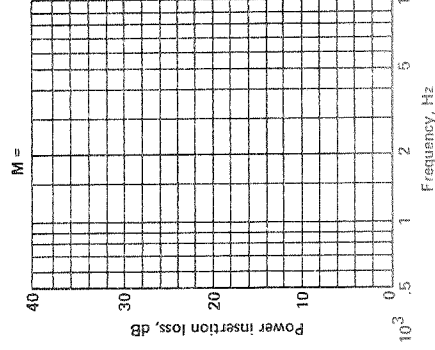
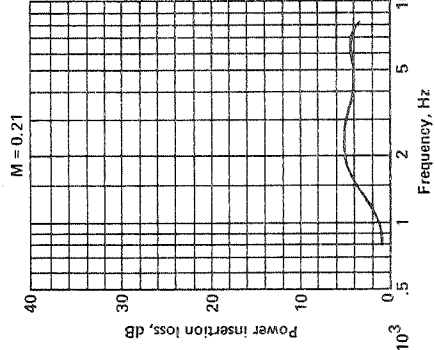
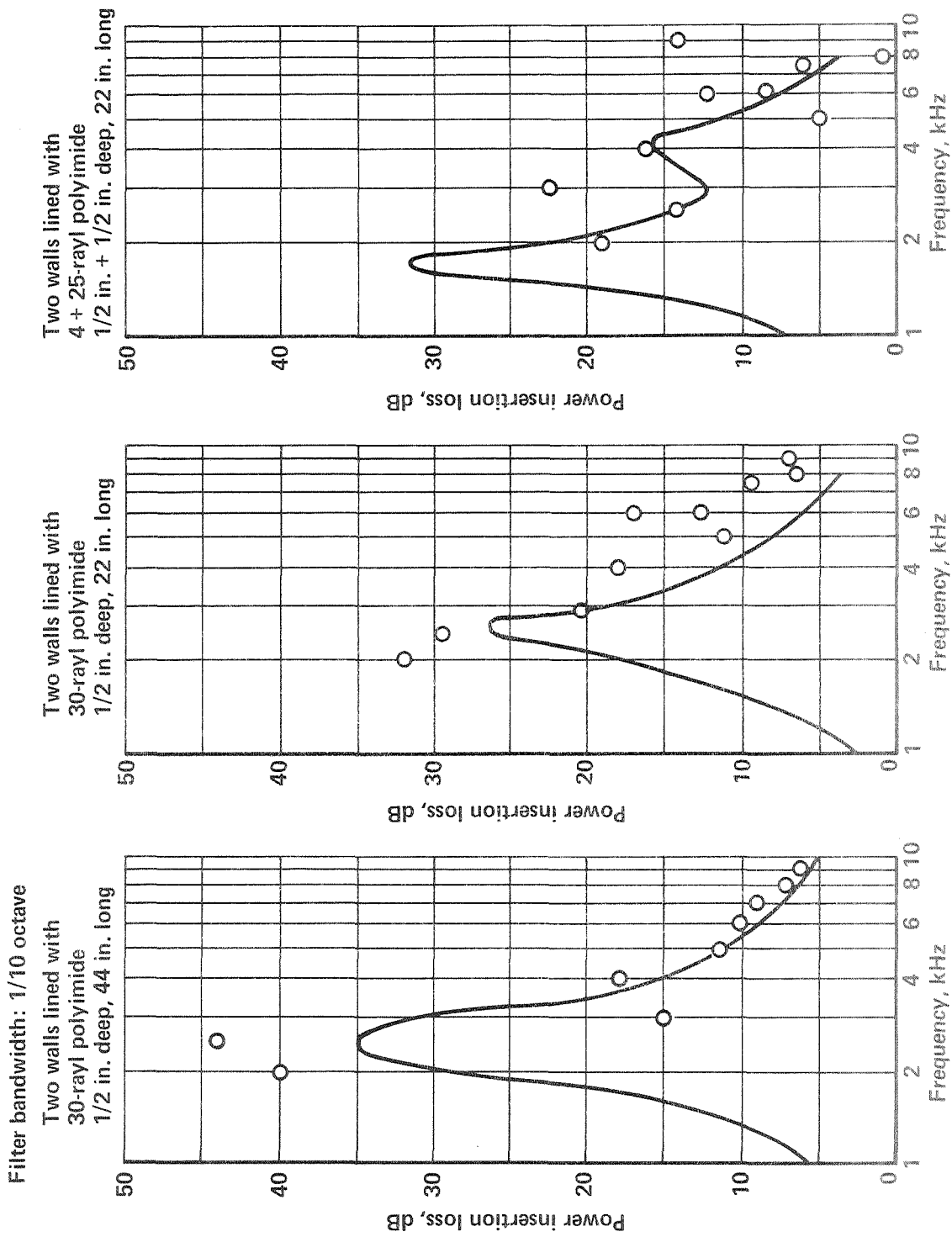


Figure A-183.

Figure A-182.



Note: Curves correspond to flow Mach no. = 0.12—Broadband noise  
 Points correspond to flow Mach no. = 0—air siren noise

Figure A-184.

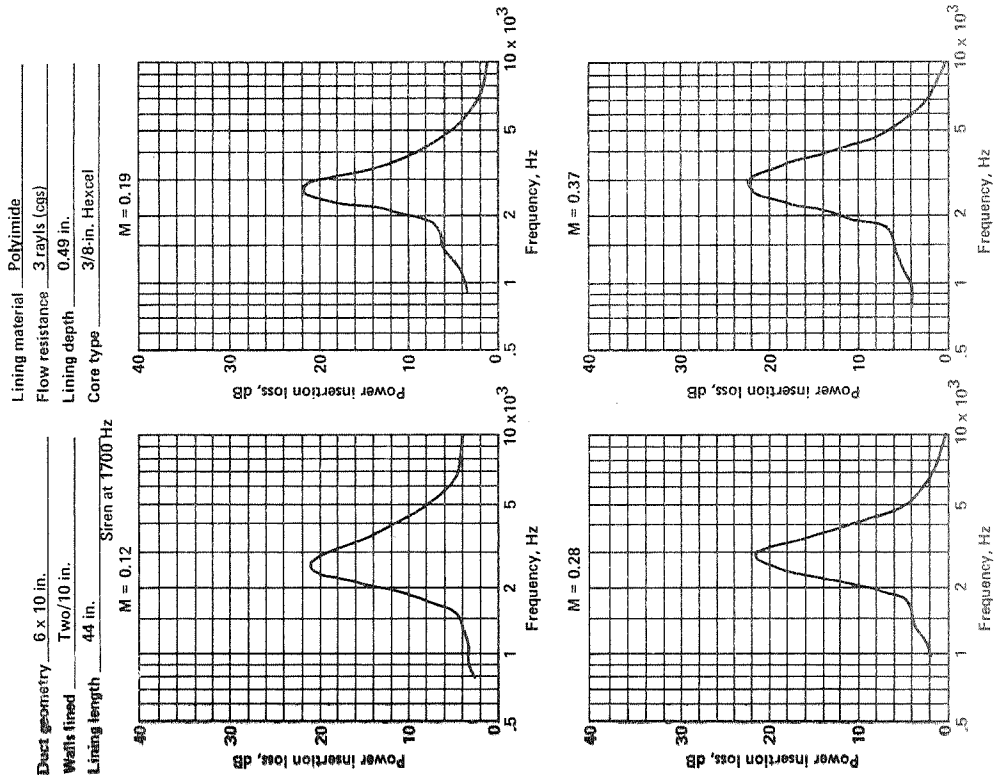


Figure A-185.

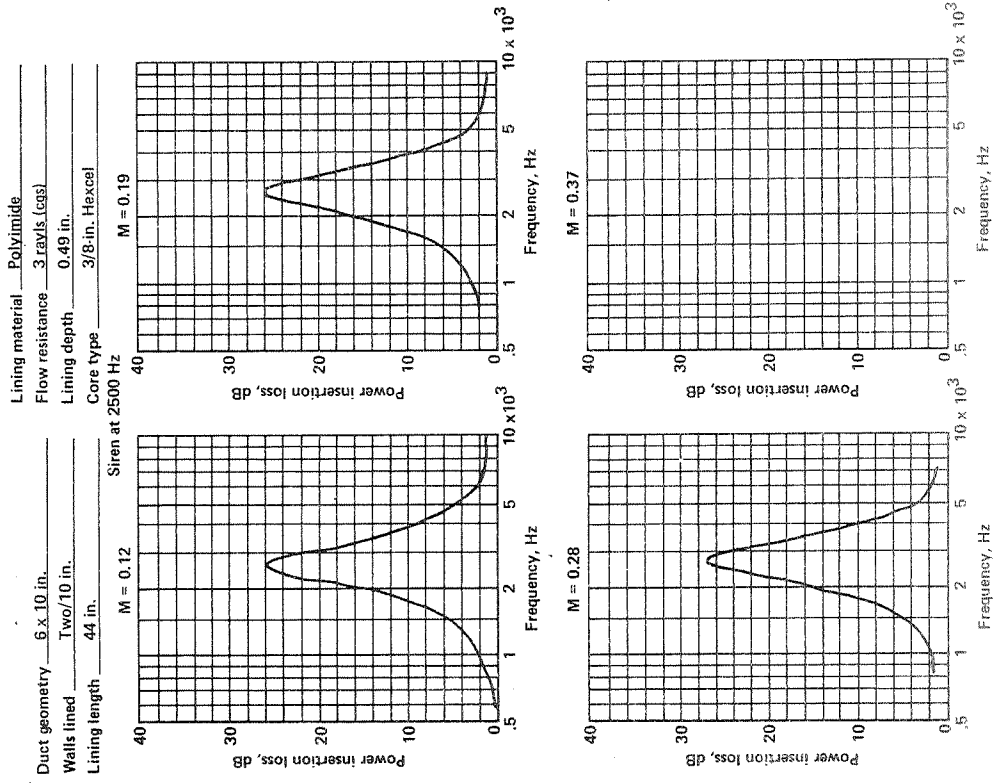


Figure A-186.

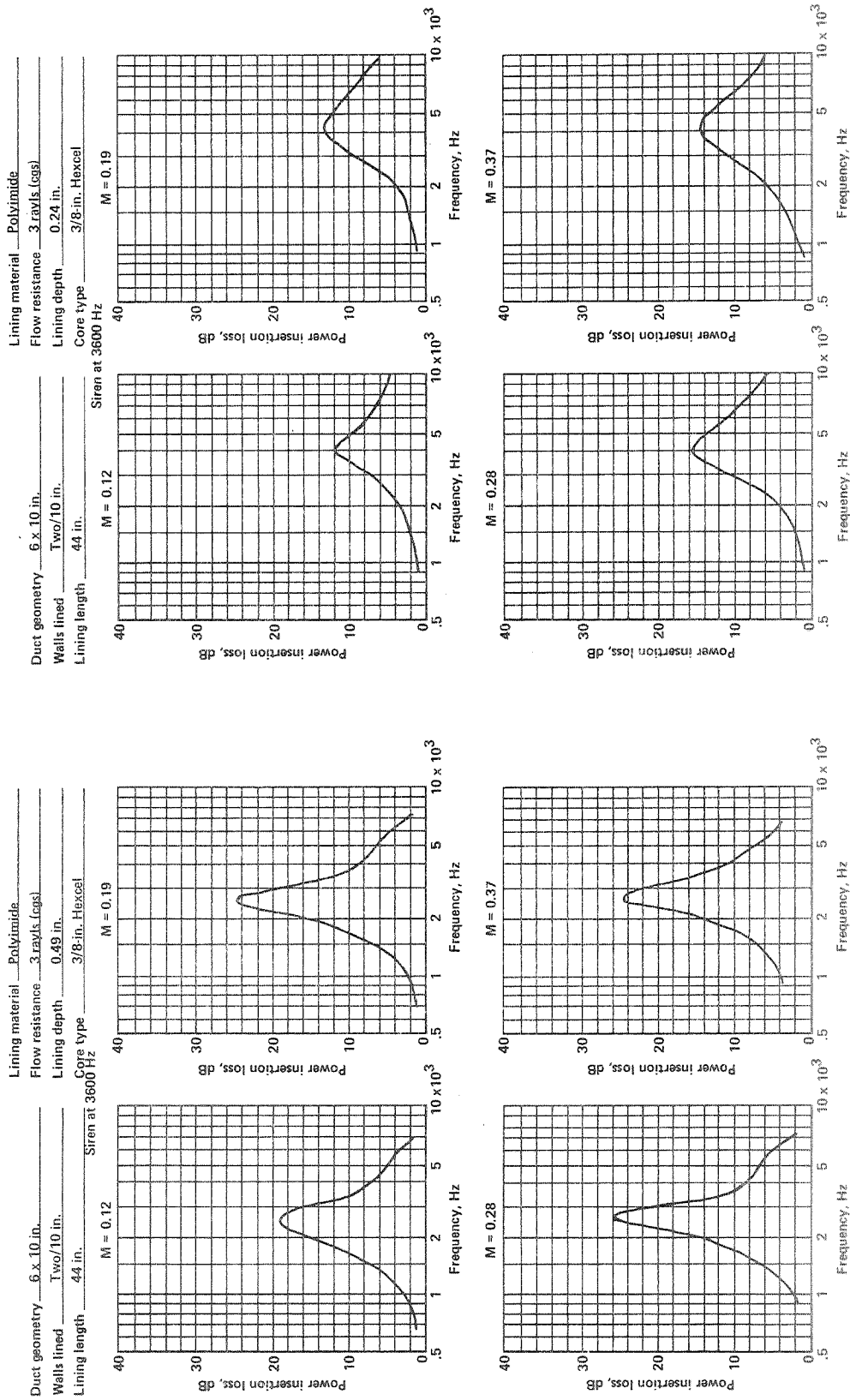


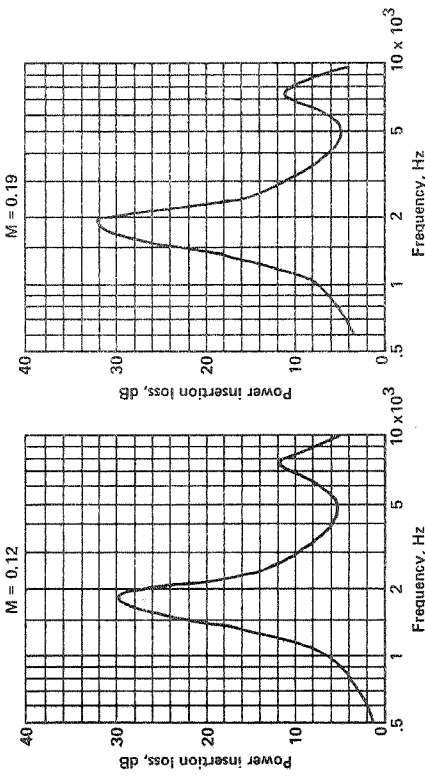
Figure A-188.

Figure A-187.



Duct geometry 6 x 10 in.  
 Walls lined Two/10 in.  
 Lining length 44 in.  
 Siren at 1700 Hz

Lining material Polyimide  
 Flow resistance 3 rayls (cgs)  
 Lining depth 1.01 in.  
 Core type 3/8-in. Hexcel



Duct geometry 6 x 10 in.  
 Walls lined Two/10 in.  
 Lining length 44 in.  
 Siren at 2500 Hz

Lining material Polyimide  
 Flow resistance 50 rayls (cgs)  
 Lining depth 0.47 in.  
 Core type 3/8-in. Hexcel

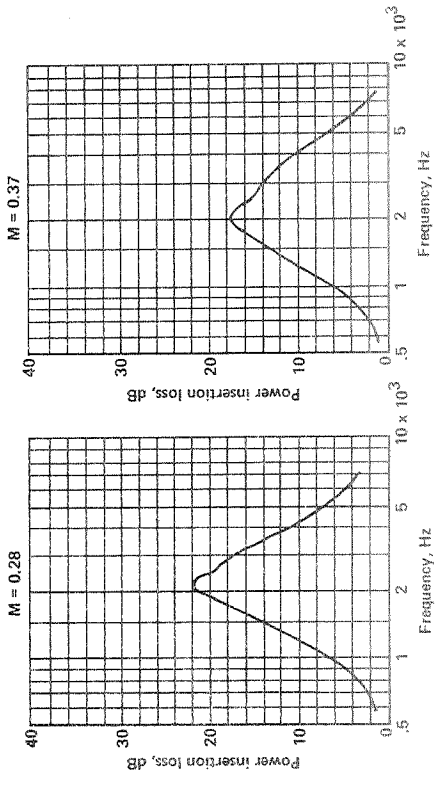
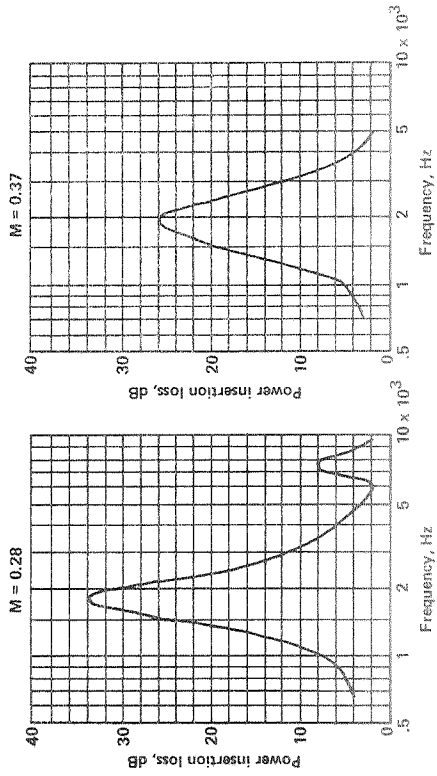
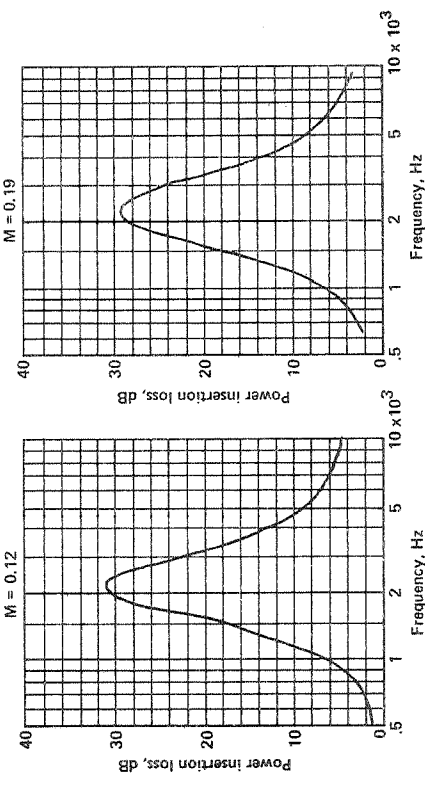


Figure A-189.

Figure A-190.

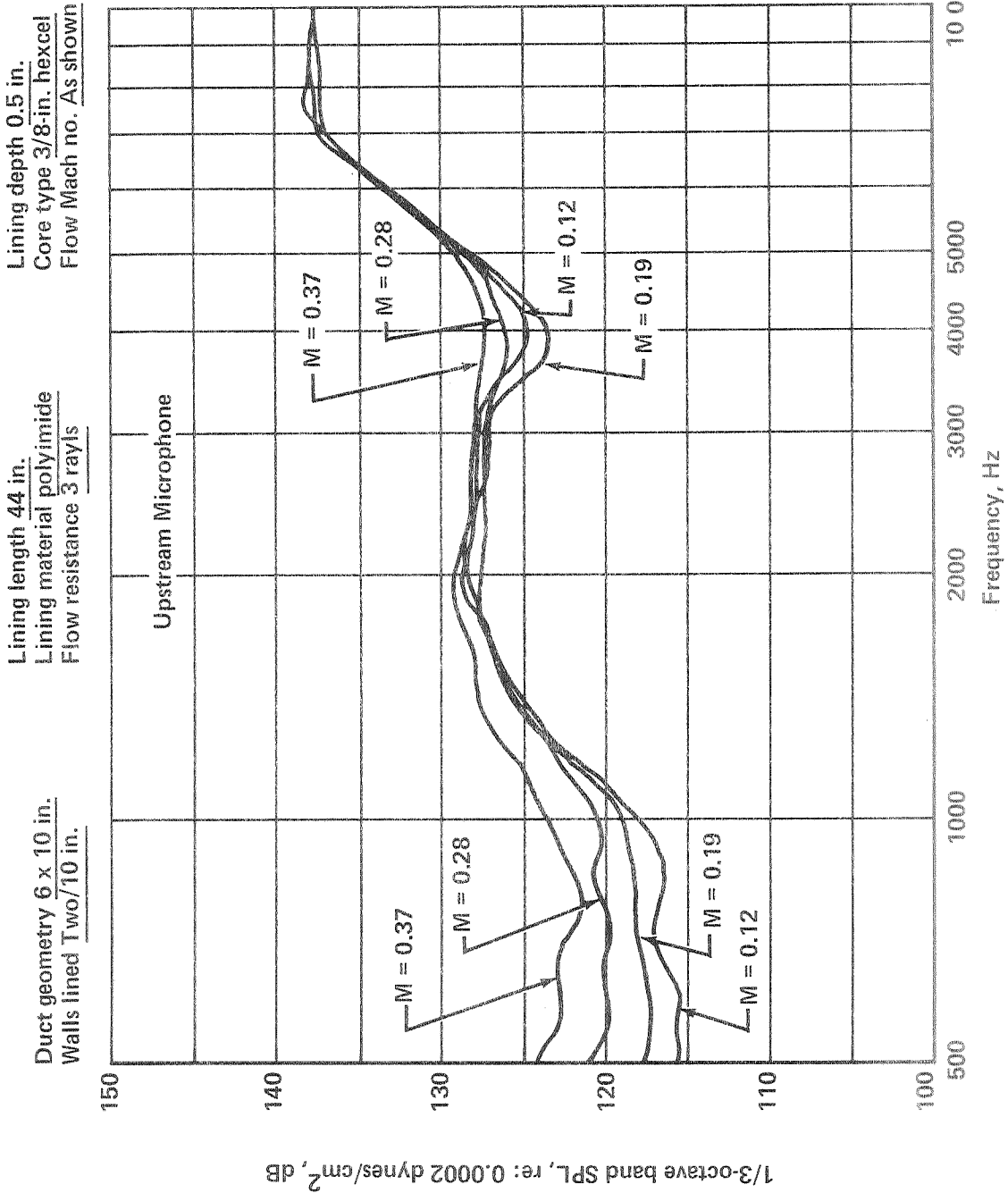


Figure A-191.

Lining depth 0.5 in.  
 Core type 3/8-in. Hexcel  
 Flow Mach no. As shown

Lining length 44 in.  
 Lining material Polyimide  
 Flow resistance 3 rayls

Duct geometry 6 x 10 in.  
 Walls lined Two/10 in.

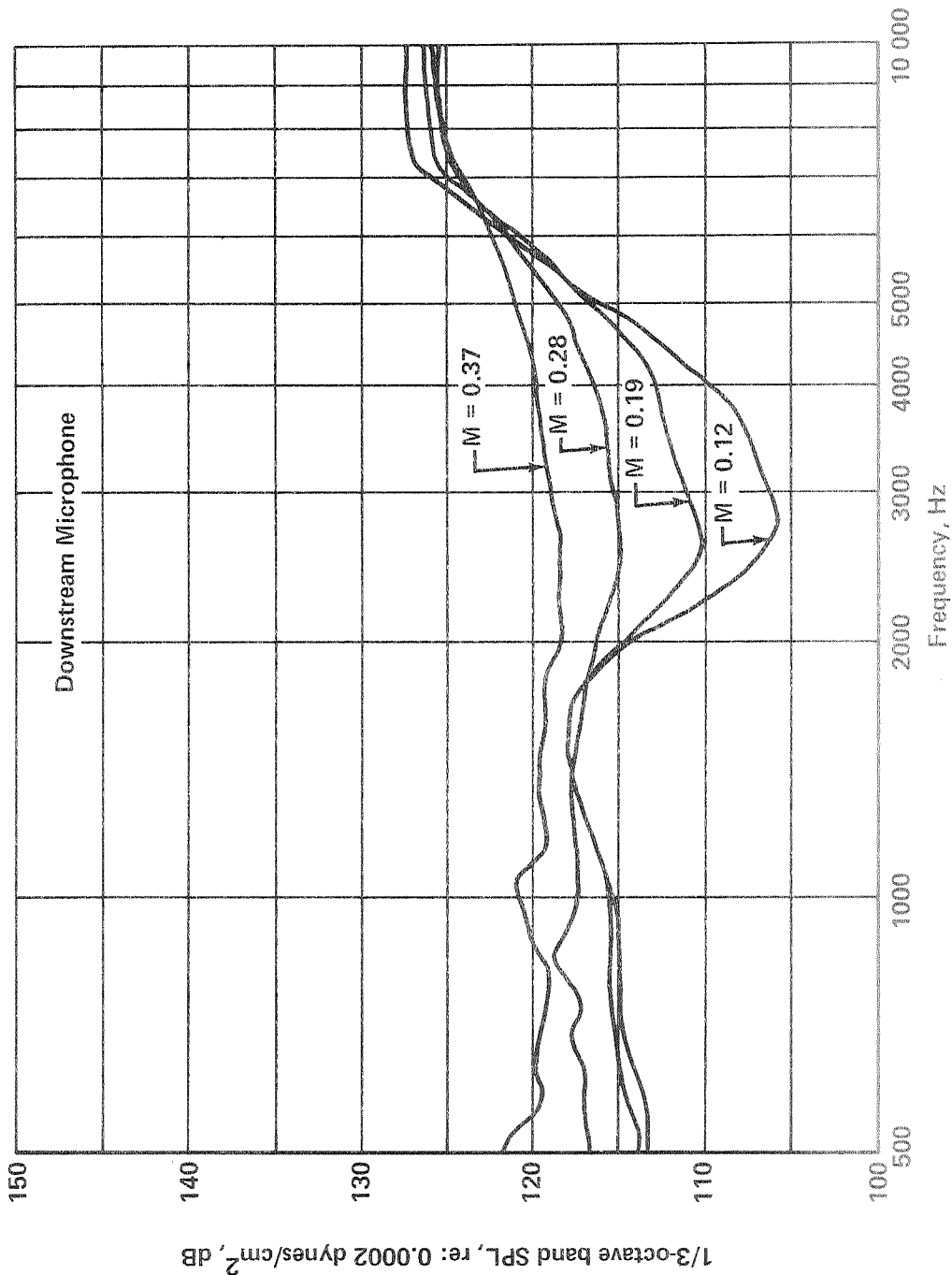


Figure A-192.

Duct geometry 6 x 10 in.  
 Wall lined Two/10 in.

Lining length 44 in.  
 Lining material Polyimide  
 Flow resistance 9 rayls

Lining depth 0.5 in.  
 Core type 3/8-in. Hexcel  
 Flow Mach no. As shown

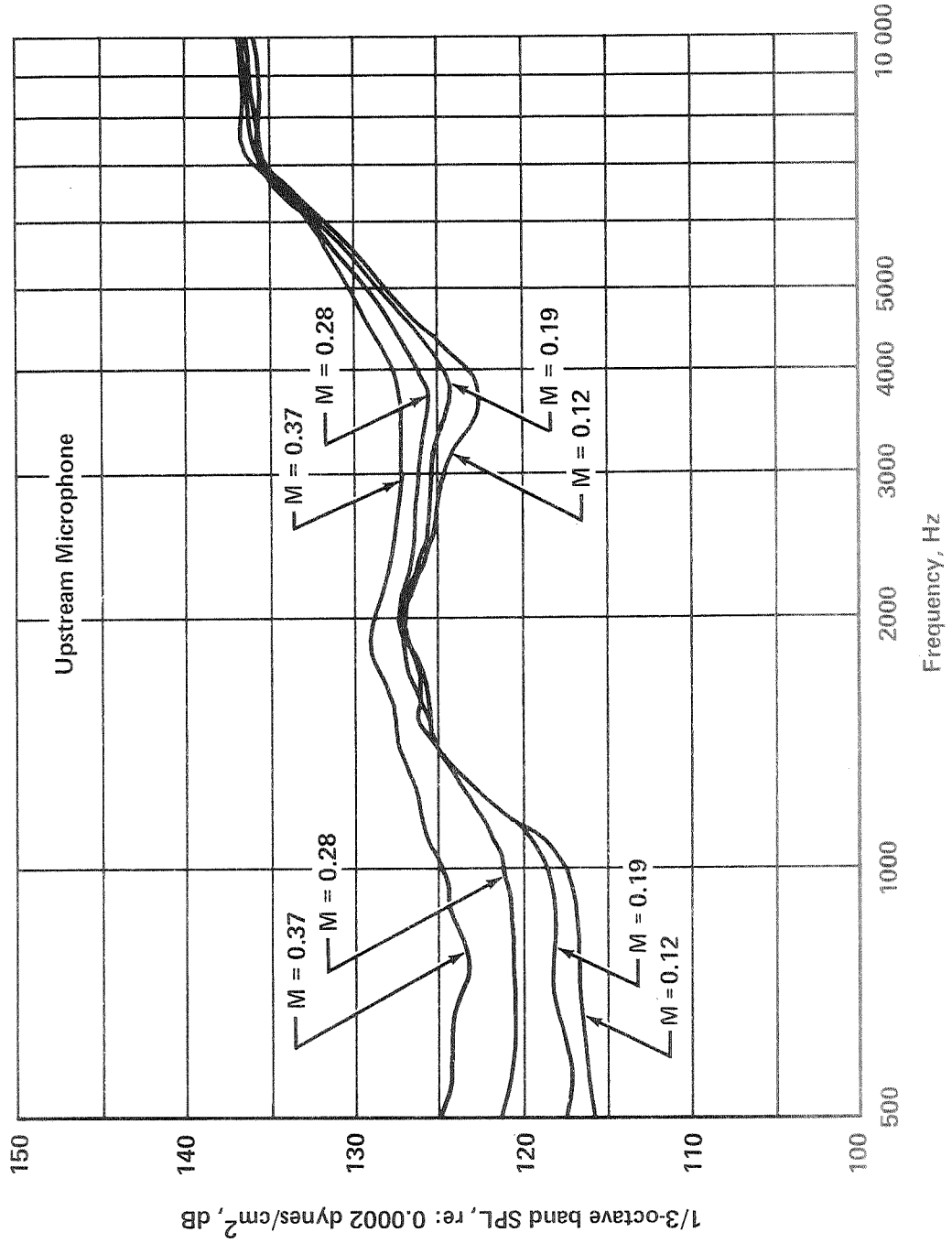


Figure A-193.

Lining depth 0.5 in.  
 Core type 3/8-in. Hexcel  
 Flow Mach no. As shown

Lining length 44 in.  
 Lining material Polyimide  
 Flow resistance 9 rays

Duct geometry 6 x 10 in.  
 Walls lined Two/10 in.

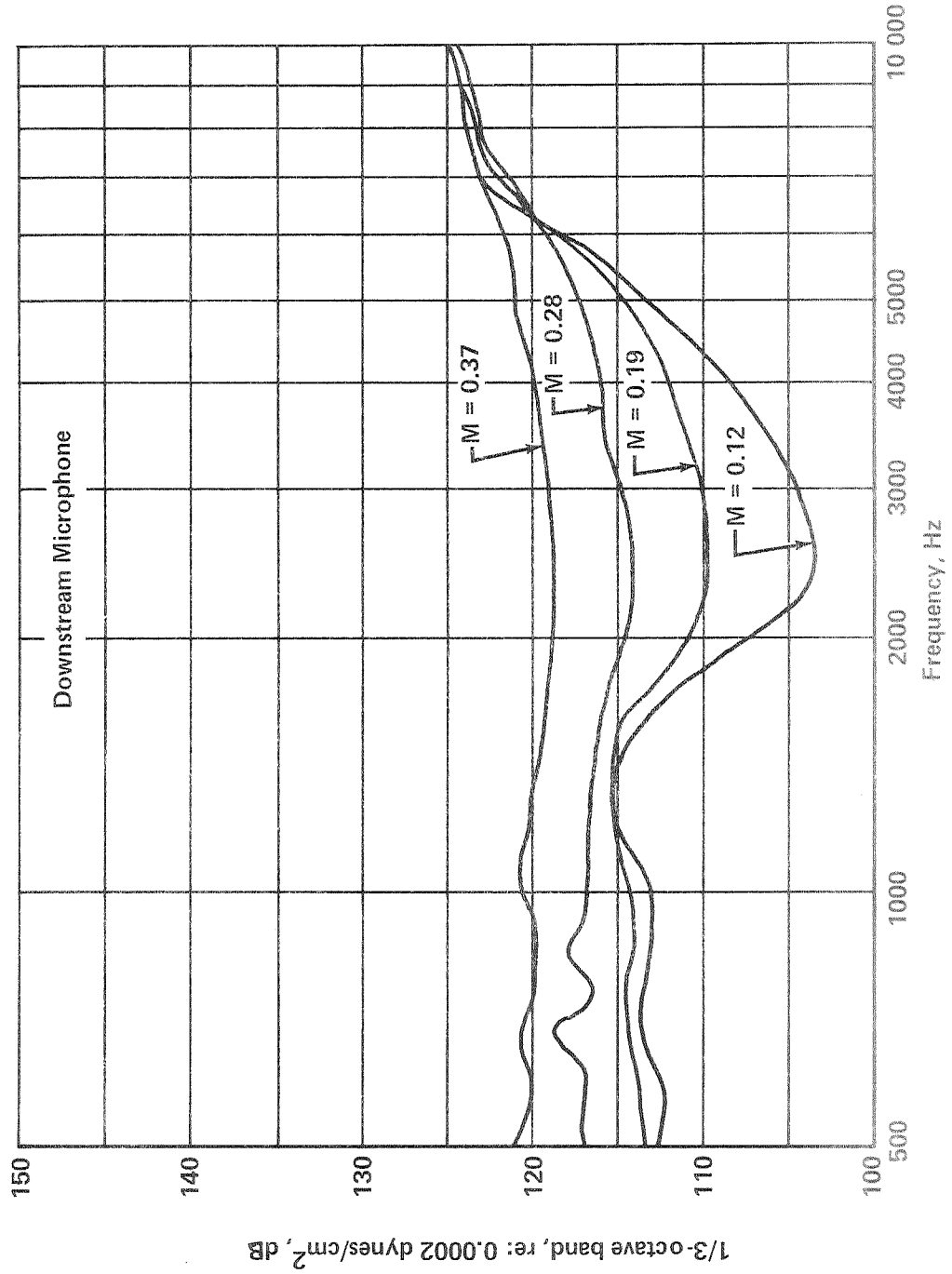


Figure A-194.

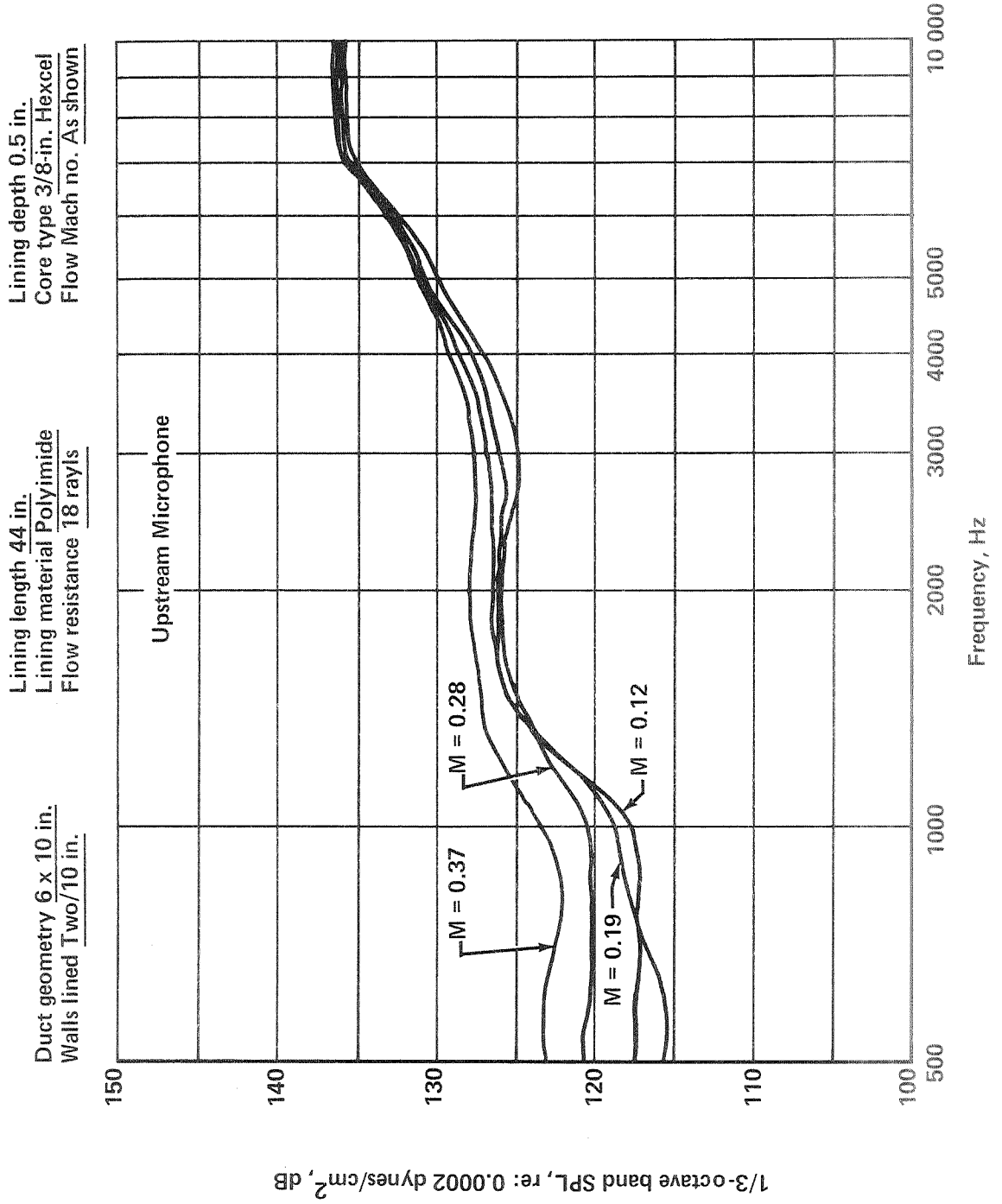


Figure A-195.

Lining depth 0.5 in.  
 Core type 3/8-in. Hexcel  
 Flow Mach no. As shown

Lining length 44 in.  
 Lining material Polyimide  
 Flow resistance 18 rays

Duct geometry 6 x 10 in.  
 Walls lined Two/10 in.

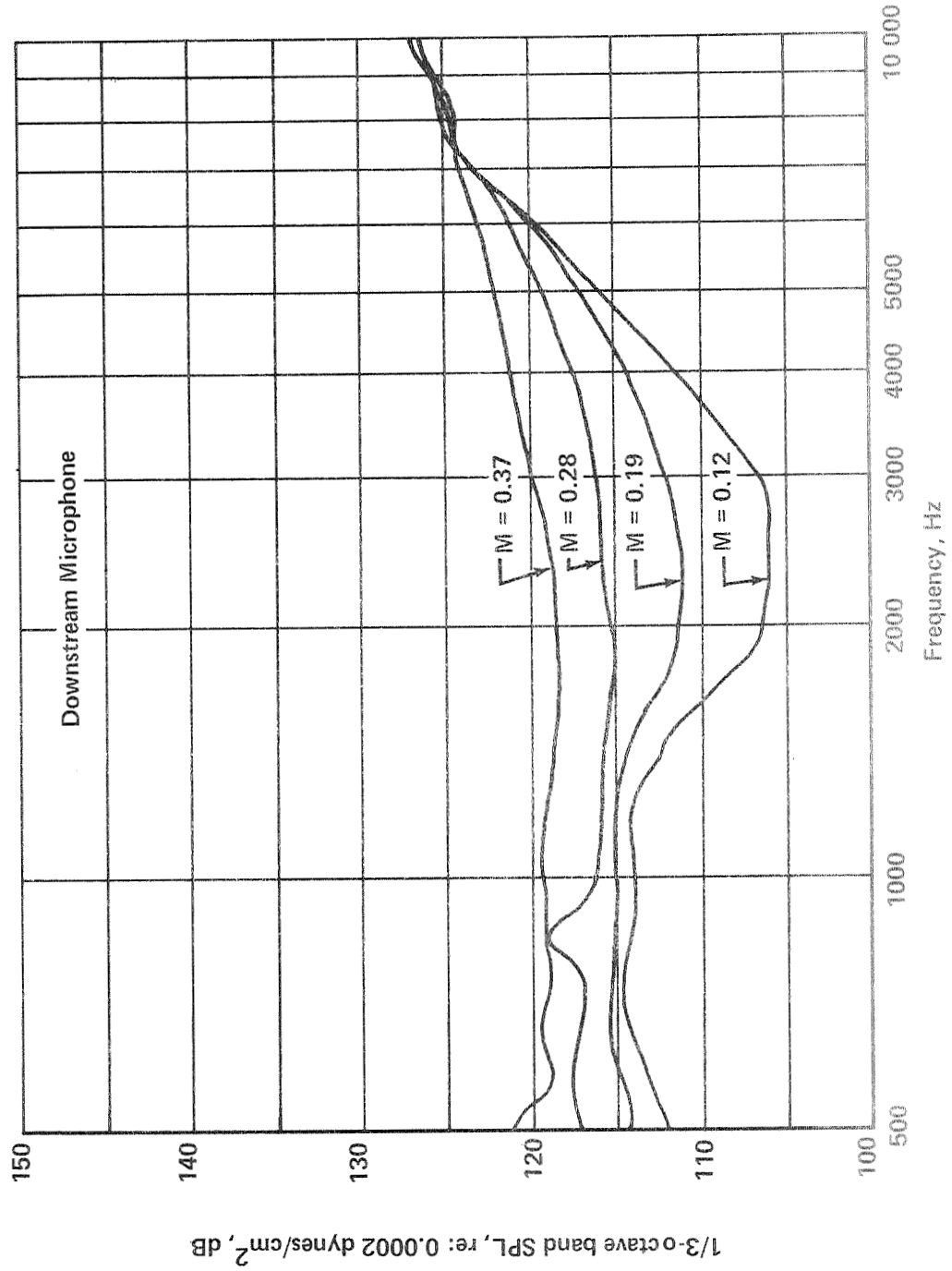


Figure A-196.

Duct geometry 6 x 10 in.  
 Walls lined Two/10 in.

Lining length 44 in.  
 Lining material Polyimide  
 Flow resistance 30 rays

Lining depth 0.5 in.  
 Core type 3/8-in. Hexcel  
 Flow Mach no. As shown

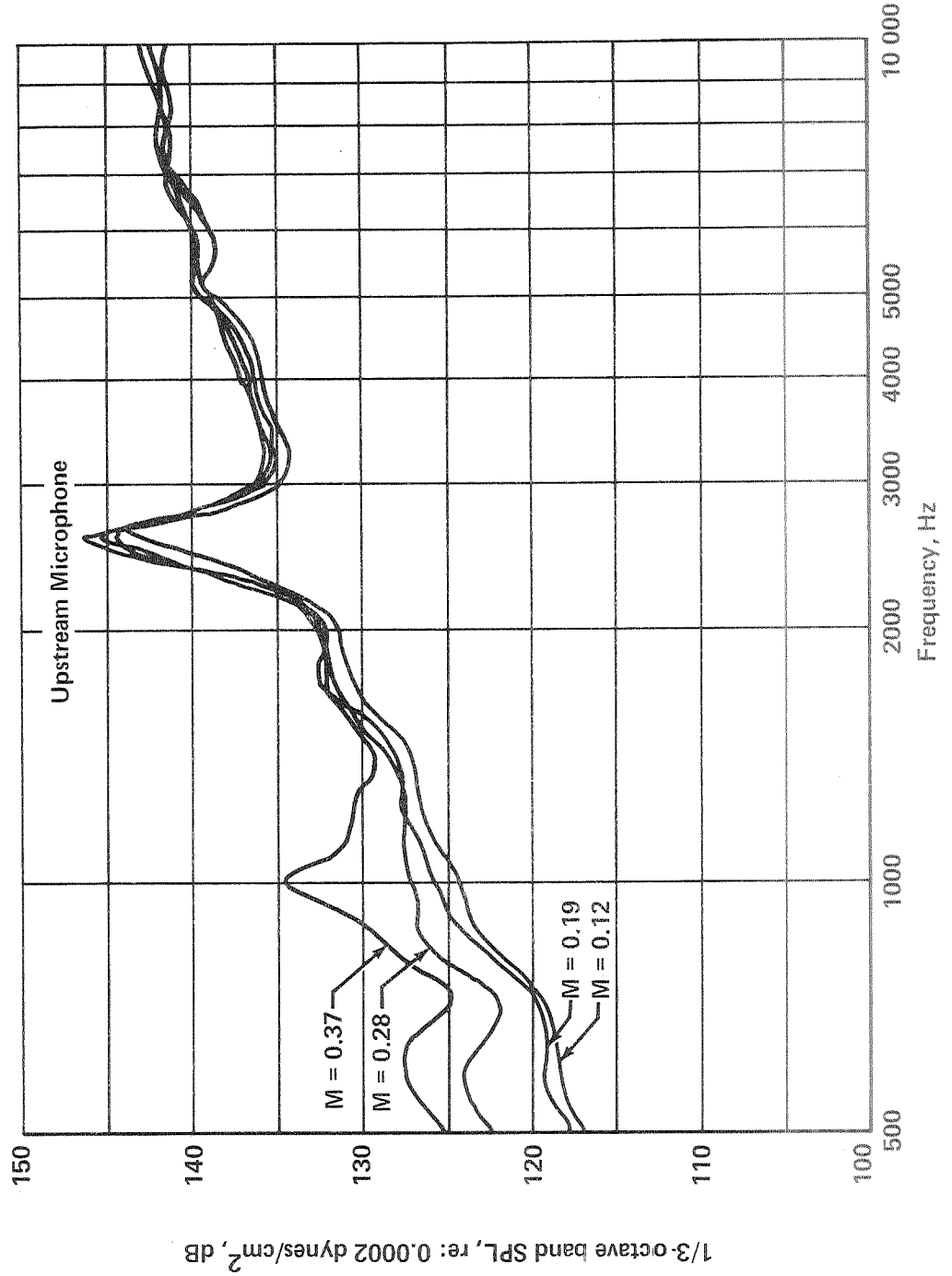


Figure A-197.



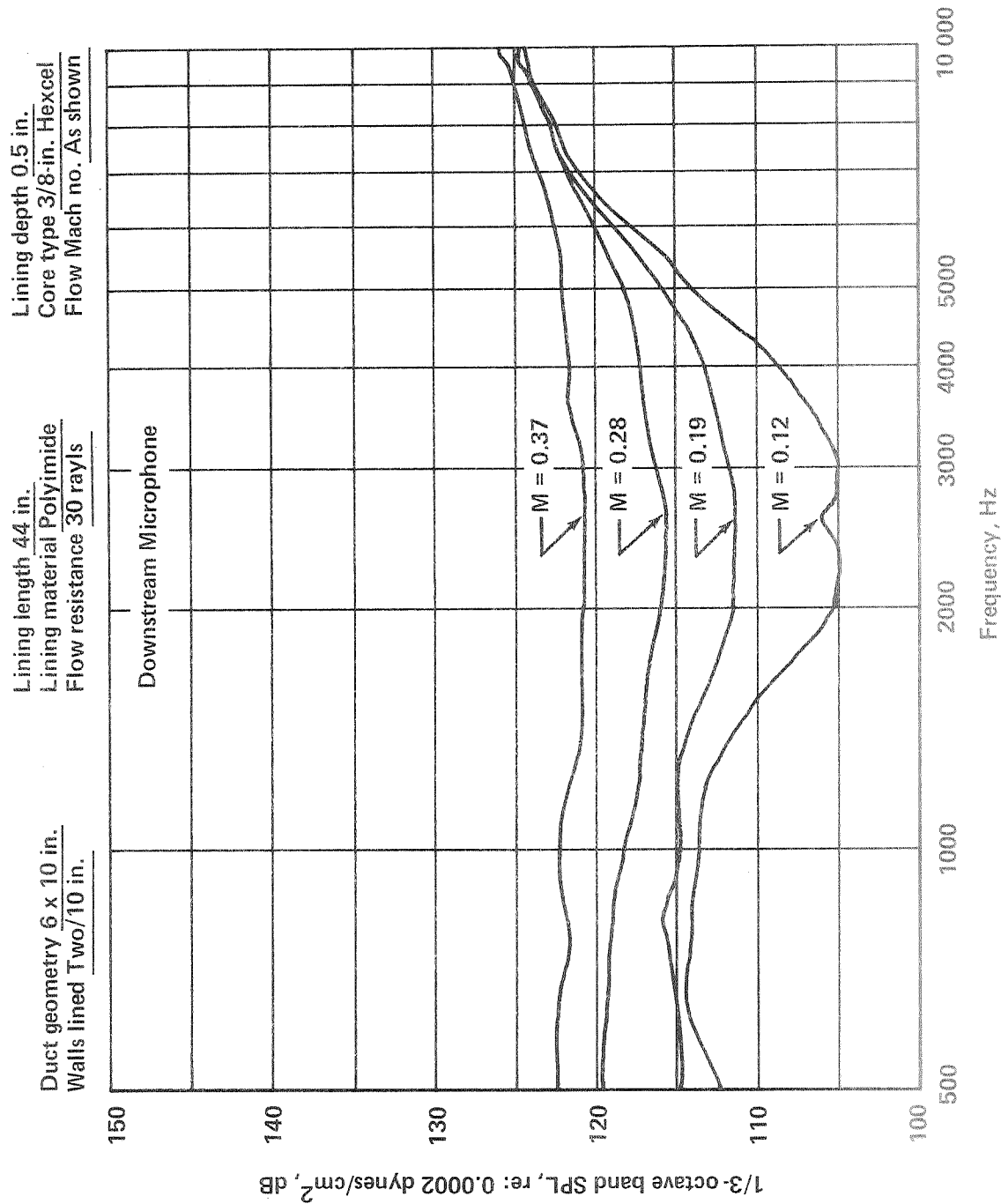


Figure A-198.

Duct geometry 6 x 10 in.  
 Walls lined Two/10 in.

Lining length 44 in.  
 Lining material Polyimide  
 Flow resistance 50 rays

Lining depth 0.5 in.  
 Core type 3/8-in. Hexcel  
 Flow Mach no. As shown

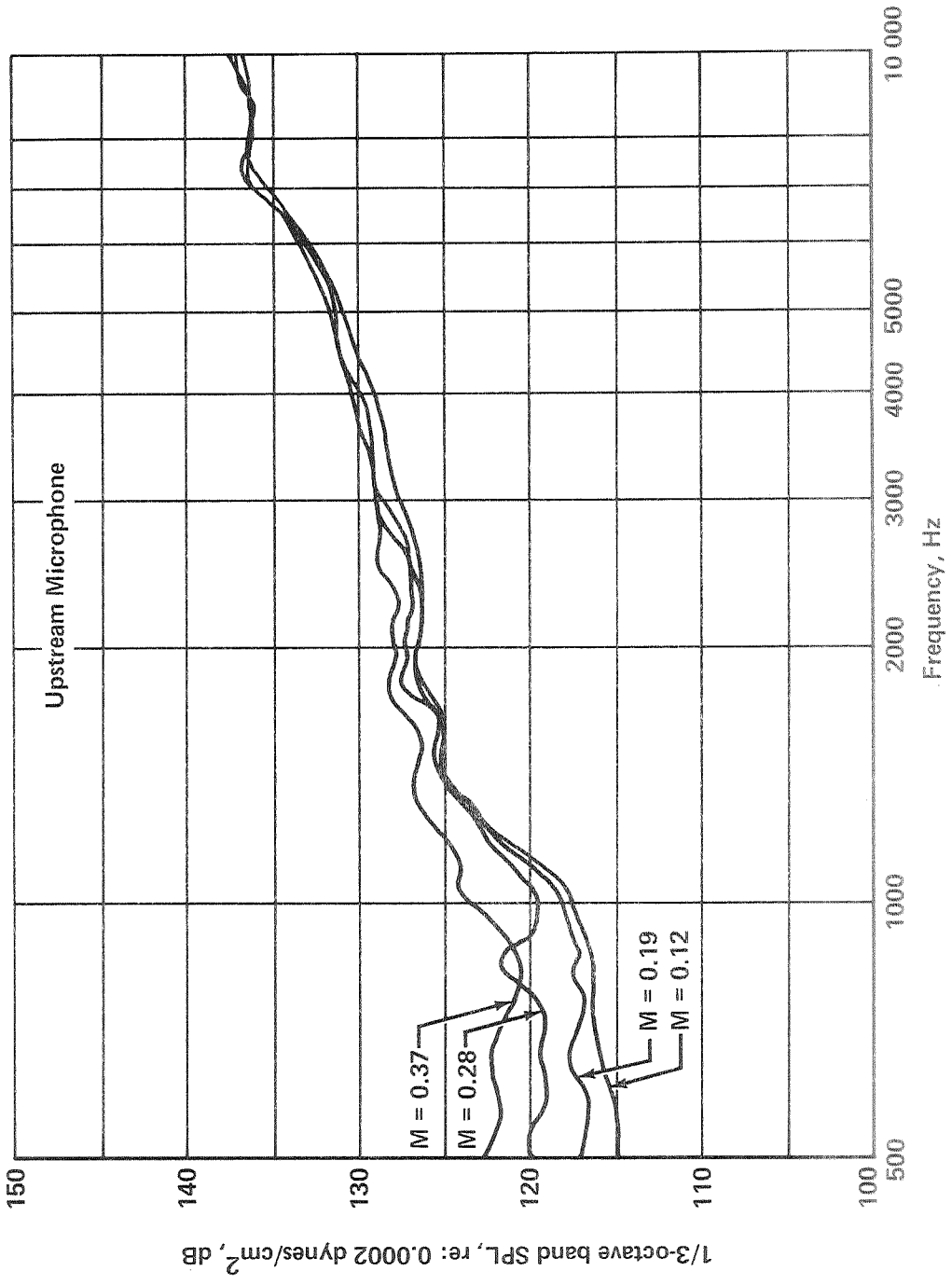


Figure A-199.

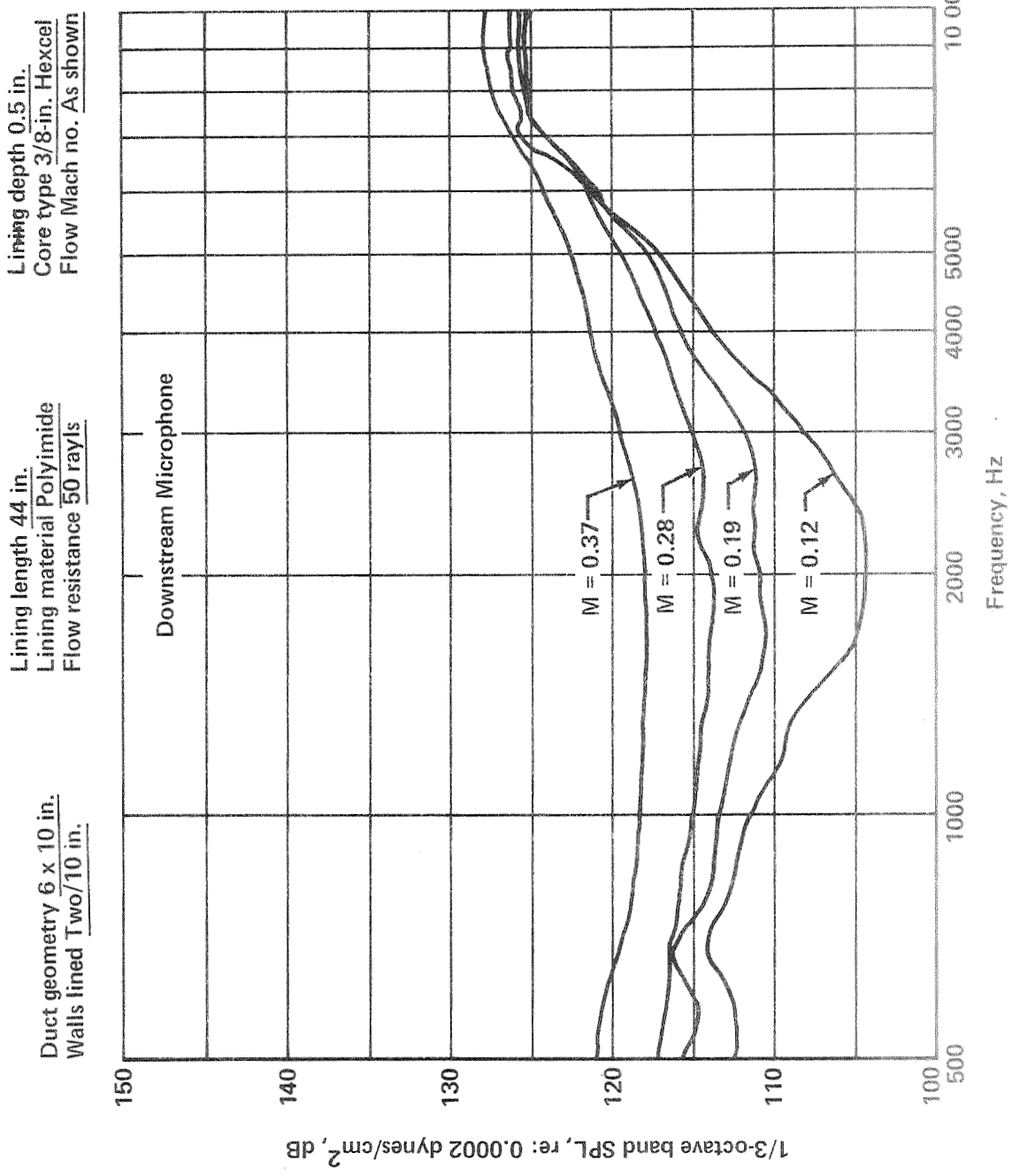


Figure A-200.

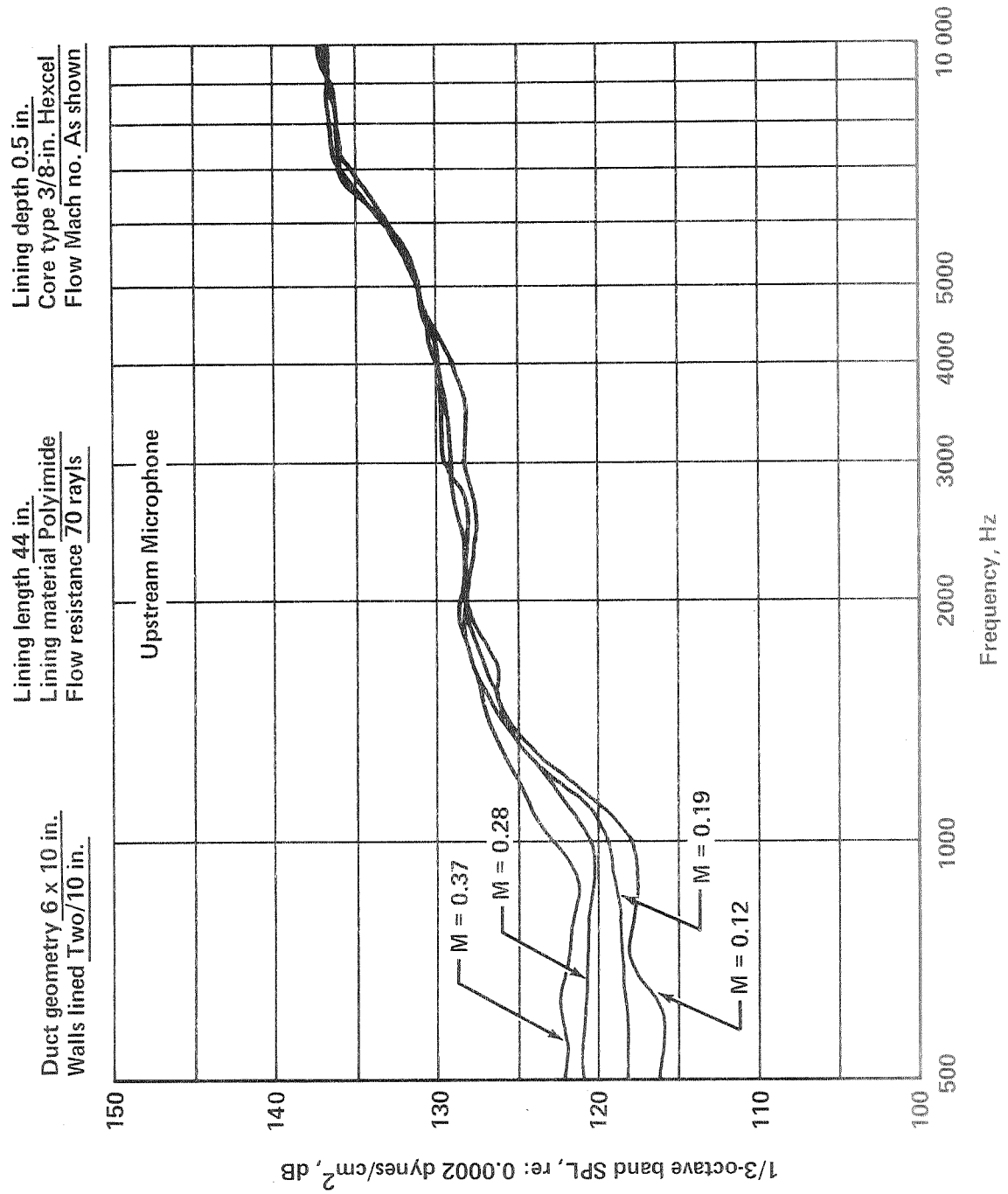


Figure A-201.

Duct geometry 6 x 10 in.  
 Walls lined Two/10 in.

Lining length 44 in.  
 Lining material Polyimide  
 Flow resistance 70 rays

Lining depth 0.15 in.  
 Core type 3/8-in. Hexcel  
 Flow Mach no. As shown

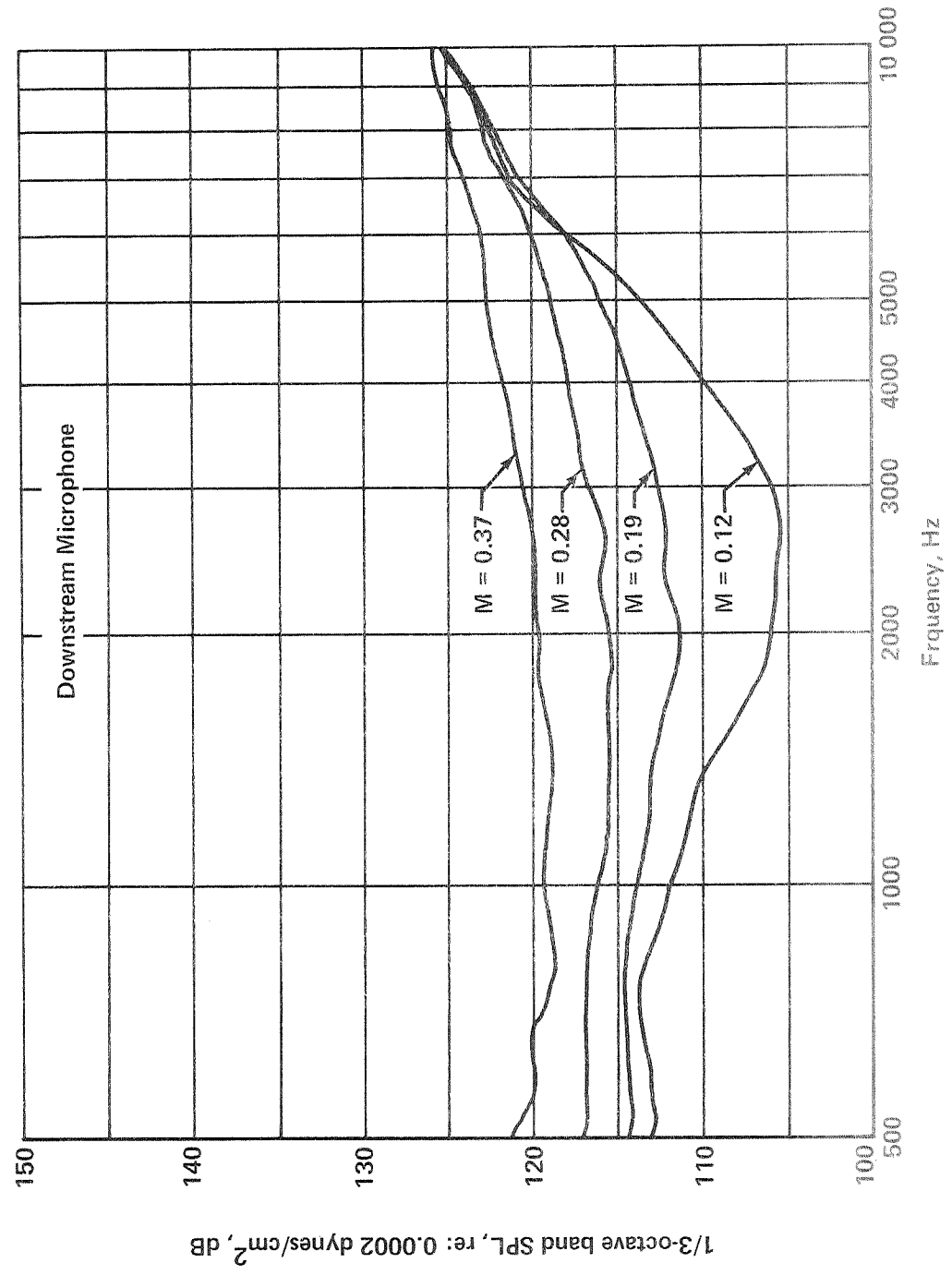


Figure A-202.

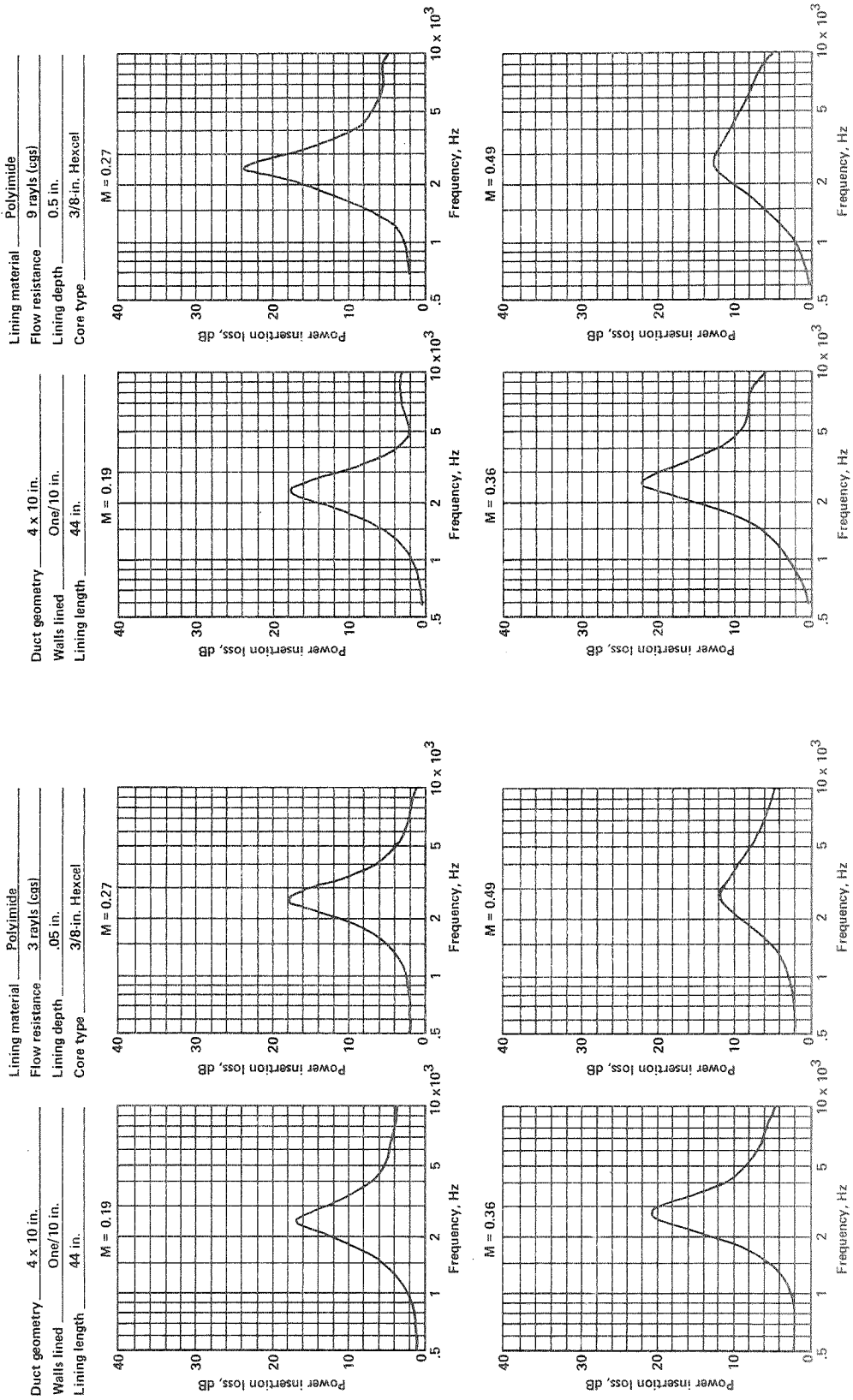


Figure A-203.

Figure A-204.

Lining material Polyimide  
 Flow resistance 30 rays (cgs)  
 Lining depth 0.5 in.  
 Core type 3/8-in. Hexcel

Duct geometry 4 x 10 in.  
 Walls lined One/10 in.  
 Lining length 44 in.

Lining material Polyimide  
 Flow resistance 18 rays (cgs)  
 Lining depth 0.5 in.  
 Core type 3/8-in. Hexcel

Duct geometry 4 x 10 in.  
 Walls lined One/10 in.  
 Lining length 44 in.

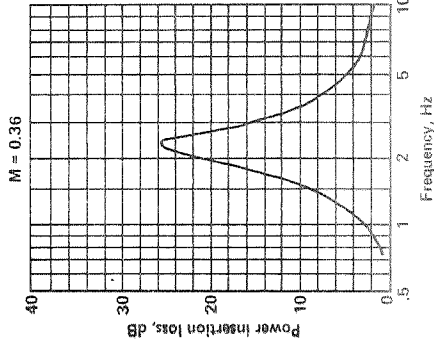
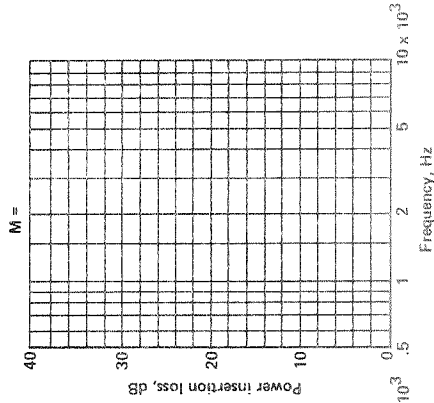
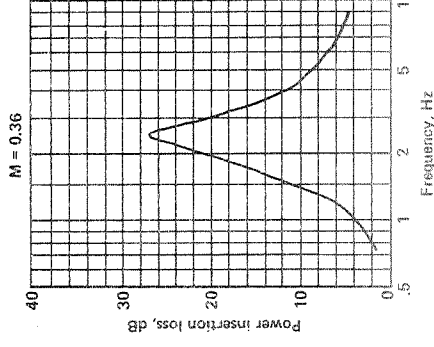
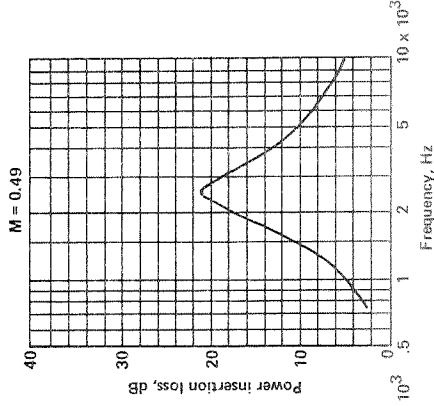
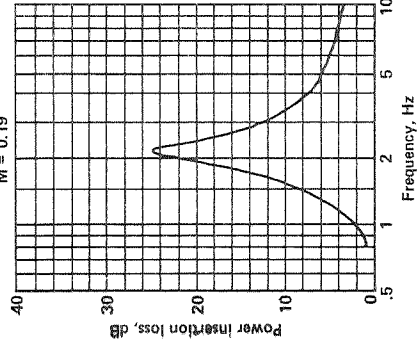
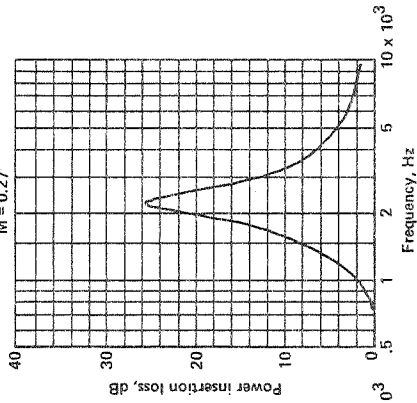
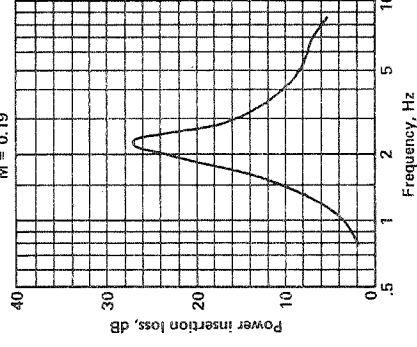
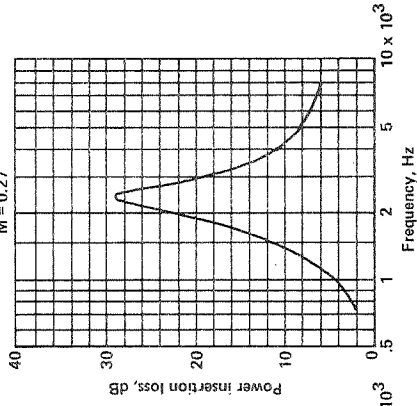


Figure A-206.

Figure A-205.

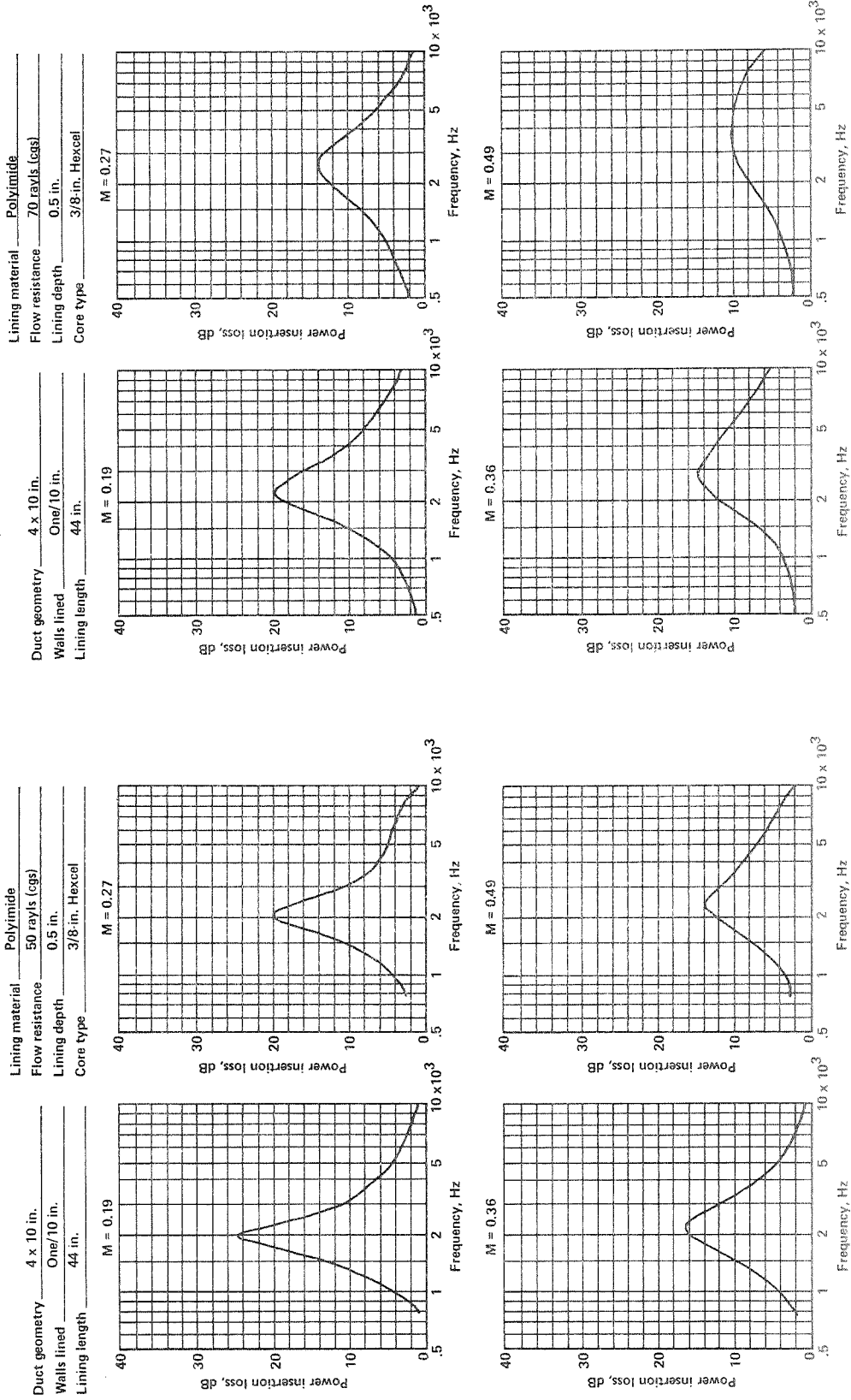


Figure A-207.

Figure A-208.



Lining material Polyimide  
 Flow resistance 9 rays/cs  
 Lining depth 0.5 in.  
 Core type 3/8-in. Hexcel

Duct geometry 4 x 10 in.  
 Walls lined Two/10 in.  
 Lining length 22 in.

Lining material Polyimide  
 Flow resistance 3 rays/cs  
 Lining depth 0.5 in.  
 Core type 3/8-in. Hexcel

Duct geometry 4 x 10 in.  
 Walls lined Two/10 in.  
 Lining length 22 in.

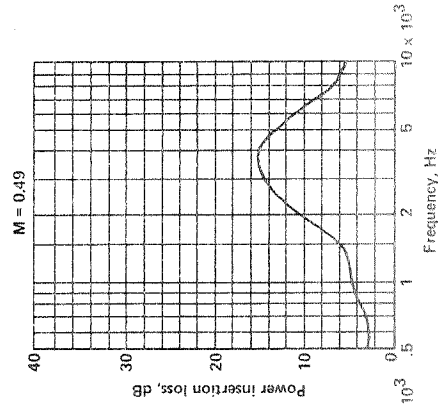
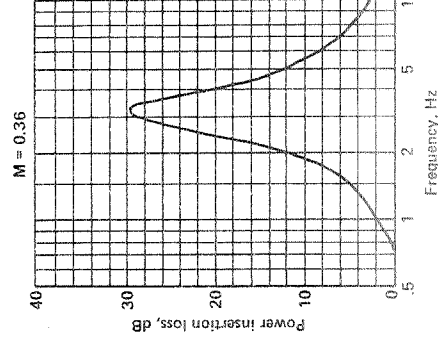
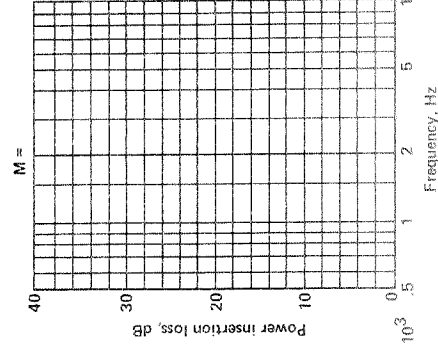
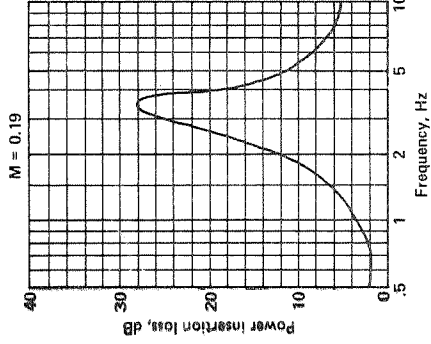
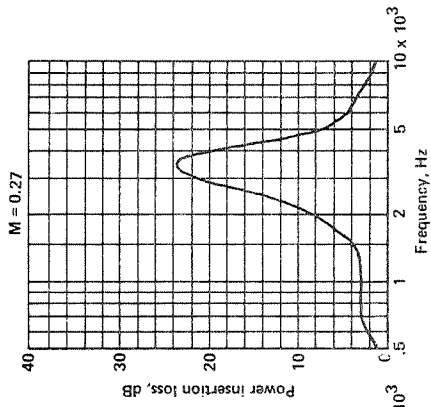
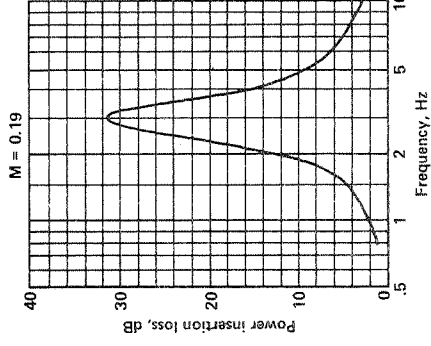
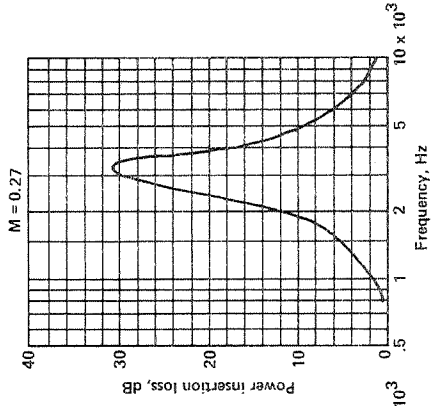
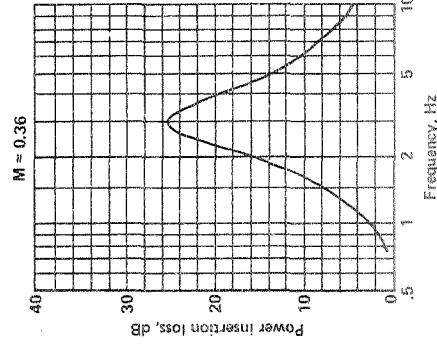
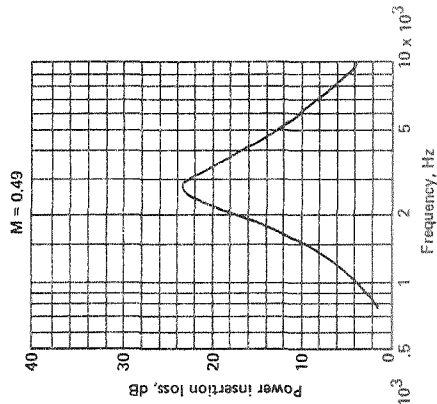
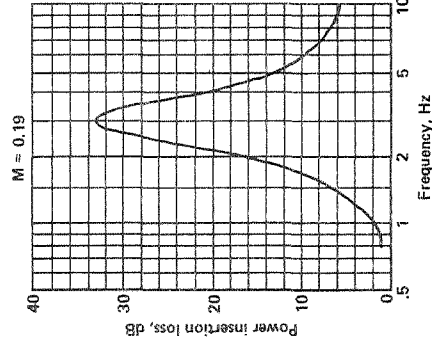
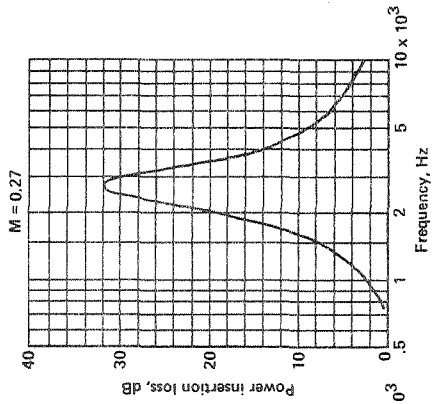


Figure A-210.

Figure A-209.

Lining material Polyimide  
 Flow resistance 18 rayls (cgs)  
 Lining depth 0.5 in.  
 Core type 3/8-in. Hexcel

Duct geometry 4 x 10 in.  
 Walls lined Two/10 in.  
 Lining length 22 in.



Lining material Polyimide  
 Flow resistance 30 rayls (cgs)  
 Lining depth 0.5 in.  
 Core type 3/8-in. Hexcel

Duct geometry 4 x 10 in.  
 Walls lined Two/10 in.  
 Lining length 22 in.

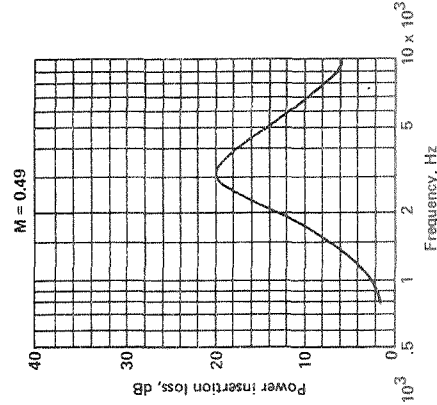
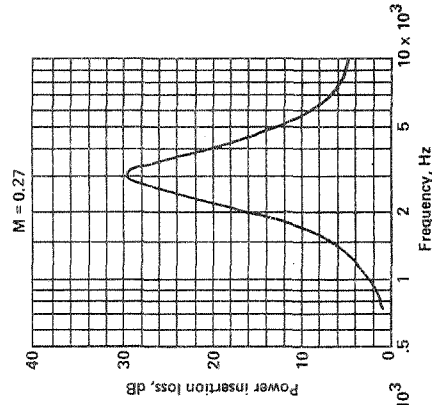
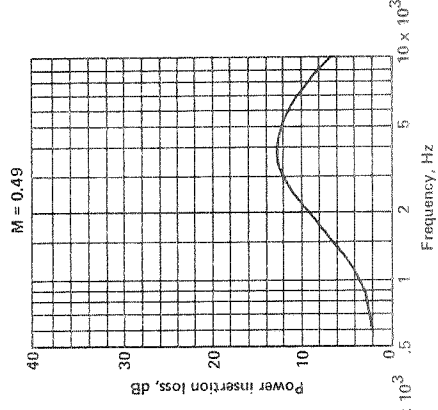
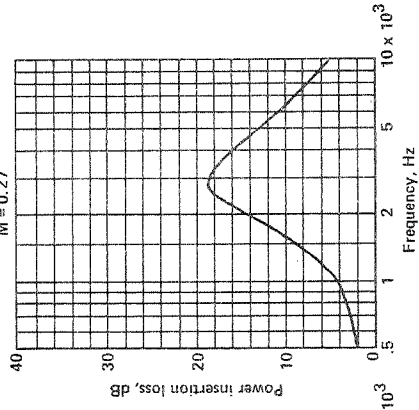


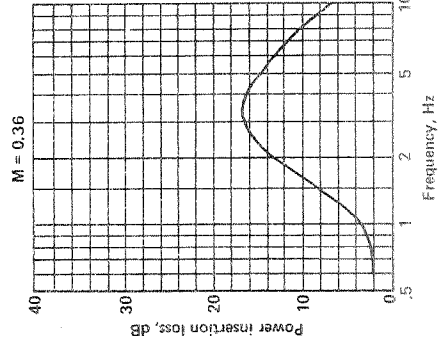
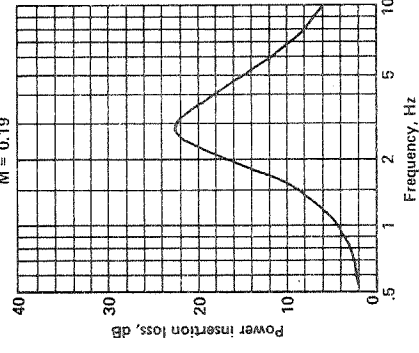
Figure A-211.

Figure A-212.

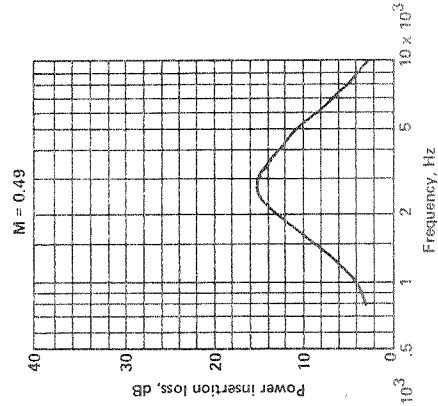
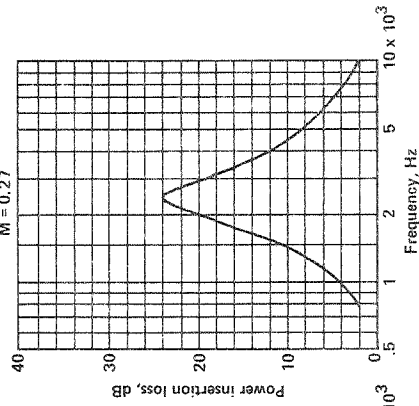
Lining material Polyimide  
 Flow resistance 70 rays/ls. (eqs)  
 Lining depth 0.5 in.  
 Core type 3/8-in. Hexcel



Duct geometry 4 x 10 in.  
 Walls lined Two/10 in.  
 Lining length 22 in.



Lining material Polyimide  
 Flow resistance 50 rays/ls. (eqs)  
 Lining depth 0.5 in.  
 Core type 3/8-in. Hexcel



Duct geometry 4 x 10 in.  
 Walls lined Two/10 in.  
 Lining length 22 in.

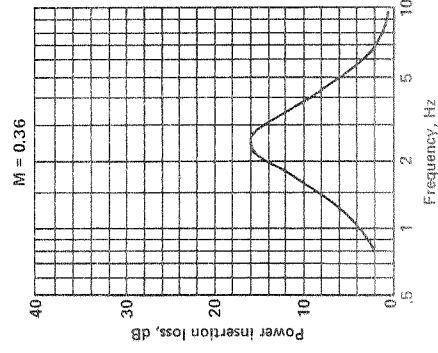
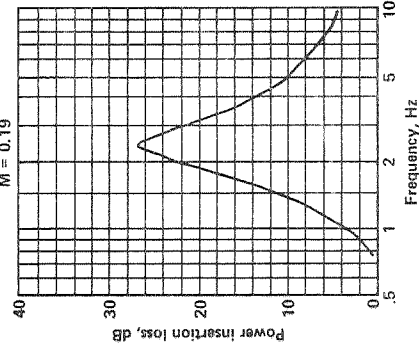


Figure A.214.

Figure A.213.

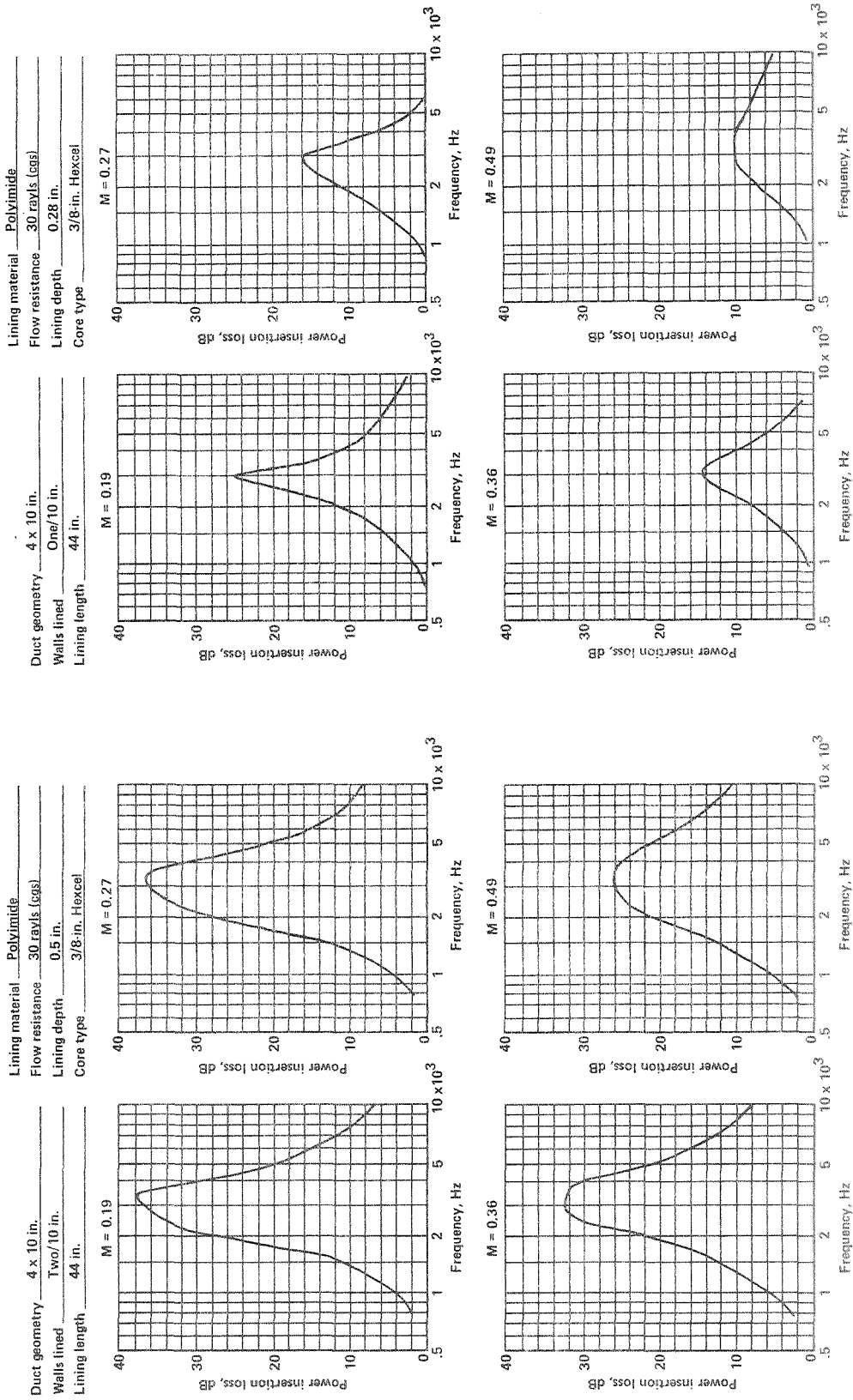
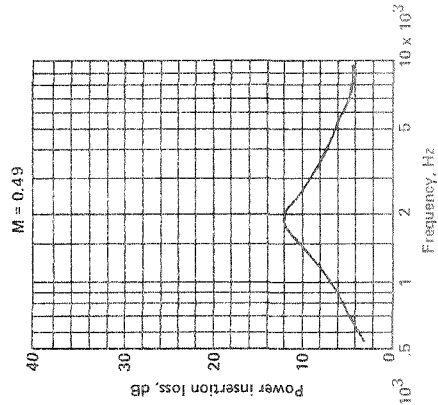
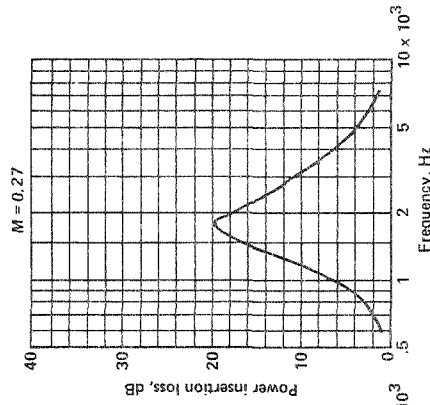


Figure A-215.

Figure A-216.

Lining material Polyimide  
 Flow resistance 30 rays/lcs  
 Lining depth 0.75 in.  
 Core type 3/8-in. Hexcel

Duct geometry 4 x 10 in.  
 Walls lined One/10 in.  
 Lining length 44 in.



Lining material Polyimide  
 Flow resistance 50 rays/lcs  
 Lining depth 1 in.  
 Core type 3/8-in. Hexcel

Duct geometry 4 x 10 in.  
 Walls lined One/10 in.  
 Lining length 44 in.

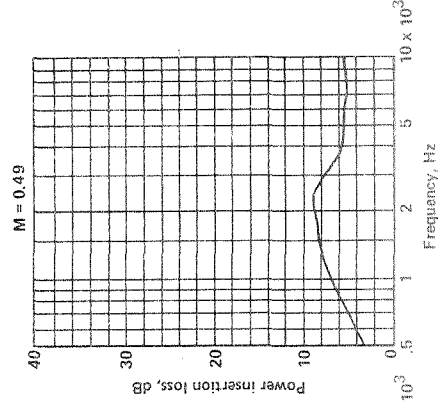
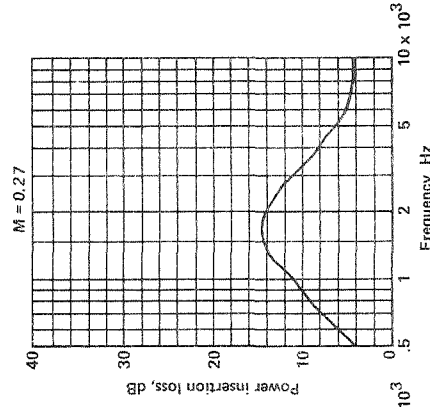


Figure A-217.

Figure A-218.

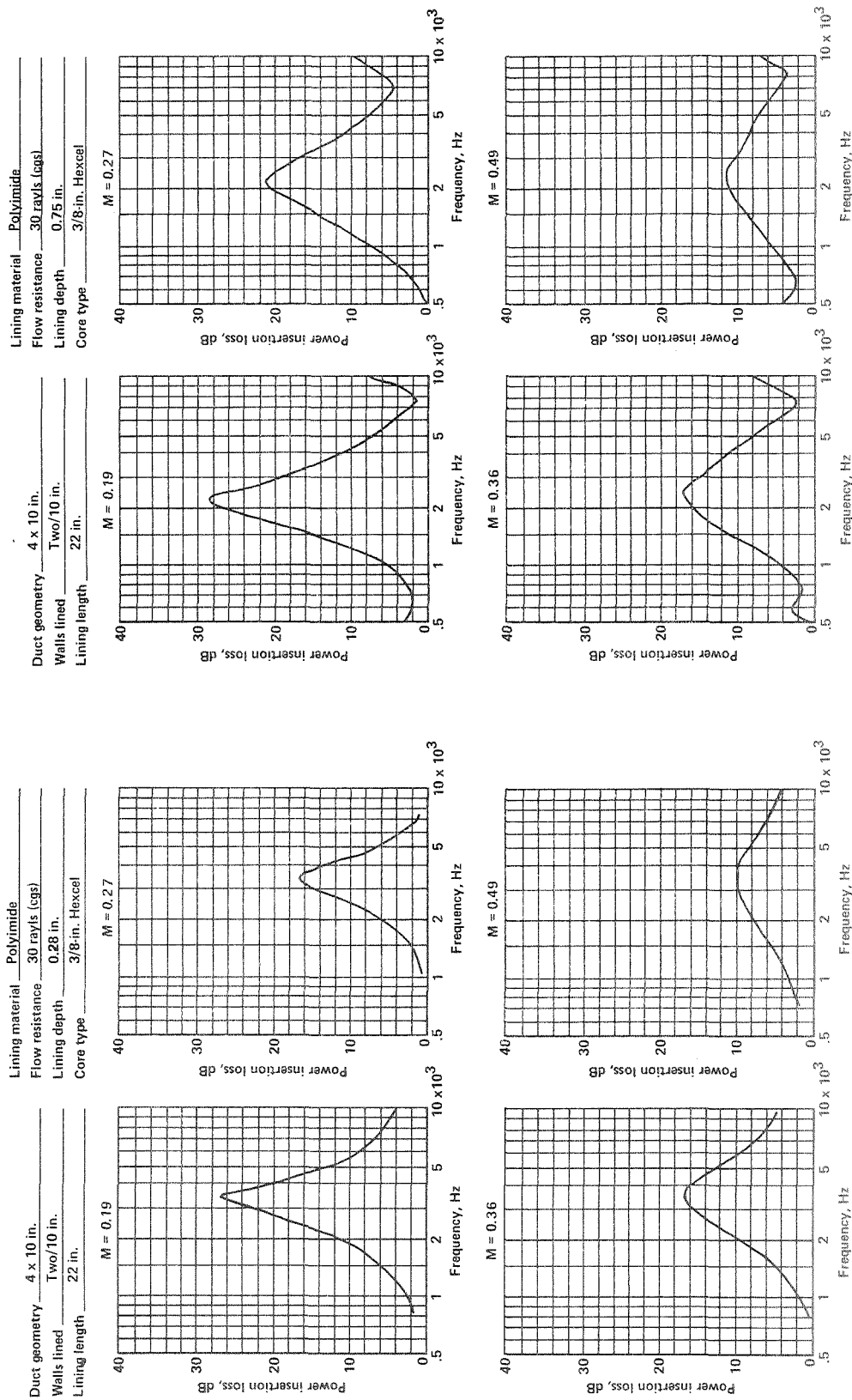


Figure A-219.

Figure A-220.

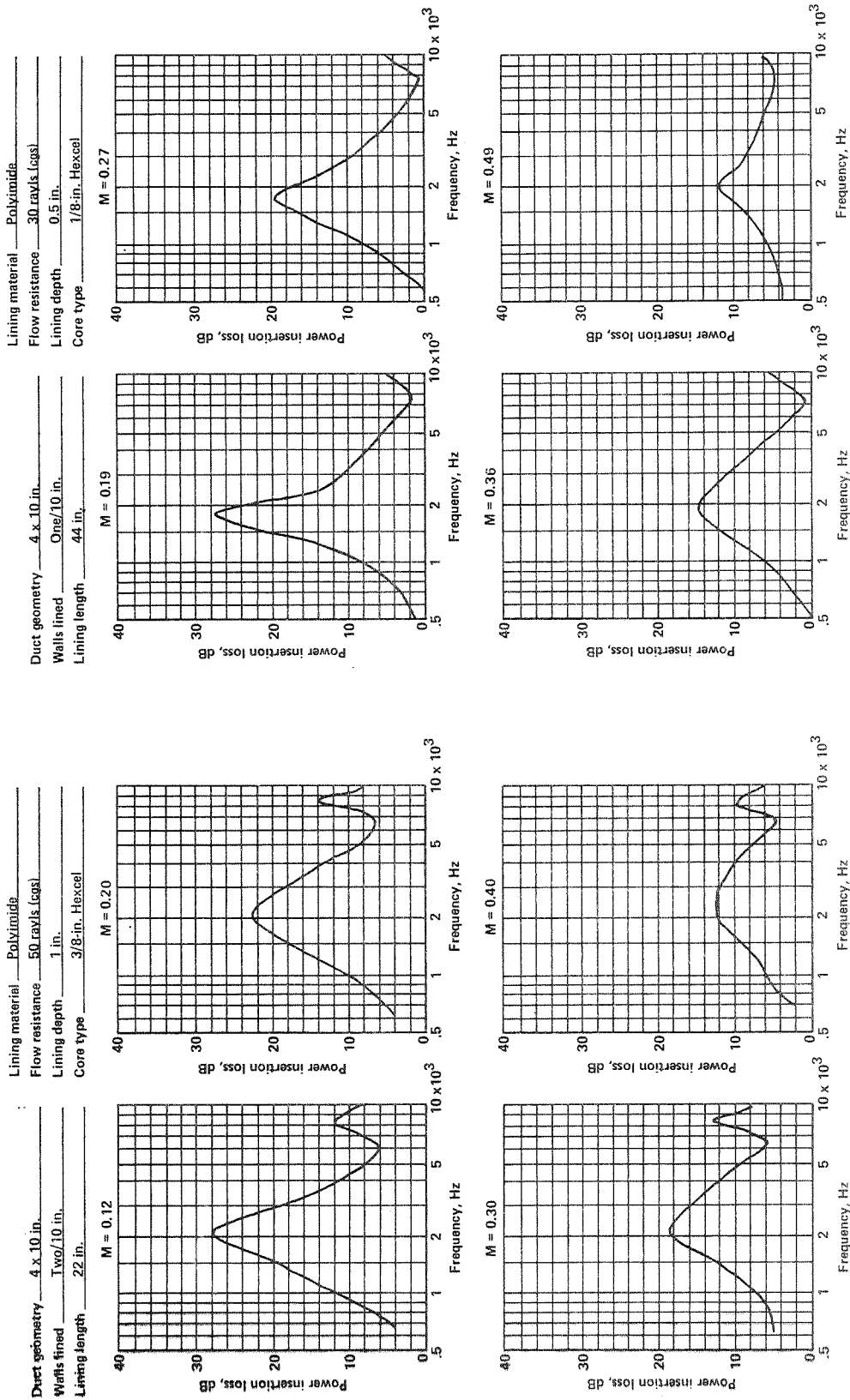


Figure A-222.

Figure A-221.

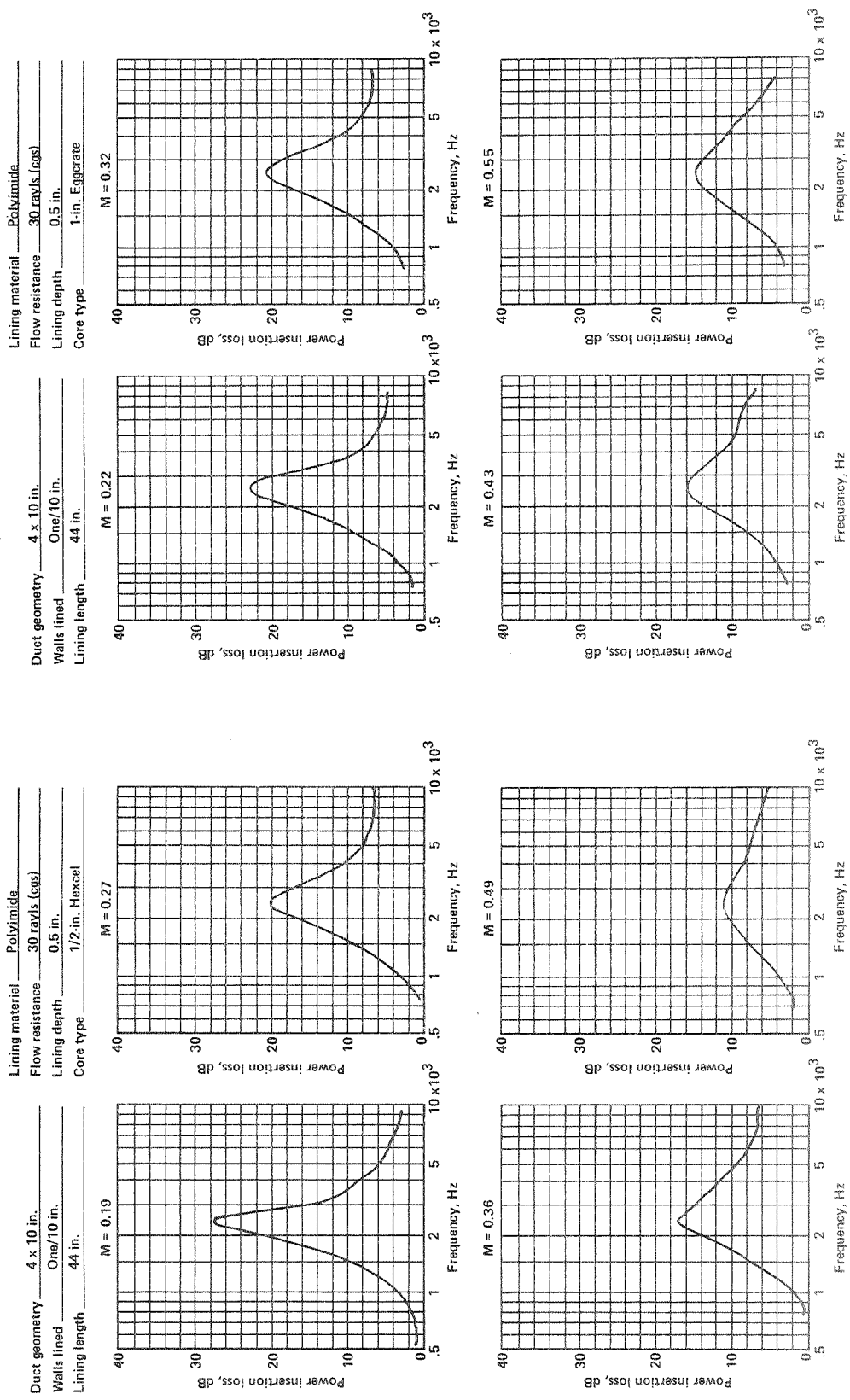


Figure A-224.

Figure A-223.



Lining material Polyimide  
 Flow resistance 30 rayls (cps)  
 Lining depth 0.5 in.  
 Core type 1/2-in. Hexcel

Duct geometry 4 x 10 in.  
 Walls lined Two/10 in.  
 Lining length 22 in.

Lining material Polyimide  
 Flow resistance 30 rayls (cps)  
 Lining depth 0.5 in.  
 Core type 1/8-in. Hexcel

Duct geometry 4 x 10 in.  
 Walls lined Two/10 in.  
 Lining length 22 in.

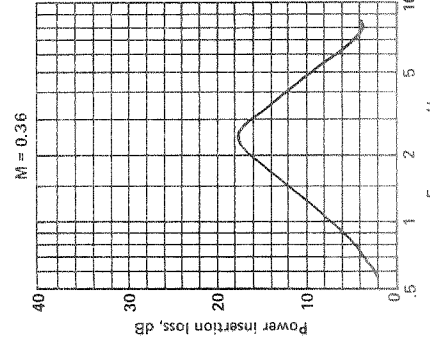
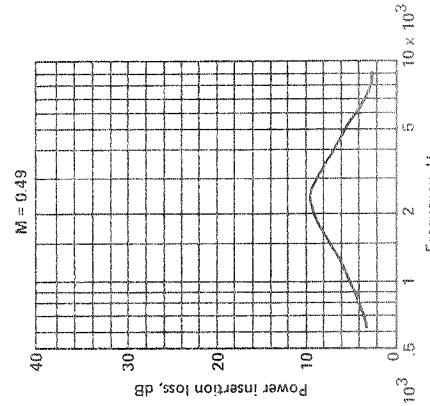
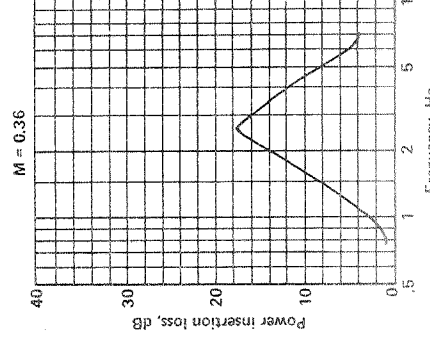
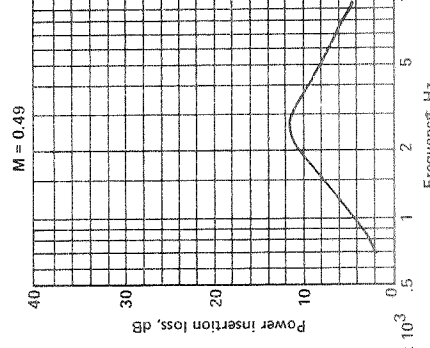
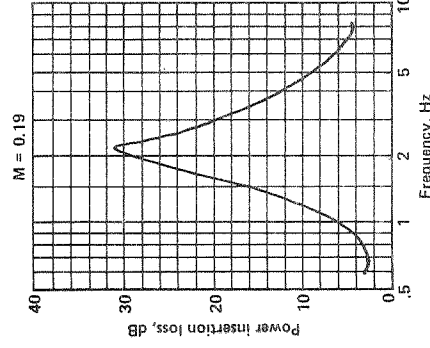
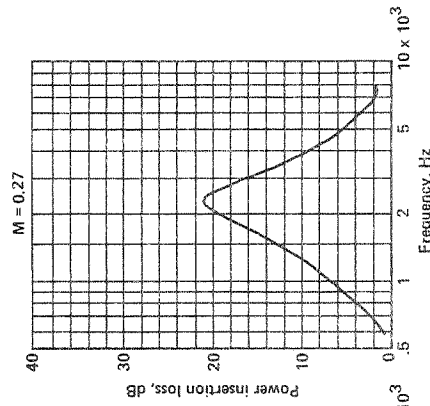
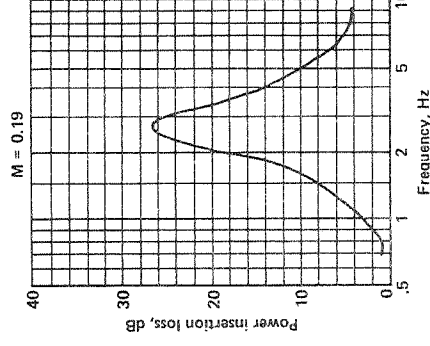
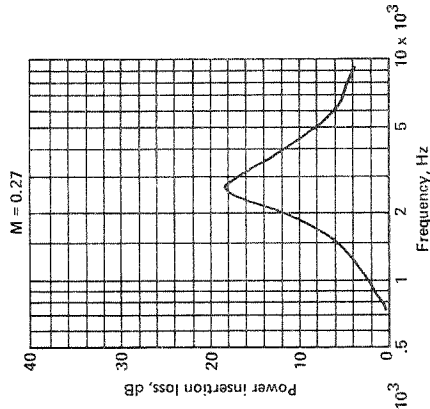


Figure A-226.

Figure A-225.

Lining material Polyimide  
 Flow resistance 30 rayls (cgs)  
 Lining depth 0.5 in.  
 Core type 1-in. Eggcrate

Duct geometry 4 x 10 in.  
 Walls lined Two/10 in.  
 Lining length 44 in.

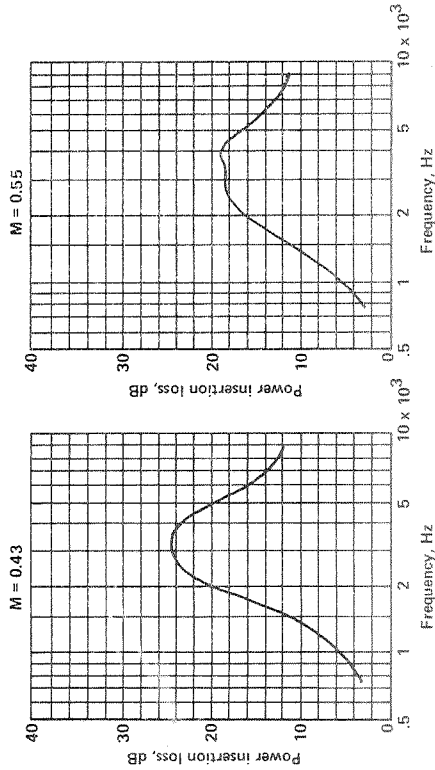
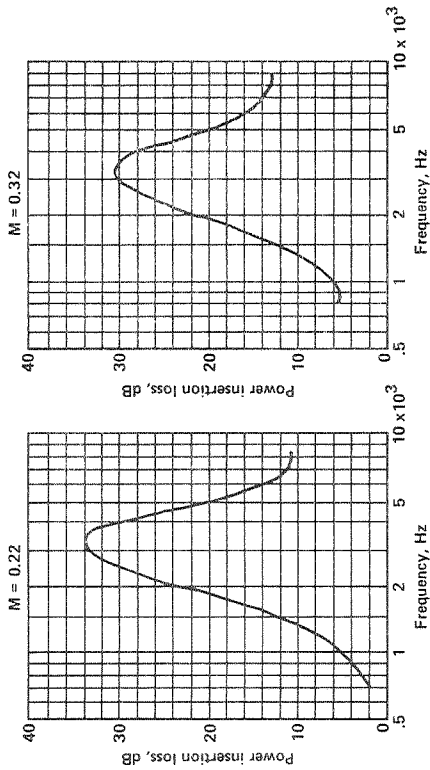


Figure A-227.

Duct geometry 4 x 10 in.  
 Walls lined One/10 in.  
 Lining length 44 in.

Lining material Woven metal fiber  
 Flow resistance 30 rayls (cgs)  
 Lining depth 0.5 in.  
 Core type 3/8-in. Hexcel

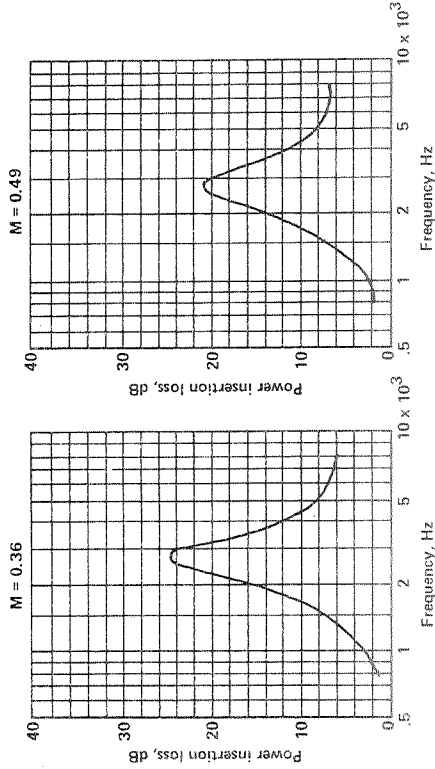
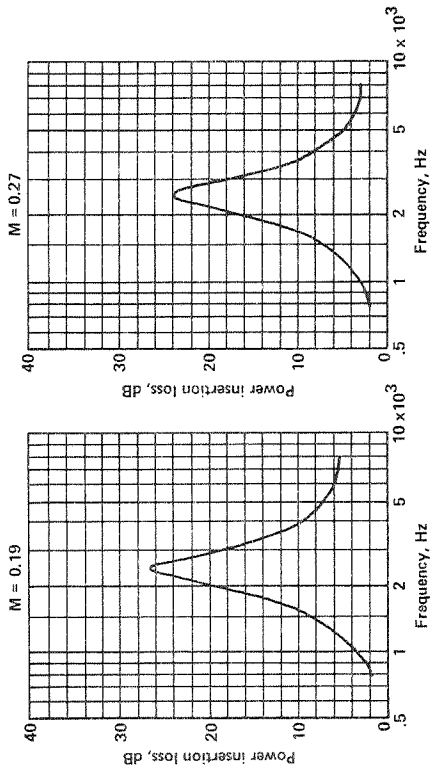
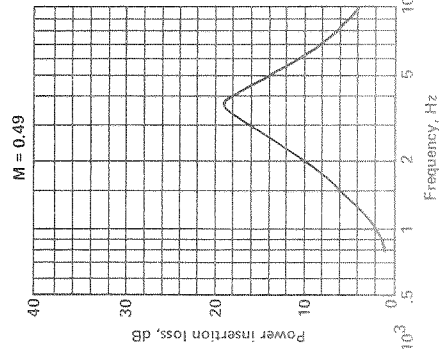
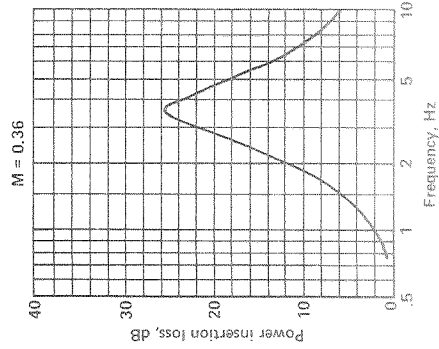
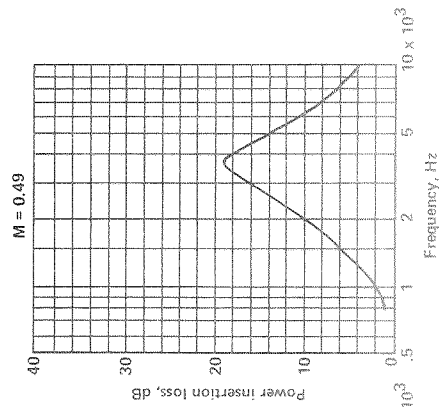
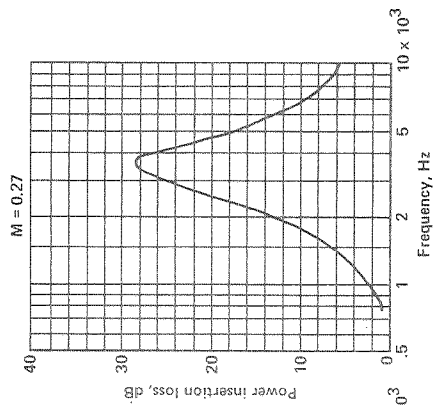


Figure A-228.

Lining material Woven metal fiber  
 Flow resistance 30 rays/ft (logs)  
 Lining depth 0.5 in.  
 Core type 3/8-in. Hexcel

Duct geometry 4 x 10 in.  
 Walls lined Two/10 in.  
 Lining length 22 in.



Duct geometry 4 x 10 in.  
 Walls lined One/10 in.  
 Lining length 44 in.

Lining material Metallic felt  
 Flow resistance 30 rays/ft (logs)  
 Lining depth 0.5 in.  
 Core type 3/8-in. Hexcel

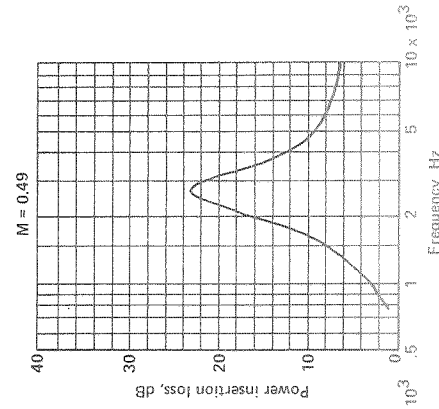
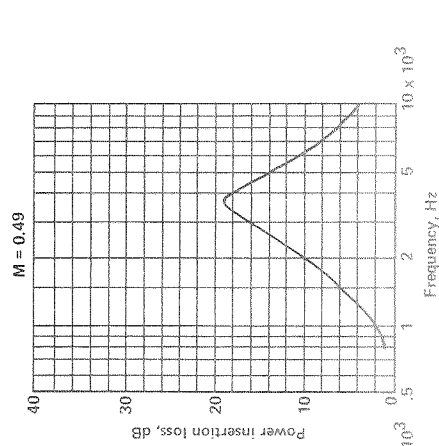
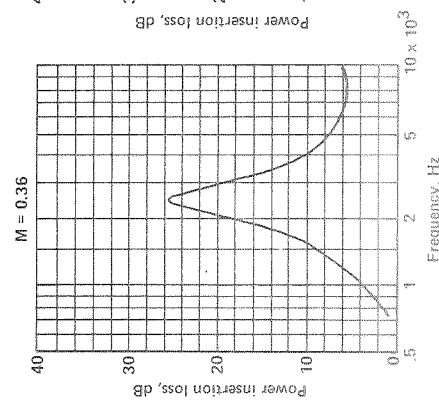
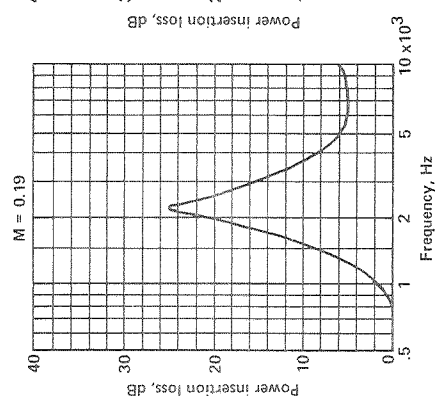


Figure A-229.

Figure A-230.

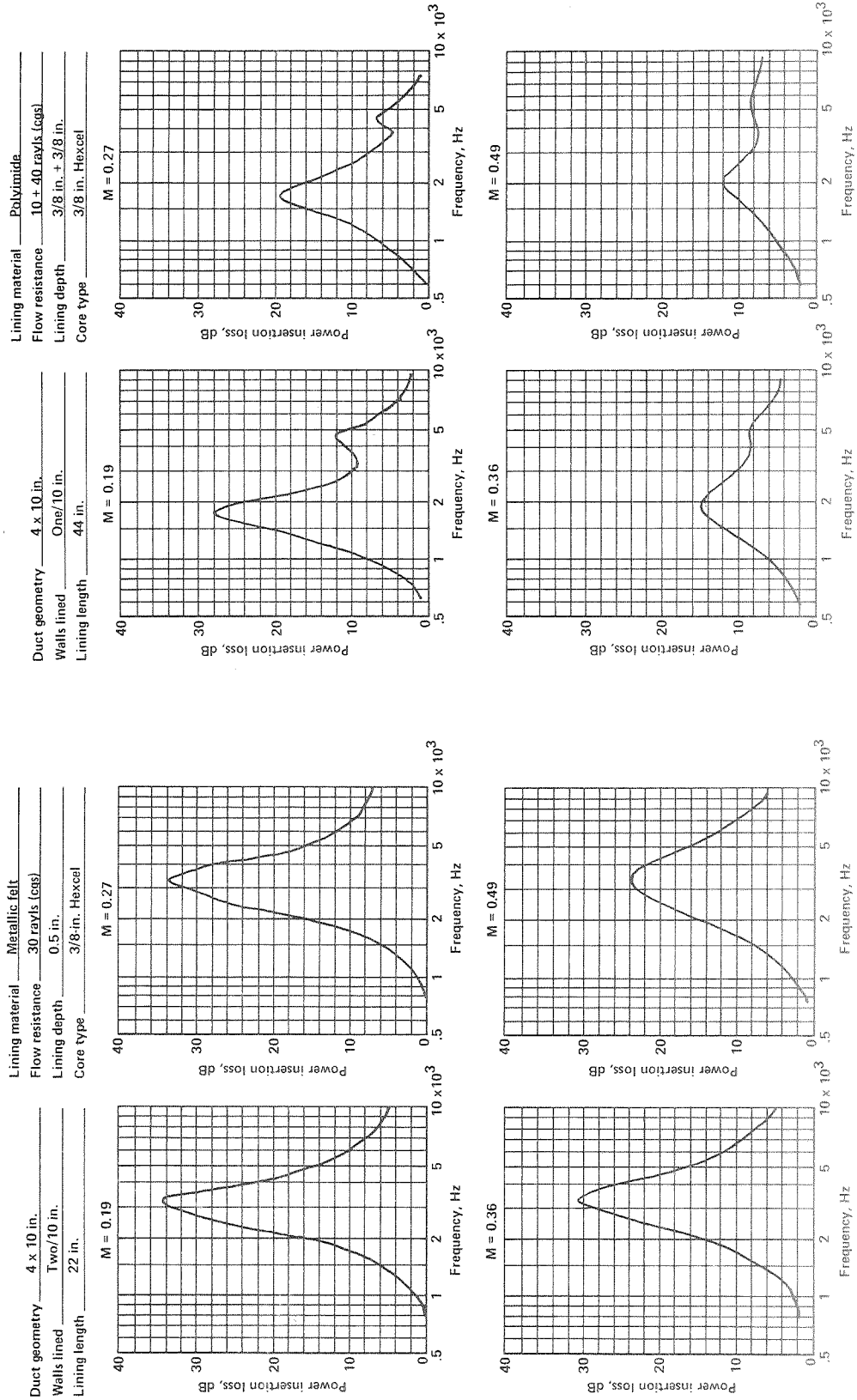
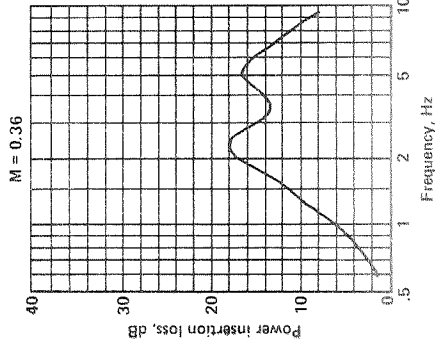
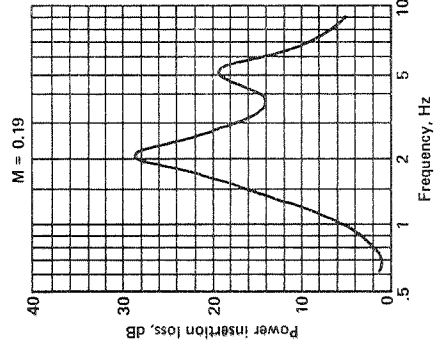
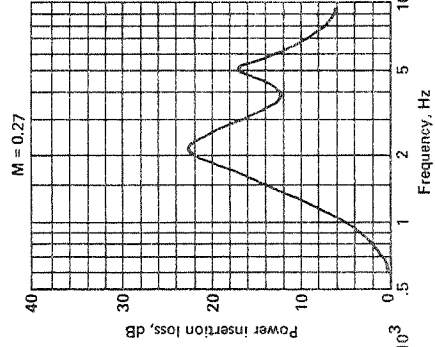


Figure A-232.

Figure A-231.

Lining material Polyimide  
 Flow resistance 10 + 40 rays (cgs)  
 Lining depth 3/8 in. + 3/8 in.  
 Core type 3/8 in. Hexcel

Duct geometry 4 x 10 in.  
 Walls lined Two/10 in.  
 Lining length 22 in.



Lining material Polyimide  
 Flow resistance 10 + 40 rays (cgs)  
 Lining depth 1/2 in. + 1/2 in.  
 Core type 3/8 in. Hexcel

Duct geometry 4 x 10 in.  
 Walls lined One/10 in.  
 Lining length 44 in.

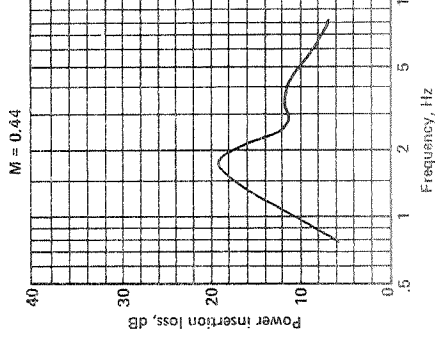
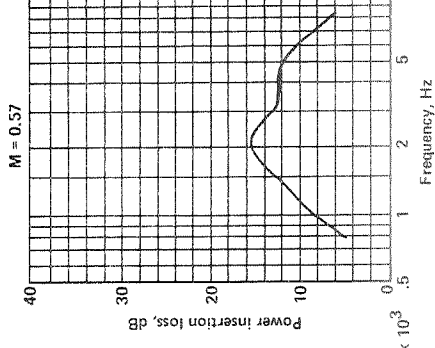
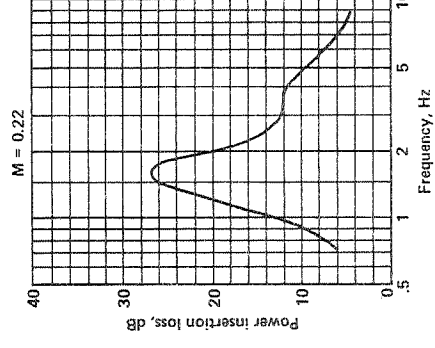
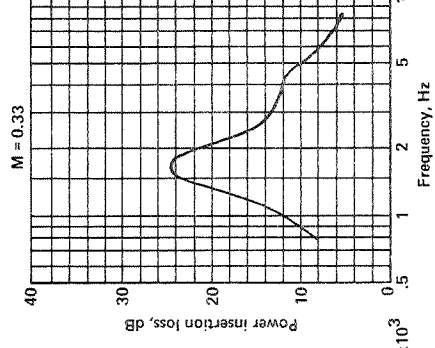


Figure A-234.

Figure A-233.

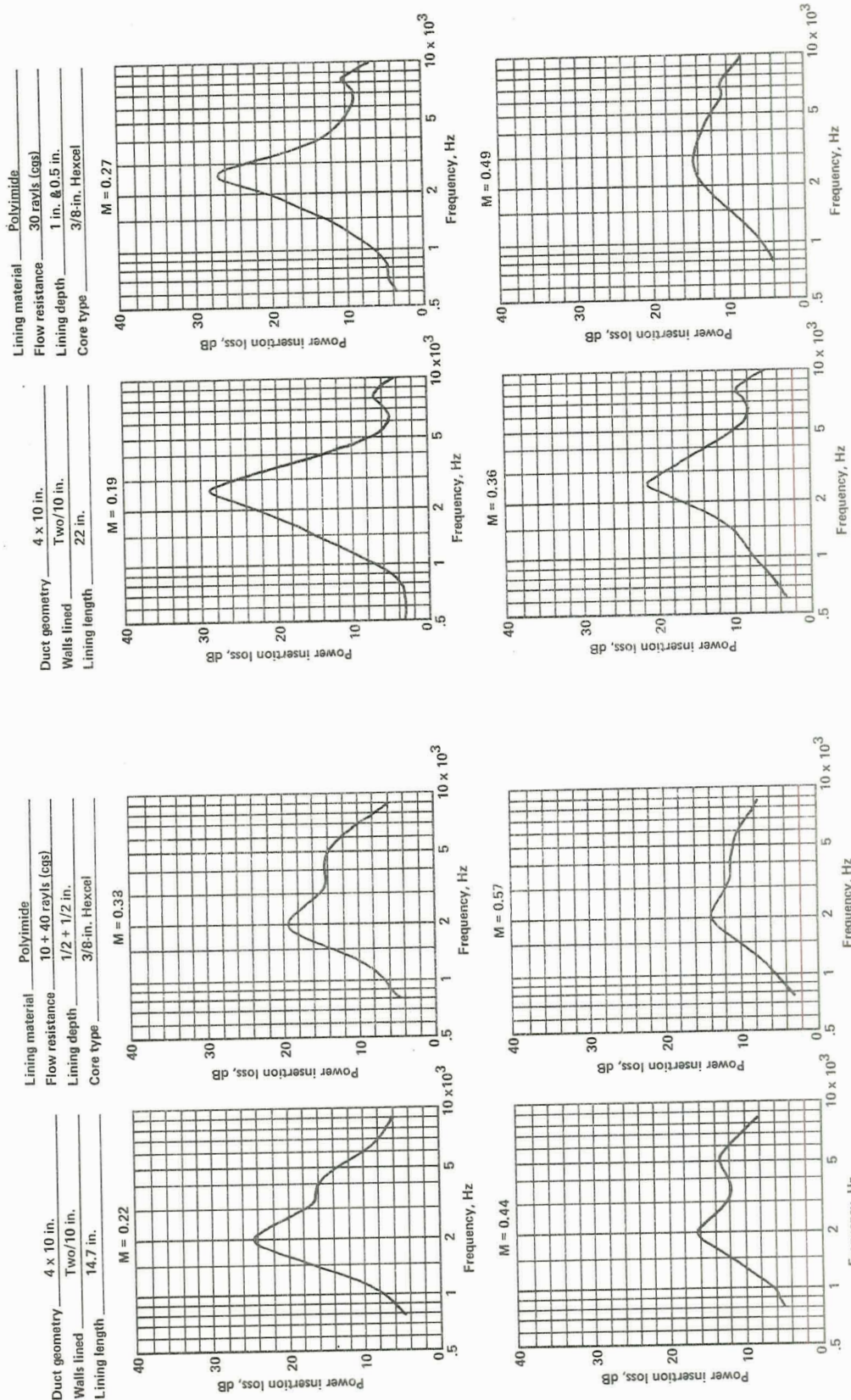
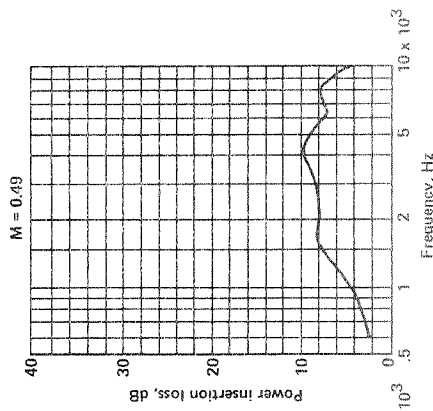
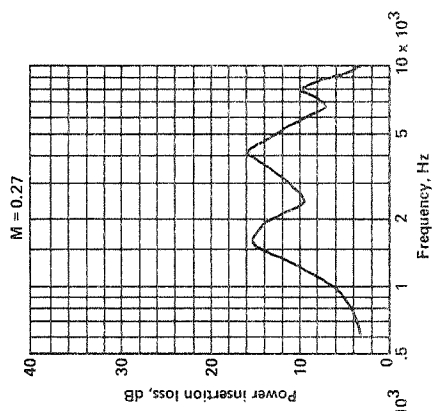


Figure A-236.

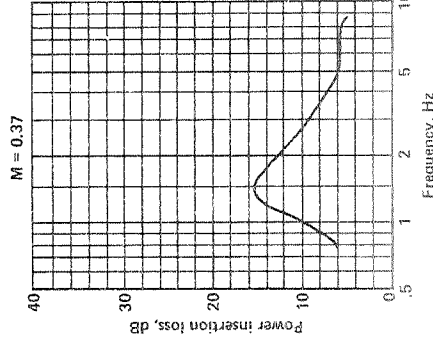
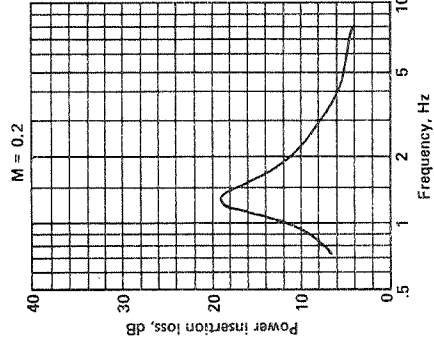
Figure A-235.

Lining material Polyimide  
 Flow resistance 30 rays (cgs)  
 Lining depth 1.0 in. & .28 in.  
 Core type 3/8-Hexcel

Duct geometry 4 x 10 in.  
 Walls lined Two/10 in.  
 Lining length 22 in.



Duct geometry 6 x 7 in.  
 Walls lined One/7 in.  
 Lining length 44 in.



Lining material Polyimide  
 Flow resistance 10/40 rays (cgs)  
 Lining depth 1/2 in. + 1/2 in.  
 Core type 3/8-in. Hexcel

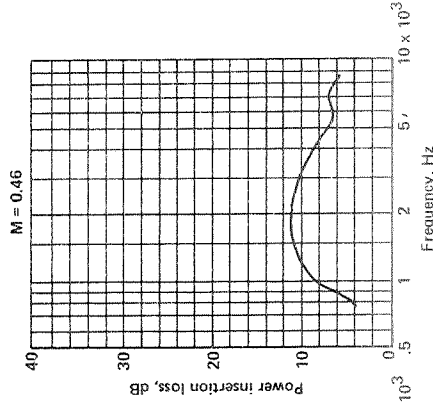
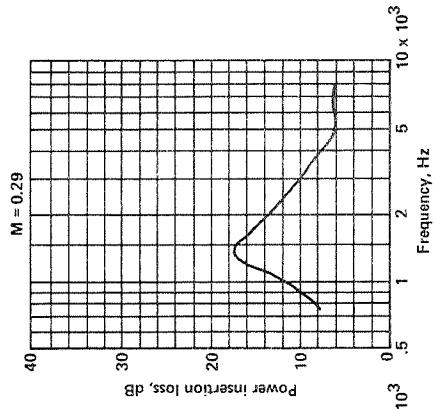


Figure A-237.

Figure A-238.

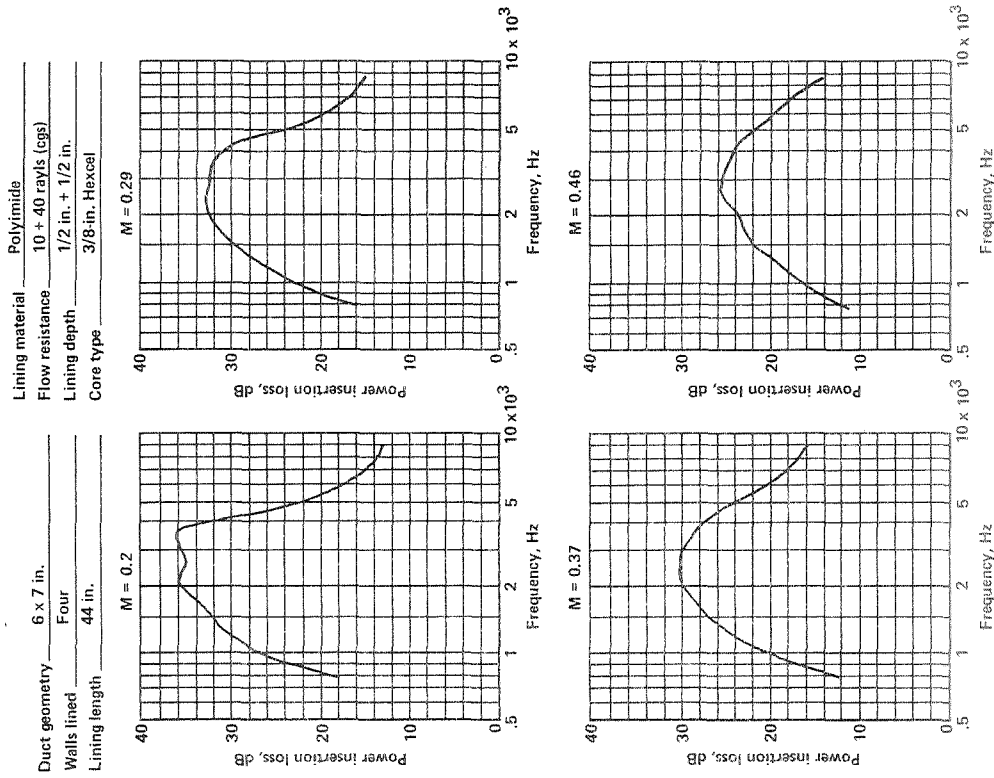


Figure A-240.

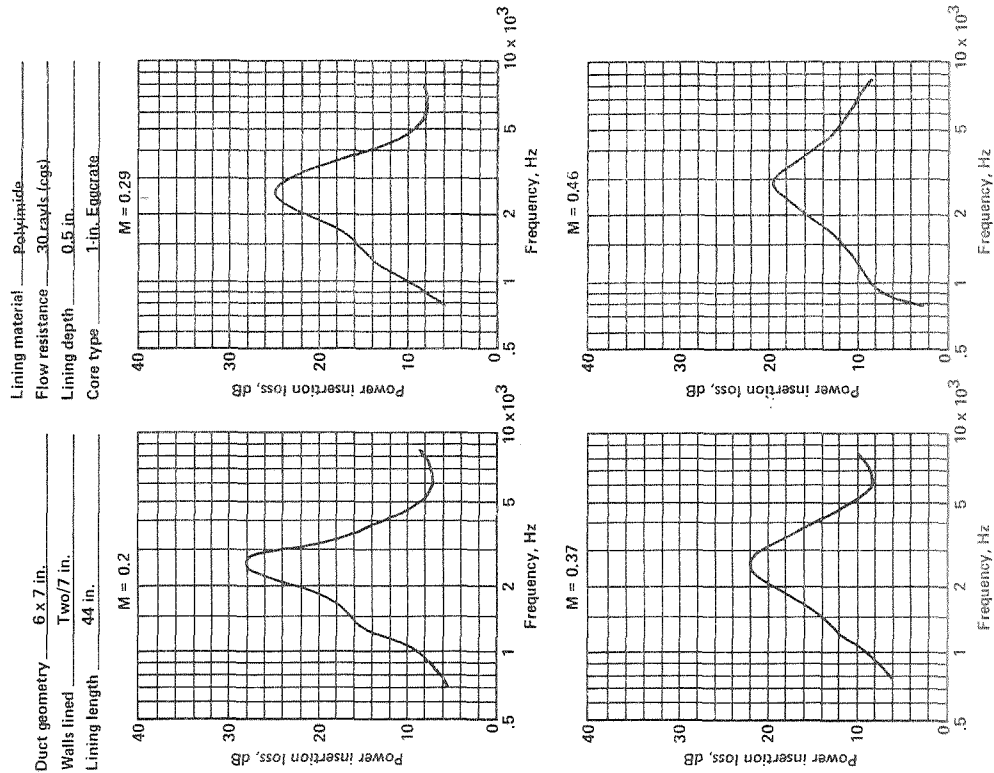


Figure A-239.



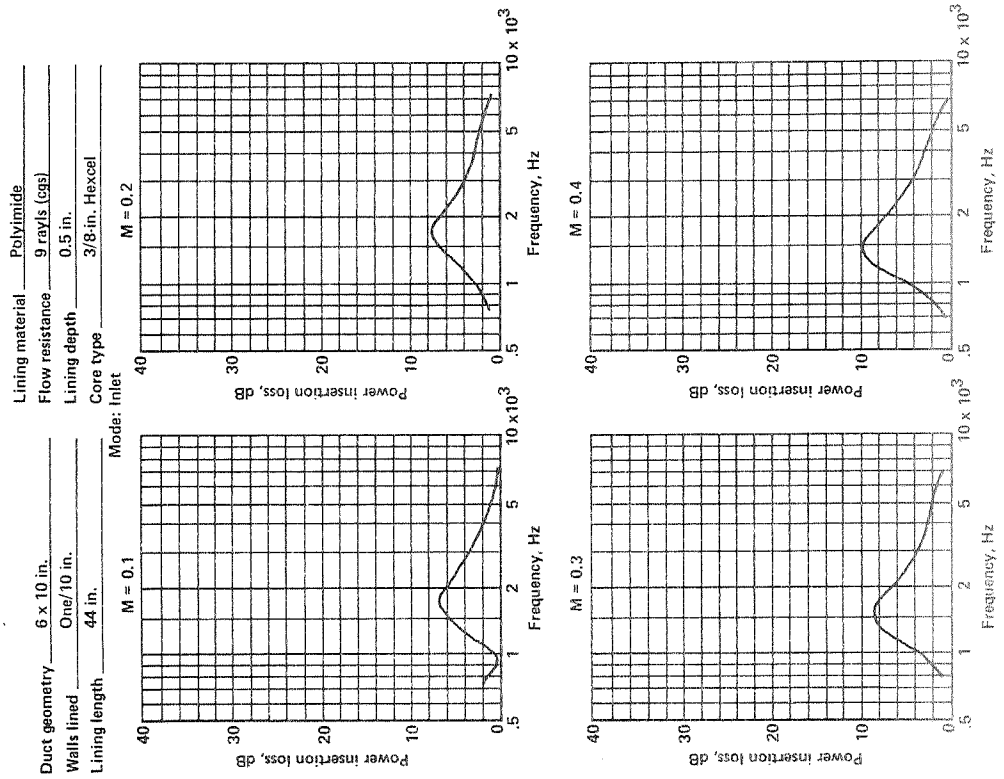


Figure A-242.

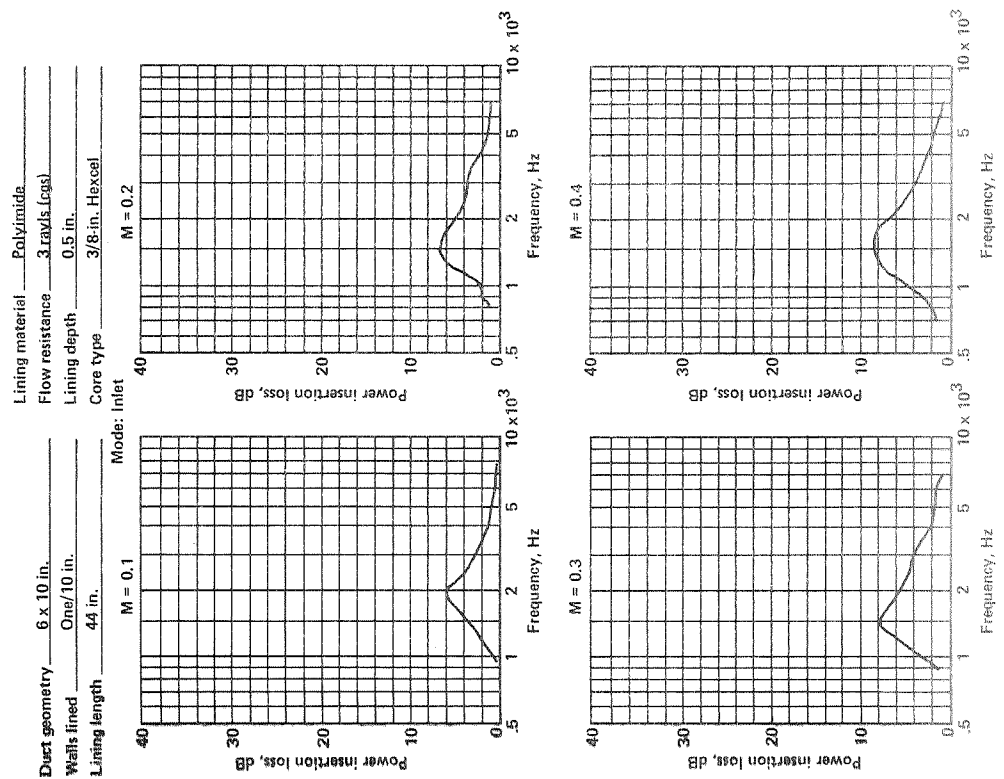


Figure A-241.

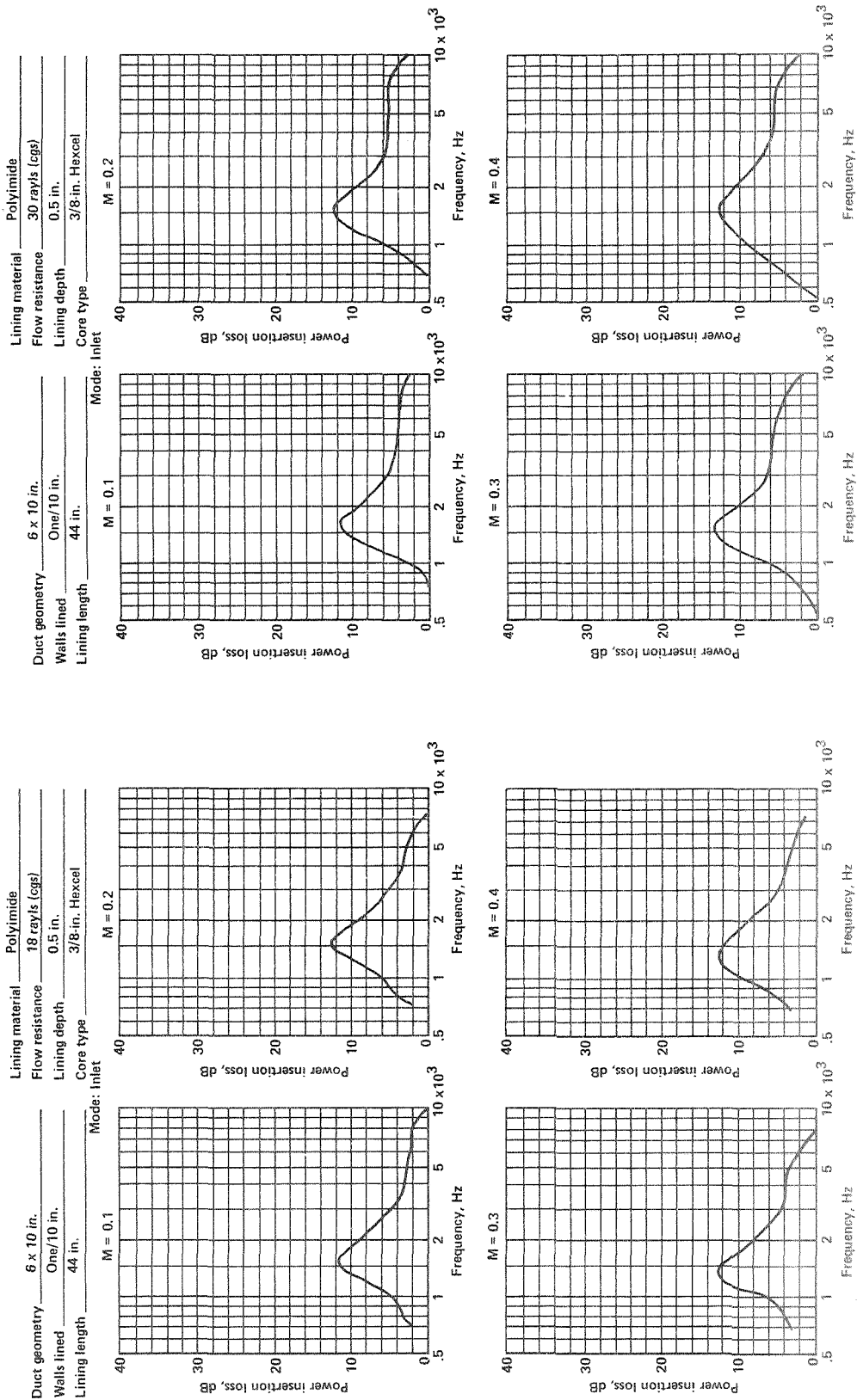


Figure A-243.

Figure A-244.

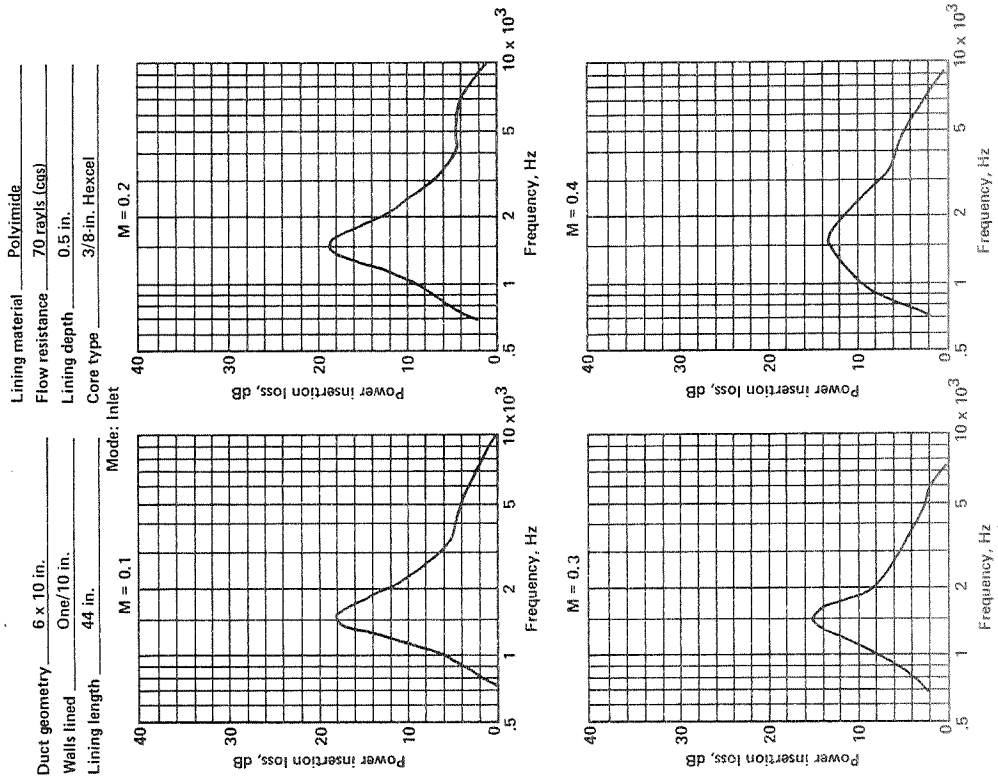


Figure A-246.

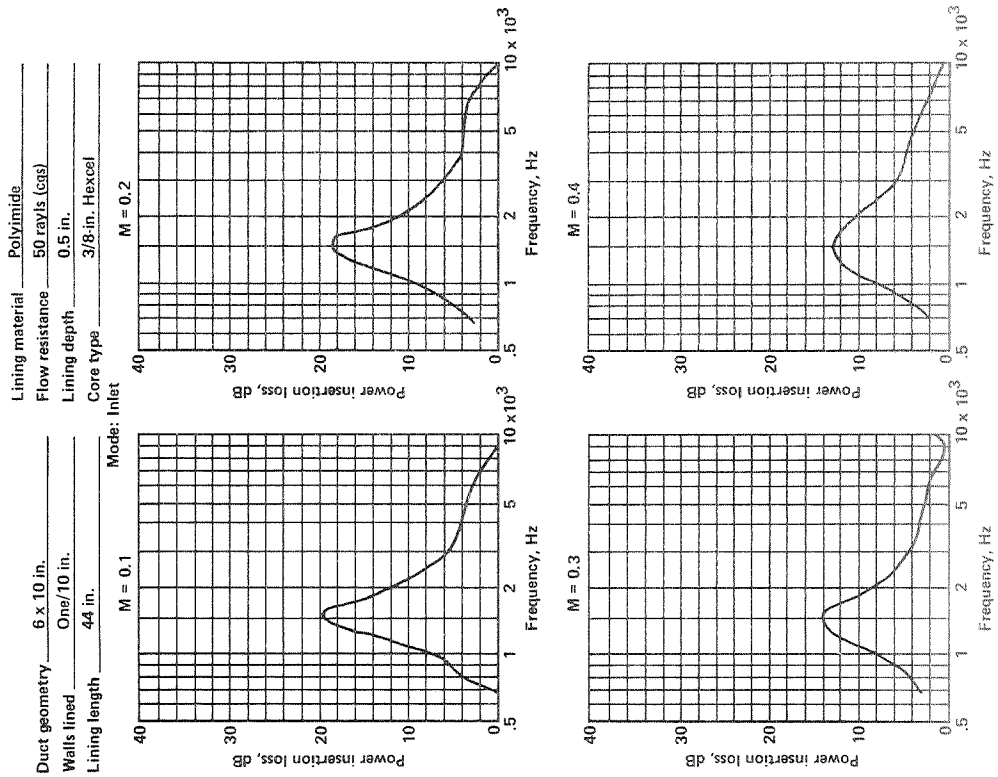


Figure A-245.

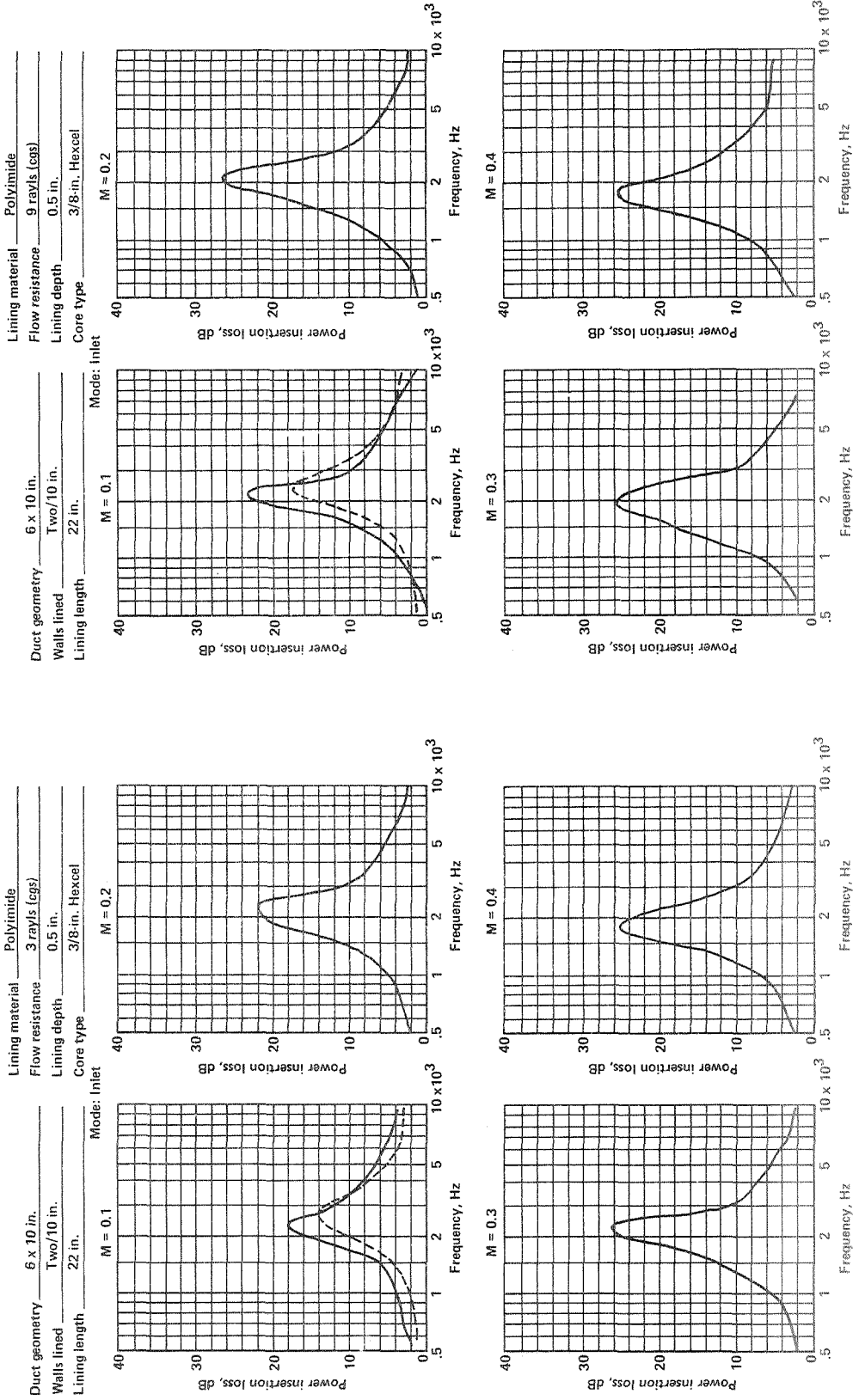


Figure A-247.

Figure A-248.

Lining material Polyimide  
 Flow resistance 18 rayls (cgs)  
 Lining depth 0.5 in.  
 Core type 3/8-in. Hexcel

Lining material Polyimide  
 Flow resistance 30 rayls (cgs)  
 Lining depth 0.5 in.  
 Core type 3/8-in. Hexcel

Duct geometry 6 x 10 in.  
 Walls lined Two/10 in.  
 Lining length 22 in.

Duct geometry 6 x 10 in.  
 Walls lined Two/10 in.  
 Lining length 22 in.

Mode: Inlet

Mode: Inlet

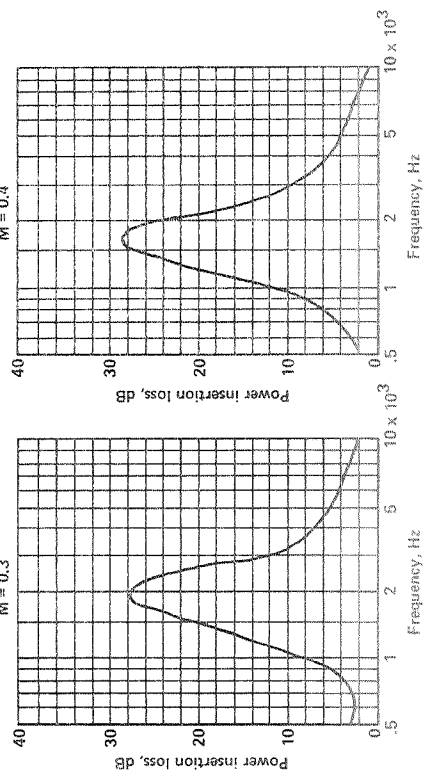
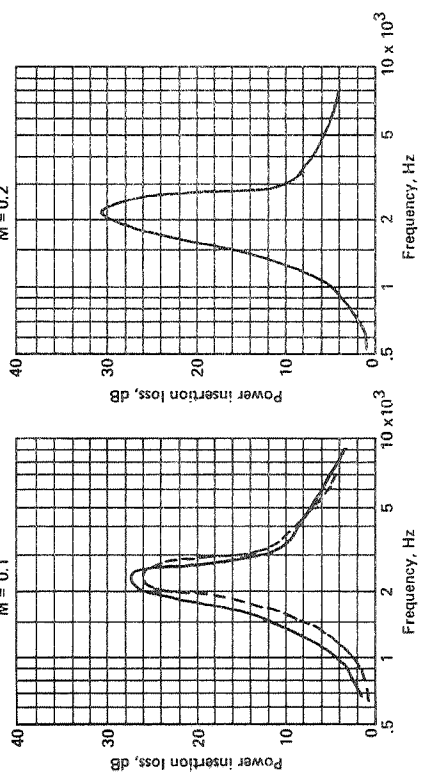


Figure A-249.

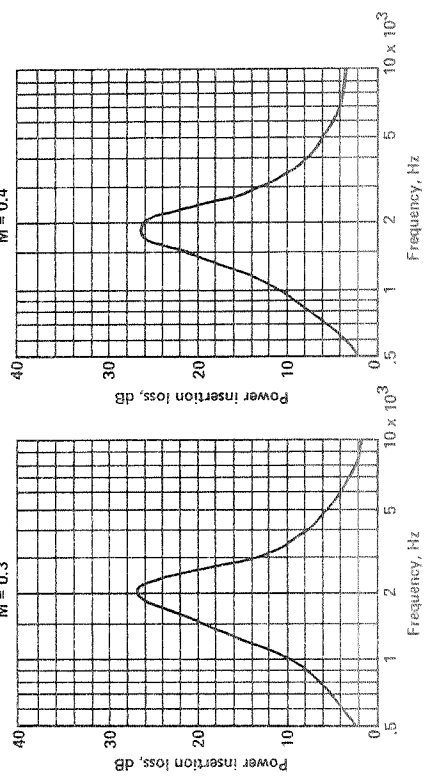
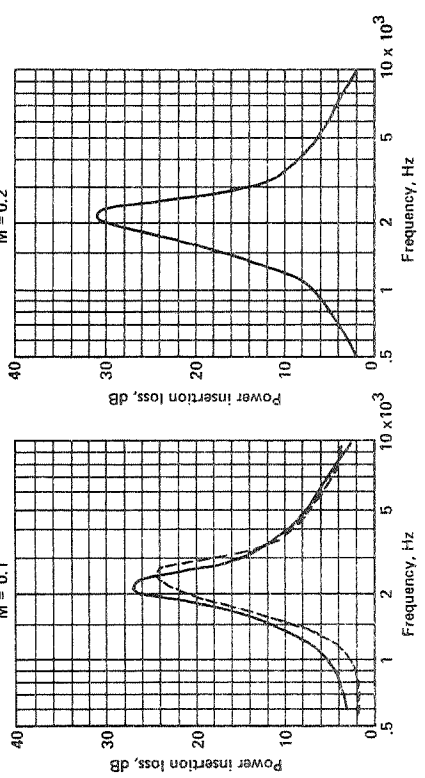


Figure A-250.

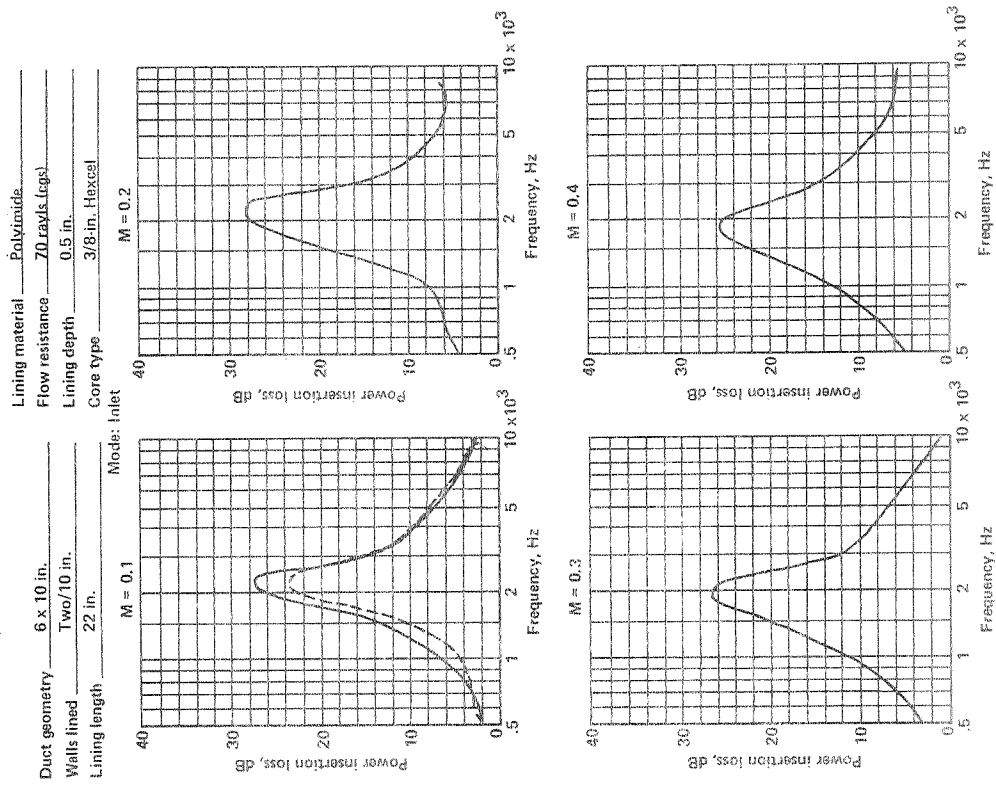


Figure A-252.

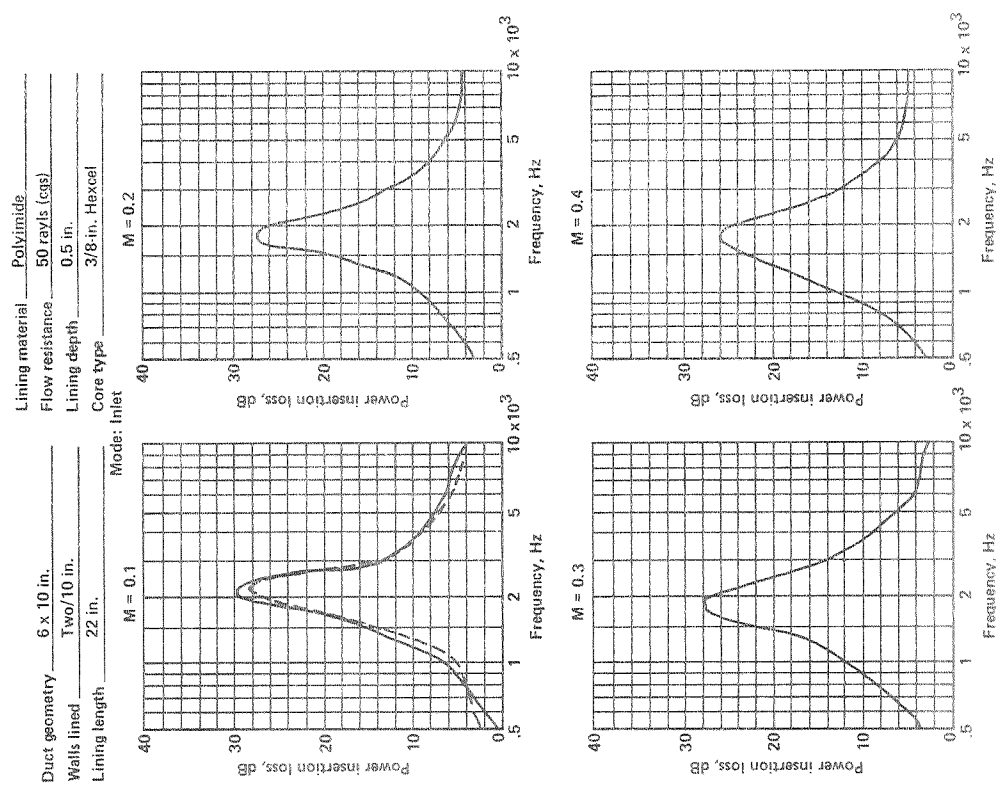


Figure A-251.

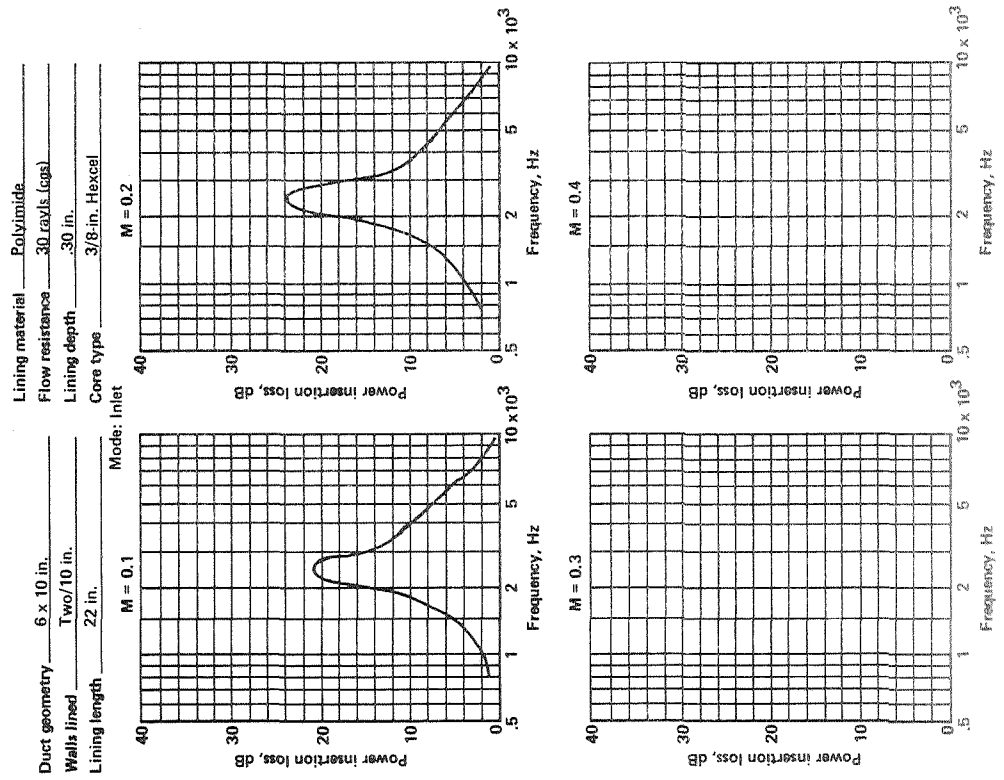


Figure A-253.

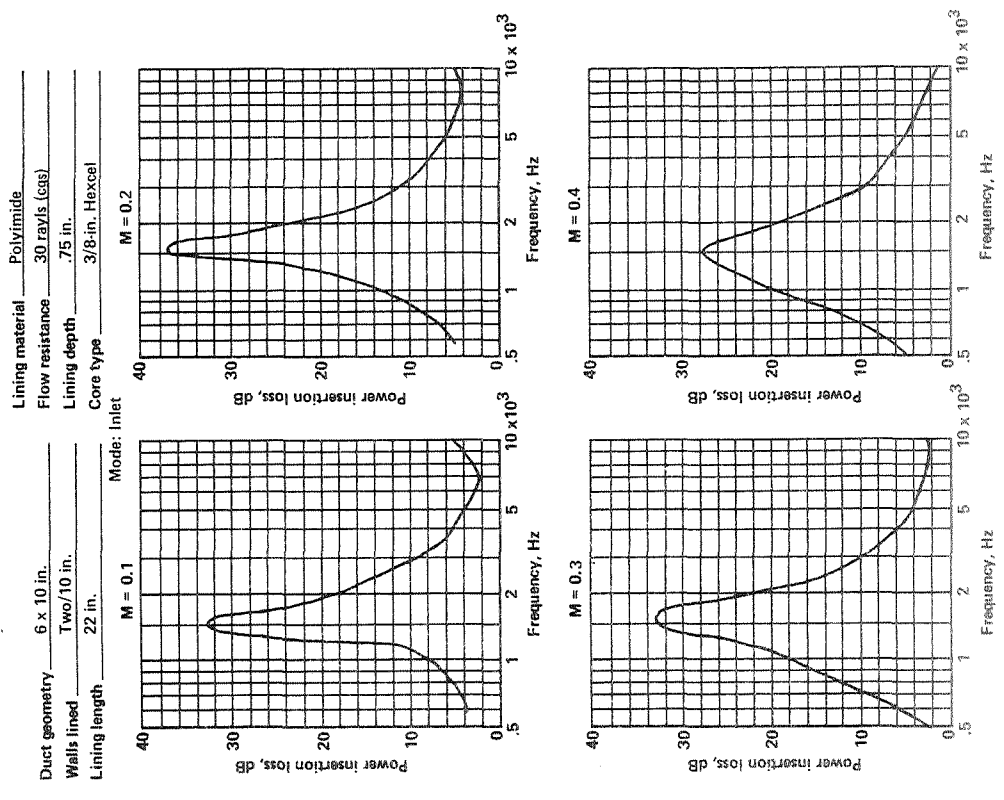


Figure A-254.

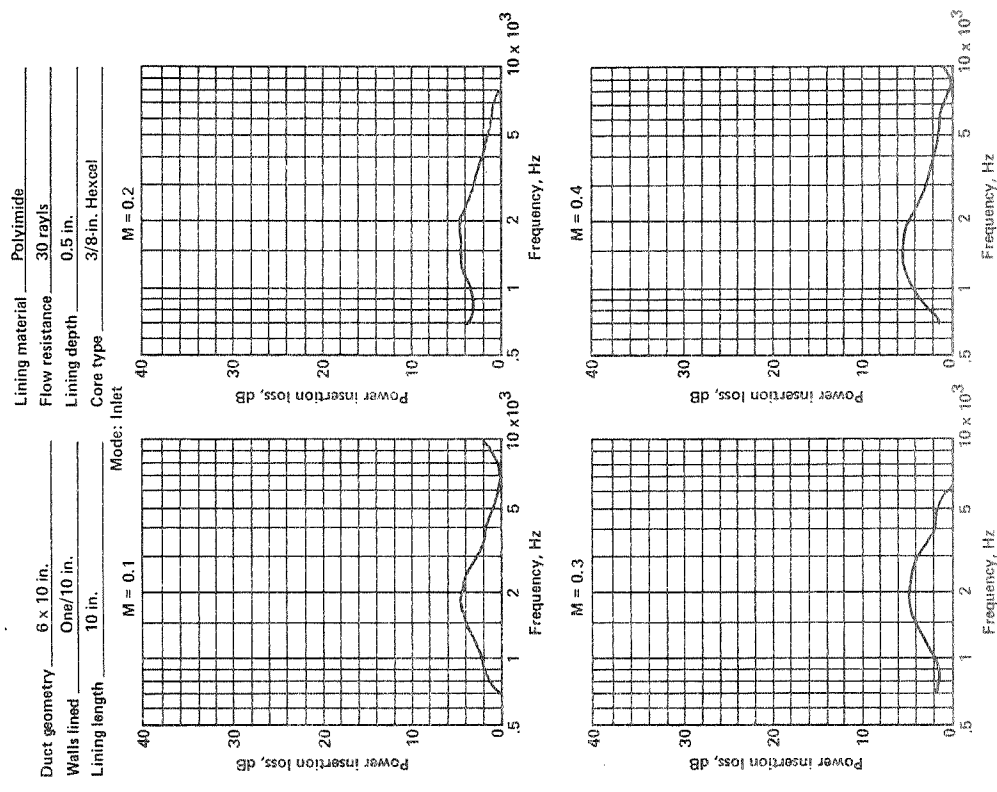


Figure A-256.

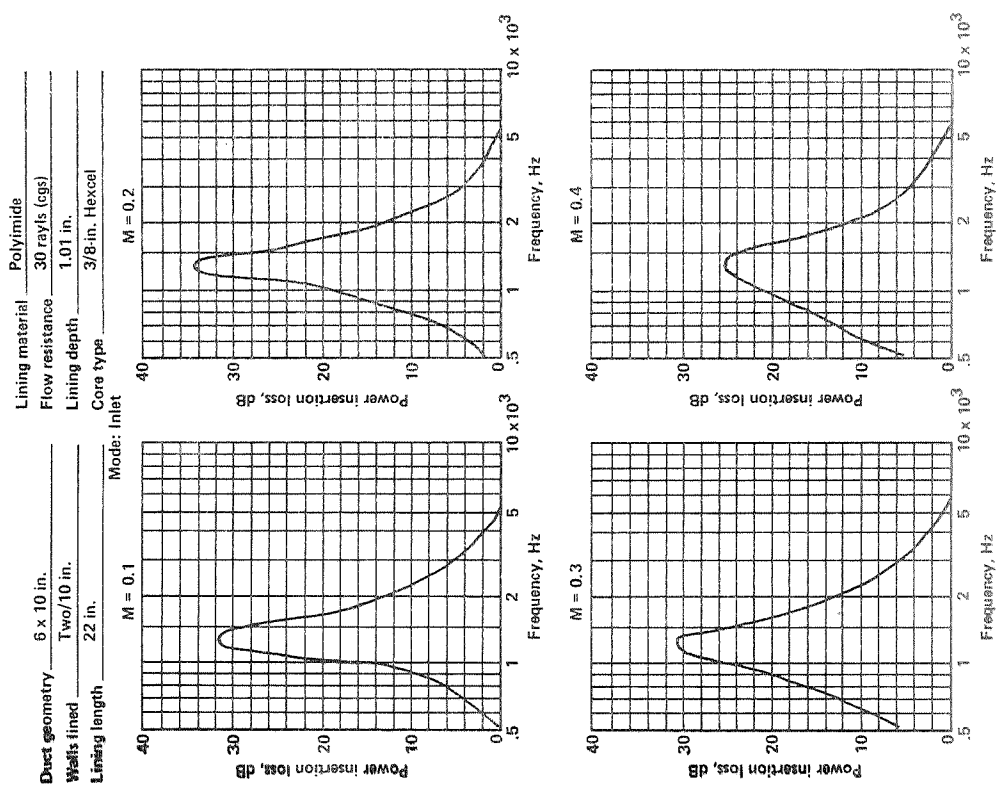


Figure A-255.



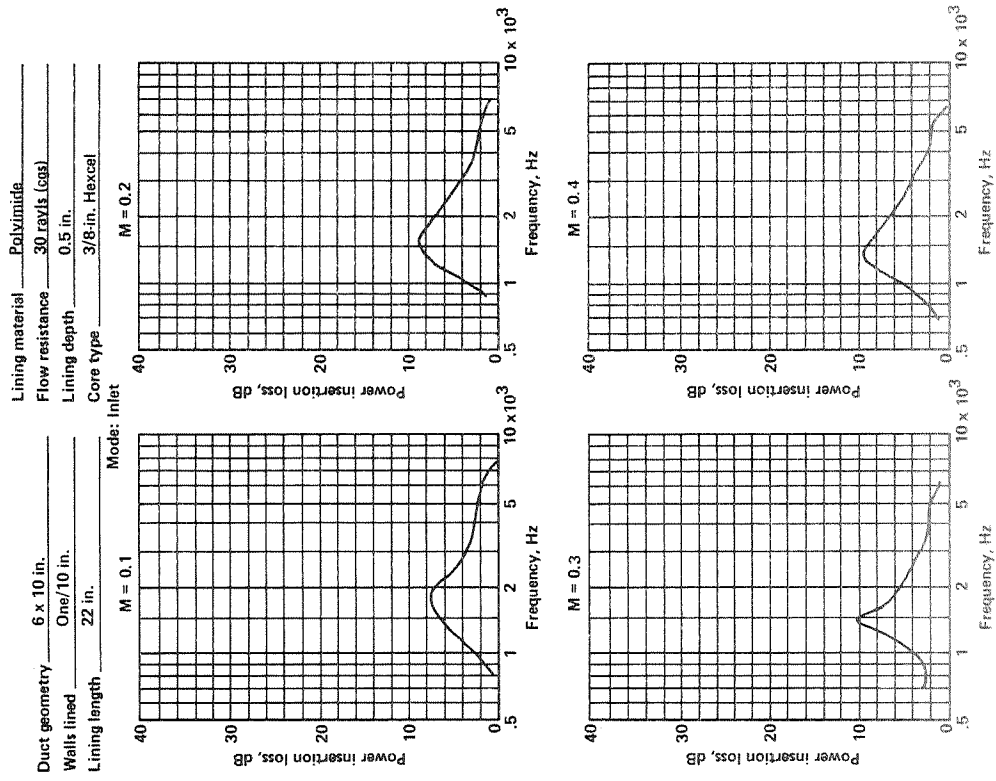


Figure A-257.

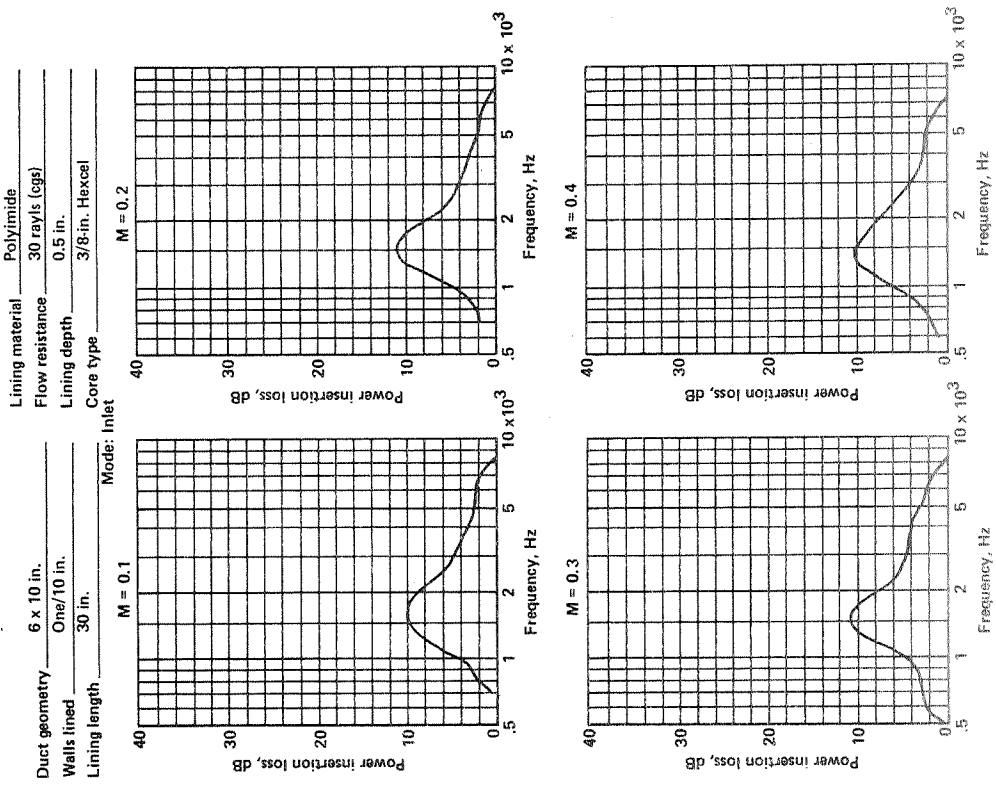


Figure A-258.

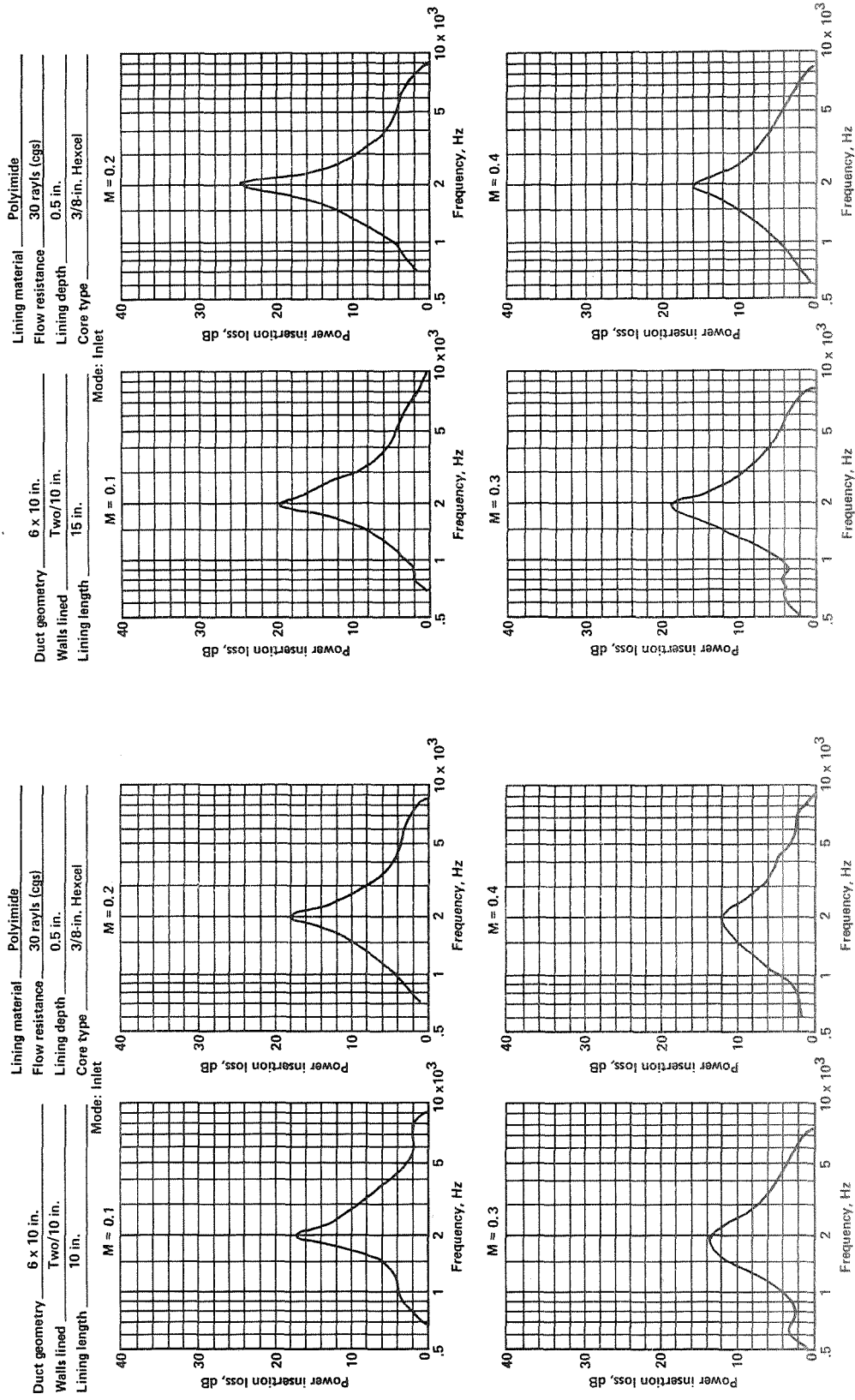
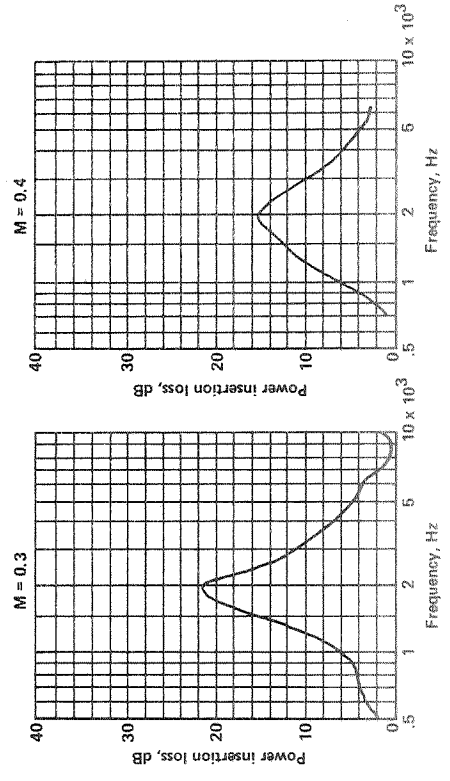
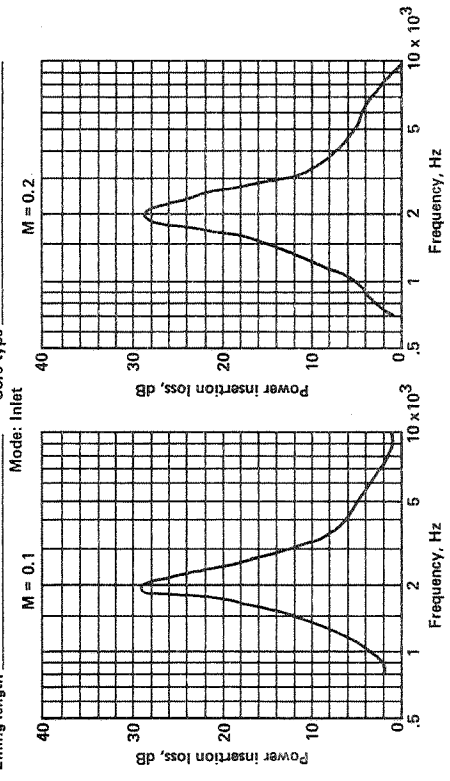


Figure A-260.

Figure A-259.

Lining material Polyimide  
 Flow resistance 30 rayls (cgs)  
 Lining depth 0.5 in.  
 Core type 3/8-in. Hexcel

Duct geometry 6 x 10 in.  
 Walls lined Two/10 in.  
 Lining length 30 in.



Lining material Polyimide  
 Flow resistance 30 rayls (cgs)  
 Lining depth 0.5 in.  
 Core type 3/8-in. Hexcel

Duct geometry 6 x 10 in.  
 Walls lined Two/10 in.  
 Lining length 44 in.

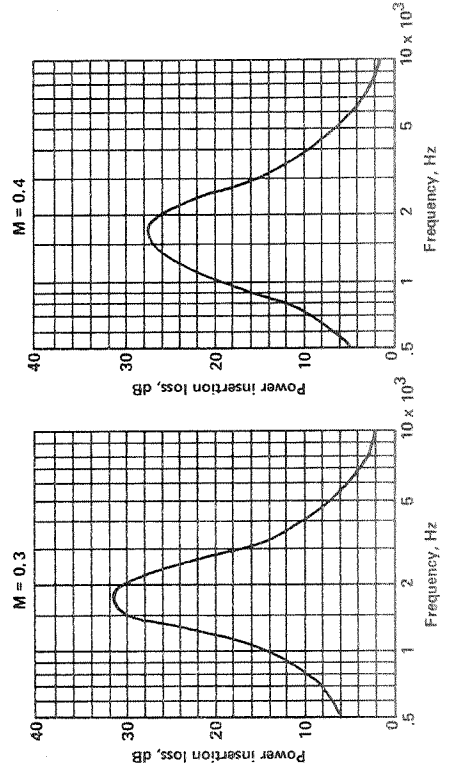
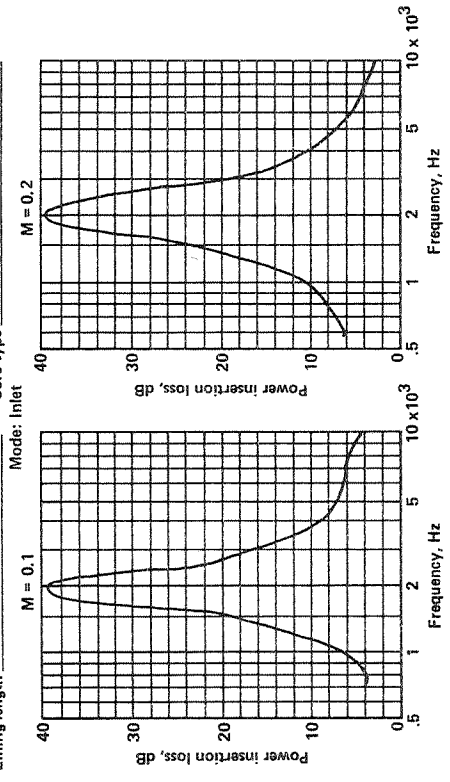


Figure A-262.

Figure A-261.

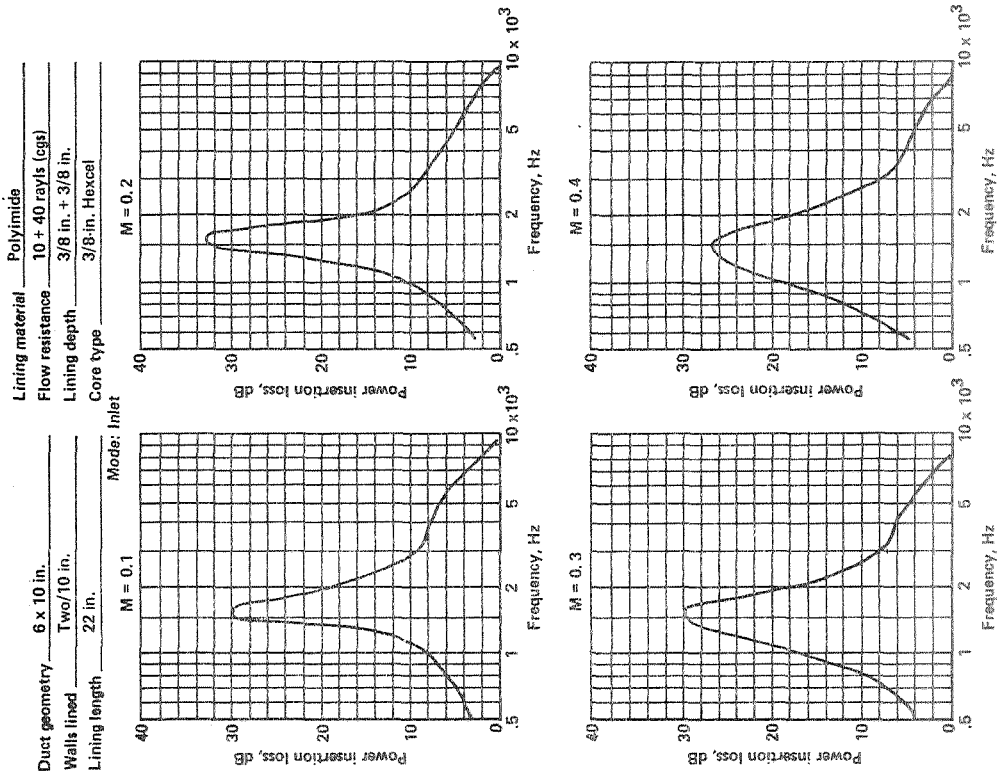


Figure A-263.

1. Report No. NASA CR-	2. Government Accession No.	3. Recipient's Catalog No.	
4. Title and Subtitle Parametric Studies of the Acoustic Behavior of Lined Ducts and Duct-Lining Materials for Turbofan Engine Applications		5. Report Date	
		6. Performing Organization Code	
7. Author(s) J. Atvars		8. Performing Organization Report No.	
		10. Work Unit No.	
9. Performing Organization Name and Address The Boeing Company Commercial Airplane Group P.O. Box 3707, Seattle, Washington 98124		11. Contract or Grant No. NAS 1-10272	
		13. Type of Report and Period Covered Contract Report	
12. Sponsoring Agency Name and Address National Aeronautics and Space Administration Langley Research Center Langley, Virginia		14. Sponsoring Agency Code	
		15. Supplementary Notes	
16. Abstract			
<p>Fan noise radiated from the engine inlet and fan discharge ducts of turbofan airplanes makes the largest contribution to perceived noise during landing approach. This noise can be reduced by lining the engine inlet and duct walls with sound-absorbing materials. In this report, a description is given of an experimental program that was conducted to investigate the influence of acoustic and geometric duct lining parameters on fan-noise attenuation. Test results showed that the significant design parameters are the lining acoustic impedance, treatment length, treatment depth, core cell dimensions, duct size, number of walls lined, number of layers in the lining, and air velocity and direction. The influence of these parameters is discussed.</p>			
17. Key Words (Suggested by Author(s)) Turbofan engine noise Engine noise reduction Acoustically lined ducts Acoustic linings Flow-duct test facility Flow-duct testing		18. Distribution Statement  Unclassified—Unlimited	
19. Security Classif. (of this report) Unclassified	20. Security Classif. (of this page) Unclassified	21. No. of Pages	22. Price*